Oxidative Medicine and Cellular Longevity

The Role of Oxidative Stress in the Pathophysiology of Chronic Inflammatory Diseases 2021

Lead Guest Editor: Daniela Ribeiro
Guest Editors: Marisa Freitas and Marilia Oliveira Fonseca Goulart

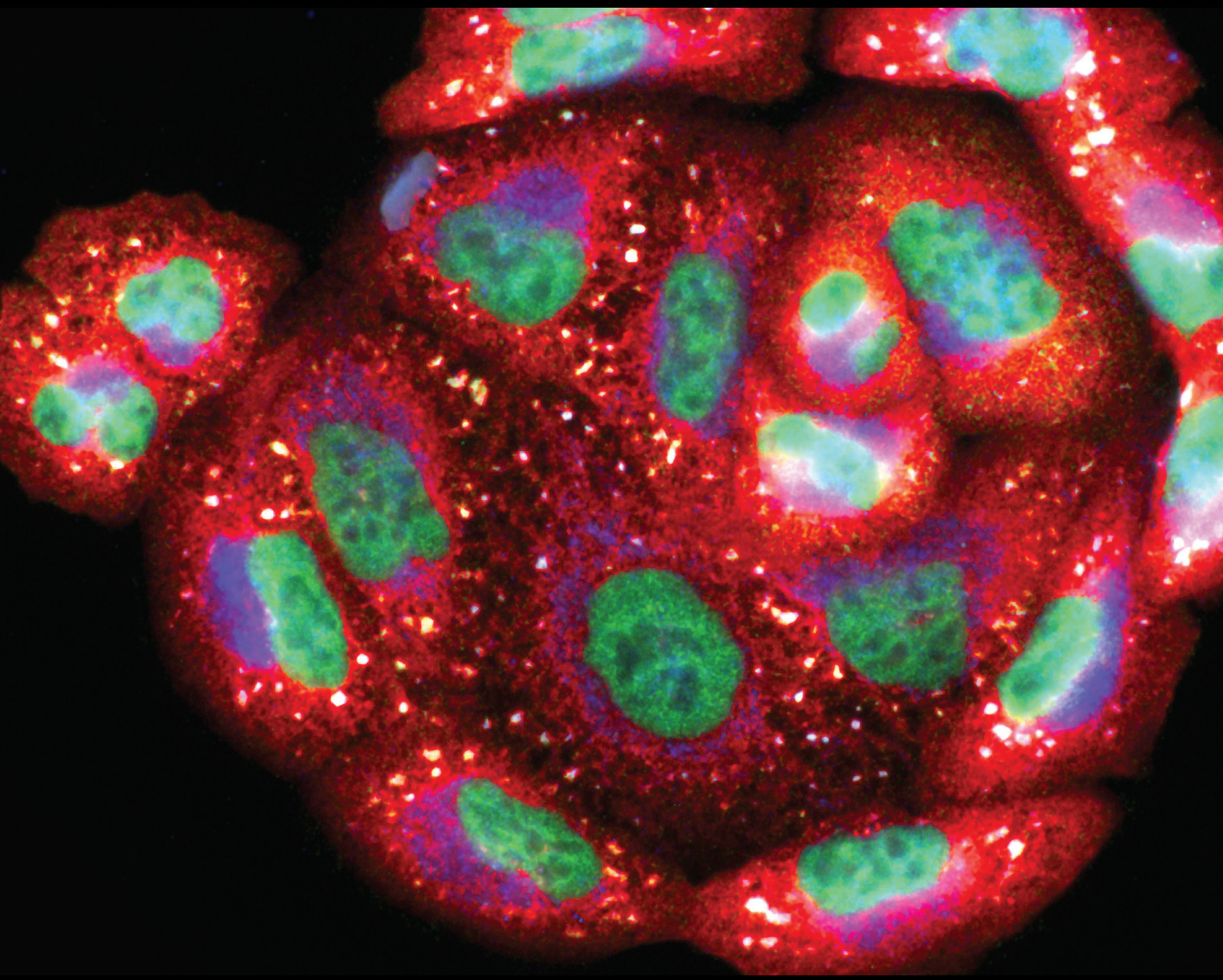

The Role of Oxidative Stress in the Pathophysiology of Chronic Inflammatory Diseases 2021

Oxidative Medicine and Cellular Longevity

The Role of Oxidative Stress in the Pathophysiology of Chronic Inflammatory Diseases 2021

Lead Guest Editor: Daniela Ribeiro
Guest Editors: Marisa Freitas and Marilia Oliveira Fonseca Goulart

Contents

Hindawi
Oxidative Medicine and Cellular Longevity
Volume 2022, Article ID 2457687, 17 pages
https://doi.org/10.1155/2022/2457687

Research Article

T Lymphocyte-Derived Exosomes Transport MEK1/2 and ERK1/2 and Induce NOX4-Dependent Oxidative Stress in Cardiac Microvascular Endothelial Cells

Filip Rolski,[1] **Marcin Czepiel**,[1] **Karolina Tkacz**,[1] **Katarzyna Fryt**,[1] **Maciej Siedlar**,[1] **Gabriela Kania**,[2] **and Przemysław Błyszczuk**[1,2]

[1]*Department of Clinical Immunology, Jagiellonian University Medical College, Cracow, Poland*
[2]*Center of Experimental Rheumatology, Department of Rheumatology, University Hospital Zurich, Switzerland*

Correspondence should be addressed to Przemysław Błyszczuk; przemyslaw.blyszczuk@uj.edu.pl

Received 25 November 2021; Revised 23 August 2022; Accepted 8 September 2022; Published 28 September 2022

Academic Editor: Franco J L

Background. Activation of endothelial cells by inflammatory mediators secreted by $CD4^+$ T lymphocytes plays a key role in the inflammatory response. Exosomes represent a specific class of signaling cues transporting a mixture of proteins, nucleic acids, and other biomolecules. So far, the impact of exosomes shed by T lymphocytes on cardiac endothelial cells remained unknown. *Methods and Results*. Supernatants of $CD4^+$ T cells activated with anti-CD3/CD28 beads were used to isolate exosomes by differential centrifugation. Activation of $CD4^+$ T cells enhanced exosome production, and these exosomes (CD4-exosomes) induced oxidative stress in cardiac microvascular endothelial cells (cMVECs) without affecting their adhesive properties. Furthermore, CD4-exosome treatment aggravated the generation of mitochondrial reactive oxygen species (ROS), reduced nitric oxide (NO) levels, and enhanced the proliferation of cMVECs. These effects were reversed by adding the antioxidant apocynin. On the molecular level, CD4-exosomes increased NOX2, NOX4, ERK1/2, and MEK1/2 in cMVECs, and ERK1/2 and MEK1/2 proteins were found in CD4-exosomes. Inhibition of either MEK/ERK with U0126 or ERK with FR180204 successfully protected cMVECs from increased ROS levels and reduced NO bioavailability. Treatment with NOX1/4 inhibitor GKT136901 effectively blocked excessive ROS and superoxide production, reversed impaired NO levels, and reversed enhanced cMVEC proliferation triggered by CD4-exosomes. The siRNA-mediated silencing of *Nox4* in cMVECs confirmed the key role of NOX4 in CD4-exosome-induced oxidative stress. To address the properties of exosomes under inflammatory conditions, we used the mouse model of $CD4^+$ T cell-dependent experimental autoimmune myocarditis. In contrast to exosomes obtained from control hearts, exosomes obtained from inflamed hearts upregulated NOX2, NOX4, ERK1/2, MEK1/2, increased ROS and superoxide levels, and reduced NO bioavailability in treated cMVECs, and these changes were reversed by apocynin. *Conclusion*. Our results point to exosomes as a novel class of bioactive factors secreted by $CD4^+$ T cells in immune response and represent potential important triggers of NOX4-dependent endothelial dysfunction. Neutralization of the prooxidative aspect of CD4-exosomes could open perspectives for the development of new therapeutic strategies in inflammatory cardiovascular diseases.

1. Introduction

Cardiovascular diseases are the leading cause of morbidity and mortality in the world, and coronary heart disease is the most common form of cardiovascular disease [1]. Chronic oxidative stress in endothelial cells that leads to their dysfunction plays a key role in the pathogenesis of atherosclerosis and coronary microcirculation dysfunction [2, 3]. More recently, endothelial dysfunction was implicated in life-threatening complications in COVID-19 patients [4].

The endothelial barrier is composed of vascular endothelial cells, endothelial glycocalyx, and basement membrane. The main function of this barrier is not only the separation of blood from underlying tissues but also the control of

nutrient delivery, metabolic homeostasis, prevention of thrombotic events, management of immune cell trafficking, and regulation of blood pressure. In a healthy condition, the production of nitric oxide (NO) exerting vasodilating properties represent a particularly important aspect of endothelial cell activity. Loss or impairment of physiological properties of the endothelium is termed endothelial dysfunction [5]. Oxidative stress is characterized by an increase of reactive oxygen species (ROS), which include hydrogen peroxide (H_2O_2), superoxide anion (O_2^-), and hydroxyl radicals. Increased ROS production together with reduced endothelial nitric oxide synthase (eNOS) activity and NO bioavailability plays a pivotal role in endothelial dysfunction [6]. ROS serve as signal transmitters regulating numerous cellular processes, and their excessive production affects cellular metabolism, transcriptomic profile, and signaling pathway activities leading to abnormal cellular function [7, 8]. In endothelial cells, ROS are produced by several cellular sources including mitochondria, membrane-bound NADPH oxidases (NOX) 1-5, and other enzymes, such as oxidases, peroxidases, cytochromes, mono- and dioxygenases, and uncoupled eNOS. Regulation of the NOX expression is not completely understood. It involves a complex interplay between several transcription factors, co-activators/repressors, nuclear receptors, and epigenetic mechanisms [9].

Inflammation has been implicated in the activation of endothelial cells. Chronic inflammatory conditions can affect coronary microvascular function and contribute to the development of myocardial ischemia and cardiovascular events. Furthermore, chronic, low-grade inflammation of the arterial wall is a typical feature of atherosclerosis [3]. In response to inflammation, endothelial cells upregulate adhesion molecules to interact with circulating leucocytes and downregulate endothelial junctional structures to increase vascular permeability. A growing body of evidence indicates that inflammation affects ROS/NO balance in endothelial cells leading to endothelial dysfunction [8]. The inflammatory response in chronic inflammatory diseases is orchestrated mainly by cells of myeloid lineage and T lymphocytes. Activation of naïve T lymphocytes through T cell receptor (TCR) leads to expansion of the effector pool of antigen-specific T lymphocytes. Activated naïve T cells turn into effector T cells, and antigen-presenting cells direct their polarization into the specific T helper subtype [10]. TCR activation results in the production and secretion of several primary inflammatory cytokines and chemokines, which often exaggerate inflammatory response.

Mid- and long-distance cell-to-cell interaction is not limited to secretory proteins but can also be mediated by extracellular vesicles, which are shed by one class of cells and absorbed by others [11]. Extracellular vesicles represent fragments of the cytoplasm that carry molecular cargo that includes membrane and cytosolic proteins, lipids, and various RNAs. Practically, all cells actively release various types of membrane vesicles of endosomal and plasma membrane origin in the process of exocytosis. Extracellular vesicles are classified by size and are usually separated by differential centrifugation. The larger size class called microvesicles is heterogeneous (200 to ~1,500 nm), while the smaller size class called exosomes is relatively homogeneous in size (50 - 150 nm). Exosomes bear specific surface markers and adhesion molecules, transport various lipids, proteins, mRNAs, and microRNAs, and therefore have to be considered as a separate class of immunomodulatory molecules [11]. Extracellular vesicles have been demonstrated to play a modulatory role in various cardiovascular disorders. So far, the proinflammatory potential of T cell-derived exosomes has not been extensively investigated. In this work, we specifically analyzed the effect of exosomes produced by activated T lymphocytes in the context of endothelial cell activation.

2. Materials and Methods

2.1. Experimental Autoimmune Myocarditis (EAM) Model. EAM was induced in 6–8 week-old Balb/c mice by subcutaneous injection of 200 μg of α-MyHC$_{614\text{-}634}$ peptide (Ac-RSLKLMATLFSTYASADR-OH, Caslo, Denmark) emulsified in 1 : 1 ratio with complete Freund's adjuvant (Difco, USA) at days 0 and 7. Mice were anesthetized by intraperitoneal injection of ketamine (75 mg/kg) and euthanized by cervical dislocation on day 21. All experiments were performed in accordance with Polish law and were approved by local authorities (license number 234/2019). Animal experiments followed the guidelines of Directive 2010/63/EU of the European Parliament on the protection of animals used for scientific purposes.

2.2. Isolation and Culture of Cardiac Microvascular Endothelial Cells. Preliminary experiments were performed using commercially available primary cardiac microvascular endothelial cells (cMVECs) from Balb/c mice (Cedarlane, Canada). Further experiments were performed on primary cMVECs isolated from 4 weeks old Balb/c mice. Briefly, mice were euthanized, and hearts were perfused with ice-cold PBS supplemented with 5 mM EDTA. Three hearts were cut into small pieces, suspended in 1 ml of RPMI 1640 (Corning, USA) supplemented with 50 μg/ml Liberase TL (Roche, Switzerland), and incubated at 37°C. Every 10 minutes, hearts were pipetted until tissues were completely disintegrated. Cell suspension was filtered through 70 μm and 40 μm cell strainers and centrifuged for 1 minute at 400 g. Single cell suspension was resuspended in the growth medium: RPMI 1640 containing 10% fetal bovine serum (FBS; USA, Gibco), 0.5 ng/ml mouse recombinant endothelial growth factor (BioLegend, USA), and 1 ng/ml mouse recombinant fibroblast growth factor (BioLegend, USA). Cells isolated from a single mouse heart were seeded in a 10 cm cell culture dish (Falcon, USA) coated with 0.2% gelatine and incubated at 37°C for 60 minutes. Next, nonadhesive cells were removed, and cMVECs were cultured in the growth medium and were passaged after reaching at least 90% confluence. The purity of all cultures was confirmed by CD31 staining using flow cytometry (over 90% of CD31$^+$ cells). Cells between passages 3 and 7 were used in the experiments. In selected experiments, the cMVECs were treated with 50 μM apocynin (Sigma, USA), 2 μM GKT136901 (NOX inhibitor, Merck, Germany), 5 μM FR180204 (ERK inhibitor, Tocris Bioscience, GB), or 5 μM U0126 (MEK

inhibitor, Tocris Bioscience, GB). Apocynin, inhibitors, and exosomes were added at the same time. All treatments were performed 1 day after cMVECs reached full confluence.

2.3. Isolation and Culture of CD4$^+$ T Lymphocytes. CD4$^+$ T lymphocytes were isolated from spleens of 4-6 weeks old Balb/c mice. Briefly, spleens were mechanically mashed through a 70 μm cell strainer following erythrocyte lysis using the ammonium-chloride-potassium buffer, and the obtained cell suspension was filtered through a 40 μm cell strainer. CD4$^+$ T cells were isolated using Dynabeads Untouched Mouse CD4 Cells Kit (ThermoFisher, USA) according to the manufacturer's instructions. Isolated CD4$^+$ T cells were cultured in RPMI 1640 supplemented with 10% FBS. The medium used in T cell cultures was depleted from exosomes by 1-hour centrifugation at 100 000 g. T cell activation was performed with Mouse T-Activator CD3/CD28 Dynabeads (ThermoFisher, USA). After 3 days of culture (density about 4×10^6 T cells/ml), the medium was collected for exosome isolation or used as conditional medium.

2.4. Isolation and Measurement of Exosomes. CD4$^+$ T cell-derived exosomes were isolated from conditioned medium of activated CD4$^+$ T cells as described previously [12]. Heart exosomes were isolated from mice hearts with induced EAM and healthy age-matched mice. Each heart was perfused with ice-cold PBS, cut into small pieces, and suspended in 1 ml of RPMI 1640 (Corning, USA) supplemented with 50 μg/ml Liberase TL and incubated at 37°C for approximately 40 minutes. Tissue pieces were pipetted every 10 minutes until single-cell suspension was obtained. Liberase TL was neutralized by the addition of 2 ml RPMI 1640 containing 10% FBS. The suspension was further diluted to 10 ml with PBS and centrifuged for 5 minutes at 4 000 g. To obtain exosomes, conditioned medium or collected supernatants were centrifuged at 20 000 g for 30 minutes to remove cell debris. Next, obtained supernatants were centrifuged for 1 hour at 100 000 g, and pellets were resuspended in 100 μl PBS and stored at -20°C for up to a month. Exosomes were used at concentration of 10^8 particles/ml unless otherwise stated. 10^8 particles/ml represented a typical concentration of exosomes in medium conditioned of activated T lymphocytes. Exosomes were measured using the NanoSight tracking analysis (NTA) system: the LM10HS microscope was equipped with the LM14 488 nm laser module (Malvern Instruments Ltd., Malvern, UK). Samples were diluted in PBS to provide counts within the detection range of the instrument. One-minute duration videos were recorded for each batch of exosomes. Particle movement was analyzed with the NTA 3.1 NanoSight software according to the manufacturer's protocol.

2.5. Exosome Labeling. Isolated exosomes were labeled with PKH26 Red Fluorescent Cell Linker Kit (Sigma-Aldrich) according to manufacturer's protocol and washed and resuspended in PBS. cMVECs were grown to full confluence on 24-well plates and treated with 4x10^8 PKH26 labeled exosomes for 18 h, washed with PBS, and resuspended in growth medium. The immunofluorescence of live cells was analyzed using an Olympus BX53 microscope equipped with Olympus XC50 camera (Olympus, Tokyo, Japan).

2.6. Flow Cytometry. Cells were cultured in 24-well plates coated with 0.2% gelatin. Before the experiment medium was removed, cells were rinsed 3 times with PBS, collected using trypsin, and washed 2 times in PBS. Total ROS production was measured by staining with 0.5 ml of 10 μM 2′,7′-dichlorofluorescein diacetate (H_2DCFDA, ThermoFisher, USA) diluted in PBS in the dark at 37°C for 10 minutes. The superoxide production by mitochondria was evaluated using the MitoSOX™ Red reagent (ThermoFisher, USA). cMVECs were suspended in 0.25 ml growth medium containing 2 μM MitoSox and incubated in the dark at 37°C for 30 minutes. Nitric oxide levels were determined with 4,5-diaminofluorescein diacetate (DAF2 DA, Abcam, UK). Cells were incubated in PBS containing 5 μM DAF2 DA in the dark at 37°C for 20 minutes. To perform membrane adhesion molecules measurements, cultured cMVECs were labeled with anti-ICAM1-PE (1 : 500, clone YN1/1.7.4, Thermo Fisher, USA), anti-VCAM1-PE-Cy7 (1 : 500, clone 429, Biolegend, USA) anti-P-selectin-APC (1 : 500, clone RMP-1, BioLegend, USA), and anti-CD31-FITC (1 : 500, clone 390, ThermoFisher, USA) using standard procedure. Dead cells were determined using propidium iodide (ThermoFisher, USA) staining and excluded from the analysis. After each respective staining, cells were washed with growth medium, centrifuged at 300 g for 5 minutes, washed again with PBS, and resuspended in flow cytometry buffer (2% FBS, 1 mM EDTA in PBS). All samples were acquired using the BD FACSCanto II analyzer (BD Biosciences), and the data were analyzed with the FlowJo software (Tree Star, FlowJo X 10.0.7., USA).

2.7. Peroxynitrite Measurement. Production of peroxynitrite was determined using Cell Meter™ Fluorimetric Intracellular Peroxynitrite Assay Kit ∗Green Fluorescence∗ (ATT Bioquest, USA). Briefly, cMVECs were seeded onto 96-well plate coated with 0.2% gelatine. The dye was diluted according to manufacturer instructions in growth medium. Cells were incubated for 30 minutes in the dark at 37°C in 50 μl of staining solution. Cells were washed twice with PBS, and fluorescence was measured using M200 PRO plate reader (TECAN Instruments, Switzerland).

2.8. Proliferation Assay. 5000 cMVECs per well in 0.2 ml of growth medium were seeded onto 96-well plates coated with 0.2% gelatin. Cells were stimulated with T cell-derived exosomes alone or in combination with 50 μM apocynin, 2 μM GKT136901, NOX inhibitor, 5 μM FR180204, or 5 μM U0126. Cell proliferation was measured after 2 days using CyQUANT™ Cell Proliferation Assay (ThermoFisher, USA) according to the manufacturer's instructions.

2.9. Adhesion Assay under Shear Stress. The BioFlux 200 48-well plate 0-20 dyn (Fluxion, USA) microcapillaries were coated with 1% gelatin (ThermoFisher, USA) and 25 μg/ml human fibronectin (ThermoFisher, USA) solution in growth medium for 24 h at 37°C. Single cell suspension of MVECs

(2.5×10^6/ml) in growth medium was loaded into capillaries using the BioFlux 200 system (Fluxion, USA), and cells were cultured inside the microcapillaries until the formation of a confluent monolayer. Cells were stimulated with either 5 ng/ml recombinant mouse TNF-α (BioLegend), T cell-derived exosomes, or a combination of both for 16 hours. For the adhesion assay, single cell suspension of freshly isolated mouse splenocytes was labelled with the CellTrace CFSE (ThermoFisher, USA) and used at concentration of 3×10^5 cells/ml. The flow of splenocytes at 1 dyn/cm^3 through the microcapillaries coated with cMVECs was induced for 30 minutes, and adhesion of CFSE-labeled splenocytes was analyzed with a fluorescence microscope (LS720, Etaluma, USA).

2.10. RT-PCR. Total RNA was extracted with TRIzol (Invitrogen) according to manufacturer recommendations. 100 ng total RNA was used for reverse transcription using the NG dART RT Kit (EURx, Poland). Quantitative real-time PCR was performed using the SYBR Green PCR Master Mix (EURx, Poland) and oligonucleotides complementary to transcripts of the analyzed genes using the Quant Studio 6 Real-Time PCR system (Applied Biosystems, USA). The following oligonucleotides were used in this study: 5′-GAGC GACTCAAACTGCCCT-3′, *Mapk3* 5′-GGTTGTTCCCA AATGCTGACT-3′ and 5′-CAACTTCAATCCTCTTGTG AGGG-3′, *Map2k1* 5′-AAGGTGGGGGAACTGAAGGAT-3′ and 5′-CGGATTGCGGGTTTGATCTC-3′, *Ywhaz* 5′-GAAAAGTTCTTGATCCCCAATGC-3′ and 5′-TGTGAC TGGTCCACAATTCCTT-3′, *Nox3* 5′-CAACGCACAGG CTCAAATGG-3′ and 5′-CACTCTCGTTCAGAATCCA GC-3′, *Cyba* 5′-TGCCAGTGTGATCTATCTGCT-3′ and 5′-TCGGCTTCTTTCGGACCTCT-3′, *Nox1* 5′-AGCTTT CTGAGTAGGTGTGCAT-3′ and 5′-CCCAACCAGGAA ACCAGAAACA-3′, *Nox2* 5′-CCTCTACCAAAACCATT CGGAG-3′ and 5′-CTGTCCACGTACAATTCGTTCA-3′, *Nox4* 5′-GAAGGGGTTAAACACCTCTGC-3′ and 5′-AT GCTCTGCTTAAACACAATCCT-3′, *Sod1* 5′-AACCAGT TGTGTTGTCAGGAC-3′ and 5′-CCACCATGTTTCTTA GAGTGAGG-3′, and *Sod2* 5′-CAGACCTGCCTTACGA CTATGG-3′ and 5′-CTCGGTGGCGTTGAGATTGTT-3′. Transcript levels of *Ywhaz* were used as endogenous reference, and the relative gene expression was calculated using the $2^{-\Delta\Delta Ct}$ method.

2.11. Immunoblotting. cMVECs, CD4$^+$ T lymphocytes, and exosomes were lysed in RIPA buffer supplemented with protease and phosphatase inhibitors (ThermoFisher, USA). Immunoblotting procedure was performed as described previously [13] using the following antibodies: anti-MEK1/2 (1 : 1000, clone D1A5, Cell Signaling, USA), anti-phospho-MEK1/2 (1 : 1000, clone S217/221, Cell Signaling USA), anti-Erk1/2 (1 : 1000, clone 137F5, Cell Signaling, USA), anti-phospho-Erk1/2 (1 : 1000, clone D13.14.4E, Cell Signaling USA), anti-eNOS antibody (1 : 1000, polyclonal, Invitrogen, USA), anti-phospho-eNOS Thr495 (1 : 1000, polyclonal, Invitrogen, USA), anti-phospho-eNOS Ser1177 (1 : 1000, polyclonal, Invitrogen, USA), anti-NOX2 (1 : 1000, clone ARC0181, Invitrogen USA), anti-NOX4 (1 : 500, clone SY0214, Invitrogen, USA), β-tubulin (1 : 1000, clone 228.33, Invitrogen, USA), goat anti-mouse IgG (H + L)-HRP (ThermoFisher, USA), and goat anti-rabbit IgG (H + L)-HRP (ThermoFisher, USA). The protein signal was detected using the Western Blotting Substrate (ThermoFisher, USA) and imaged with the ChemiDoc instrument (Bio-Rad, ChemiDoc Imaging System, USA). Results were analyzed with the ImageJ software (Version 1.52a, NIH, Bethesda, USA). Protein abundance was normalized to β-tubulin levels. To detect eNOS dimers, cell lysates were incubated in Laemmli buffer without 2-mercaptoethanol at 37°C for 5 min. For the monomer control, a sample was incubated with reducing agents at 80°C for 5 minutes. The samples were subjected to low temperature SDS-PAGE. Buffers and gels were equilibrated at 4°C, samples were separated in 6% gels at 80 V for 90 minutes, and the electrophoresis was performed in the fridge.

2.12. Nox4 Silencing. Nox4 silencing in cMVECs was performed with anti-*Nox4* siRNA (m) (Santa Cruz Biotechnology, USA). cMVECs were seeded onto 24-well plates coated with 0.2% gelatine. Cells were transfected with Lipofectamine 3000 (Thermofisher) after reaching 90% confluence. Briefly, cells were incubated in 0.3 ml transfection mix (6 μl Lipofectamine 3000, 100 nM anti-*Nox4* siRNA) for 24 hours. Afterwards, 0.2 ml of growth medium was added, and cells were stimulated with CD4-derived exosomes for another 24 hours. Cells transfected with Lipofectamine 3000 without siRNA were used as controls. Optimalization of transfection was performed using Control siRNA (FITC Conjugate)-A (Santa Cruz Biotechnology, USA).

2.13. Histology. Mouse hearts were fixed in 4% formalin and embedded in paraffin. Standard hematoxylin/eosin staining was performed to visualize and grade the size of leukocyte infiltrates. Immunohistochemistry of CD3 cells was performed as described previously [14].

2.14. Statistic. Data was analyzed using Student's *t*-test or one-way ANOVA followed by Fisher's least significant difference (LSD) *post hoc* test. Differences were considered statistically significant for $p < 0.05$. All analyses were performed with GraphPad Prism 6 software (San Diego, USA), and values are expressed as mean with standard deviation (SD) as described in figure legends.

3. Results

3.1. Exosomes Shed by Activated CD4$^+$ T Lymphocytes Induce Endothelial Dysfunction but Do Not Affect the Adhesive Properties of cMVECs. In the immune response, activation of CD4$^+$ T cells with antigen leads to the production of pro-inflammatory mediators causing activation and dysfunction of endothelial cells. We could confirm that conditional medium of CD4$^+$ T cells activated with anti-CD3/CD28 effectively increased membrane levels of cell adhesion antigens ICAM-1, VCAM-1, and P-selectin, induced oxidative stress in cMVECs as indicated by elevated total ROS levels,

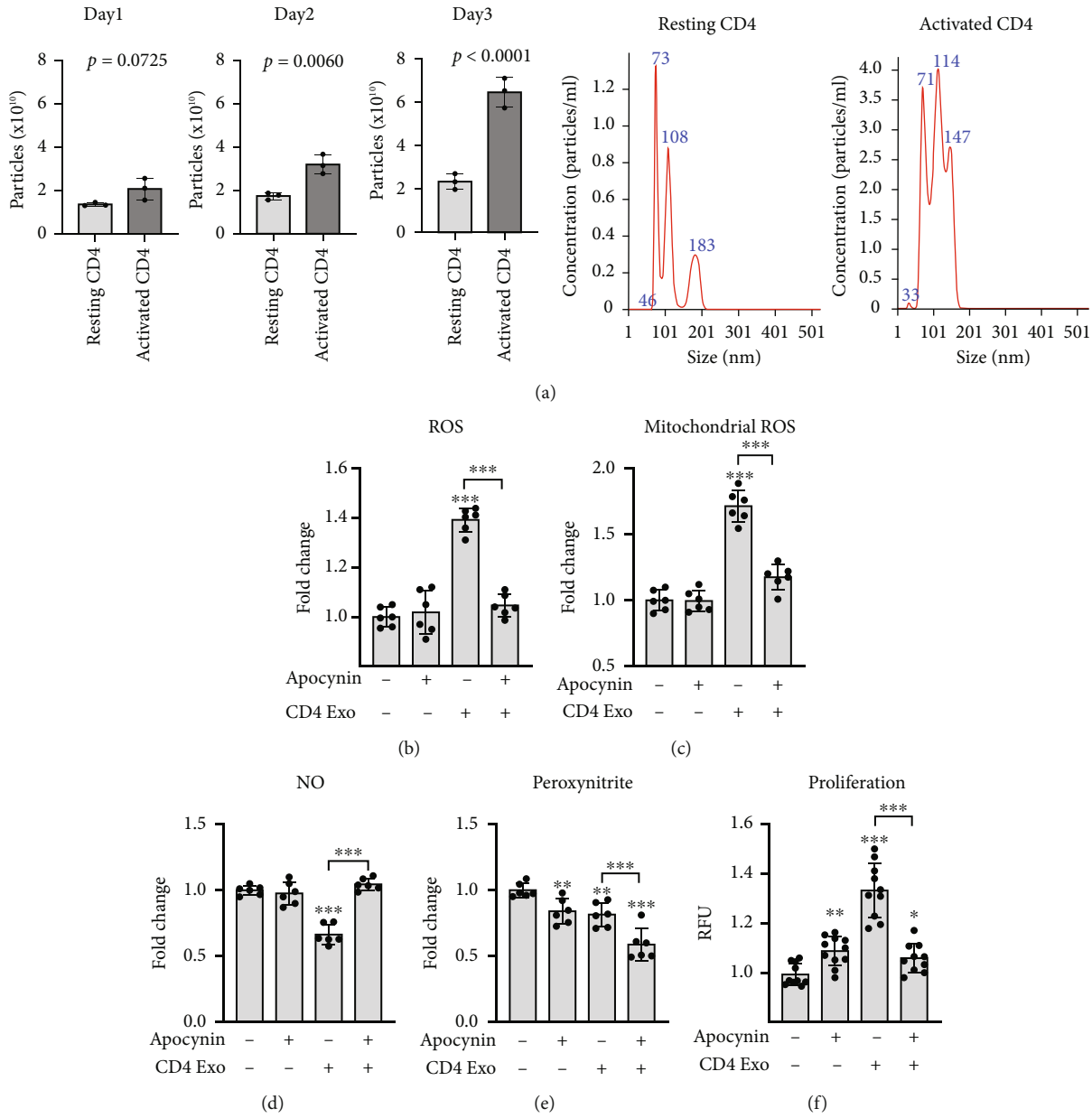

Figure 1: CD4-exosomes induce oxidative stress in cMVECs. Panel (a) shows quantification and representative NTA analysis of exosomes produced by resting and activated $CD4^+$ T lymphocytes, $n = 3$. p values calculated with Student's t-test. Panels (b)–(e) demonstrate effect of CD4-exosomes (CD4 Exo) on cMVEC's total ROS levels (b), $n = 6$, mitochondrial ROS generation (c), $n = 6$, NO levels (d), $n = 6$, peroxynitrite levels (e), $n = 6$, and cell proliferation (f), $n = 10$, in the presence or absence of apocynin. $^*p < 0.05$, $^{**}p < 0.01$, and $^{***}p < 0.001$ calculated by one-way ANOVA followed by Fisher's LSD post hoc test versus control group or for indicated groups.

and increased mitochondrial superoxide production, and showed defective NO production (Suppl. Figure 1A).

Activated T cells secrete not only cytokines and chemokines but also shed exosomes; therefore, we asked how these exosomes could affect the physiology of cMVECs. Activation with anti-CD3/CD28 induced secretion of exosomes by $CD4^+$ T cells (Figure 1(a)). Stimulation with these CD4-exosomes (10^8 particles/ml) for 16 hours increased ROS levels and increased mitochondrial superoxide production in cMVECs (Figures 1(b) and 1(c)). It is well known that oxidative stress can reduce NO bioavailability. Indeed, we observed reduced NO levels in cMVECs treated with exosomes (Figure 1(d)). Peroxynitrite is a highly reactive coupling product of NO and superoxide, and we observed reduced peroxynitrite levels in cells treated with CD4-exosomes (Figure 1(e)). Antioxidant apocynin can efficiently inhibit oxidative stress in endothelial cells by scavenging ROS [15, 16]. Accordingly, treatment with apocynin nearly completely protected cMVECs from CD4-exosome-induced oxidative stress and impaired NO production (Figures 1(b)–1(d)). Furthermore, treatment with CD4-exosomes enhanced cMVEC proliferation that was abolished by treatment with

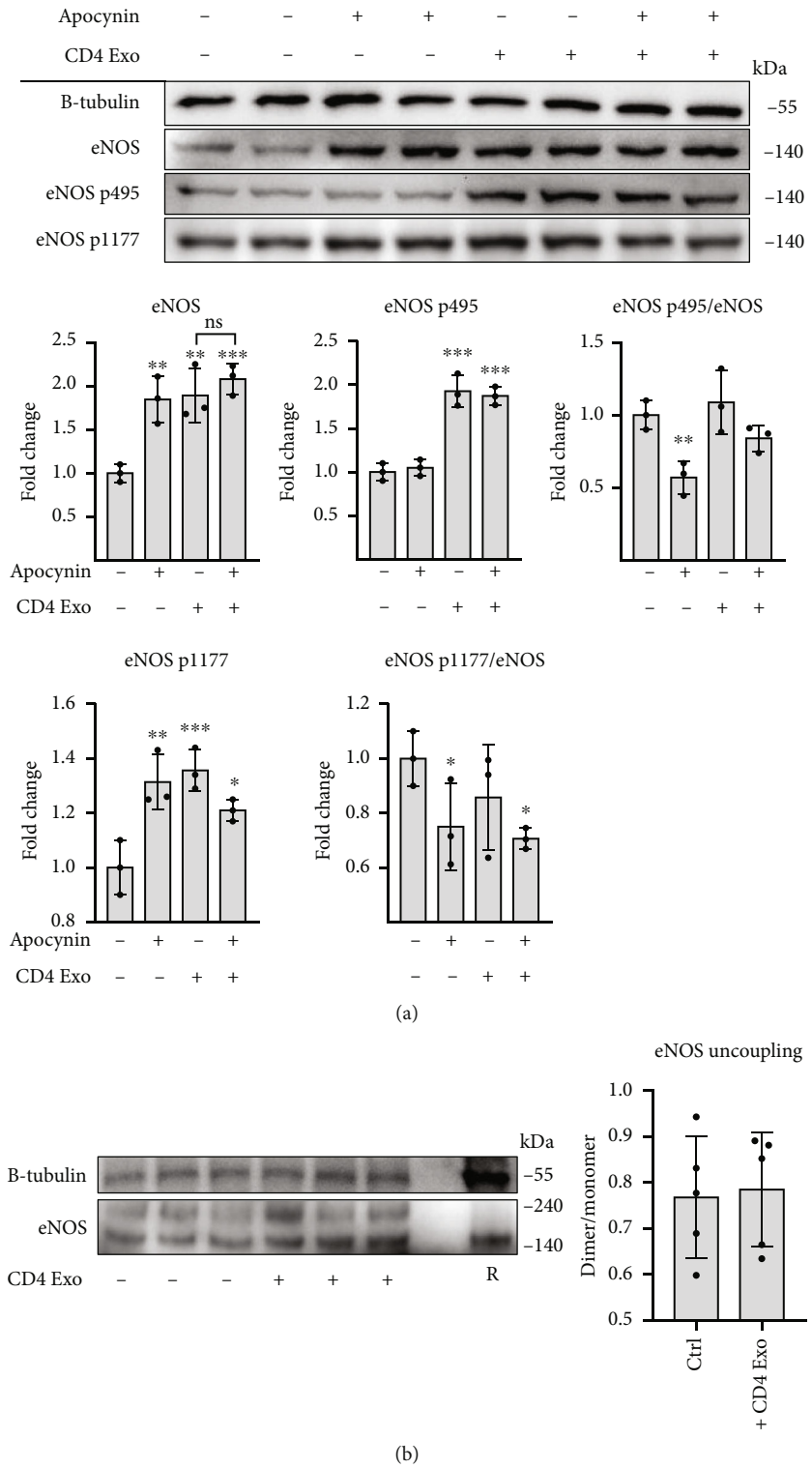

Figure 2: CD4-exosomes upregulate the eNOS expression in cMVECs independently of oxidative stress. Panel (a) shows representative immunoblots and densitometry of total levels of eNOS, eNOS-p495 (inhibitory site), and eNOS-p1177 (activation site) in cMVECs treated with CD4-exosomes and/or apocynin, $n = 3$. Protein levels were normalized to beta-tubulin or to total eNOS. Panel (b) shows representative immunoblots and densitometry of eNOS dimer/monomer ratio in cMVECs stimulated with CD4-exosomes, $n = 5$. *R* indicates sample with reducing agent. In each experiment, cMVECs were stimulated for 16 h. $^{*}p < 0.05$, $^{**}p < 0.01$, and $^{***}p < 0.001$ calculated by one-way ANOVA followed by Fisher's LSD post hoc test versus control group or for indicated groups.

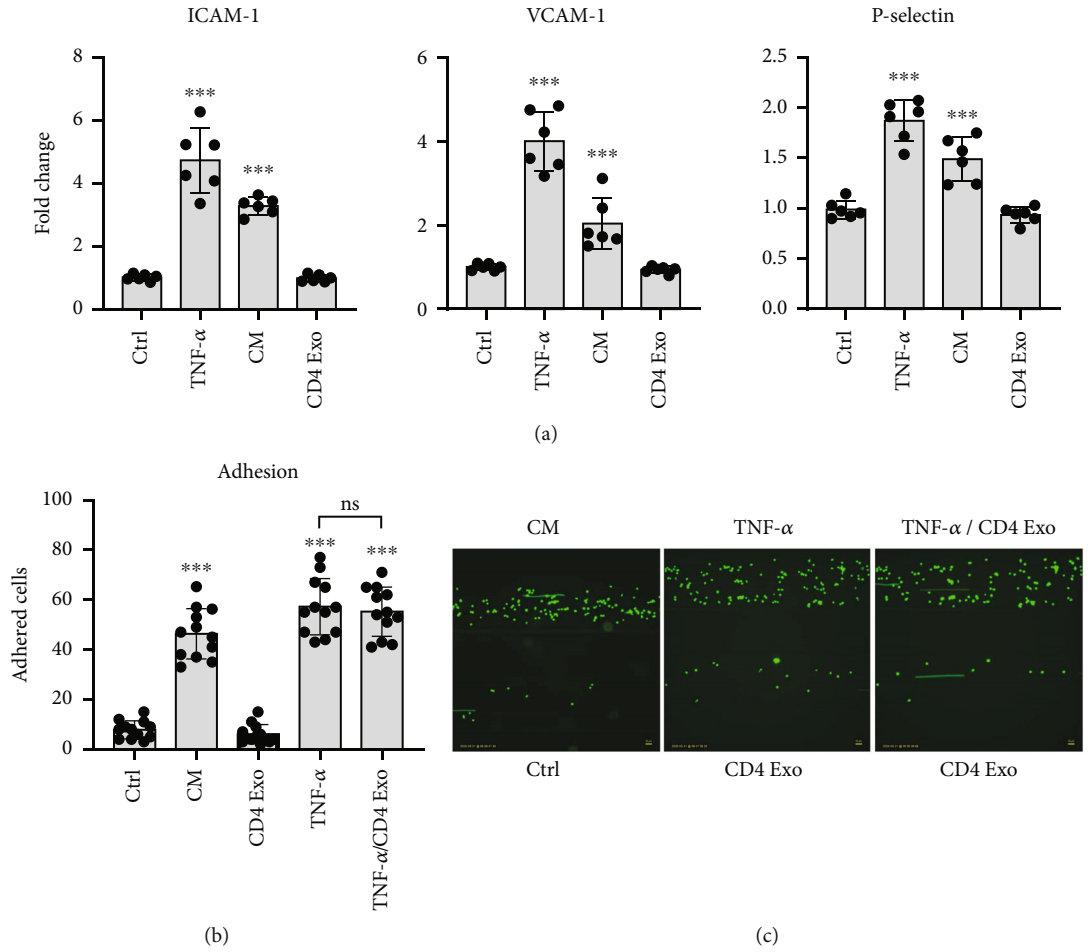

Figure 3: No effect of CD4-exosomes on cMVEC's adhesive properties. Panel (a) shows changes in membrane levels of adhesion molecules VCAM-1, ICAM-1, and p-selectin in cMVECs stimulated with TNF-α, medium conditioned of activated T lymphocytes (CM), or CD4-exosomes (CD4 Exo) for 16 h, $n = 6$. Panel (b) represents capability of treated cMVECs (for 16 h) to bind leukocytes under shear-flow conditions. Results are expressed as average number of leukocytes that firmly adhered to cMVECs after 30 minutes of shear flow, $n = 12$. Panel (c) shows representative microphotographs used in adhesion analysis. ns-$p > 0.05$, $^{*}p < 0.05$, $^{**}p < 0.01$, and $^{***}p < 0.001$ calculated by one-way ANOVA followed by Fisher's LSD post hoc test versus control group or for indicated groups.

apocynin (Figure 1(f)). NO is produced by eNOS, which is activated by dephosphorylation at Thr495 and phosphorylation at Ser1177. Treatment with CD4-exosomes elevated total eNOS levels in cMVECs but relative phosphorylations at both sites remained unaffected (Figure 2(a)). Importantly, uncoupled eNOS represents a source of ROS rather than NO. Our data showed, however, no changes in dimer/monomer eNOS ratio in cMVECs following treatment with CD4-exosomes (Figure 2(b)). Of note, exosomes derived from resting $CD4^+$ T cells lowered ROS in cMVECs and did not affect NO levels (Suppl. Figure 1B).

Oxidative stress has been associated with endothelial activation [17]. cMVECs treated with CD4-exosomes were analyzed for membrane levels of integrins involved in endothelial-leukocyte adhesion. In contrast to treatment with TNF-α, stimulation with CD4-exosomes did not upregulate ICAM-1, VCAM-1, and P-selectin in cMVECs (Figure 3(a)). In line with these results, the functional adhesive properties of cMVECs to bind leukocytes under shear flow were unchanged after treatment with CD4-exosomes. As expected, in activation of cMVECs with TNF-α induced adhesion of leukocytes, however, the addition of CD4-exosomes did not alter this response (Figure 3(b)).

3.2. $CD4^+$ T Cell-Derived Exosomes Transport MEK1/2 and ERK1/2 and Activate NADPH Oxidases in cMVECs. We assumed that CD4-exosome-induced oxidative stress was associated with the upregulation of endogenous NOXs in these cells. The obtained results confirmed the upregulation of *Nox2*, *Nox4*, *Cyba* (the gene that encodes P22 – a common subunit for NOX2 and NOX4 complexes), *Sod1*, and *Sod2*, but not *Nox1* at the mRNA level (Figure 4(a)). The increased levels of *Nox2* and *Nox4* in cMVECs were further confirmed at the protein level (Figure 4(b)). In the next step, we addressed the expression of transcription factors that control NOXs, such as MEK1/2 and ERK1/2. We found significant upregulation of total MEK1/2, and ERK1/2 but also p-MEK1/2 and p-ERK1/2 protein levels as early as 2-4 h after treatment with CD4-exosomes (Figure 4(b)). In contrast to the protein level, mRNA levels of *Mapk3* and

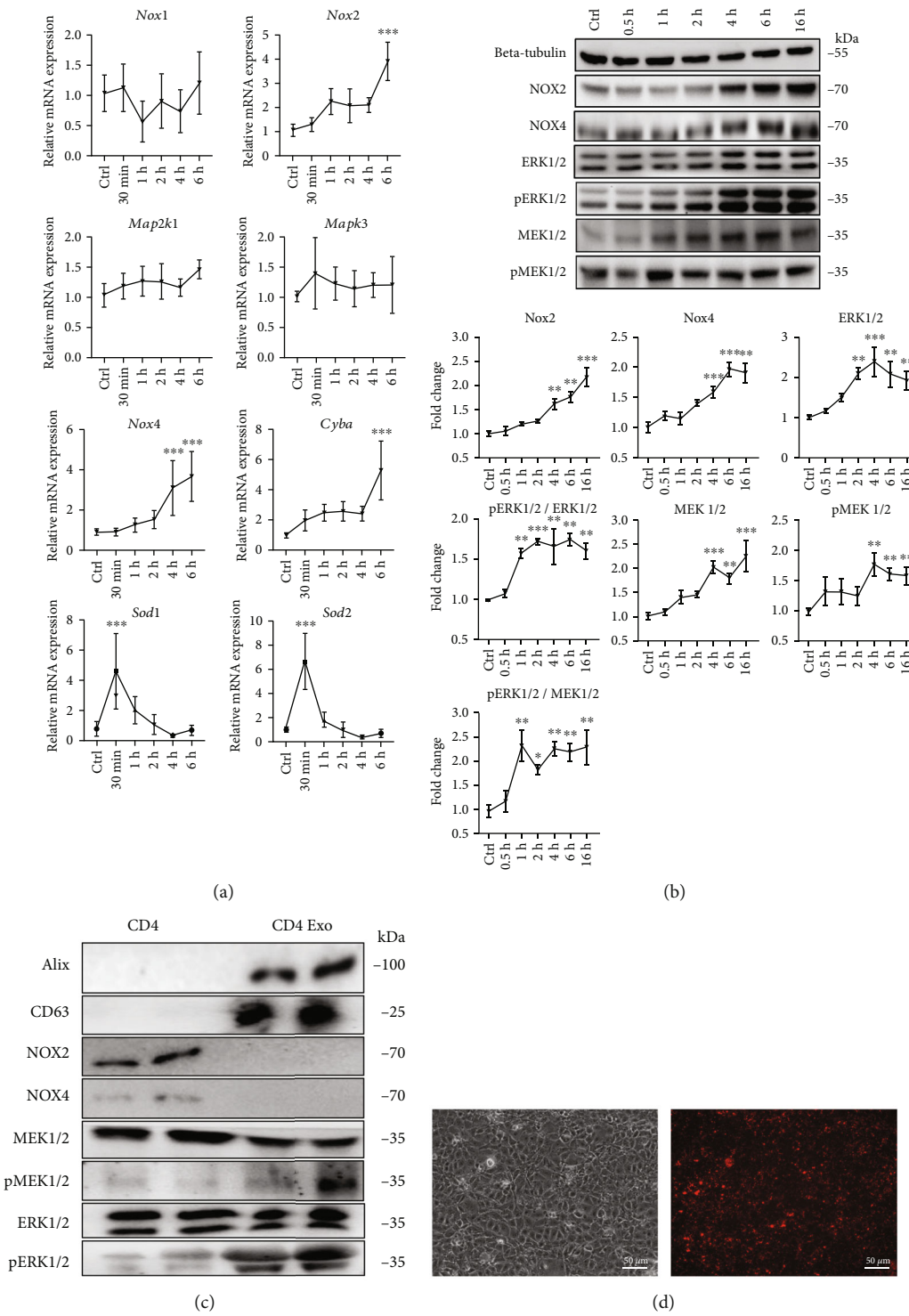

Figure 4: CD4-exosomes activate ERK1/2 and MEK1/2 pathway in cMVECs. Panel (a) shows changes at mRNA levels in cMVECs stimulated with CD4-exosomes for up to 6 hours, $n = 10$, for NOX4 and P22, $n = 7$, for other genes. Changes in protein levels of NOX2, NOX4, ERK1/2, ERK1/2 phosphorylation (pERK1/2), MEK1/2 and MEK1/2 phosphorylation (pMEK1/2), phosphorylation sites in cMVECs stimulated with CD4-exosomes for 16 h, and representative immunoblots are shown in panel (b), $n = 4$. Protein levels were normalized to beta-tubulin, and phosphorylated proteins were additionally normalized to their respective nonphosphorylated forms. Immunoblots of lysates (equal amounts of proteins were loaded on gel) from activated T lymphocytes (CD4) and CD4-exosomes (CD4 Exo) for indicated proteins are shown in panel (c). Panel (d) shows representative microphotographs demonstrating binding of PKH26-stained CD4-exosomes (red fluorescence) to MVECs 16 h after treatment. Scale bar = 50 μm. $^{*}p < 0.05$, $^{**}p < 0.01$, and $^{***}p < 0.001$ calculated by one-way ANOVA followed by Fisher's LSD post hoc test versus control group.

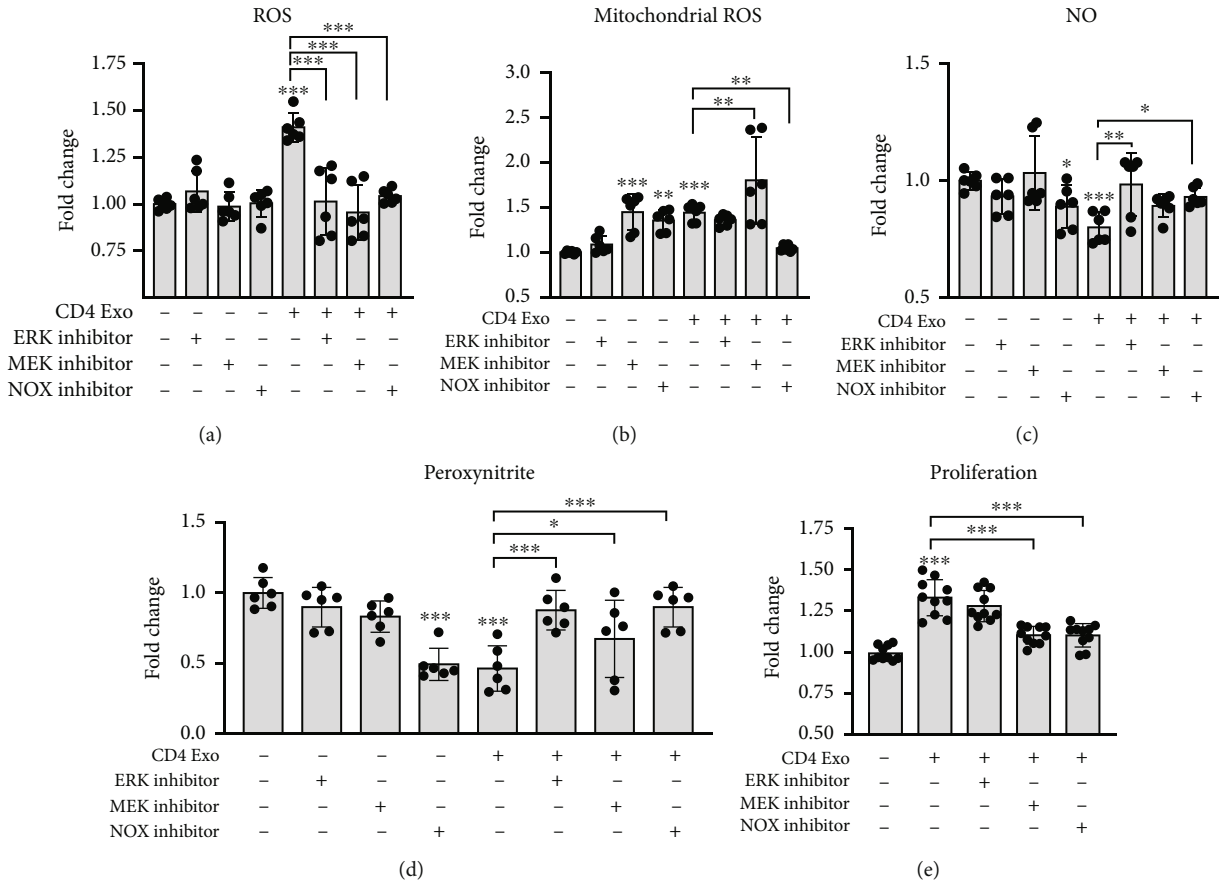

Figure 5: Oxidative stress induced in cMVECs by CD4-exosomes is regulated by ERK1/2 and MEK1/2 pathway. cMVECs were stimulated for 16 h with CD4-exosomes (CD4 Exo) in the presence or absence of ERK1/2 inhibitor (FR180204), MEK1/2 inhibitor (U0126), and NOX inhibitor (GKT136901). Panels (a)–(e) show effect of indicated treatment on total ROS levels (a), $n = 6$, mitochondrial ROS generation (b), $n = 6$, NO bioavailability (c), $n = 6$, peroxynitrite levels (d), $n = 6$, and cell proliferation (e), $n = 10$. $^{*}p < 0.05$, $^{**}p < 0.01$, and $^{***}p < 0.001$ calculated by one-way ANOVA followed by Fisher's LSD post hoc test versus control group or for indicated groups.

*Mapk2k1 (*genes encoding ERK1 and MEK1, respectively) remained unchanged (Figure 4(a)), suggesting that *de novo* transcription was not responsible for the elevated protein levels in activated cMVECs.

To address whether NOXs and transcription factors could be delivered to cMVECs with exosomes, we analyzed their presence in activated $CD4^+$ T cells and CD4-exosomes. Although NOX2 and NOX4 were found in $CD4^+$ T cells, they were not detected in the exosomes (Figure 4(c)). However, in contrast to NOXs, exosomes shed by $CD4^+$ T cells were rich in MEK1/2 and ERK1/2 (Figure 4(c)). Furthermore, the uptake of PKH26-stained CD4-exosomes by cMVECs was confirmed by fluorescence imaging (Figure 4(d)). These data suggest that activated $CD4^+$ T cells release MEK1/2 and ERK1/2 in exosomes, which can be taken up by cMVECs.

3.3. MEK/ERK Pathway Controls NOX4-Dependent Endothelial Dysfunction in Exosome-Activated cMVECs. In the next step, by using pharmacological inhibitors, we analyzed the contribution of NOXs and MEK-ERK pathways to regulate CD4-exosome-induced oxidative stress in cMVECs. We observed that NOX-1/4 inhibitor GKT136901 effectively blocked excessive ROS and superoxide production and reversed reduced NO levels triggered by CD4-exosomes (Figures 5(a)–5(c)). Inhibition of either MEK/ERK (with U0126) or ERK (with FR180204) also successfully protected cMVECs from increased ROS and reduced NO production and peroxynitrate levels but failed to suppress mitochondrial superoxide production in stimulated cells (Figures 5(a)–5(d)). Similarly, treatment with GKT136901 or U0126 reversed the enhanced proliferation of cMVECs triggered by CD4-exosomes (Figure 5(e)).

As expected, ERK but also p-ERK/ERK levels were downregulated in cells treated with U0126 or FR180204 (Figure 6). As shown above, CD4-exosomes induced NOX4 production in cMVECs. We found that treatment with U0126 or with FR180204 effectively reduced NOX4 (but not NOX2) protein levels in cMVECs exposed to CD4-exosomes (Figure 6). Of note, protein levels of the MEK/ERK pathway as well as of NOX2 and NOX4 upregulated by CD4-exosomes were maintained in cMVECs treated with GKT136901 (Figure 6). To confirm the key role of NOX4 in oxidative stress in our model, we silenced *Nox4* in cMVECs prior treatments with CD4-exosomes. Silencing resulted in nearly 50% reduced NOX4 protein level (Figure 7(a)). Cells with the reduced NOX4 were protected from CD4-exosome-

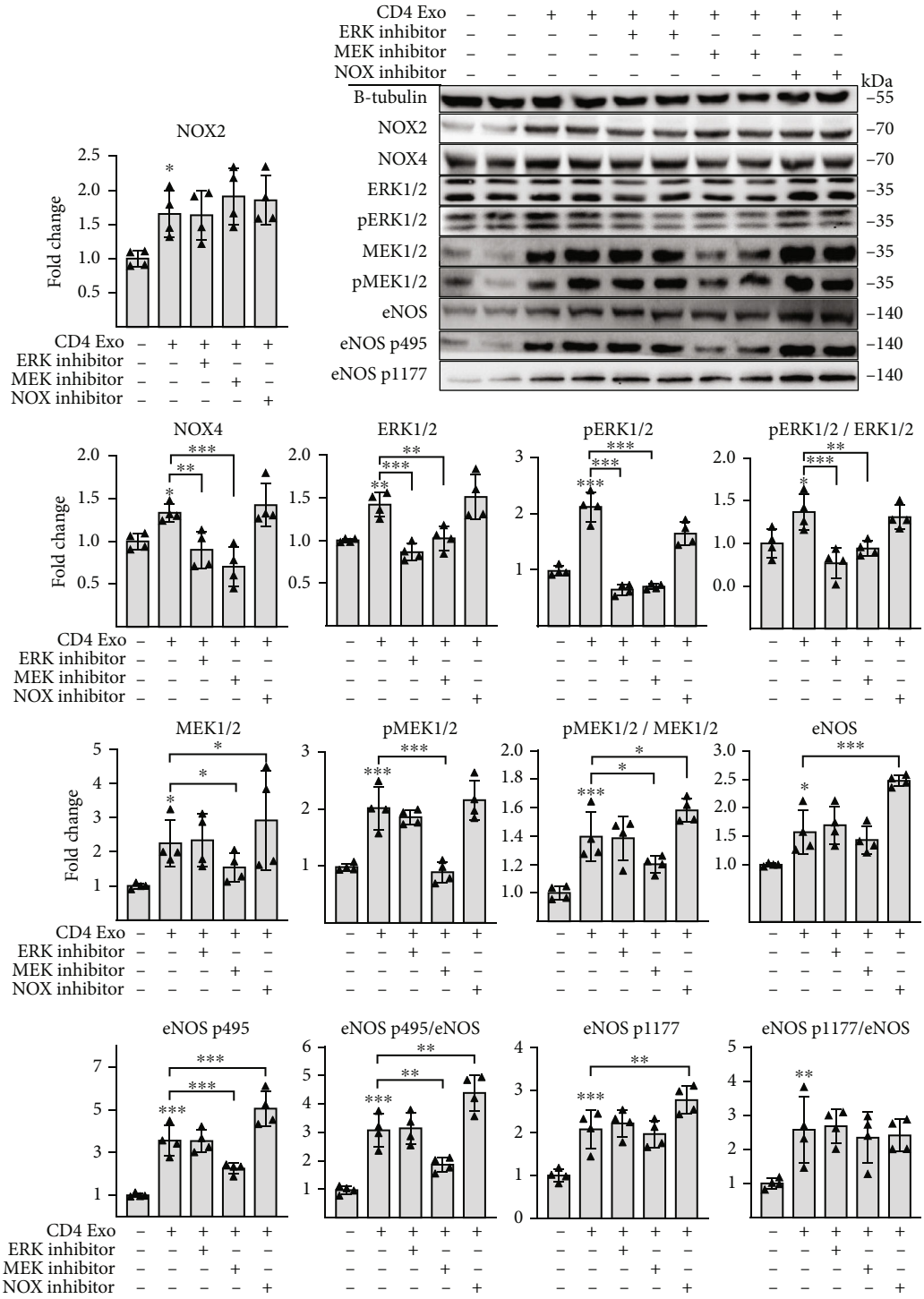

Figure 6: T cell-derived exosomes upregulate NOX4 in cMVECs through ERK1/2 and MEK1/2 pathway. This panel shows representative microphotographs of immunoblots and changes in levels of selected proteins in cMVECs in response to CD-4 exosomes in presence of ERK1/2 inhibitor (FR180204), MEK1/2 inhibitor (U0126), and NOX inhibitor (GKT136901). Cells were stimulated with exosomes for 16 h, $n = 4$. Protein levels were normalized to beta-tubulin, and phosphorylated proteins were additionally normalized to their respective nonphosphorylated forms. $^{*}p < 0.05$, $^{**}p < 0.01$, and $^{***}p < 0.001$ calculated by one-way ANOVA followed by Fisher's LSD post hoc test versus control group or for indicated groups.

induced oxidative stress and showed elevated NO levels (Figure 7(b)). Collectively, these data point to NOX4 as a key enzyme in oxidative stress caused by CD4-exosomes and to MEK/ERK as a regulatory pathway.

3.4. Inflamed Hearts Contain Oxidative Stress-Inducing Exosomes. In the next step, we analyzed whether cardiac inflammation is associated with generation of oxidative stress-inducing exosomes in vivo. Experimental

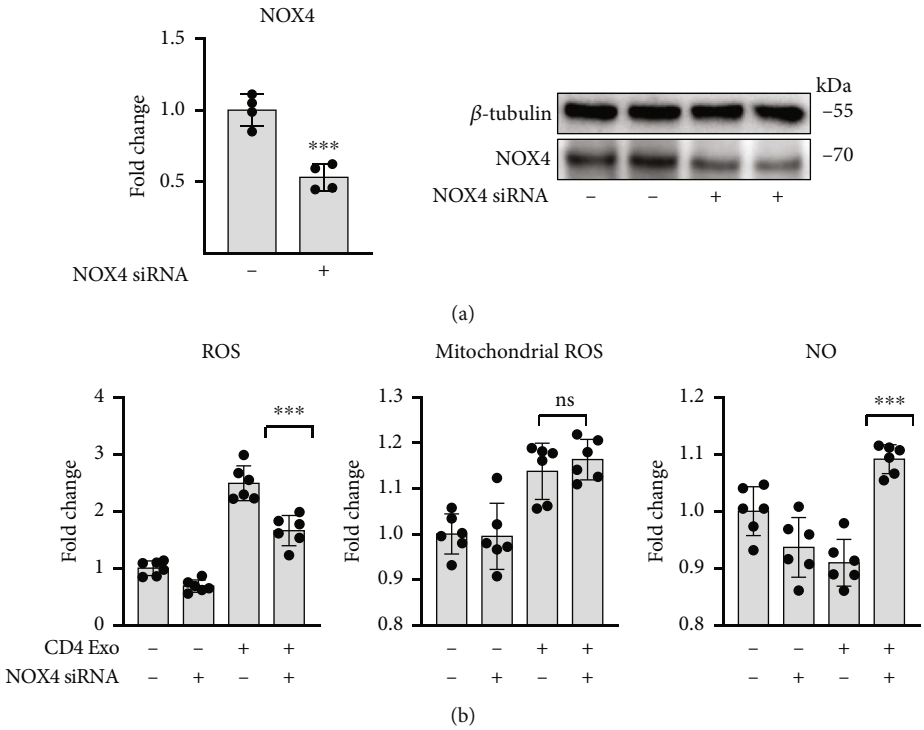

Figure 7: Oxidative stress caused by T cell-derived exosomes is mediated by NOX4. Panel (a) shows densitometry and representative immunoblots of cMVECs incubated with anti-*Nox4* siRNA for 36 h, $n = 4$. Panel (b) shows changes in total ROS, mitochondrial ROS, and NO levels in cMVECs transfected with anti-*Nox4* siRNA for 24 h and stimulated with CD4-exosomes for another 16 h, $n = 6$. ns-$p > 0.05$ and $^{***}p < 0.001$ calculated by Student's t-test in (a) and one-way ANOVA followed by Fisher's LSD post hoc test versus indicated groups in (b).

autoimmune myocarditis (EAM) represents a model of $CD4^+$ T cell-mediated cardiac inflammation, in which the heart is infiltrated with T lymphocytes during the acute inflammatory phase (d18-21, Figure 8(a)). We isolated exosomes from hearts of control and EAM groups at d19 (EAM-exosomes) and observed that inflammation was associated with an increased number of microvesicles in the cardiac tissue (Figure 8(b)). Treatment with exosomes (10^8 particles/ml) obtained from healthy hearts showed no effect on ROS, NO levels, and mitochondrial superoxide production in cMVECs. In contrast, EAM-exosomes (10^8 particles/ml) increased ROS and superoxide levels and reduced NO bioavailability in the treated cells, and these changes were reversed by apocynin (Figure 8(c)). Uptake of microvesicles isolated from EAM hearts by cMVECs was confirmed by fluorescence imaging (Figure 8(d)). In line with the CD4-exosome data, cMVECs treated with EAM-exosomes upregulated NOX2, NOX4, ERK1/2, MEK1/2, and eNOS protein levels (Figure 8(e)). Of note, this upregulation remained unaffected in the presence of apocynin, suggesting MEK/ERK activation, and the subsequent increase of NOXs was mediated by exosomes and independent of the induced oxidative stress in cMVECs.

4. Discussion

Secreted bioactive factors mediate mid- and long-distance cell-to-cell communication. Exosomes represent a specific class of signaling cues as they transport a mixture of proteins, nucleic acids, and other biomolecules [18]. Their cargo depends on the cell type they were shed off, and therefore, cell type-specific exosomes are expected to trigger unique responses. In this work, we specifically examined the role of exosomes shed by $CD4^+$ T cells in the activation of cMVECs. Involvement of $CD4^+$ T cells has been recognized in the pathogenesis of several cardiovascular diseases including atherosclerosis, myocardial infarction, and myocarditis [19–21]. It is well established that following activation of TCR, $CD4^+$ T cells secrete a number of proinflammatory cytokines such as TNF-α, IL-6, IL-17, and others, which upregulate adhesive molecules in endothelial cells leading to tissue inflammation [22]. Unlike cytokines, CD4-exosomes do not modulate adhesive properties of endothelial cells suggesting that they are not transporting proinflammatory agents. This was a surprising finding, as oxidative stress has been often implicated in upregulation of adhesion molecules in endothelial cells. Thus, increased ROS was expected to induce adhesive properties of cMVECs. We can only speculate that either CD4-exosomes negatively regulate proadhesive mechanisms or ROS induces adhesion in preactivated endothelial cells only. In fact, prooxidative agents typically show pleiotropic effects and coactivate multiple molecular pathways; therefore, the exact mechanism of ROS-induced adhesion requires further investigation and may not be the same for all conditions. In line with our findings, infiltration of leukocytes into tissue induces oxidative

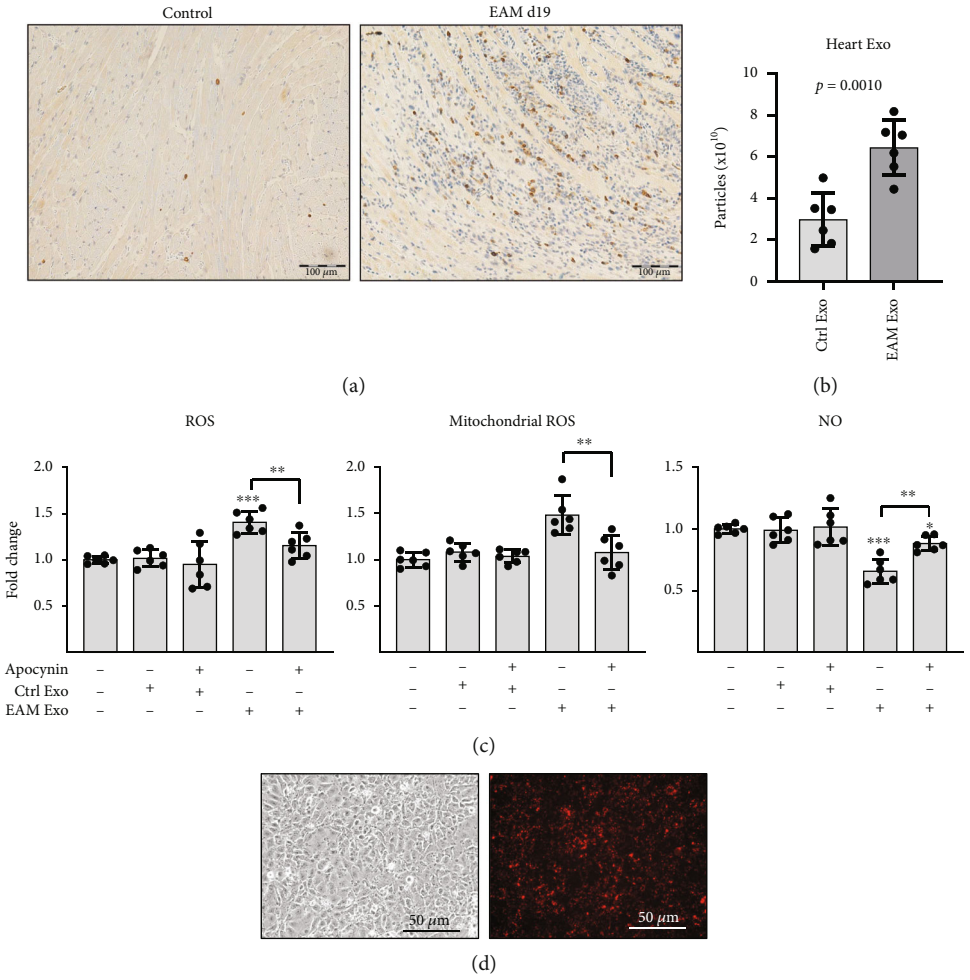

Figure 8: Continued.

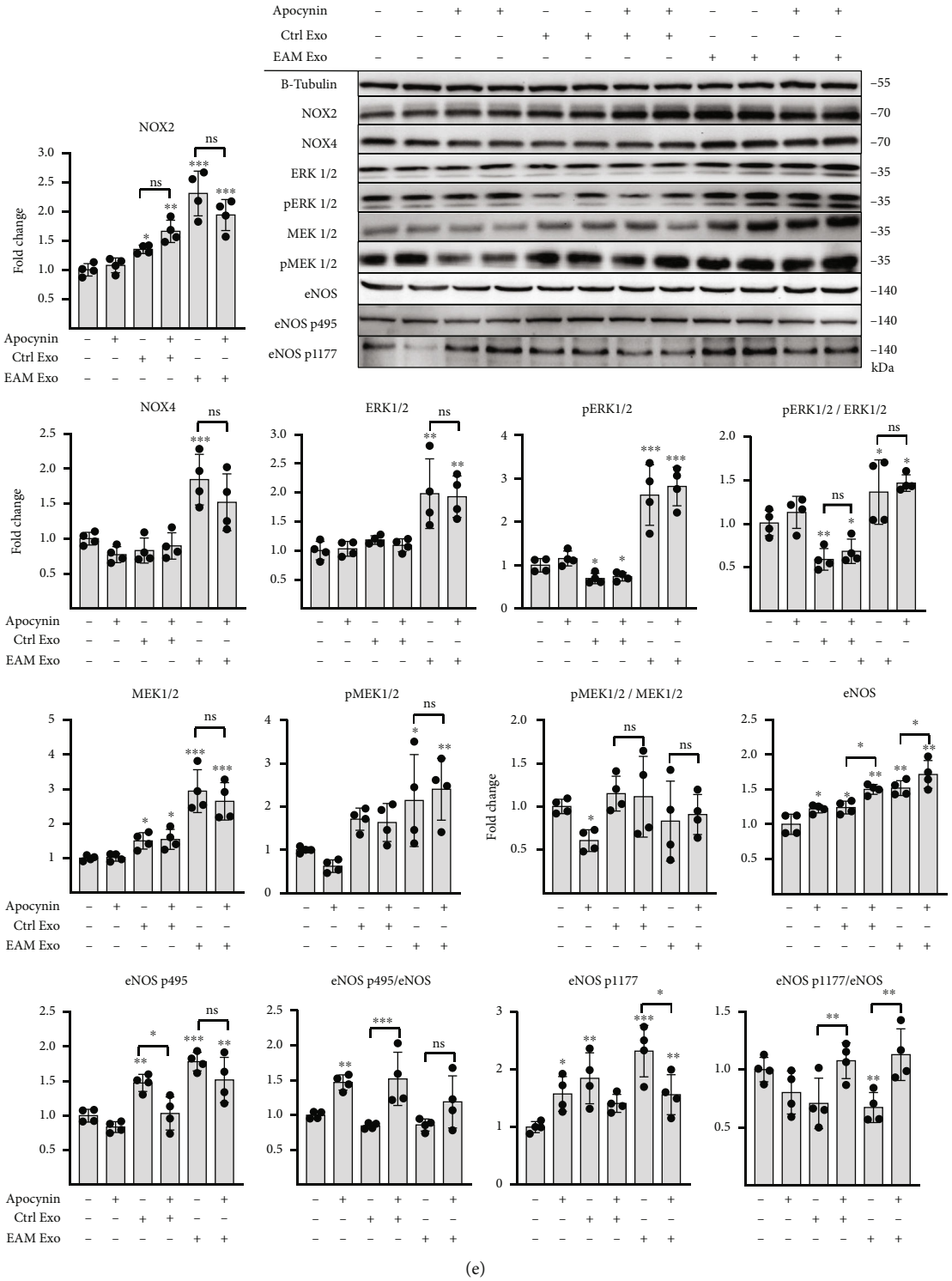

(e)

Figure 8: Exosomes isolated from inflamed hearts induce oxidative stress in cMVECs. Panel (a) shows representative microphotographs of CD3 staining in hearts of healthy controls and mice at day 19 of EAM. Scale bar = 100 μm. Panel (b) represents quantification of exosomes isolated from hearts of healthy mice (Ctrl Exo) and hearts of mice at day 19 of EAM (EAM Exo), $n = 6$. Panel (c) shows relative changes in levels of total ROS, mitochondrial ROS, and NO in cMVECs in response to 16 h of incubation with Ctrl Exo or EAM Exo in presence or absence of apocynin (Apo), $n = 6$. Panel (d) shows representative microphotographs of PKH26-stained exosomes (red) bound to cMVECs after 16 h of incubation. Representative immunoblots and quantification of selected proteins in cMVECs stimulated for 16 hours with exosomes obtained from healthy or inflamed hearts are presented in panel (e). Protein levels were normalized to beta tubulin, and phosphorylated proteins were additionally normalized to their respective nonphosphorylated forms, $n = 4$. $p > 0.05$, $^{*}p < 0.05$, $^{**}p < 0.01$, and $^{***}p < 0.001$ calculated by one-way ANOVA followed by Fisher's LSD post hoc test versus control group or for indicated groups.

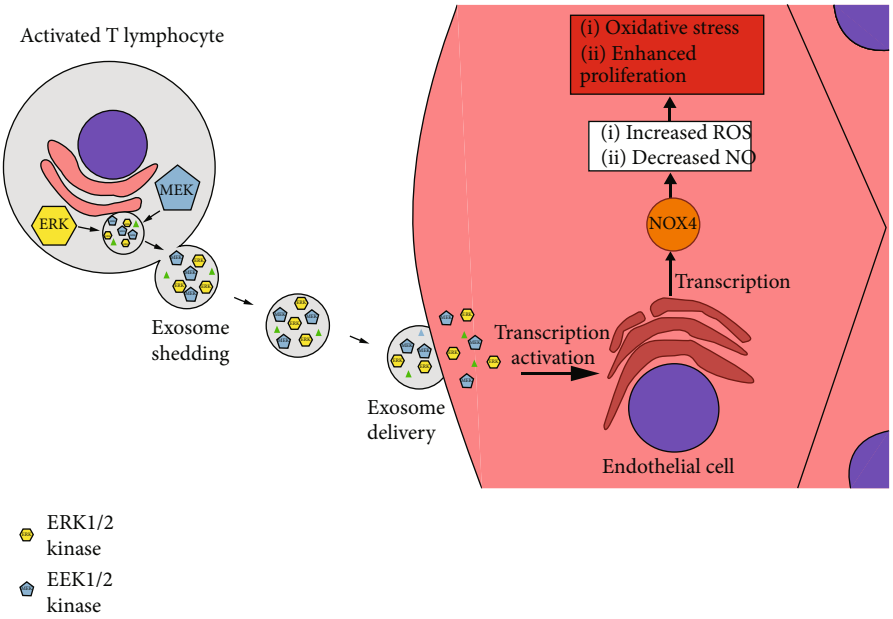

Figure 9: Schematic presentation of proposed mechanism. Activated T lymphocytes shed exosomes containing ERK1/2 and MEK1/2 kinases. These exosomes taken up by endothelial cells cause upregulation of NOX4 leading to oxidative stress and enhanced proliferation.

stress [23]. Our *in vitro* results suggest that not only the secretome but specifically the exosomes shed by activated $CD4^+$ T lymphocytes contribute to oxidative stress. Therefore, our results add exosomes to the list of bioactive factors secreted by $CD4^+$ T cells and highlight them as potential important deregulators of ROS/NO balance in the inflammatory response in the heart. A growing body of evidence indicates that exosomes can modulate oxidative stress in recipient cells. For example, macrophage-derived exosomes can increase ROS production in neurons [24], microparticles derived from ischemic muscles, and blood platelets from septic patients induce oxidative stress in endothelial cells by increasing NOX levels and their activity [25] [26],'. Furthermore, exosomes have been associated with oxidative stress in human diseases. Exosomes containing miR-137 are elevated in Parkinson's disease and have been shown to induce oxidative stress in neurons [27]. Similarly, the serum of HIV infected patients is enriched in exosomes that carry proteins involved in oxidative stress and immune activation [28]. Importantly, not all types of exosomes induce oxidative stress. Published data demonstrate that exosomes derived from mesenchymal stem cells ameliorate ROS and inflammatory response [29–31]. Similarly, microvesicles derived of an activated T cell line were shown to protect human umbilical vein endothelial cells from actinomycin D-induced apoptosis by ameliorating ROS production [32].

Exosomes can either up- or downregulate oxidative stress; therefore, it seems that their molecular cargo determines the ultimate effect in the recipient cell. In the case of $CD4^+$ T cell-derived exosomes, we found no evidence for the presence of NOX2 and NOX4 in exosomes despite the presence of these enzymes in the activated $CD4^+$ T cells. These data suggest a highly selective accumulation of cytoplasmic content into exosomes in $CD4^+$ T cells. Unlike T lymphocytes, macrophage-derived exosomes were reported to contain functional NOX2 [24]. Instead, we detected ERK1/2 and MEK1/2 in exosomes, and these transcription factors are known to control NOXs levels in endothelial cells [33, 34]. As $CD4^+$ T cell-derived exosomes transport ERK1/2 and MEK1/2 but not NOXs, we suggest that endothelial cells take up ERK1/2- and MEK1/2-rich exosomes and thereby increase their intracellular ERK1/2 and MEK1/2 levels. This leads to transcriptional upregulation of *Nox*s and eventually to oxidative stress (Figure 9). Consistent with this hypothesis, we observed a relatively quick (2 h after treatment with exosomes) increase in intracellular ERK1/2 and MEK1/2 protein levels, while the corresponding mRNAs remained unchanged. However, we cannot exclude an alternative mechanism that upregulates ERK1/2 and MEK1/2 in our experimental model.

Experiments with ERK1/2 and MEK1/2 inhibitors showed that the MEK-ERK pathway controlled ROS and mediated upregulation of specifically NOX4 and *Nox4* silencing confirmed the key role of this enzyme in exosome-induced oxidative stress. In the cardiovascular system, NOX4 generates superoxide constitutively, whereas NOX2 is an inducible enzyme [35]. It seems that NOX4 represents the most important NOX isoform in endothelial cells. In line with our findings, the expression of NOX4 in cardiomyocytes involved in mediating oxidative stress is responsible for the impairment of cardiac functions in a pressure overload model [35]. In endothelial cells, NOX4 appears to positively regulate functions related to angiogenesis. Increased levels of this enzyme promote proliferation, migration, and angiogenesis, which are connected to activation of ERK1/2 pathway [36].

Oxidative stress induced by exosomes enhanced mitochondrial ROS production, reduced NO bioavailability, and triggered proliferation of endothelial cells. It seems that elevated ROS levels due to upregulated NOXs affected normal

mitochondrial metabolism and triggered mitochondrial ROS production. Such oxidative stress positive feedback mechanism is known as ROS-induced ROS release and has been described in endothelial cells [37]. Our data did not indicate the key involvement of NOX4 in mitochondrial ROS production; therefore, this process might be linked with NOX2 activity as described previously [38]. Elevated NOX2 levels were shown to be associated with increased antioxidant enzyme and eNOS protein levels. NOX2 was also shown to regulate the hemodynamic response to angiotensin II leading to endothelial dysfunction and increased mitochondrial ROS generation in aortic cells [39, 40]. ROS generation in mitochondria was originally thought to be a toxic byproduct of ATP synthesis, whereas more recent views point to mitochondrial ROS as important signal transducers in regulating endothelial metabolism [41]. Nevertheless, a prolonged increment of ROS generation above basal levels can be detrimental and underlie the development of endothelial dysfunction, and atherosclerosis and cause hyperglycaemic damage [42, 43]. NO acts as a reversible inhibitor of the respiratory chain limiting mitochondrial activity and thus regulates respiration and ROS generation. In case of elevated systemic oxidative stress, NO reacts with excessive ROS forming peroxynitrite that irreversibly blocks multiple elements of the respiratory chain [44, 45]. Obtained data indicated that in our model, NO level was regulated by NOX4 and preserved by the addition of antioxidant apocynin. This suggests that CD4-exosomes trigger a reaction of NO with NOX4-derived superoxide radical and thereby reduce NO bioavailability in cMVECs. However, despite of increased ROS production, measured peroxynitrite levels in cMVECs were low. This unexpected result could be explained by enhanced processes utilizing peroxynitrite as a substrate, like SOD- or myeloperoxidase-dependent tyrosine nitration, or by enhanced peroxynitrite decomposition [46].

Cell damage is known to trigger apoptosis-induced compensatory proliferation, serving as a mechanism to maintain homeostasis during tissue regeneration [47]. Increased oxidative stress fuels this process through NOX-derived ROS, which activate pathways responsible for the proliferation [48]. In line with our data, in human dermal microvascular endothelial cells, NOX4- but not NOX2-derived ROS were shown to promote proliferation via ERK1/2 pathway [49].

Despite a straightforward effect in vitro, the actual contribution of $CD4^+$ T cell-derived exosomes to endothelial dysfunction in vivo remains unclear. Currently, there are no available tools to specifically block exosome shedding or to modulate exosomal cargo in vivo to prove their impact on disease. Nevertheless, our findings could confirm the presence of pathogenic exosomes in inflamed hearts containing inflammatory $CD4^+$ T lymphocytes; although, it should be acknowledged that these exosomes were not exclusively derived from $CD4^+$ T cells. However, taking into account that myocarditis is associated with coronary microvascular dysfunction [50], exosomes produced by heart inflammatory cells should be considered as potential triggers of this pathogenic vascular condition. Furthermore, we believe that $CD4^+$ T cell-derived exosomes could potentially contribute to the pathogenesis of other vascular diseases. For example, atherosclerosis represents a chronic inflammatory disease of arterial walls with the involvement of $CD4^+$ T cells [19], and exosomes shed locally by these cells could exaggerate oxidative stress and promote endothelial dysfunction. However, more research is still needed to verify this hypothesis.

In conclusion, in this work, we identified exosomes as potentially important mediators in $CD4^+$ T cell-dependent immune response, which can induce oxidative stress by delivering transcription factors. Specific neutralization of exosomal cargo might prevent from the induction of self-fuelling oxidative stress and endothelial dysfunction. Thus, the identification of a novel mechanism of intercellular communication opens up perspectives for the development of new therapeutic strategies for inflammatory cardiovascular diseases.

Data Availability

The data used to support the findings of this study are available from the corresponding author upon reasonable request.

Conflicts of Interest

The authors declare that they have no conflicts of interest.

Acknowledgments

This work has been supported by the National Science Centre (Poland), grant 2016/21/B/NZ5/01397.

Supplementary Materials

Supplementary figure 1: Effect of medium conditioned of activated $CD4^+$ T lymphocytes and exosomes derived of resting $CD4^+$ T lymphocytes on activation and oxidative stress in cMVECs. Panel (a) shows changes in membrane levels of adhesion molecules VCAM-1, ICAM-1, and p-selectin in cMVECs stimulated with medium conditioned of activated T lymphocytes (CM) or exosomes shed by resting $CD4^+$ T lymphocytes (1×10^8 particles/ml, rCD4 Exo) for 16 h, $n = 6$. In panel (b), influence of MVEC stimulation with CM or rCD4 Exo for 16 h on levels of total reactive oxygen species (total ROS), mitochondrial activity (mitochondrial ROS), and nitric oxide generation (NO) is shown, $n = 6$. $^{***}p < 0.001$ calculated by one-way ANOVA followed by Fisher's LSD post hoc test versus control group. *(Supplementary Materials)*

References

[1] A. D. Lopez and T. Adair, "Is the long-term decline in cardiovascular-disease mortality in high-income countries over? Evidence from national vital statistics," *International Journal of Epidemiology*, vol. 48, no. 6, pp. 1815–1823, 2019.

[2] M. A. Incalza, R. D'Oria, A. Natalicchio, S. Perrini, L. Laviola, and F. Giorgino, "Oxidative stress and reactive oxygen species in endothelial dysfunction associated with cardiovascular and metabolic diseases," *Vascular Pharmacology*, vol. 100, pp. 1–19, 2018.

[3] P. G. Camici, G. D'Amati, and O. Rimoldi, "Coronary microvascular dysfunction: Mechanisms and functional assessment," *Nature Reviews Cardiology*, vol. 12, pp. 48–62, 2015.

[4] E. Gavriilaki, P. Anyfanti, M. Gavriilaki, A. Lazaridis, S. Douma, and E. Gkaliagkousi, "Endothelial Dysfunction in COVID-19: Lessons Learned from Coronaviruses," *Current Hypertension Reports*, vol. 22, no. 9, 2020.

[5] D. Konukoglu and H. Uzun, "Endothelial Dysfunction and Hypertension," *Advances in Experimental Medicine and Biology*, vol. 956, pp. 511–540, 2016.

[6] F. Fleissner and T. Thum, "Critical role of the nitric oxide/reactive oxygen species balance in endothelial progenitor dysfunction," *Antioxidants & Redox Signaling*, vol. 15, no. 4, pp. 933–948, 2011.

[7] L. Krishnamoorthy and C. J. Chang, "Exosomal NADPH Oxidase: Delivering Redox Signaling for Healing," *Biochemistry*, vol. 57, no. 27, pp. 3993-3994, 2018.

[8] J. Tejero, S. Shiva, and M. T. Gladwin, "Sources of vascular nitric oxide and reactive oxygen species and their regulation," *Physiological Reviews*, vol. 99, no. 1, pp. 311–379, 2019.

[9] G. A. Knock, "NADPH oxidase in the vasculature: expression, regulation and signalling pathways; role in normal cardiovascular physiology and its dysregulation in hypertension," *Free Radical Biology and Medicine*, vol. 145, pp. 385–427, 2019.

[10] L. Zhou, M. M. W. Chong, and D. R. Littman, "Plasticity of CD4+ T cell lineage differentiation," *Immunity*, vol. 30, no. 5, pp. 646–655, 2009.

[11] R. Xu, D. W. Greening, H. J. Zhu, N. Takahashi, and R. J. Simpson, "Extracellular vesicle isolation and characterization: Toward clinical application," *Journal of Clinical Investigation*, vol. 126, no. 4, pp. 1152–1162, 2016.

[12] E. Działo, M. Rudnik, R. I. Koning et al., "WNT3a and WNT5a transported by exosomes activate WNT signaling pathways in human cardiac fibroblasts," *International Journal of Molecular Sciences*, vol. 20, no. 6, p. 1436, 2019.

[13] K. Tkacz, F. Rolski, M. Czepiel et al., "Haploinsufficient rock 1 +/- and rock 2+/- mice are not protected from cardiac inflammation and postinflammatory fibrosis in experimental autoimmune myocarditis," *Cells*, vol. 9, no. 3, p. 700, 2020.

[14] M. Zarak-Crnkovic, G. Kania, A. Jaźwa-Kusior et al., "Heart non-specific effector CD4+ T cells protect from postinflammatory fibrosis and cardiac dysfunction in experimental autoimmune *myocarditis*," *Basic Research in Cardiology*, vol. 115, no. 1, p. 115, 2020.

[15] M. Vejražka, R. Míček, and S. Štípek, "Apocynin inhibits NADPH oxidase in phagocytes but stimulates ROS production in non-phagocytic cells," *Biochimica et Biophysica Acta (BBA) - General Subjects*, vol. 1722, no. 2, pp. 143–147, 2005.

[16] S. Heumüller, S. Wind, E. Barbosa-Sicard et al., "Apocynin is not an inhibitor of vascular NADPH oxidases but an antioxidant," *Hypertension*, vol. 51, no. 2, pp. 211–217, 2008.

[17] S. R. Kim, Y. H. Bae, S. K. Bae et al., "Visfatin enhances ICAM-1 and VCAM-1 expression through ROS-dependent NF-κB activation in endothelial cells," *Biochimica et Biophysica Acta (BBA) - Molecular Cell Research*, vol. 1783, no. 5, pp. 886–895, 2008.

[18] D. M. Pegtel and S. J. Gould, "Exosomes," *Annual Review of Biochemistry*, vol. 88, no. 1, pp. 487–514, 2019.

[19] R. Saigusa, H. Winkels, and K. Ley, "T cell subsets and functions in atherosclerosis," *Nature Reviews Cardiology*, vol. 17, no. 7, pp. 387–401, 2020.

[20] K. Tse, H. Tse, J. Sidney, A. Sette, and K. Ley, "T cells in atherosclerosis," *International Immunology*, vol. 25, no. 11, pp. 615–622, 2013.

[21] P. L. Schwimmbeck, C. Badorff, G. Rohn, K. Schulze, and H. P. Schultheiss, "The role of sensitized T-cells in myocarditis and dilated cardiomyopathy," *International Journal of Cardiology*, vol. 54, no. 2, pp. 117–125, 1996.

[22] L. Cosmi, L. Maggi, V. Santarlasci, F. Liotta, and F. Annunziato, "*T helper cells plasticity in inflammation*," *Cytometry Part A*, vol. 85, no. 1, pp. 36–42, 2014.

[23] C. de Miguel, C. Guo, H. Lund, D. Feng, and D. L. Mattson, "Infiltrating T lymphocytes in the kidney increase oxidative stress and participate in the development of hypertension and renal disease," *American Journal of Physiology-Renal Physiology*, vol. 300, no. 3, pp. F734–F742, 2011.

[24] A. Hervera, F. De Virgiliis, I. Palmisano et al., "Reactive oxygen species regulate axonal regeneration through the release of exosomal NADPH oxidase 2 complexes into injured axons," *Nature Cell Biology*, vol. 20, no. 3, pp. 307–319, 2018.

[25] A. S. Leroyer, T. G. Ebrahimian, C. Cochain et al., "Microparticles from ischemic muscle promotes postnatal vasculogenesis," *Circulation*, vol. 119, no. 21, pp. 2808–2817, 2009.

[26] M. Janiszewski, C. A. O. Do, M. A. Pedro, E. Silva, E. Knobel, and F. R. M. Laurindo, "Platelet-derived exosomes of septic individuals possess proapoptotic NAD(P) H oxidase activity: a novel vascular redox pathway," *Critical Care Medicine*, vol. 32, no. 3, pp. 818–825, 2004.

[27] Y. Jiang, J. Liu, L. Chen et al., "Serum secreted miR-137-containing exosomes affects oxidative stress of neurons by regulating OXR1 in Parkinson's disease," *Brain Research*, vol. 1722, article 146331, 2019.

[28] S. Chettimada, D. R. Lorenz, V. Misra et al., "Exosome markers associated with immune activation and oxidative stress in HIV patients on antiretroviral therapy," *Scientific Reports*, vol. 8, no. 1, 2018.

[29] F. Arslan, R. C. Lai, M. B. Smeets et al., "Mesenchymal stem cell-derived exosomes increase ATP levels, decrease oxidative stress and activate PI3K/Akt pathway to enhance myocardial viability and prevent adverse remodeling after myocardial ischemia/reperfusion injury," *Stem Cell Research*, vol. 10, no. 3, pp. 301–312, 2013.

[30] T. Wang, Z. Jian, A. Baskys et al., "MSC-derived exosomes protect against oxidative stress-induced skin injury _via_ adaptive regulation of the NRF2 defense system," *Biomaterials*, vol. 257, article 120264, 2020.

[31] C. R. Harrell, N. Jovicic, V. Djonov, N. Arsenijevic, and V. Volarevic, "Mesenchymal Stem Cell-Derived Exosomes and Other Extracellular Vesicles as New Remedies in the Therapy of Inflammatory Diseases," *Cells*, vol. 8, no. 12, article 1605, 2019.

[32] R. Soleti, E. Lauret, R. Andriantsitohaina, and M. M. Carmen, "Internalization and induction of antioxidant messages by microvesicles contribute to the antiapoptotic effects on human endothelial cells," *Free Radical Biology and Medicine*, vol. 53, no. 11, pp. 2159–2170, 2012.

[33] N. Azouzi, J. Cailloux, J. M. Cazarin et al., "NADPH oxidase NOX4 is a critical mediator of BRAFV600E-induced downregulation of the sodium/iodide symporter in papillary thyroid Carcinomas," *Antioxidants & Redox Signaling*, vol. 26, no. 15, pp. 864–877, 2017.

[34] N. Y. Hakami, H. Wong, M. H. Shah, G. J. Dusting, F. Jiang, and H. M. Peshavariya, "Smad-independent pathway involved in transforming growth factor β1-induced Nox4 expression and proliferation of endothelial cells," *Naunyn-Schmiedeberg's Archives of Pharmacology*, vol. 388, no. 3, pp. 319–326, 2015.

[35] J. Kuroda, T. Ago, S. Matsushima, P. Zhai, M. D. Schneider, and J. Sadoshima, "NADPH oxidase 4 (Nox4) is a major source of oxidative stress in the failing heart," *Proceedings of the National Academy of Sciences*, vol. 107, no. 35, pp. 15565–15570, 2010.

[36] S. R. Datla, H. Peshavariya, G. J. Dusting, K. Mahadev, B. J. Goldstein, and F. Jiang, "Important role of Nox4 type NADPH oxidase in angiogenic responses in human microvascular endothelial cells in vitro," *Arteriosclerosis, Thrombosis, and Vascular Biology*, vol. 27, no. 11, pp. 2319–2324, 2007.

[37] E. Shafique, A. Torina, K. Reichert et al., "Mitochondrial redox plays a critical role in the paradoxical effects of NAPDH oxidase-derived ROS on coronary endothelium," *Cardiovascular Research*, vol. 113, no. 2, pp. 234–246, 2017.

[38] S. I. Dikalov, R. R. Nazarewicz, A. Bikineyeva et al., "Nox2-induced production of mitochondrial superoxide in angiotensin ii-mediated endothelial oxidative stress and hypertension," *Antioxidants & Redox Signaling*, vol. 20, no. 2, pp. 281–294, 2014.

[39] J. K. Bendall, R. Rinze, D. Adlam, A. L. Tatham, J. De Bono, and K. M. Channon, "Endothelial Nox2 overexpression potentiates vascular oxidative stress and hemodynamic response to angiotensin II," *Circulation Research*, vol. 100, no. 7, pp. 1016–1025, 2007.

[40] C. E. Murdoch, S. P. Alom-Ruiz, M. Wang et al., "Role of endothelial Nox2 NADPH oxidase in angiotensin II-induced hypertension and vasomotor dysfunction," *Basic Research in Cardiology*, vol. 106, no. 4, pp. 527–538, 2011.

[41] M. E. Widlansky and D. D. Gutterman, "Regulation of endothelial function by mitochondrial reactive oxygen species," *Antioxidants & Redox Signaling*, vol. 15, no. 6, pp. 1517–1530, 2011.

[42] M. G. Scioli, G. Storti, F. D'amico et al., "Oxidative stress and new pathogenetic mechanisms in endothelial dysfunction: potential diagnostic biomarkers and therapeutic targets," *Journal of Clinical Medicine*, vol. 9, no. 6, p. 1995, 2020.

[43] F. Cheng, J. Lan, W. Xia et al., "Folic acid attenuates vascular endothelial cell injury caused by hypoxia via the inhibition of ERK1/2/NOX4/ROS pathway," *Cell Biochemistry and Biophysics*, vol. 74, no. 2, pp. 205–211, 2016.

[44] J. D. Erusalimsky and S. Moncada, "Nitric oxide and mitochondrial signaling," *Arteriosclerosis, Thrombosis, and Vascular Biology*, vol. 27, no. 12, pp. 2524–2531, 2007.

[45] P. Pacher, J. S. Beckman, and L. Liaudet, "Nitric oxide and peroxynitrite in health and disease," *Physiological Reviews*, vol. 87, no. 1, pp. 315–424, 2007.

[46] S. Bartesaghi and R. Radi, "Fundamentals on the biochemistry of peroxynitrite and protein tyrosine nitration," *Redox Biology*, vol. 14, pp. 618–625, 2018.

[47] N. Diwanji and A. Bergmann, "An unexpected friend – ROS in apoptosis-induced compensatory proliferation: implications for regeneration and cancer," *Seminars in Cell & Developmental Biology*, vol. 80, pp. 74–82, 2018.

[48] P. S. Hole, J. Zabkiewicz, C. Munje et al., "Overproduction of NOX-derived ROS in AML promotes proliferation and is associated with defective oxidative stress signaling," *Blood*, vol. 122, no. 19, pp. 3322–3330, 2013.

[49] H. Peshavariya, G. J. Dusting, F. Jiang et al., "NADPH oxidase isoform selective regulation of endothelial cell proliferation and survival," *Naunyn-Schmiedeberg's Archives of Pharmacology*, vol. 380, no. 2, pp. 193–204, 2009.

[50] A. Saraste, V. Kytö, M. Saraste, T. Vuorinen, J. Hartiala, and P. Saukko, "Coronary flow reserve and heart failure in experimental coxsackievirus myocarditis. A transthoracic Doppler echocardiography study," *American Journal of Physiology-Heart and Circulatory Physiology*, vol. 291, no. 2, pp. H871–H875, 2006.

Hindawi
Oxidative Medicine and Cellular Longevity
Volume 2022, Article ID 8133310, 23 pages
https://doi.org/10.1155/2022/8133310

Research Article

The Role of *Aeromonas*-Goblet Cell Interactions in Melatonin-Mediated Improvements in Sleep Deprivation-Induced Colitis

Ting Gao,[1] Zixu Wang,[1] Jing Cao,[1] Yulan Dong,[1] and Yaoxing Chen [1,2]

[1]*College of Veterinary Medicine, China Agricultural University, Haidian, Beijing 100193, China*
[2]*Department of Nutrition and Health, China Agricultural University, Haidian, Beijing 100193, China*

Correspondence should be addressed to Yaoxing Chen; yxchen@cau.edu.cn

Received 10 September 2021; Revised 26 January 2022; Accepted 17 February 2022; Published 20 March 2022

Academic Editor: Daniela Ribeiro

Background. Our previous studies demonstrated that melatonin could effectively ameliorate sleep deprivation- (SD-) caused oxidative stress-mediated gut microbiota disorder and colitis. The research further clarified the mechanism of melatonin in improving colitis from the perspective of the interaction between *Aeromonas* and goblet cells. *Methods*. A seventy-two hours SD mouse model with or without melatonin intervention and fecal microbiota transplantation (FMT) to explore the vital position of *Aeromonas*-goblet cell interactions in melatonin improving SD-induced colitis. Moreover, *Aeromonas* or LPS-supplied mice were assessed, and the influence of melatonin on *Aeromonas*-goblet cell interactions-mediated oxidative stress caused colitis. Furthermore, in vitro experiment investigated the regulation mechanism of melatonin.*Results*. Our study showed that SD induced colitis, with upregulation of *Aeromonas* and LPS levels and reductions in goblet cells number and MUC2 protein. Similarly, FMT from SD mice, *Aeromonas* veronii colonization, and LPS treatment restored the SD-like goblet cells number and MUC2 protein decrease and colitis. Moreover, LPS treatment downregulated the colonic antioxidant capacity. Yet, melatonin intervention reversed all consequence in SD, *A*.veronii colonization, and LPS-treated mice. In vitro, melatonin reversed *A*. veronii- or LPS-induced MUC2 depletion in mucus-secreting human HT-29 cells via increasing the expression level of Villin, Tff3, p-GSK-3β, β-catenin, and melatonin receptor 2 (MT2) and decreasing the level of p-IκB, p-P65, ROS, TLR4, and MyD88 proteins, while the improvement effect was blocked with pretreatment with a MT2 antagonist but were mimicked by TLR4 and GSK-3β antagonists and ROS scavengers. *Conclusions*. Our results demonstrated that melatonin-mediated MT2 inhibits *Aeromonas*-goblet cell interactions to restore the level of MUC2 production via LPS/TLR4/MyD88/GSK-3β/ROS/NF-κB loop, further improving colitis in SD mice.

1. Introduction

Sleep has a vital effect on the homeostasis of gastrointestinal mucosal barriers and intestinal microbiota [1, 2]. Insufficient sleep is closely related to lots of adverse outcomes, including higher risk of cardiovascular disease, diabetes mellitus, coronary heart disease, hypertension [3], and inflammatory bowel disease (IBD) [4]. In fact, some researches have indicated that sleep disorders may disrupt the immune homeostasis in the intestines, further inducing inflammatory response, and resulting in the occurrence of IBD [4]. Conversely, IBD patients also suffer from poor sleep quality and markedly prolonged sleep latency, as well as frequently sleep fragmentation [5], which highlights the closely correlation between IBD and sleep deficiency.

The intestinal homeostasis relies on closely regulated cross-talk between the mucosal immune, intestinal microbiota, and intestinal epithelial cells (IECs) [6]. Mucus layer damage accelerates intestinal epithelium-pathogen interactions and the pathogen invasion [7]. O-glycosylated mucin (MUC)2, produced by goblet cells, constitutes the major component of the intestinal mucus layer of the rodents' intestines and is a mechanical barrier by forming a huge network of mucus polymer barrier [8]. Importantly, the reduction of MUC2 content and goblet cells number means a thinner mucus layer, which is closely related to IBD [9].

Considering that mucin has a positive effect on offering protection resist the multiple inflammation caused by toxins and invading pathogenic bacteria, it is vital to distinguish the elements that regulate MUC2 gene expression exposed to insufficient sleep [10–12].

Melatonin (N-acetyl-5-methoxytryptamine, MT), synthesized from tryptophan, often used to regulate sleep. MT can regulate a series of molecular process, such as circadian rhythms, sleep control, immune pathway, oxidative stress, apoptosis, and autophagy [13]. Moreover, MT is a neurotransmitter among intestinal hormones, and it affects physiological functions of the gastrointestinal tract (GI), including bicarbonate secretion, motility, permeability, energy utilization, and tight junction proteins in intestines [14]. Specifically, consider that mucin influences the abundance of intestinal microbiota [15] and that some microbiota treats glycan as a nutrient [16, 17], bacteria modulation via melatonin may be due to goblet cells differentiation-mediated mucin regulation. Therefore, MT is expected to treat a variety of GI diseases, such as necrotizing enterocolitis, ischemic injuries, and IBD [13]. However, it remains unknown whether MT mediated the regulation of MUC2 synthesis and secretion improves IBD in response to SD. Thus, we aim to determine the influence of SD on MUC2 depletion and the roles of MT using a continuous 72 h SD mouse model and *Aeromonas* veronii or LPS-treated mucus-secreting human HT-29 cells.

2. Materials and Methods

All experiments were operated which subject to the Guide for the Care and Use of Laboratory Animals published by the Animal Welfare Committee of the Agricultural Research Organization, China Agricultural University (Approval No. CAU20170911-2).

2.1. Animal Model Establishment. 168 male ICR mice (eight weeks old; Vital River Laboratory Animal Technology Co. Ltd., Beijing, China) were fed in 28 cages (six mice/cage) in general environments (temperature: 21 ± 1°C, relative humidity: 50 ± 10%) with a regular 10 h dark: 14 h light cycle (lights on at 7 : 00 am.). The mice eat and drink freely. One week acclimatization later, the mice were casually distributed to 14 groups and used to carry out four experiments: the sleep deprivation experiment: sleep deprivation (SD), SD + melatonin supplementation (SD + MT), and nonsleep-deprived control (CON) groups, the ZT time of day that SD started and MT administration were previously described by Gao et al. and Zhang et al.; [18, 19]; fecal microbiota transplantation (FMT) experiment: F-CON, F-SD, F – SD + MT (F-SM), and F-R group, FMT was performed via oral gavage of a feces into wild mice as described Stebegg et al.; [20] *Aeromonas* veronii colonization experiment: C-CON, C-*Aeromonas* (C-A), and C – *Aeromonas* + MT (C-AM) groups; and LPS experiment: LPS, LPS + melatonin supplementation (LPS + MT), LPS + TAK – 242 supplementation (LPS + TAK – 242), and non-LPS control (CON) groups.

Table 1: DAI score evaluation.

Weight loss	Score	Blood in stool	Score	Stool consistency	Score
<1%	0	Absence	0	Normal	0
1-5%	1		1	Soft stools	1
5-10%	2	Slight bleeding	2	Loose stools	2
10-15%	3		3	Mild diarrhea	3
>15%	4	Gross bleeding	4	Watery diarrhea	4

Colitis was evaluated daily based on the overall rating of body weight, stool consistency, and fecal occult blood to count the disease activity index (DAI), which indicated in Table 1. The scoring range for DAI scores is 0-4, as previously recorded by Murthy et al. [21]. Specific study design is supplied in the Supplementary Material.

2.2. Fecal Occult Blood Test. Specific study design is supplied in the Supplementary Material. The judgment criterion is negative: (-) there is no rose red or cherry red after 3 minutes; positive: (+) rose red or cherry red appears within 30-60 s; strong positive: (++) rose red or cherry red appears immediately; and the strongest positive: (+++) a deep rose red or deep cherry red appears immediately.

2.3. Intestinal Permeability to Fluorescein Isothiocyanate-(FITC-) Dextran. Two hours before the end of the experiment (6 : 00 am), all mice were given oral administration of 0.6 mg/g body weight of 4-kDa FITC-dextran at a concentration of 80 mg/mL and fasted for 2 hours. Euthanasia was subsequently carried out. Blood was collected by retroorbital ocular hemorrhage and centrifuged (500 × *g*, 10 minutes) to collect serum. A fluorescence spectrophotometer with emission at 535 nm and excitation at 485 nm was used to calculate the fluorescence value in the serum. Create a standard curve via diluting FITC-dextran within PBS using a standard curve to calculate the content of FITC-dextran of the serum.

2.4. Histological Staining. Specific study design is supplied in the Supplementary Material. The scoring criteria are (I) 0: no obvious inflammation; (II) 2: low-grade inflammation, scattered infiltrating monocytes (1~2 lesions); (III) 4: multifocal lighter inflammation; (IV) 6: high level of inflammatory response and upregulated blood vessel density, as well as obvious thickening of the wall; and (V) 8: the most severe inflammation, accompanied by transmural leukocyte infiltration.

2.5. Immunohistochemical Staining. Using immunohistochemistry to stain for MUC2 in paraffin intestinal sections, tissues were infiltrated overnight at 4°C in the monoclonal rabbit anti-mouse primary antibody (MUC2, 1 : 500; TLR4, 1 : 200; Abcam, Cambridge, MA, USA). Specific operation is supplied in the Supplementary Material.

2.6. Enzyme-Linked Immunosorbent Assay (ELISA). A competitive ELISA assay (Uscn Life Science, Inc., Wuhan, China) was used to assess the inflammatory factors (IL-10,

Table 2: Primers of target genes and reference gene.

Gene	Sense	Antisense
MyD88	CCTGCGGTTCATCACTAT	GGCTCCGCATCAGTCT
MUC2	CTGCACCAAGACCGTCCTCATG	GCAAGGACTGAACAAAGACTCAGAC
Tff3	GGCTGCTGCTTTGACTC	AGCCTGGACAGCTTCAA
Villin	TCGGCCTCCAGTATGTAG	CGTCTTCGGGGTAGAACT
GAPDH	CCGAGAATGGGAAGCTTGTC	TTCTCGTGGTTCACACCCATC
Firmicutes	GGAGCATGTGGTTTAATTCGAAGCA	AGCTGACGACAACCATGCAC
Bacteroidetes	GAGAGGAAGGTCCCCCAC	CGCTACTTGGCTGGTTCAG
Proteobacteria	GGTTCTGAGAGGAGGTCCC	GCTGGCTCCCGTAGGAGT
Aeromonas	AGAGTTTGATCCTGGCTCAG	GGCTACCTTGTTACGACTT
Escherichia coli	GGAGCAAACAGGATTAGATACCC	AACCCAACATTTCACAACACG

TNF-α, IFN-γ, and IL-1β) and fecal LPS of colonic tissue. The operations were operated on the basis of the manufacturer's instructions. There were 8 samples in every group, and every sample was detected in triplicate. A microplate reader (Model 680, Bio-Rad, St. Louis, MO, USA) equipped with a 450 nm filter was used to calculate the data. The data were written as pg/mg protein for the IL-10, TNF-α, IFN-γ, and IL-1β levels of the colonic tissue and μg/mL for the LPS of the colonic content.

2.7. PAS Staining. Colon tissues were soaked in 4% paraformaldehyde in 0.1 M phosphate-buffered saline (pH 7.4, 4°C) immediately for forty-eight hours and infiltrated in paraffin for sectioning (5 μm, cross-section). All colonic tissues were embedded in periodic acid-schiff (PAS). 30 random fields in 6 sections of every sample from PAS staining were photographed at 400x magnification with a microscope (BX51; Olympus, Tokyo, Japan), and a total of at least 360 fields (12 mice) were analysed per group. The goblet cells number per μm^2 were counted.

2.8. Colonic RNA and Fecal DNA Isolation and Quantitative RT-PCR Analysis. Specific operation is supplied in the Supplementary Material. The primers used are shown in Table 2.

2.9. Cell Culture and Treatment. We use 96-well culture plates (5×10^6cells/mL) and 12-well culture plates (5×10^5 cells/mL) to culture the human colonic intestinal epithelial cells (HT-29, CL-0118, China). The LPS-treated cells (10 nM, Solarbio Ltd., Beijing, China) were treated with 100 μM NAC (a ROS scavenger; MCE, New Jersey, USA; LPS + NAC-cells), 100 μM TAK-242 (a TLR4 antagonist; MCE, New Jersey, USA; LPS + TAK-242-cells), 2 μM TWS119 (a selective GSK-3β antagonist; MCE, New Jersey, USA; LPS + TWS-cells), or 10^{-8} M MT (Sigma-Aldrich, St. Louis, USA; LPS + MT-cells). After MT supplementation for 30 min, the LPS + MT-cells were sequentially treated with 50 μM 4P-PDOT (a nonselective MT2 antagonist; MCE, New Jersey, USA; LPS + MT + 4P-PDOT-cells). Incubate each treated cells for 24 h. Meanwhile, some *Aeromonas* veronii-supplied cells (ATCC35624, *Aeromonas* cells) were treated with 10^{-10}-10^{-8} M MT (*Aeromonas* + MT-cells). Each plate was inoculated with a bacterial suspension at a ratio of 1 : 5-5 : 1 (bacteria: host cells) for 0-12 h.

The IECs collected from the 96-well culture plates were detected for ROS (Nanjingjianchen, Beijing, China) assay and proliferation activity using MTT (3-(4,5)-dimethylthiahiazo (-z-y1)-3,5-di-phenytetrazoliumromide; Sigma, St. Louis, MO, USA) assay. A microplate reader (Model 680, Bio-Rad, St. Louis, MO, USA) equipped with a 570 nm wavelength filter was used to determine the optical density. Meanwhile, the cells collected from the 12-well culture plates was assessed for lactate dehydrogenase (LDH) assessment, quantitative RT-PCR, and western blotting analysis. Each operation used a repeat of 8 wells.

2.10. LDH Assessment. Consistent with the manufacturer's instructions, we use a LDH test kit (Solarbio Ltd., Beijing, China) to detected the cell supernatants. The test data were assessed at 450 nm wavelength via a microplate reader (Model 680, Bio-Rad, St. Louis, MO, USA) and were expressed as U/10^4 cells. Every sample was assayed three times.

2.11. Determination of ROS Formation. Consistent with the manufacturer's instructions, we use a ROS test kit, purchased from Sigma-Aldrich to detect the ROS content ($n = 9$). A flow cytometer with an oxidation-sensitive DCFH-DA fluorescent probe was used to measure the intracellular ROS generation. Specific operation is supplied in the Supplementary Material.

2.12. Western Blotting. The appropriate amount of colon segment was quickly homogenized in liquid nitrogen and stored at -80°C refrigerator for western blotting analysis. Specific operation is supplied in the Supplementary Material.

2.13. Statistical Analysis of Data. We use SPSS 10.0 statistical software (SPSS, Inc., Chicago, IL, USA) to analysed the data and showed as themean ± standard error. Differences between groups were statistically analysed using one-way ANOVA, which was used to indicated the significance of differences among groups ($P < 0.05$ and $P < 0.01$).

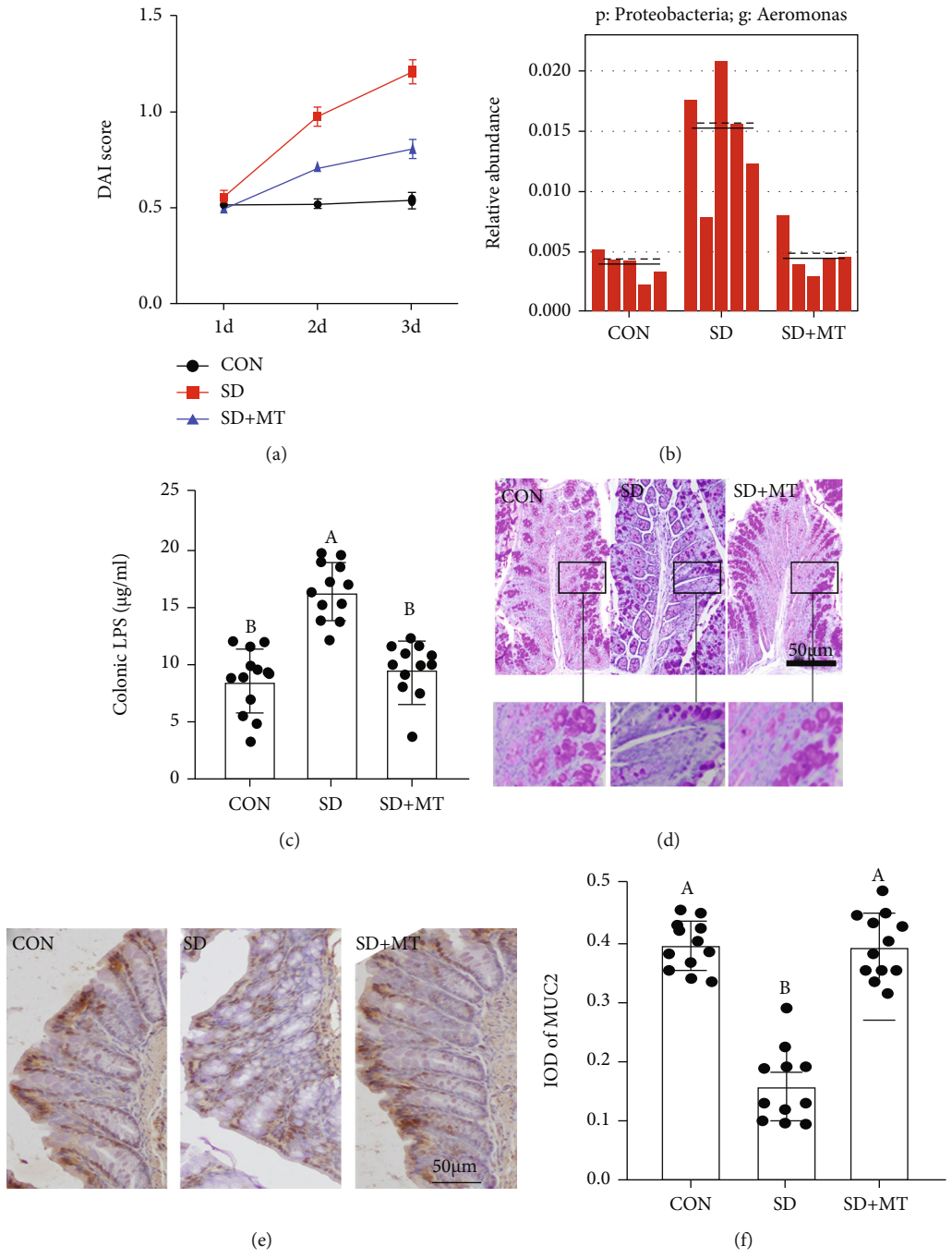

Figure 1: Continued.

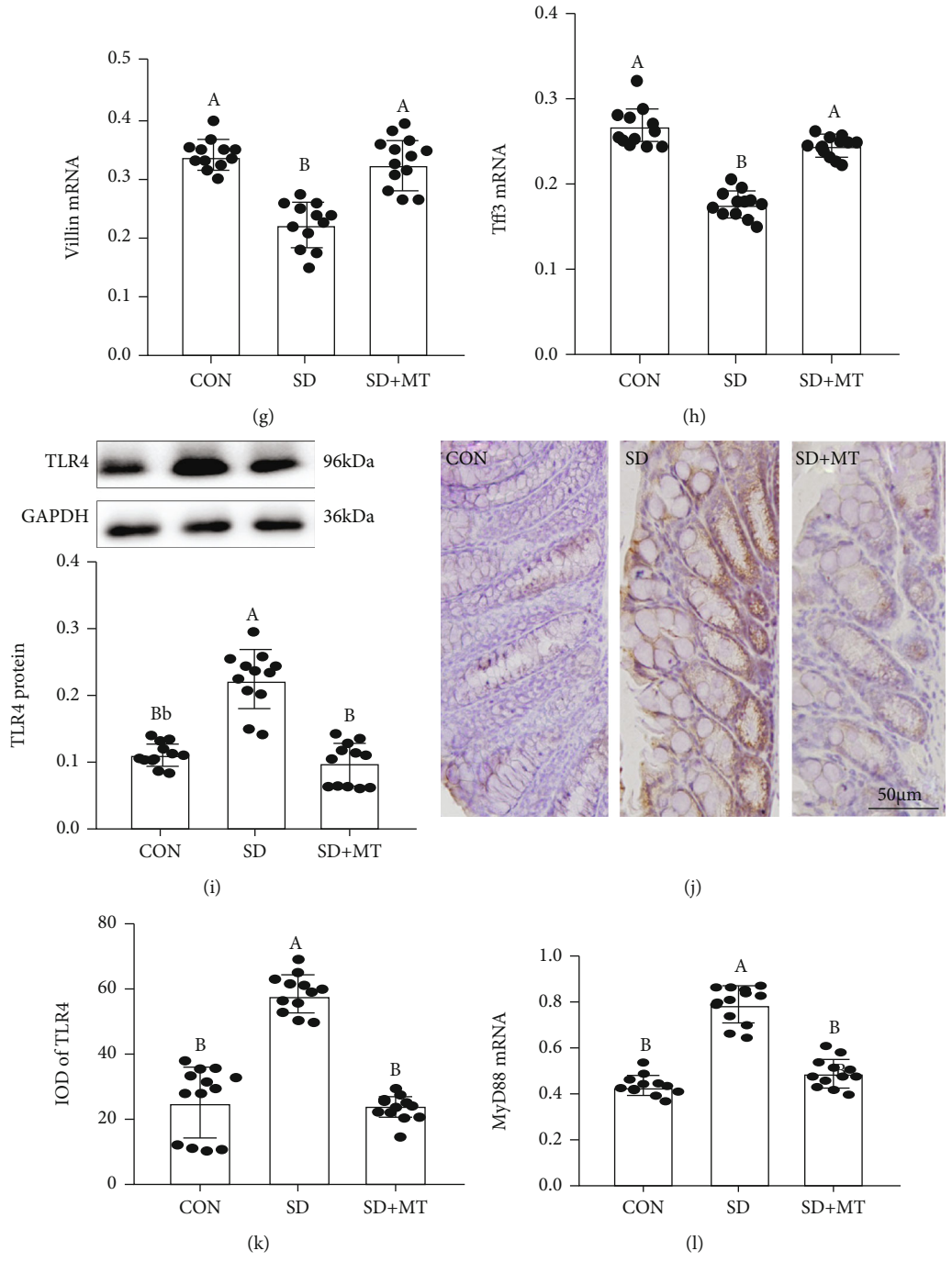

Figure 1: Continued.

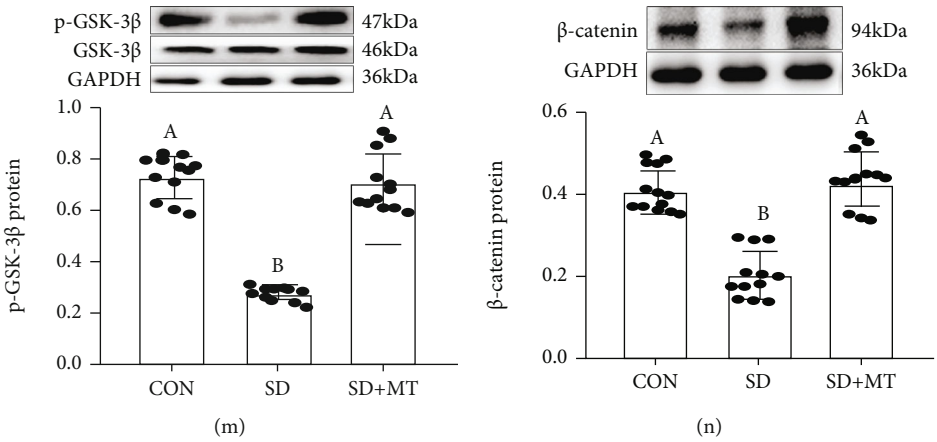

Figure 1: Melatonin improved SD-induced *Aeromonas* and LPS level increase and MUC2 deficiency in mice. (a) DAI score; relative abundance of colonic *Aeromonas* (b) and LPS (c); (d) PAS staining of colon tissue sections (scale: 50 μm); (e) immunohistochemical staining of MUC2 in colon sections (scale: 50 μm); (f) IOD of MUC2 protein; (g) Villin mRNA; (h) Tff3 mRNA; (i) TLR4 protein; (j) immunohistochemical staining of TLR4 in colon sections (scale: 50 μm); (k) IOD of TLR4 protein; (l) MyD88 mRNA; (m) p-GSK-3β and (n) β-catenin proteins in CON, SD, and SD+MT groups. Values are presented as mean ± SE. Differences were assessed using ANOVA and are denoted as follows: different lowercase letters: $P < 0.05$; different uppercase letters: $P < 0.01$; same letter: $P > 0.05$. The bottom is the same.

3. Results

3.1. Melatonin Improved SD-Induced Aeromonas and LPS Increase and MUC2 Deficiency in Mice. Results showed the occurrence of colitis in SD mice, including weight loss (Figure S1A), colon shortening (Figures S1B, C), fecal occult blood (Figure S1F), the increase of histological score (Figures S1D, E), intestinal permeability (Figure S1G), and IL-17 levels (Figure S1H), compared with CON group. Our researches demonstrated that SD induced an elevation in the DAI score (Figure 1(a)). Moreover, there was an upregulation of relative abundance in colonic *Aeromonas* (Figure 1(b)) and LPS (Figure 1(c)) and a reduction in the goblet cells number (Figure 1(d)) in the SD group relative to the CON group. Meanwhile, compared with the CON group, there was a decrease in MUC2 protein (Figures 1(e) and 1(f)), Villin (Figure 1(g)), and Tff3 mRNA (Figure 1(h)). Furthermore, there was an upregulation in the expression levels of TLR4 (Figures 1(i–k)) and MyD88 (Figure 1(l)), and a reduction in the expression levels of p-GSK-3β (Figure 1(m)) and β-catenin (Figure 1(n)) in the SD groups relative to the CON group.

MT-supplied elevated the colitis phenotype, goblet cells number and expression level of MUC2, Villin, Tff3, p-GSK-3β and β-catenin and reduced the DAI score, level of Aeromonas and LPS, and contents of TLR4 and MyD88, and there was no obviously difference between the SD+MT and control groups ($P > 0.063$).

3.2. FMT Promotes Reestablishment of the Intestinal Microecology. As illustrated in Figure 2, compared with the F-CON group, the body weight, colonic length, the level of IL-10, and IFN-γ, the goblet cells number and expression levels of MUC2, p-GSK-3β, and β-catenin proteins decreased by 2.3 ± 0.669% (Figure S2A), 56.8 ± 0.134% (Figures S2D, E), 42.3 ± 1.004% (Figure S2H), 34.2 ± 2.115 % (Figure S2I), 4.3 ± 3.314% (Figures 2(a) and 2(b)), 54.3 ± 0.015% (Figure 2(c)), 48.9 ± 0.006% (Figure 2(i)), and 62.1 ± 0.002% (Figure 2(j)), respectively, while the intestinal permeability, histological score, the level of IL-1β and IL-6, F:B ratio, relative abundance of *Aeromonas* and LPS, and expression levels of TLR4, MyD88, p-P65, and p-IκB proteins increased by 43.9 ± 0.006% (Figure S2C), 52.1 ± 0.007% (Figures S2F, G), 29.8 ± 0.150% (Figure S2J), 35.6 ± 0.009% (Figure S2K), 38.1 ± 0.343% (Figure 2(d)), 51.5 ± 0.009% (Figure 2(e)), 48.1 ± 0.221% (Figure 2(f)), 35.7 ± 0.005% (Figure 2(g)), 45.2 ± 0.008% (Figure 2(h)), 32.1 ± 0.004% (Figure 2(k)), and 26.9 ± 0.005% (Figure 2(l)) in the F-SD group, with fecal occult blood (Figure S2B). Moreover, there was an upregulation of the relative abundance in Firmicutes and proteobacteria (Figures S3B, C) and a downregulation of bacteroidetes and Faecalibacterium (Figures S3A, D) in F-SD group related to F-CON group. Yet, the stimulating effects of F-SD on changes in colitis and intestinal microbiota imbalance were improved in the colon via F-MT supplementation.

3.3. A. veronii Colonization Promoted the Occurrence of Colitis and MUC2 Deficiency in Mice. To verify the core role of the *Aeromonas* level increase in SD-induced MUC2 deficiency, we established an *A.* veronii colonization mouse model. After *A.* veronii colonization, we observed an upregulation of the relative level of *Aeromonas* and LPS by 31.2 ± 0.254%, $P = 0.024$ (Figure S4A) and 29.1 ± 0.061%, $P = 0.025$ (Figure S4B), respectively, and Pearson correlation analysis demonstrated a positive correlation between the relative content of *Aeromonas* and the colonic LPS level ($r^2 = 0.9131$, $P < 0.0001$, Figure S4C) in mice. Moreover, the mice exhibited a more serious fecal occult blood level (Figure 3(a)), elevations of permeability (Figure 3(b)), and clinical score (Figures 3(c) and 3(d)) and

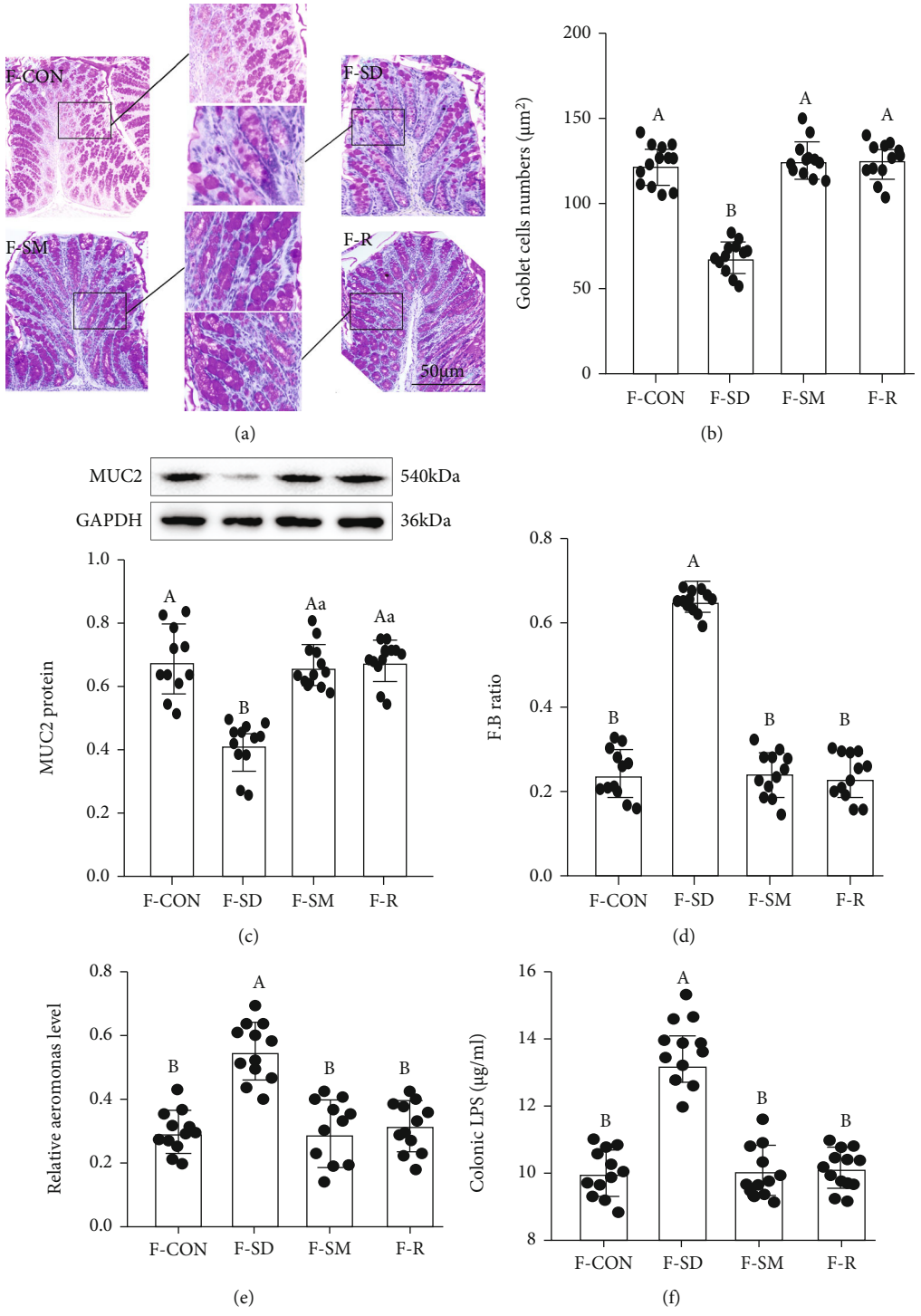

Figure 2: Continued.

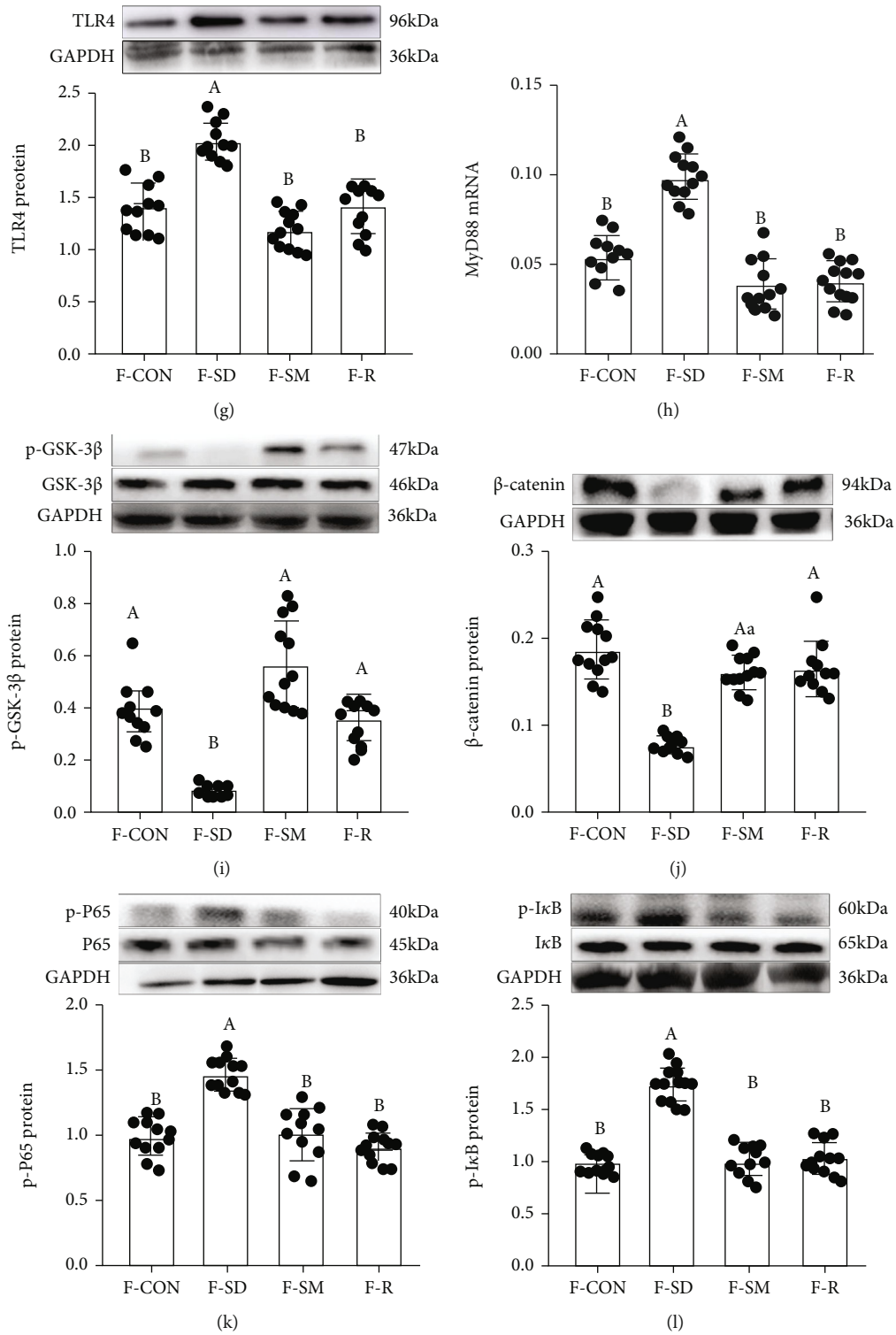

Figure 2: FMT reestablished the intestinal microecology similar to CON, SD, and SD+MT mice. (a) PAS staining of colon tissue sections (scale: 50 μm); (b) the number of goblet cells per um^2 in the colon; (c) MUC2 protein; (d) the ratio of F:B; Relative abundance of *Aeromonas* (e) and LPS (f) in the colonic content; colonic TLR4 (g), MyD88 (h), GSK-3β (i), β-cateinin (j), p-P65 (k), and p-IκB (l) mRNA and proteins of the F-CON, F-SD, F-SM, and F-MT groups.

levels of TNF-α (Figure 3(e)) and IL-1β (Figure 3(f)), as well as reductions of IL-10 (Figure 3(g)) and IFN-γ (Figure 3(h)) levels, goblet cells' number (Figures 3(i) and 3(j)), and expression levels of MUC2 (Figure 3(k)), Villin (Figure 3(l)), and Tff3 (Figure 3(m)), relative to the C-CON group. However, MT supplementation suppressed this process and caused no obvious differences between the C-CON and C-AM groups ($P > 0.053$).

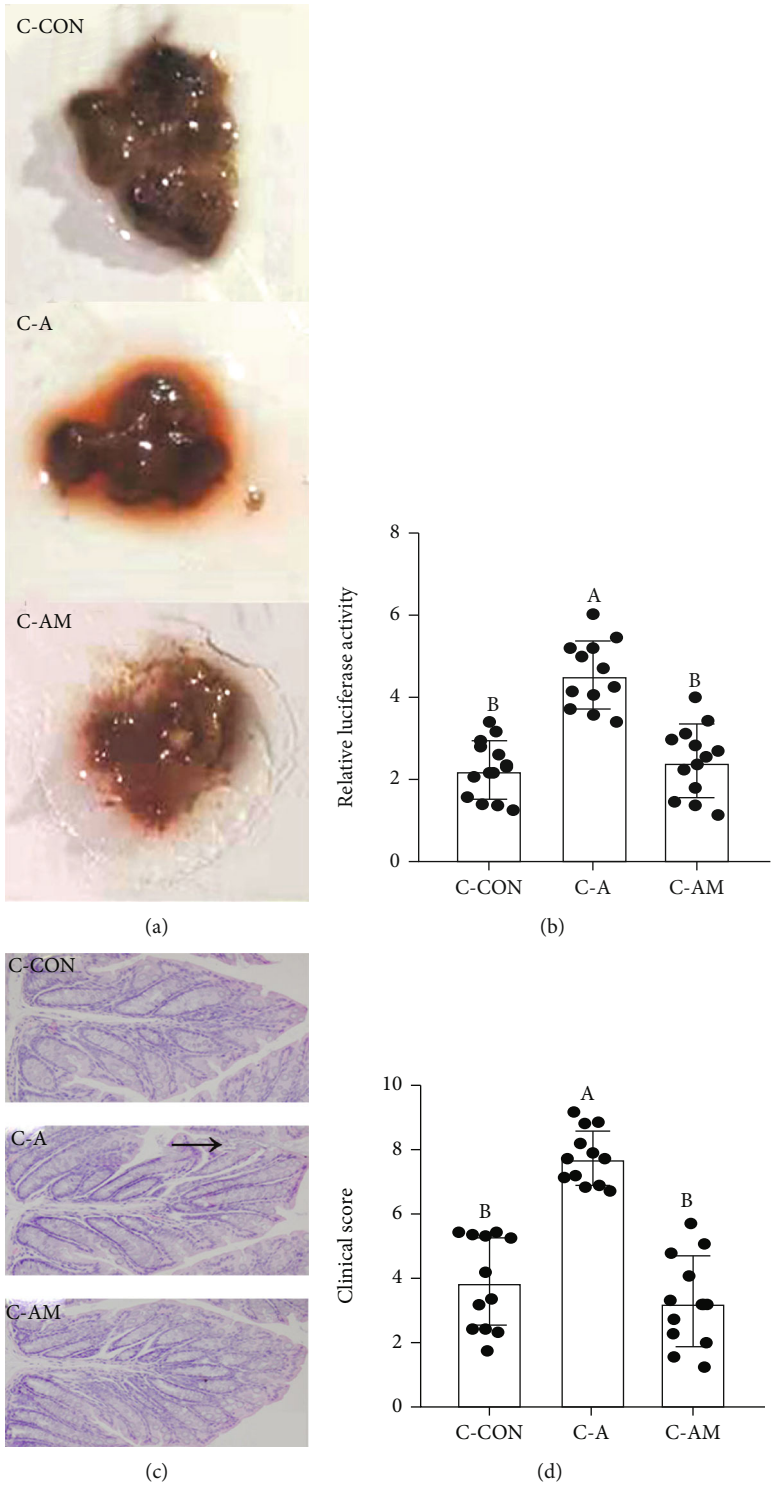

Figure 3: Continued.

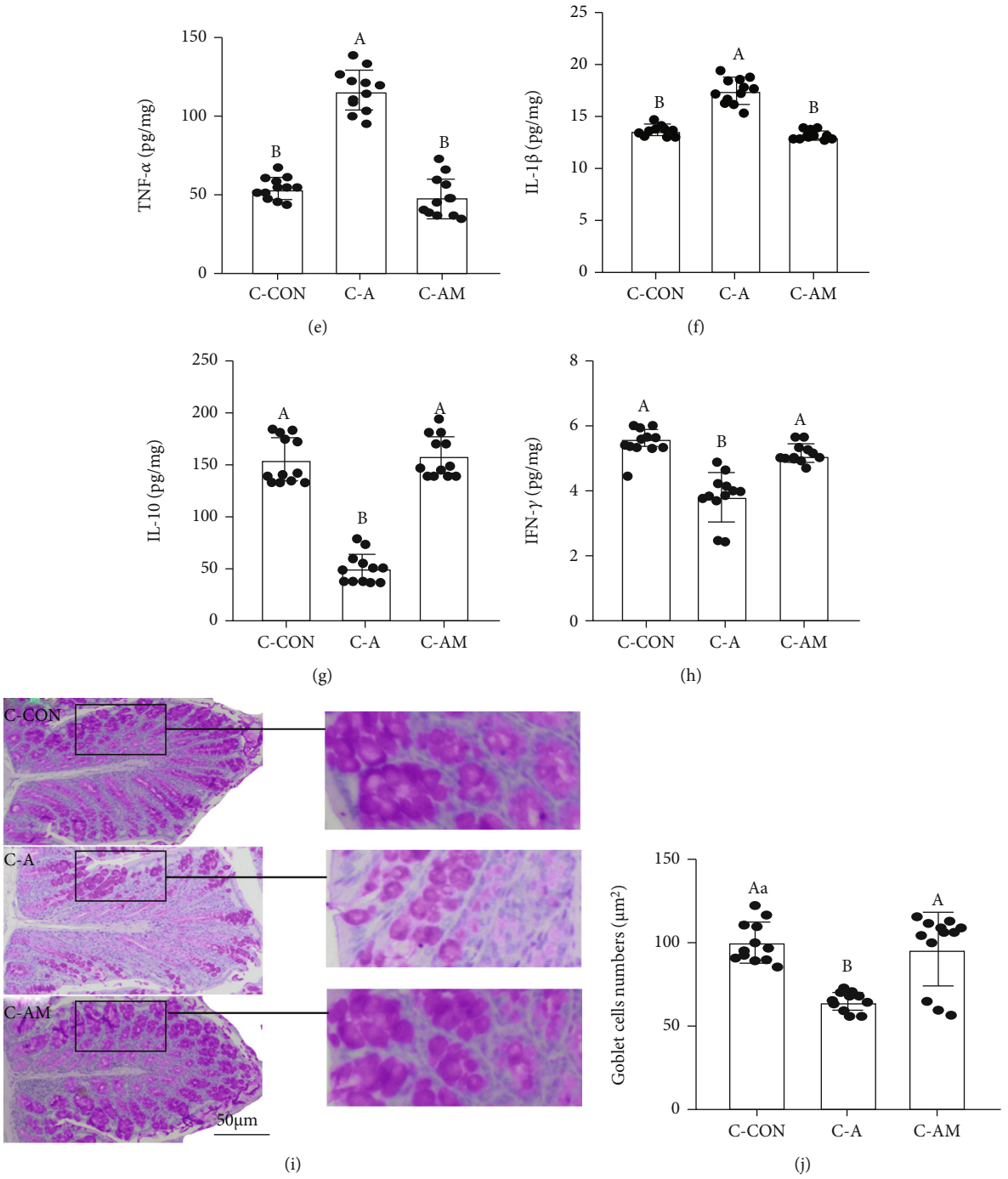

Figure 3: Continued.

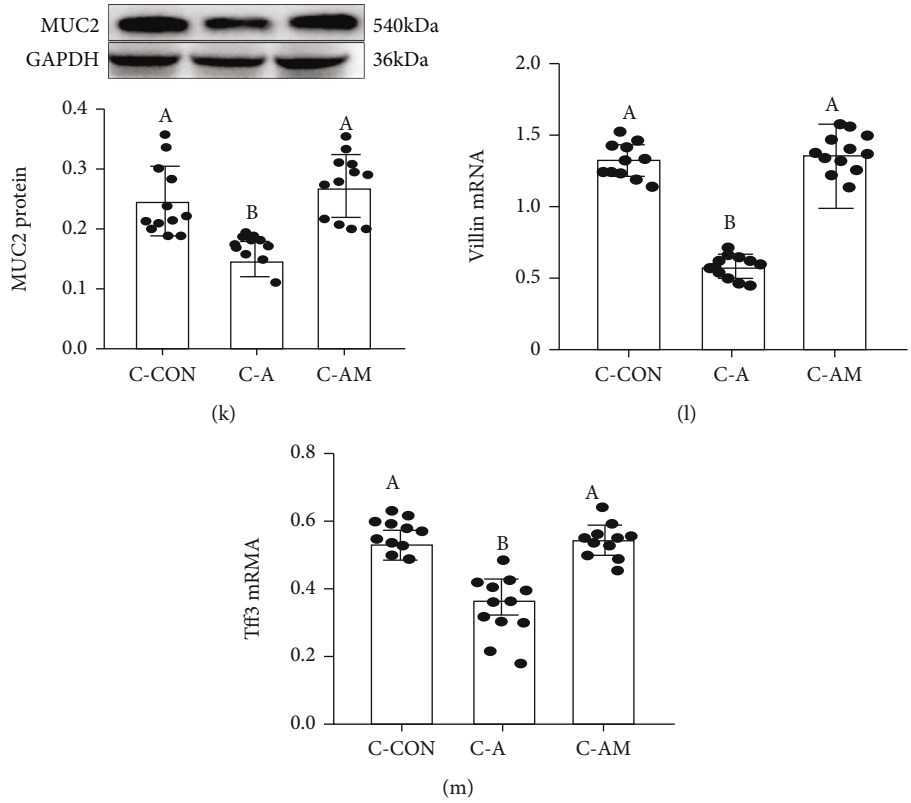

Figure 3: *Aeromonas* veronii colonization promoted the occurrence of colitis in mice. (a): fecal occult blood; (b) relative luciferase activity for colonic permeability; (c) H&E staining photographs (scale: 50 μm); (d) histopathological score; colonic TNF-α (e), IL-1β (f), and IL-10 (g), and IFN-γ (h) concentrations were measured by ELISA; (i) PAS staining of colon tissue sections (scale: 50 μm); (j) the number of goblet cells per um^2 in the colon; (k) MUC2 protein; (l) Villin mRNA; (m) Tff3 mRNA in C-CON, C-A, and C-AM groups.

3.4. Melatonin Ameliorates LPS-Induced Colitis. To evaluate the clinical relevance of MT and LPS-mediated mucin deficiency, we established a LPS-induced mouse colitis model with or without MT and TAK-242 supplementation. We observed no significant changes in liver morphology (Figure S5A) and levels of inflammatory factors (IL-6, TNF-α, IFN-γ, and IL-10, Figures S5B-E) in mice of CON, LPS and, LPS+MT groups. However, compared with the CON group, the LPS-treated group showed a decrease in body weight (Figure 4(a)), colon length (Figures 4(b) and 4(c)), IL-10 (Figure 4I), and IFN-γ (Figure 4(j)) as well as an upregulation in histopathological score (Figures 4(d) and 4(e)), permeability (Figure 4(f)), TNF-α (Figure 4(g)), and IL-1β (Figure 4(h)).

In contrast, MT and TAK-242 supplementation reversed the LPS-induced changes in colitis and the inflammatory response; no significant difference was showed in body weight ($P > 0.052$), colonic length ($P > 0.556$), colonic permeability ($P > 0.345$), histopathological score ($P > 0.643$), proinflammatory cytokines (TNF-α and IL-1β, $P > 0.772$), or anti-inflammatory factors (IL-10 and IFN-γ, $P > 0.558$) among the LPS+MT, LPS+NAC, LPS+TAK-242, and CON groups.

3.5. Melatonin Ameliorates LPS-Induced MUC2 Depletion and Changes in the Expression Levels of Signalling Proteins in Mice. Meanwhile, the PAS staining consequence indicated that the goblet cells number was significantly reduced by $40.6 \pm 2.513\%$ ($P = 0.035$) in the colon in the LPS group (Figures 5(a)–5(e)). An analogous effect was presented in the expression levels of MUC2 protein, Villin, and Tff3 mRNA, which was significantly decreased by $20.6 \pm 0.019\%$ (MUC2, $P = 0.009$, Figure 5(f)), $48.3 \pm 0.007\%$ (Villin, $P \leq 0.001$, Figure 5(g)), and $36.4 \pm 0.018\%$ (Tff3, $P = 0.007$, Figure 5(h)), respectively, in the LPS group related to the control group. While these diversifications were improved after MT and TAK-242 supplementation, leading to no obviously difference among these groups ($P > 0.209$).

Moreover, our researches indicated that there was an increase in the expression levels of TLR4 (Figure 5(i)), MyD88 (Figure 5(j)), p-IκB (Figure 5(m)), and p-P65 (Figure 5(n)) and a decrease in p-GSK-3β (Figure 5(k)) and β-catenin (Figure 5(l)) in the LPS group compared with the CON group. While after MT and TAK-242 supplementation, the expression levels of TLR4, MyD88, p-IκB, and p-P65 proteins downregulated by $28.7 \pm 0.020 - 35.7 \pm 0.025\%$, $36.1 \pm 0.039 - 47.3 \pm 0.028\%$, $29.4 \pm 0.047 - 48.9 \pm 0.044\%$, and $25.4 \pm 0.027 - 37.5 \pm 0.030\%$, respectively, while the expression levels of p-GSK-3β and β-catenin proteins increased by $25.4 \pm 0.039 - 32.9 \pm 0.054\%$ and $21.8 \pm 0.050 - 33.6 \pm 0.030\%$, respectively, relative to those in the LPS group, leading to no significant diversity between the CON group and the MT and TAK-242-supplied groups. Moreover, the changing trends of these proteins (TLR4, MyD88,

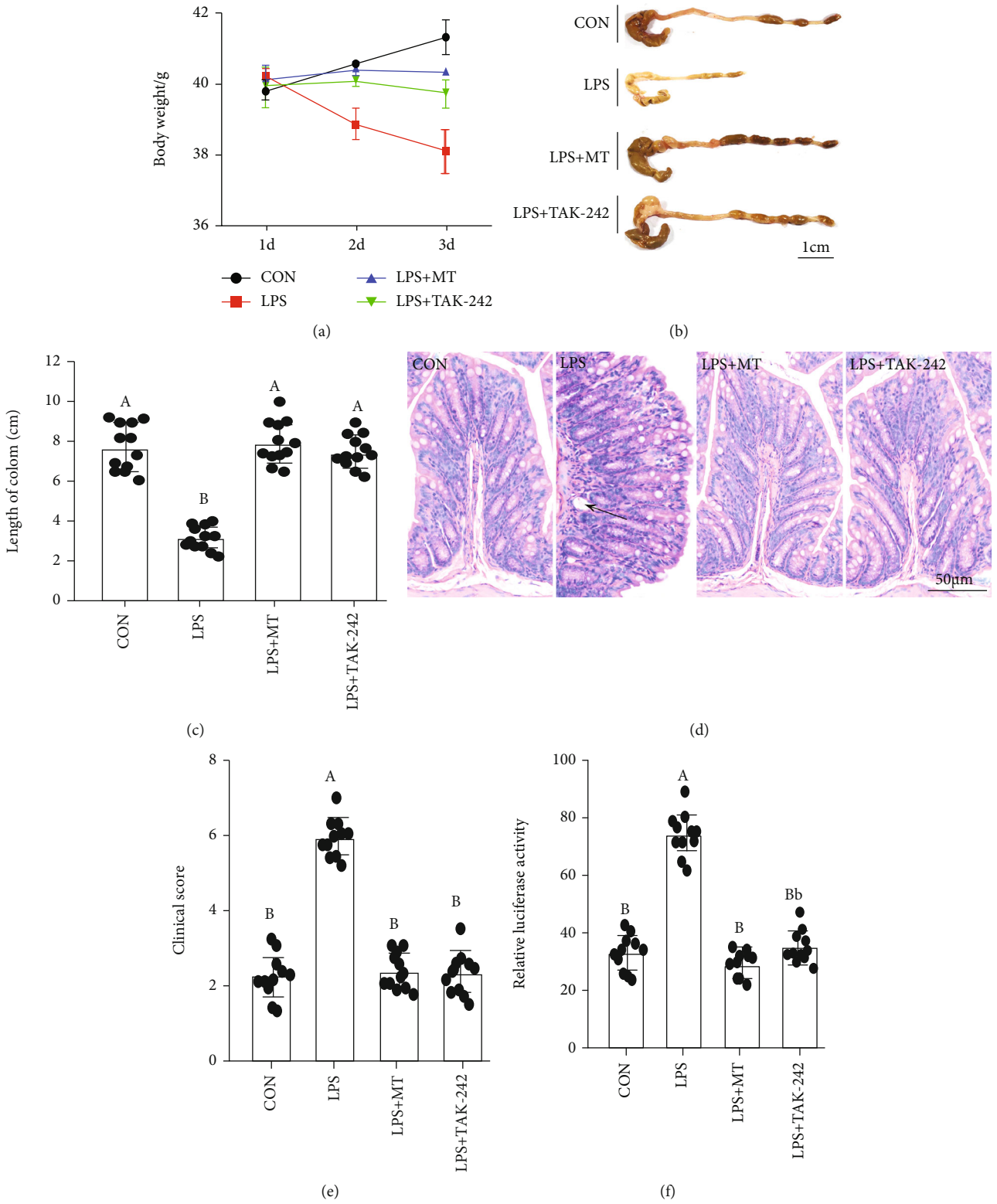

Figure 4: Continued.

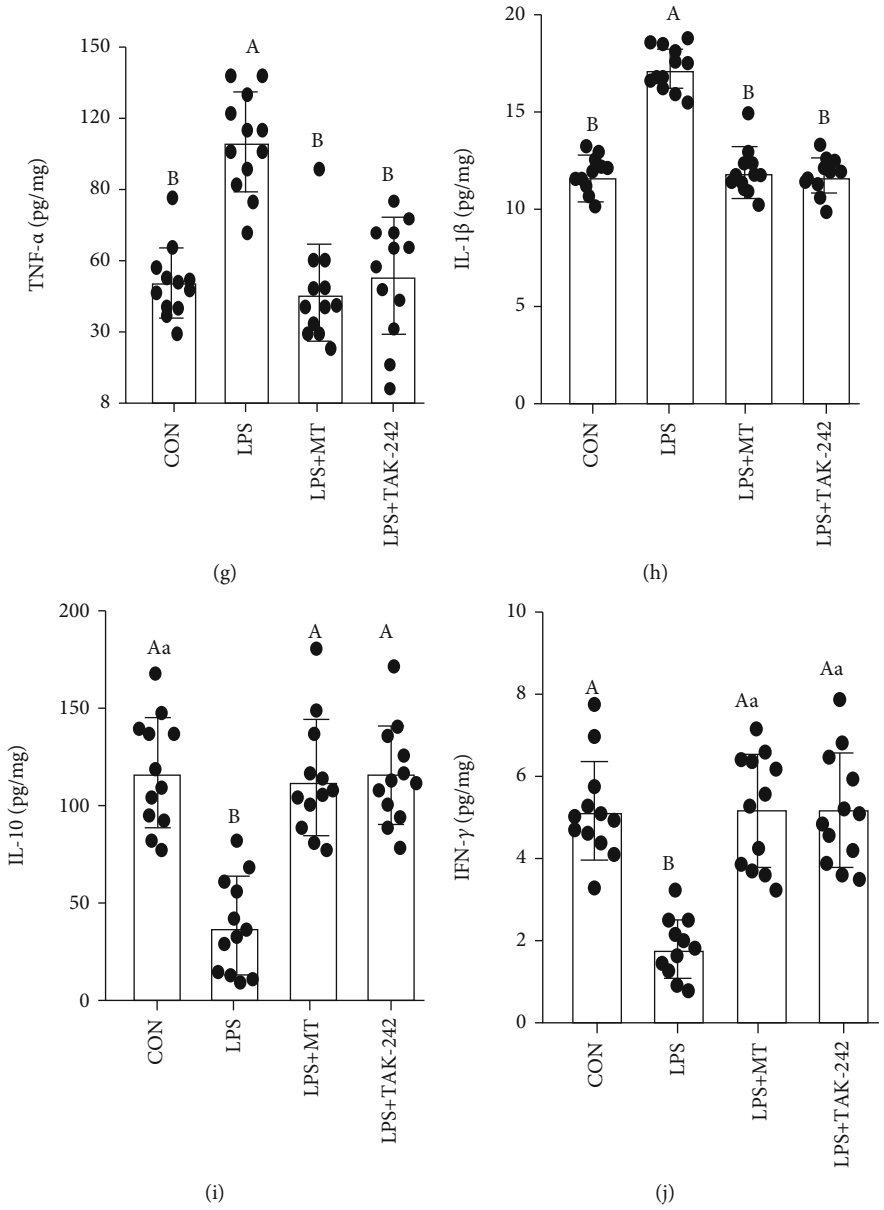

Figure 4: Melatonin improved LPS induced colitis in mice. (a) body weight; (b) and (c) colonic length; (d) H&E staining photographs (scale: 50 μm); (e) histopathological score; (f) relative luciferase activity for colonic permeability; (g–j) TNF-α (g); IL-1β (h); IL-10 (i), and IFN-γ (j) concentrations were measured by ELISA in the colon of the CON, LPS, LPS+MT, and LPS+TAK-242 groups.

p-GSK-3β, β-catenin, p-P65, and p-IκB) are consistent with the mice in C-CON, C-A, and C-AM groups (Figure S6).

3.6. Melatonin Regulates the MUC2 Level in HT-29 Cells Treated with A. veronii. To determine the vital effect of MT in MUC2 production, we selected mucin-secreting human HT-29 cells exposed to various proportions (1 : 5~5 : 1) of *A.* veronii for 12 h, which formed a homogeneous population of polarized goblet cells. Compared to the cells in the CON group, *A.* veronii treatments from 1 : 3-5 : 1 significantly inhibited the proliferation activity and MUC2 expression level of HT-29 cells, which decreased by $44.2 \pm 0.010 - 56.9 \pm 0.007\%$ (Figure S7A) and $38.6 \pm 0.011 - 62.1 \pm 0.005\%$ (Figure S7D), respectively. A decrease in proliferation activity and MUC2 level was examined after 8 h of infiltrated with 1 : 1 *A.* veronii, which reduced by $35.2 \pm 0.009\%$ (Figure S7B) and $34.1 \pm 0.040\%$ (Figure S7E), respectively. To investigate the molecular pathway via which MT regulates colonic MUC2 production, cells were supplied with MT at 10^{-10}-10^{-8} M concentrations 1 h prior to *A.* veronii treatment (1 : 1) for 8 h. We observed that the proliferation activity and expression level of MUC2 protein were decreased by $54.8 \pm 0.007\%$ (Figure S7C) and $61.2 \pm 0.033\%$ (Figure S7F) in the *A.* veronii-treated group relative to the CON group, respectively. Obviously, the inhibitory effect of *A.* veronii on proliferation activity and MUC2 expression was reversed by pretreatment with MT after 10^{-8} M MT supplementation.

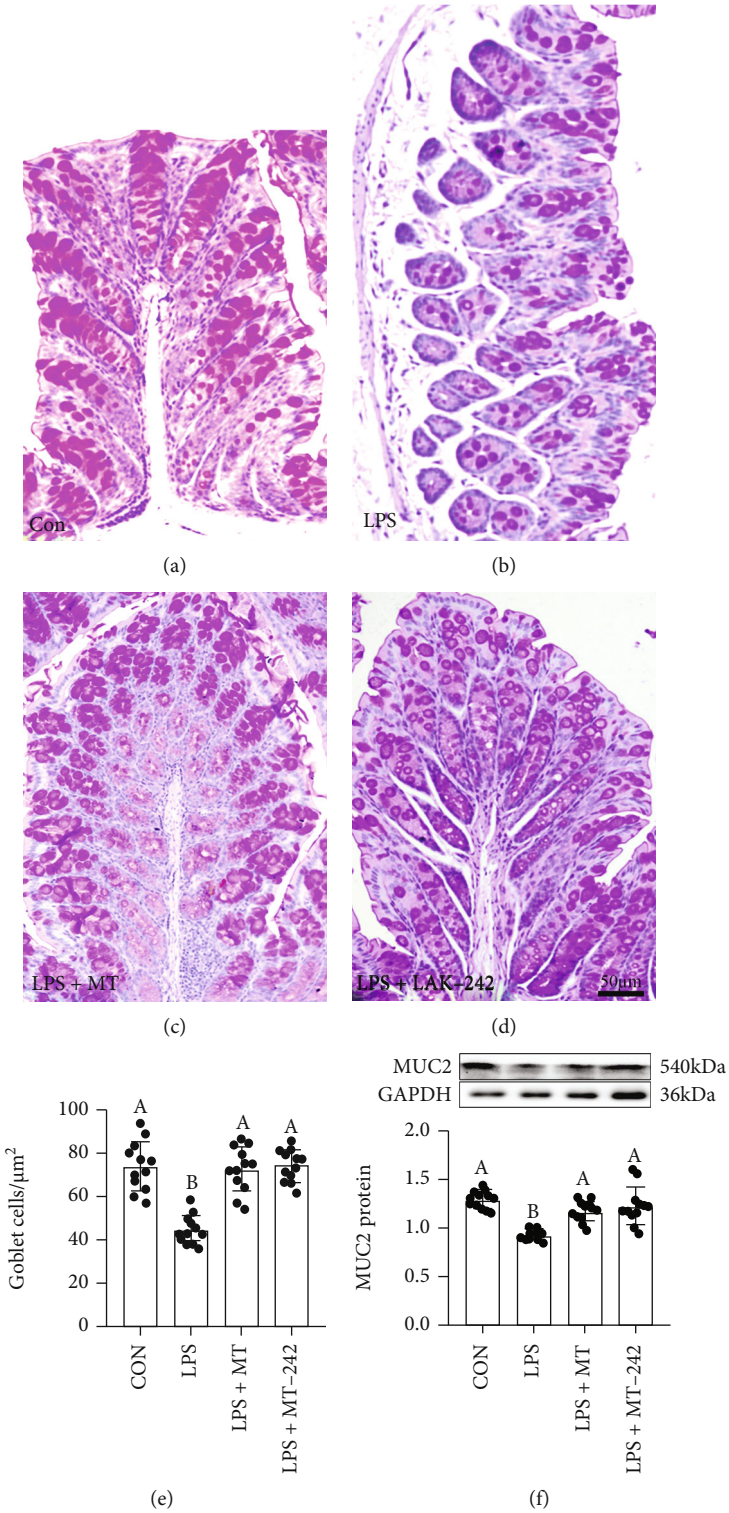

Figure 5: Continued.

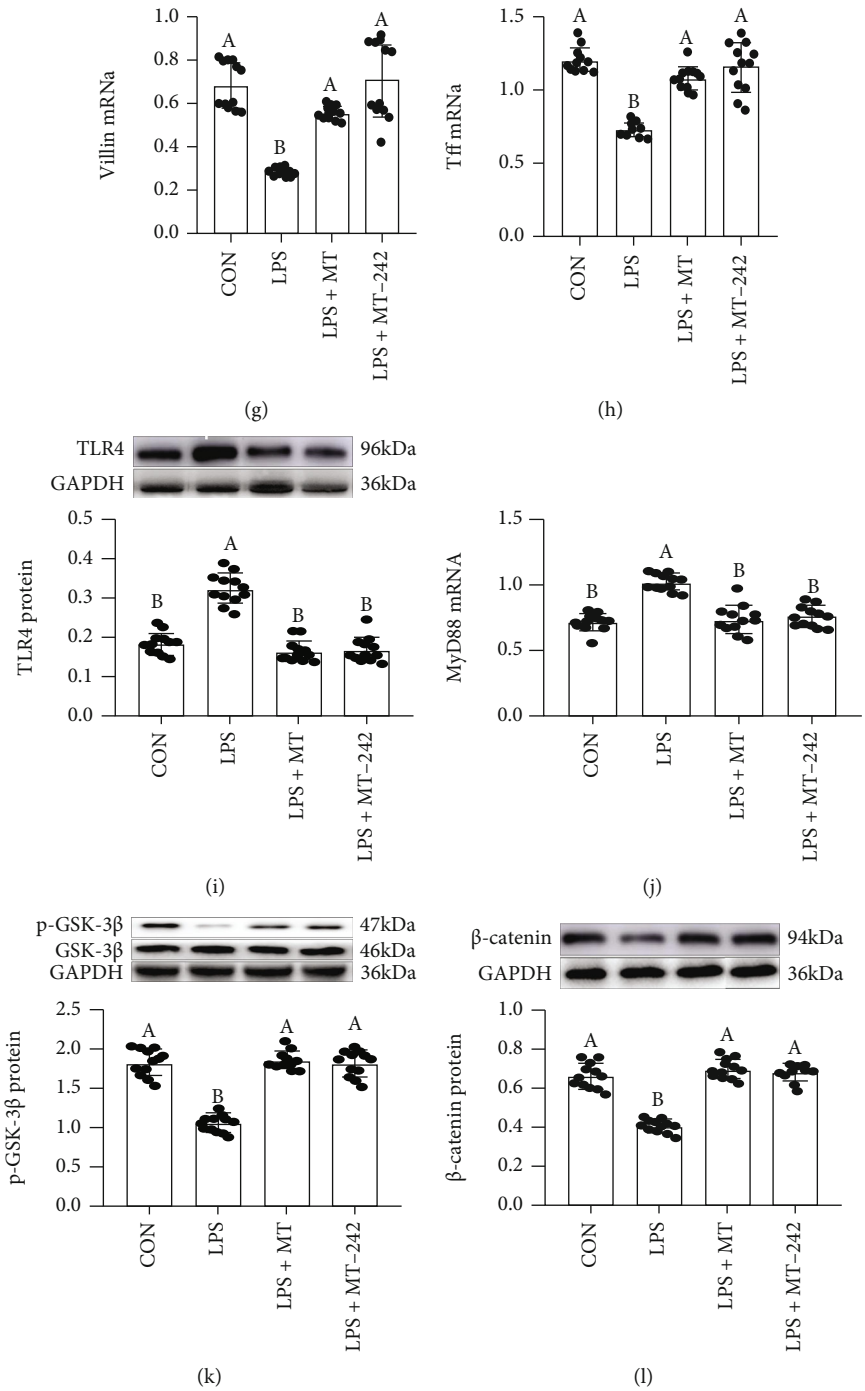

Figure 5: Continued.

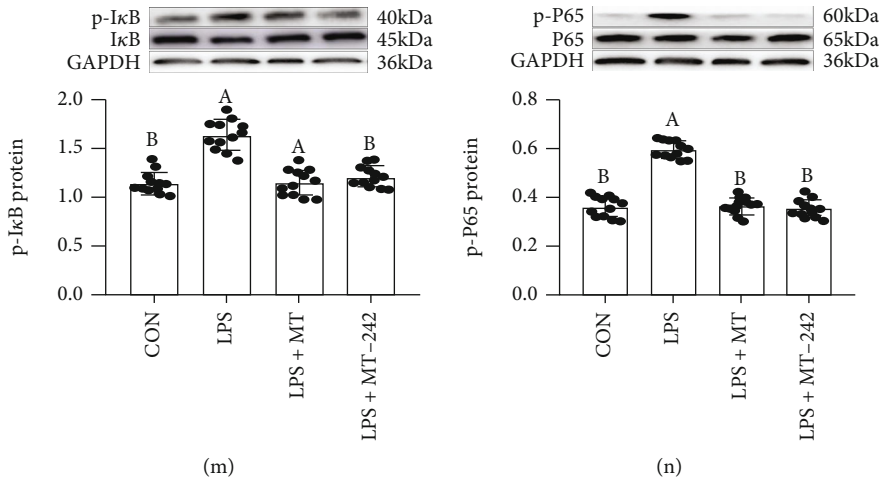

Figure 5: Melatonin improved LPS-induced MUC2 deficiency and the changes of expression levels in signalling proteins in mice. (a–d) PAS staining of colon tissue sections (scale: 50 μm); (e) the number of goblet cells per um^2 in the colon; (f) colonic MUC2 protein; (g) Villin, and (h) Tff3 mRNA; (a) colonic TLR4, (b) MyD88, (c) p-GSK-3β, (d) β-catenin, (e) p-IκB, and (f) p-P65 proteins and mRNA production in the CON, LPS, LPS+MT, and LPS+TAK-242 groups.

3.7. Regulatory Effect of Melatonin on the TLR4/MyD88/GSK-3β/β-catenin/NF-κB Loop in A. veronii-Treated HT-29 Cells. The results demonstrated that there was an obviously reduction in the expression levels of MUC2 (Figure 6(a)), Villin (Figure 6(b)), Tff3 (Figure 6(c)), p-GSK-3β (Figure 6(h)), and β-catenin (Figure 6(i)) and an upregulation in the expression levels of TLR4 (Figure 6(d)), MyD88 (Figure 6(e)), p-IκB (Figure 6(f)), and p-P65 (Figure 6(g)) in the *A.* veronii-treated group related to the vehicle group. While MT supplementation effectively improved these *A.* veronii-induced changes. In contrast, we observed a downregulation of TLR4, MyD88, p-IκB, and p-P65 and an upregulation of MUC2, Villin, Tff3, p-GSK-3β, and β-catenin related to the *A.* veronii-treated group.

3.8. Melatonin Regulates the MUC2 Level in HT-29 Cells Treated with LPS. To investigate the effect of LPS in the regulation of mucin expression levels, HT-29 cells were infiltrated with different concentrations (0-500 pg/mL) of LPS for 24 h. Compared to the cells in the CON group, LPS-treated from 100 to 500 pg/mL obviously suppressed the mucin expression levels of HT-29 cells (Figure S8A), which decreased by $54.3 \pm 0.084\%$ and $58.4 \pm 0.084\%$, respectively. A reduction in MUC2 expression level was presented after 24 h of exposed to 100 pg/mL LPS (Figure S8B), which was reduced by $35.2 \pm 0.078\%$. To verify the molecular pathways by which MT regulates colonic MUC2 production, the cells were treated with 10^{-8} M MT thirty min prior to LPS (100 pg/mL) for 24 hours. We observed that the expression level of MUC2 protein was decreased by $12.3 \pm 0.065\%$ in the LPS-treated group relative to the CON group. Obviously, the inhibitory effect of LPS on MUC2 expression was reversed by supplementation with MT (Figure S8C). We also explored the ability of MT to improve cell viability in LPS-treated IECs in an LDH assay. Compared with the control cells, LPS caused a large amount of cell death and released LDH (Figure S8D). Statistically, the LDH level was obviously upregulated (Figure S8E) in the LPS-treated group relative to the vehicle group. Conversely, the MTT assay indicated that LPS caused a decrease in proliferation index (Figures S8F, G). However, after MT supplementation, the LDH index was significantly reduced by $12.5 \pm 0.094\%$, while the proliferation capacity observably increased by $17.1 \pm 0.075\%$, which almost returned to the vehicle level.

3.9. Melatonin Inhibited TLR4/MyD88 Pathway-Mediated Oxidative Stress Activation-Induced MUC2 Depletion in HT-29 Cells Treated with LPS. Consistent with the anticipation, LPS-treated obviously caused a decrease in the expression levels of MUC2 protein (Figure 7(a)), Tff3 (Figure 7(b)), and Villin mRNA (Figure 7(c)) as well as an upregulation in the expression levels of TLR4 protein (Figure 7(d)), MyD88 mRNA (Figure 7(e)), and ROS content (Figure 7(f)) compared with the vehicle group. By contrast, MT-supplied improved the stimulatory effect of LPS, leading to no significant difference between the CON group and the MT-supplied group. Moreover, the LPS-induced effect was blocked by pretreatment with TAK242, which showed an upregulation of MUC2, Tff3, and Villin mRNA and a downregulation of TLR4, MyD88, and ROS contents in the LPS+TAK242-treated IECs relative to the LPS-treated group. Similarly, TW119 supplementation effectively reversed these LPS-induced changes, while it had no effect on the expression levels of TLR4 and MyD88. Furthermore, our results demonstrated that NAC imitated the improvement effect of MT and upregulated the expressions of MUC2 protein, Tff3, and Villin mRNA, as well as downregulated the ROS content in LPS+NAC-treated IECs relative to the LPS-treated group. Yet, it had no influence on the expression levels of TLR4 and MyD88. These studies indicated that the inhibitory influence of MT on oxidative stress closely associates with the suppression of TLR4/MyD88 pathway induced by LPS. In contrast, 4P-PDOT

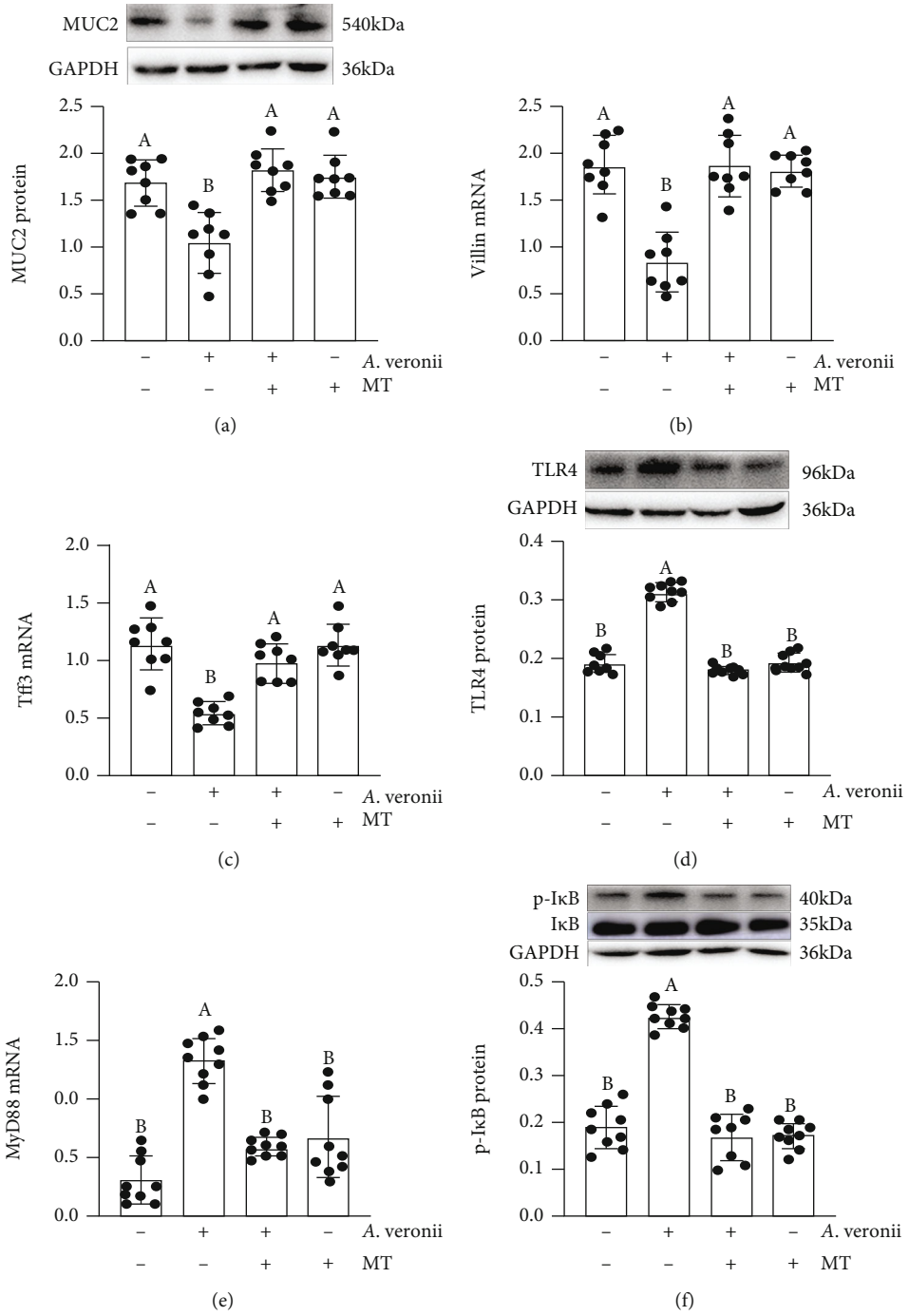

Figure 6: Continued.

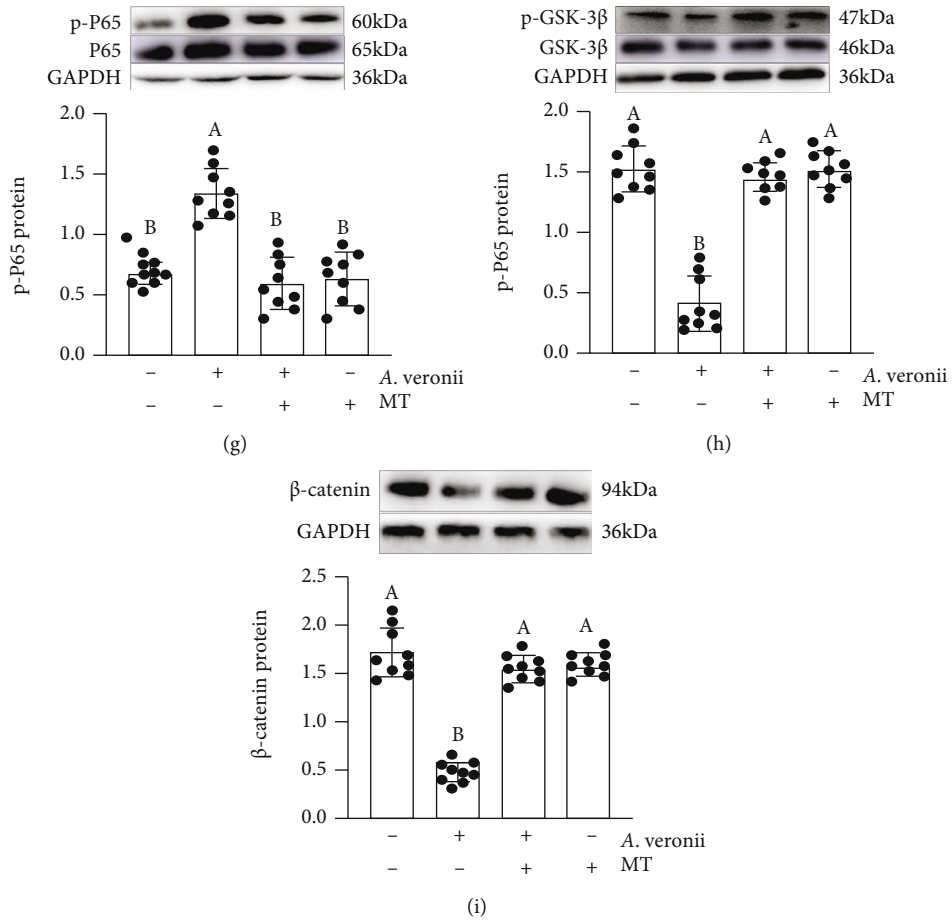

Figure 6: Melatonin suppressed the changes in expression levels of signalling proteins in *Aeromonas*-treated HT-29 cells. MUC2 (a), Villin (b), Tff3 (c), TLR4 (d), MyD88 (e), p-IκB (f), p-P65 (g), p-GSK-3β (h) and β-catenin (i) proteins, and mRNA in various treatment groups.

pretreatment counteracted the effects of MT. The expressions of MUC2, Tff3, and Villin were decreased by $33.9 \pm 0.081\%$, $35.9 \pm 0.040\%$, and $32.9 \pm 0.076\%$, while TLR4, MyD88, and ROS contents were increased by 42.9 ± 0.064 %, $35.2 \pm 0.070\%$, and $38.9 \pm 0.092\%$ in the LPS+MT+4P-PDOT group versus the LPS+MT group.

3.10. Regulatory Effect of Melatonin on the GSK-3β/β-catenin/NF-κB Loop Mediated by TLR4/MyD88 Pathway Inactivation in HT-29 Cells Treated with LPS. Next, we explored how TLR4/MyD88 activation was related to mucin deficiency. The results showed an upregulation in the expression levels of p-P65 (Figure 8(a)) and p-IκB (Figure 8(b)) and a significant reduction in the expression levels of p-GSK-3β (Figure 8(c)), β-catenin (Figure 8(d)), and MT2 (Figure 8(f)) in the LPS-treated group, relative to that in the vehicle group while the expression level of MT1 protein did not change (Figure 8(e)). While MT supplementation effectively improved these LPS-induced changes. In contrast, after treatment with TAK-242 and TWS119, we observed a downregulation of p-P65 and p-IκB and an upregulation of p-GSK-3β and β-catenin relative to the LPS group while these had no influence on the expression of MT2 protein level. Moreover, our results suggested that NAC, imitated the improvement effect of MT and downregulated the expressions of p-P65 and p-IκB proteins in LPS+NAC-treated IECs relative to the LPS-treated group while it had no influence on the expression levels of p-GSK-3β, β-catenin, and MT2 proteins. However, in treatment with 4P-PDOT, the antagonist of MT2 counteracted the therapeutic influences of MT and failed to reverse the changes induced by LPS, which further confirmed the role of the TLR4/MyD88-mediated GSK-3β/β-catenin/NF-κB/ROS pathway in LPS-treated IECs.

4. Discussion

Our previous results showed that SD induced intestinal mucosal barrier damage, including a decrease in the number of goblet cells and MUC2 protein and an upregulation of pathogen (*Aeromonas*) content [18]. Meanwhile, FMT from SD mice to wild mice recapitulates the SD-like *Aeromonas* content increase and goblet cells number and MUC2 protein level decreases, while MT improved these changes. These results demonstrated a high correlation between *Aeromonas* level increase and goblet cells number decrease. In the SD experiment, we found that the relative abundance of *Aeromonas* in the colon of the SD mice was upregulated most significantly, and after melatonin supplementation, it returned to the control level. *Aeromonas* species belong to Gram-

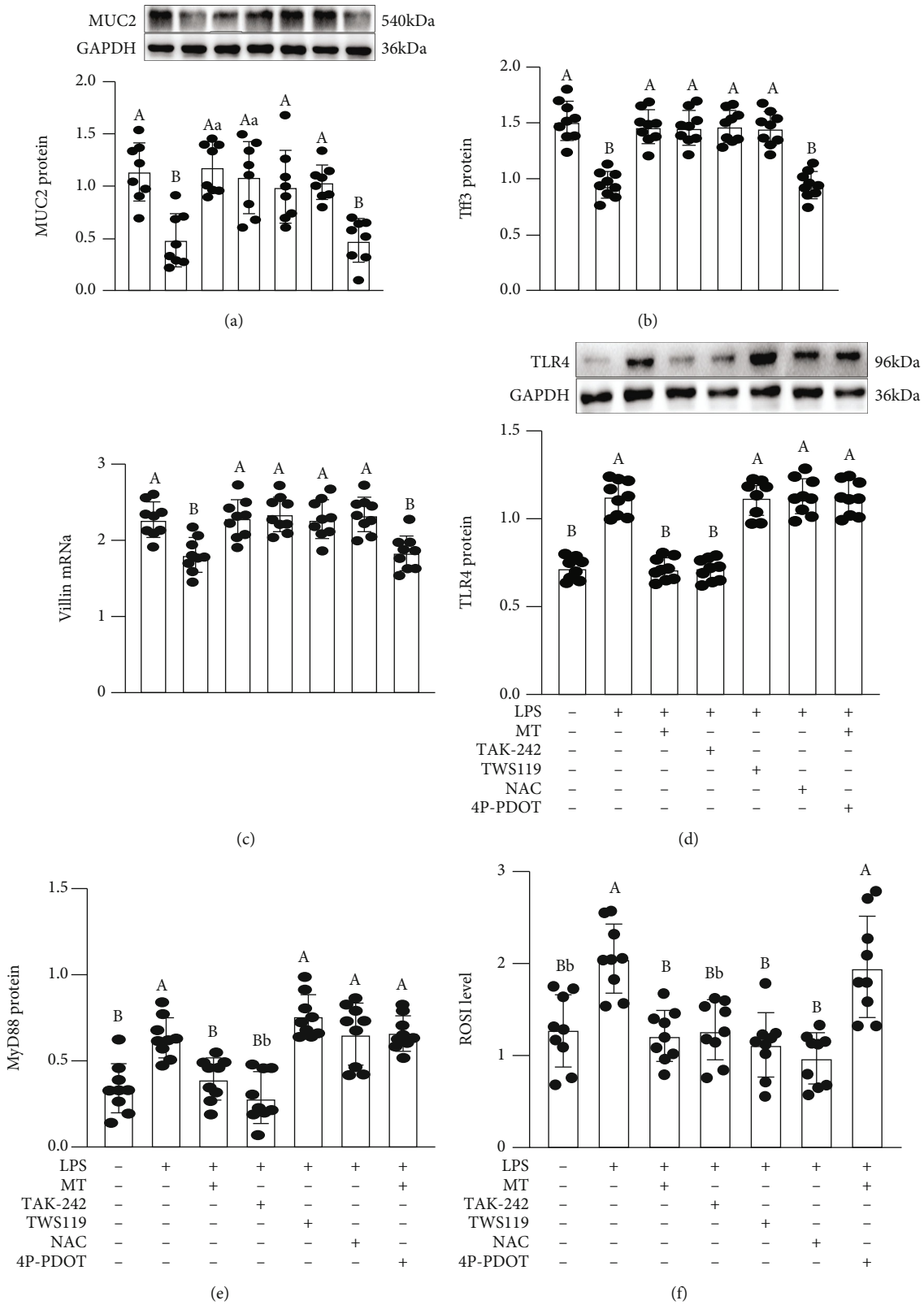

Figure 7: Melatonin suppressed the changes in expression levels of signalling proteins (MUC2, Tff3, Villin, TLR4, and MyD88) in LPS-treated HT-29 cells. MUC2 (a), Tff3 (b), Villin (v), TLR4 (d), MyD88 (e) proteins and mRNA content and ROS (f) in various treatment groups. NAC: ROS scavenger; TAK-242: an antagonist of TLR4; TWS119: an antagonist of GSK-3β; 4P-PDOT: an antagonist of MT2. The bottom is the same.

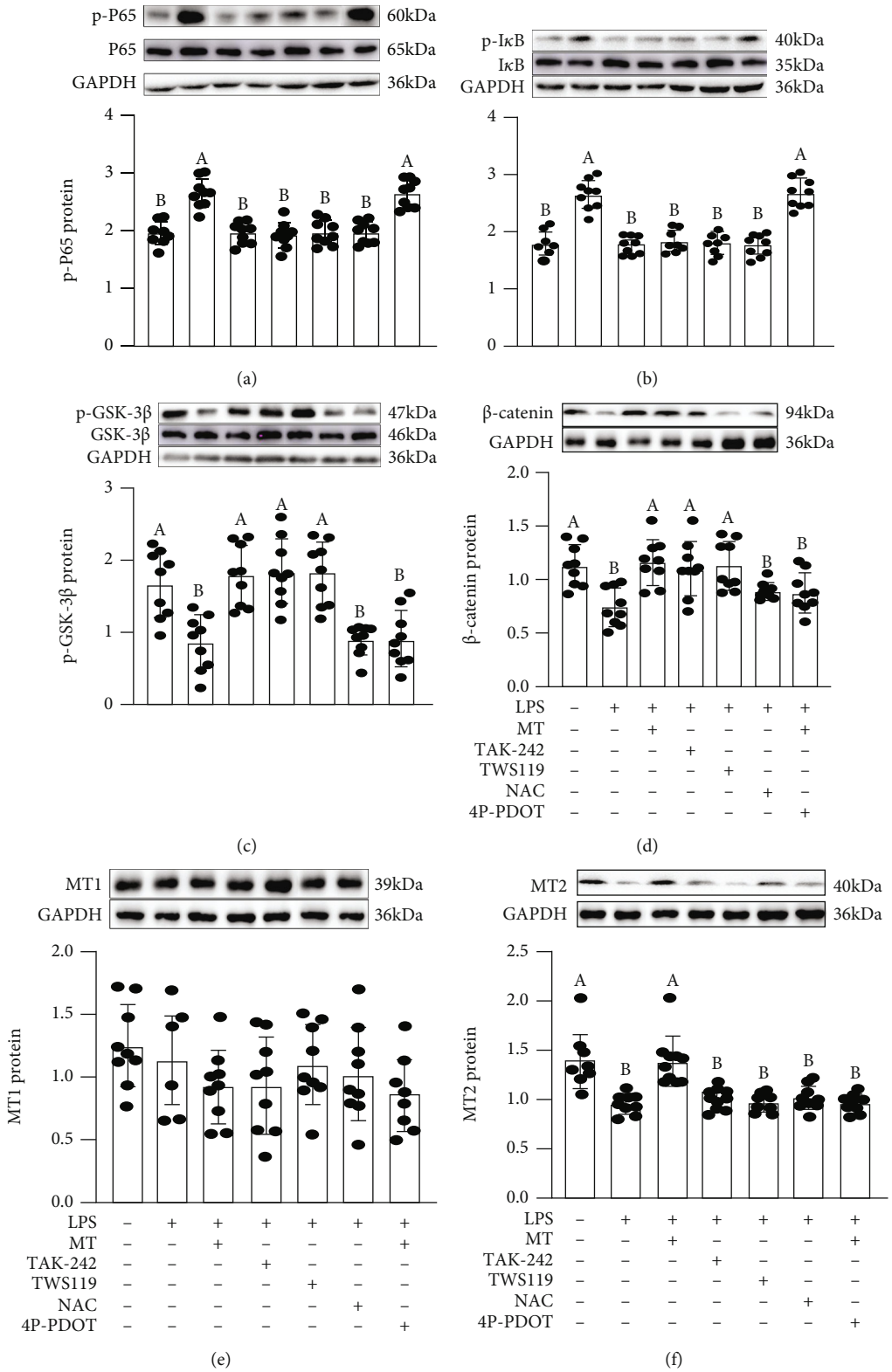

Figure 8: Melatonin suppressed the changes in expression levels of signalling proteins (p-P65, p-IκB, p-GSK-3β, β-catenin, MT1, and MT2) in LPS-treated HT-29 cells. p-P65 (a), p-IκB (b), p-GSK-3β (c), β-catenin (d), MT1 (e), and MT2 (f) proteins in various treatment groups.

negative microbiota usually resides in the intestines. Members of the genus *Aeromonas* are related to lots of inter-intestinal and extraintestinal infections in rodents [22]. *Aeromonas* obviously induces intestinal inflammation, while can frequently cause extraintestinal inflammatory responses, e.g., biliary system infection, necrotizing fasciitis, cholangitis,

surgical wounds, abdominal meningitis, and posttraumatic cellulitis [23]. To test the vital role of *Aeromonas* in SD-induced MUC2 depletion, we established an *A.* veronii colonization mouse model. The results indicated that *A.* veronii-colonized mice exhibited a colitis phenotype, including an upregulation of *Aeromonas* and its cell wall composition LPS levels and a downregulation of goblet cells' number and MUC2 protein level. However, MT supplementation significantly suppressed *A.* veronii colonization-induced proliferation of *Aeromonas* and LPS, restored MUC2 deficiency, and improved colitis, which strongly indicated that *Aeromonas* coupling with goblet cells promoted MUC2 depletion, further inducing colitis.

Furthermore, we set up a LPS-treated mouse model with or without MT supplementation to demonstrate that excessive *Aeromonas*-related LPS has a negative effect on MUC2 depletion in SD mice. The study is consistent with previous researches in mice that were exposed to LPS that caused obvious signs of colitis: shorter colonic length, lighter weight, and more serious intestinal permeability [24]. Meanwhile, there was an elevation in LPS level and a reduction in goblet cells number and MUC2 protein, Tff3, and Villin mRNA expression levels in LPS-treated mice. Importantly, the decrease of goblet cells number, MUC2 content, and a thinner intestinal mucus layer closely associates with IBD [9]. Van der Sluis et al. previously pointed that $MUC2^{-/-}$ mice behave with clinical and histological characteristics of colitis [25]. Furthermore, the present findings also showed that MT supplementation could alleviate LPS-induced colitis and the reduction of goblet cells and MUC2 protein, Villin, and Tff3 mRNA. Similarly, Shah et al. showed that MT could promote the proliferation of goblet cells to secrete mucin to resist pathogenic bacteria [26]. Therefore, we speculated that MT could improve colitis by suppressing *Aeromonas*-goblet cell interactions, thereby upregulating the goblet cells number and MUC2 protein, further improving SD-induced colitis. Meanwhile, we observed a decrease in the expression levels of p-GSK-3β and β-catenin proteins, as well as an increase in TLR4, MyD88 and p-P65, and p-IκB proteins in LPS-treated mice, while MT supplementation restored these changes. Similarly, TAK-242 (an antagonist of TLR4) supplementation mimicked the improvement effect of MT. Researches demonstrated that inappropriate TLR activation can induce prolonged inflammatory response and even autoimmune and inflammatory diseases [27]. Similarly, in rat biliary epithelia, anti-TLR2 antibodies or anti-TLR4 antibodies supplementation could reduce MUC2 expression treated with LPS [28]. It seems that boosting LPS activates the TLR4-MyD88-GSK-3β-NF-κB pathway and promotes MUC2 depletion, further inducing colitis.

In vitro, we further found that LPS and *A.* veronii could upregulate the LDH index and ROS abundance and downregulate the expression of MUC2 protein level and cell proliferation activity in mucus-secreting human HT-29 cells. However, MT supplementation effectively suppressed this process. Further, the ameliorate effect of MT could be suppressed by 4P-PDOT. However, TAK242 mimicked the effect of MT in LPS-treated cells, while it had no influence on the expression level of MT2 proteins. LPS binds innate immunity TLRs, which activates signalling cascades related to NF-κB transcription factor and mitogen-activated protein kinases (MAPKs) in adipocytes [29]. Furthermore, we found that TWS119 treatment enhanced the expressions levels of p-GSK-3β and β-catenin, ultimately suppressing NF-κB activation and promoting MUC2 secretion, while it had no influence on the expression levels of TLR4 and MT2 protein and MyD88 mRNA. Emerging date has also indicated that GSK-3β mediated the activation of the NF-κB signalling cascade via enhancing the NF-κB transcriptional activity in the nucleus to promote cancer [30]. Similarly, NAC counteracted the effect of LPS in HT-29 cells, which suppressed the activation of NF-κB pathway. Previous researches indicated that oxidative stress-mediated NF-κB activation ultimately relies on the phosphorylation and proteasomal degradation of its inhibitor IκBα, supporting nuclear NF-κB translocation. Therefore, in our study, a large number of in vivo and in vitro experiments have been demonstrated that melatonin-mediated MT2 inhibits aeromonas-goblet cell interactions to restore the level of MUC2 production via the LPS/TLR4/MyD88/GSK-3β/ROS/NF-κB loop, further improving colitis in SD mice. Certainly, additional loss-of-function experiments using knock-down or knock-out mice/cell lines would be useful.

5. Conclusions

Overall, our study revealed that MT2-mediated MT suppressed *Aeromonas* coupling with goblet cells and restored MUC2 depletion by inhibiting the TLR4/MyD88/GSK-3β/β-catenin/ROS/NF-κB loop, ultimately improving SD-induced colitis in mice. Obviously, the study supported original evidence for the useful influence of MT as a physiological controller of *Aeromonas*-induced MUC2 deficiency and supported the recent enlarging of the definition of psychobiotics to include MT-based strategies.

Data Availability

All data generated or analysed during this study are included in this published article.

Conflicts of Interest

The authors declare that they have no potential conflicts of interest, including any financial, personal, or other relationships, with other people or organizations.

Acknowledgments

Thanks to all the members of neurobiology lab. This work was supported by the Beijing Natural Science Foundation (6222019) and the Chinese National Natural Science Foundation (31873000 and 32172801).

Supplementary Materials

See supplementary methods and Figures S1-S8 in the Supplementary Material for comprehensive image analysis. *(Supplementary Materials)*

References

[1] T. Gao, Z. Wang, J. Cao, Y. Dong, and Y. Chen, "Melatonin ameliorates corticosterone-mediated oxidative stress induced colitis in sleep-deprived mice involving gut microbiota," *Oxidative Medicine and Cellular Longevity*, vol. 2021, Article ID 9981480, 2021.

[2] T. Gao, T. Wang, Z. Wang, J. Cao, Y. Dong, and Y. Chen, "Melatonin-mediated MT2 attenuates colitis induced by dextran sodium sulfate via PI3K/AKT/Nrf2/SIRT1/RORα/NF-κB signaling pathways," *International Immunopharmacology*, vol. 96, article 107779, 2021.

[3] T. Gao, Z. Wang, Y. Dong, J. Cao, and Y. Chen, "Melatonin-mediated colonic microbiota metabolite butyrate prevents acute sleep deprivation-induced colitis in mice," *International Journal of Molecular Sciences*, vol. 22, no. 21, p. 11894, 2021.

[4] T. Qazi and F. A. Farraye, "Sleep and inflammatory bowel disease: an important bi-directional relationship," *Inflammatory Bowel Diseases*, vol. 25, no. 5, pp. 843–852, 2019.

[5] G. R. Swanson, H. J. Burgess, and A. Keshavarzian, "Sleep disturbances and inflammatory bowel disease: a potential trigger for disease flare?," *Expert Review of Clinical Immunology*, vol. 7, no. 1, pp. 29–36, 2011.

[6] K. Vlantis, A. Polykratis, P. S. Welz, G. van Loo, M. Pasparakis, and A. Wullaert, "TLR-independent anti-inflammatory function of intestinal epithelial TRAF6 signalling prevents DSS-induced colitis in mice," *Gut*, vol. 65, no. 6, pp. 935–943, 2016.

[7] M. Parlato and G. Yeretssian, "NOD-like receptors in intestinal homeostasis and epithelial tissue repair," *International Journal of Molecular Sciences*, vol. 15, no. 6, pp. 9594–9627, 2014.

[8] M. Shan, M. Gentile, J. R. Yeiser et al., "Mucus enhances gut homeostasis and oral tolerance by delivering immunoregulatory signals," *Science*, vol. 342, no. 6157, pp. 447–453, 2013.

[9] I. B. Renes and I. Van Seuningen, "Mucins in intestinal inflammatory diseases: their expression patterns, regulation, and roles," in *The Epithelial Mucins: Structure/Function Roles in Cancer and Inflammatory Diseases*, I. Seuningen, Ed., pp. 211–232, Research Signpost, Lille, France, 2008.

[10] T. Hamada, M. Goto, H. Tsutsumida et al., "Mapping of the methylation pattern of the MUC2 promoter in pancreatic cancer cell lines, using bisulfite genomic sequencing," *Cancer Letters*, vol. 227, no. 2, pp. 175–184, 2005.

[11] L. Wang, H. Cao, L. Liu et al., "Activation of epidermal growth factor receptor mediates mucin production stimulated by p40, a *Lactobacillus rhamnosus* GG-derived protein∗," *The Journal of Biological Chemistry*, vol. 289, no. 29, pp. 20234–20244, 2014.

[12] A. Gopal, S. C. Iyer, U. Gopal, N. Devaraj, and D. Halagowder, "Shigella dysenteriae modulates BMP pathway to induce mucin gene expression in vivo and in vitro," *PLoS One*, vol. 9, no. 11, article e111408, 2014.

[13] N. Ma, J. Zhang, R. J. Reiter, and X. Ma, "Melatonin mediates mucosal immune cells, microbial metabolism, and rhythm crosstalk: A therapeutic target to reduce intestinal inflammation," *Medicinal Research Reviews*, vol. 40, no. 2, pp. 606–632, 2020.

[14] C. Q. Chen, J. Fichna, M. Bashashati, Y. Y. Li, and M. Storr, "Distribution, function and physiological role of melatonin in the lower gut," *World Journal of Gastroenterology*, vol. 17, no. 34, pp. 3888–3898, 2011.

[15] N. Burger-van Paassen, L. M. P. Loonen, J. Witte-Bouma et al., "Mucin Muc2 deficiency and weaning influences the expression of the innate defense genes Reg3β, Reg3γ and angiogenin-4," *PLoS One*, vol. 7, no. 6, article e38798, 2012.

[16] J. P. Ouwerkerk, W. M. de Vos, and C. Belzer, "Glycobiome: Bacteria and mucus at the epithelial interface," *Best Practice & Research. Clinical Gastroenterology*, vol. 27, no. 1, pp. 25–38, 2013.

[17] M. E. Johansson, H. E. Jakobsson, J. Holmén-Larsson et al., "Normalization of host intestinal mucus layers requires long-term microbial colonization," *Cell Host & Microbe*, vol. 18, no. 5, pp. 582–592, 2015.

[18] T. Gao, Z. X. Wang, Y. L. Dong et al., "Role of melatonin in sleep deprivation-induced intestinal barrier dysfunction in mice," *Journal of Pineal Research*, vol. 67, article e12574, 2019.

[19] L. Zhang, H. Q. Zhang, X. Y. Liang, H. F. Zhang, T. Zhang, and F. E. Liu, "Melatonin ameliorates cognitive impairment induced by sleep deprivation in rats: role of oxidative stress, BDNF and CaMKII," *Behavioural Brain Research*, vol. 256, pp. 72–81, 2013.

[20] M. Stebegg, A. Silva-Cayetano, S. Innocentin et al., "Heterochronic faecal transplantation boosts gut germinal centres in aged mice," *Nature Communications*, vol. 10, no. 1, p. 2443, 2019.

[21] S. N. Murthy, H. S. Cooper, H. Shim, R. S. Shah, S. A. Ibrahim, and D. J. Sedergran, "Treatment of dextran sulfate sodium-induced murine colitis by intracolonic cyclosporin," *Digestive Diseases and Sciences*, vol. 38, no. 9, pp. 1722–1734, 1993.

[22] J. L. Parker and J. G. Shaw, "*Aeromonas* spp. clinical microbiology and disease," *The Journal of Infection*, vol. 62, no. 2, pp. 109–118, 2011.

[23] D. Tena, A. González-Praetorius, C. Gimeno, M. Teresa Pérez-Pomata, and J. Bisquert, "Extraintestinal infection due to *Aeromonas* spp.: review of 38 cases," *Enfermedades Infecciosas y Microbiología Clínica*, vol. 25, no. 4, pp. 235–241, 2007.

[24] M. H. Derakhshan, N. J. Goodson, J. Packham et al., "Association of diverticulitis with prolonged spondyloarthritis: an analysis of the ASAS-COMOSPA international cohort," *Journal of Clinical Medicine*, vol. 8, no. 3, p. 281, 2019.

[25] M. Van der Sluis, B. A. De Koning, A. C. De Bruijn et al., "Muc2-deficient mice spontaneously develop colitis, indicating that MUC2 is critical for colonic protection," *Gastroenterology*, vol. 131, no. 1, pp. 117–129, 2006.

[26] S. A. Shah, M. Khan, M. H. Jo, M. G. Jo, F. U. Amin, and M. O. Kim, "Melatonin stimulates the SIRT1/Nrf2 signaling pathway counteracting lipopolysaccharide (LPS)-induced oxidative stress to rescue postnatal rat brain," *CNS Neuroscience & Therapeutics*, vol. 23, no. 1, pp. 33–44, 2017.

[27] X. Cao, "Self-regulation and cross-regulation of pattern-recognition receptor signalling in health and disease," *Nature Reviews. Immunology*, vol. 16, no. 1, pp. 35–50, 2016.

[28] H. Ikeda, M. Sasaki, A. Ishikawa et al., "Interaction of toll-like receptors with bacterial components induces expression of CDX2 and MUC2 in rat biliary epithelium in vivo and in culture," *Laboratory Investigation*, vol. 87, no. 6, pp. 559–571, 2007.

[29] F. L. Sage, O. Meilhac, and M. P. Gonthier, "Porphyromonas gingivalis lipopolysaccharide induces pro-inflammatory adipokine secretion and oxidative stress by regulating Toll-like receptor- mediated signaling pathways and redox enzymes in adipocytes," *Molecular and Cellular Endocrinology*, vol. 446, pp. 102–110, 2017.

[30] K. P. Hoeflich, J. Luo, E. A. Rubie, M. S. Tsao, O. Jin, and J. R. Woodgett, "Requirement for glycogen synthase kinase-3beta in cell survival and NF-kappaB activation," *Nature*, vol. 406, no. 6791, pp. 86–90, 2000.

Hindawi
Oxidative Medicine and Cellular Longevity
Volume 2022, Article ID 9151169, 14 pages
https://doi.org/10.1155/2022/9151169

Research Article

Expression of Oxidative Phosphorylation Complexes and Mitochondrial Mass in Pediatric and Adult Inflammatory Bowel Disease

Anna M. Schneider,[1] **Mihriban Özsoy**,[1] **Franz A. Zimmermann**,[1] **Susanne M. Brunner**,[1] **René G. Feichtinger**,[1] **Johannes A. Mayr**,[1] **Barbara Kofler**,[1] **Daniel Neureiter**,[2] **Eckhard Klieser**,[2] **Elmar Aigner**,[3] **Sebastian Schütz**,[4] **Nathalie Stummer**,[1] **Wolfgang Sperl**,[1] **and Daniel Weghuber**[1]

[1]*Department of Pediatrics, University Hospital Salzburg, Paracelsus Medical University, Salzburg, Austria*
[2]*Department of Pathology, University Hospital Salzburg, Paracelsus Medical University, Salzburg, Austria*
[3]*First Department of Medicine, University Hospital Salzburg, Paracelsus Medical University, Salzburg, Austria*
[4]*Department of Mathematics, Paris Lodron University, Salzburg, Austria*

Correspondence should be addressed to René G. Feichtinger; r.feichtinger@salk.at

Received 25 August 2021; Revised 23 November 2021; Accepted 6 December 2021; Published 6 January 2022

Academic Editor: Daniela Ribeiro

Introduction. Inflammatory bowel disease (IBD), which includes Crohn's disease (CD) and ulcerative colitis (UC), is a multifactorial intestinal disorder but its precise etiology remains elusive. As the cells of the intestinal mucosa have high energy demands, mitochondria may play a role in IBD pathogenesis. The present study is aimed at evaluating the expression levels of mitochondrial oxidative phosphorylation (OXPHOS) complexes in IBD. *Material and Methods*. 286 intestinal biopsy samples from the terminal ileum, ascending colon, and rectum from 124 probands (34 CD, 33 UC, and 57 controls) were stained immunohistochemically for all five OXPHOS complexes and the voltage-dependent anion-selective channel 1 protein (VDAC1 or porin). Expression levels were compared in multivariate models including disease stage (CD and UC compared to controls) and age (pediatric/adult). *Results*. Analysis of the terminal ileum of CD patients revealed a significant reduction of complex II compared to controls, and a trend to lower levels was evident for VDAC1 and the other OXPHOS complexes except complex III. A similar pattern was found in the rectum of UC patients: VDAC1, complex I, complex II, and complex IV were all significantly reduced, and complex III and V showed a trend to lower levels. Reductions were more prominent in older patients compared to pediatric patients and more marked in UC than CD. *Conclusion*. A reduced mitochondrial mass is present in UC and CD compared to controls. This is potentially a result of alterations of mitochondrial biogenesis or mitophagy. Reductions were more pronounced in older patients compared to pediatric patients, and more prominent in UC than CD. Complex I and II are more severely compromised than the other OXPHOS complexes. This has potential therapeutic implications, since treatments boosting biogenesis or influencing mitophagy could be beneficial for IBD treatment. Additionally, substances specifically stimulating complex I activity should be tested in IBD treatment.

1. Introduction

Inflammatory bowel disease (IBD) with its two major clinical forms, ulcerative colitis (UC) and Crohn's disease (CD), is a chronic relapsing inflammatory disorder of the intestine [1]. UC is defined as a continuous and superficial, mucosal, and submucosal inflammation limited to the colon. CD, on the other hand, is characterized by scattered lesions affecting any part of the gastrointestinal tract, with transmural inflammation associated with many complications [2]. Although the exact etiology of IBD is still enigmatic, it is known to be a multifactorial disease that results from a complex interplay

of genetic susceptibility, an altered immune response, changes in the intestinal microbiota, and environmental triggers [3]. Destruction of the intestinal epithelial barrier, increased permeability, dysfunctional immunoregulation, and increased invasion by immune cells are central disease mechanisms [4–6]. Although IBD may develop at any age, up to 25% of patients are diagnosed during childhood or adolescence [7, 8]. Previous reports have suggested that the age of disease onset correlates inversely with disease outcome, indicating that younger age may be an important risk factor for aggressive, treatment-resistant disease [9].

Mitochondria supply cells with energy by producing adenosine triphosphate (ATP) via the action of oxidative phosphorylation (OXPHOS) complexes I to V [10]. Cells with high energy demand, like intestinal epithelial cells, tend to be more vulnerable to the consequences of mitochondrial dysfunction. Several possible links between mitochondria and IBD have been reported. For example, elevated levels of reactive oxygen species (ROS) were observed in mitochondria of patients with IBD [11, 12], highlighting oxidative injury in IBD pathology. Furthermore, recent data suggest that mitochondrial dysfunction compromises the intestinal barrier and may contribute to IBD pathogenesis [11, 13–18]. Additionally, IBD patients have significantly higher levels of circulating mitochondrial DNA (mtDNA) in their plasma and feces. Moreover, their mtDNA levels correlate with the severity and activity of the disease, and mtDNA was found to serve as a proinflammatory damage-associated molecular pattern during active IBD [19]. Regarding mitochondrial function and morphology in the gut, several studies showed a significant deficiency in the enzyme activity of OXPHOS complexes as well as changes in morphological appearance of mitochondria [17, 18]. Another study reported loss of cytochrome c oxidase (COX; complex IV) to be an indicator of tumor progression in adults with UC [20]. Studies of mitochondrial dysfunction in pediatric IBD are scarce: there are two clinical cases and one study that focused on the interplay between the intestinal microbiota and mitochondria [21–23]. Specific mitochondrial proteins were shown to be the primary proteins downregulated in IBD, suggesting a regulatory interaction between mitochondria and the intestinal microbiota as well as a resulting imbalance of this relationship in CD patients. More recently, transcriptome analysis of rectal mucosal specimens revealed downregulation of mitochondria related genes in a large pediatric UC cohort [24].

The aim of this study was to investigate if there are defects in OXPHOS complex expression in IBD, whether the grade of inflammation correlates with alterations in OXPHOS expression, and whether there are differences in OXPHOS expression in pediatric versus adult IBD (Figure 1).

2. Material and Methods

The study was approved by the local ethics committee *(415-E/2080/5-2016)* and conducted in accordance with the Helsinki Declaration of 1975 (revised 2013).

2.1. Patients and Tissue Samples. Patients with chronic abdominal pain, elevated fecal calprotectin, or signs and symptoms of IBD underwent diagnostic colonoscopy. In routine ileocolonoscopies performed at the hospital, biopsy specimens were taken from the intestinal epithelium in a stepwise approach starting from the terminal ileum and including all segments of the colon (the cecum, ascending colon, transverse colon, descending colon, sigmoid colon, and rectum). The specimens were then analyzed by pathologists and used by clinicians to confirm the diagnosis. The remaining biopsy material was obtained from the Institute of Pathology, University Hospital Salzburg, Austria, and used for the present study.

If the diagnosis of IBD was established by macroscopic and histologic evaluation, patients were assigned to our study group. If colonoscopy did not show any abnormalities on gross or on microscopic analysis, patients were assigned to the control group. A pathologist verified that the samples in the control group had no abnormalities by using a histologic severity score (HSS) from 0 to 3, which included evaluation of crypt architecture (0-3), acute and chronic inflammation (each 0-3), and regeneration of the epithelium (0-3), resulting in a range of integer values from 0 to 12 before the average of all 4 components was determined. Only samples with an average score of less than or equal 1 were included in the control group. Some samples of the control group were used previously [25].

As CD mainly affects the terminal ileum, one biopsy per CD patient was obtained from that location. Similarly, the rectum is the most commonly affected site in UC, so one rectal biopsy per patient was obtained in the UC cohort. From each patient, a biopsy from the ascending colon was used as well, to enable comparison of all study groups based on the same anatomical site. Samples from the terminal ileum, ascending colon, and rectum were examined in the control group.

In the diseased groups (pediatric and adult IBD), only newly diagnosed patients were included, ensuring that these patients did not receive any prior IBD-specific treatment, which may have influenced the results.

2.2. Immunohistochemistry. The samples were fixed in 4% neutral- buffered formalin and embedded in paraffin and cut in 4 μm sections with a microtome, and three samples each were placed on a specimen holder. Immunohistochemical (IHC) staining was performed as previously described by Zimmermann et al. [26, 27]. The following antibodies were used: mouse monoclonal anti-complex I subunit NDUFS4 (WH0004724M1-100UG, dilution 1 : 1000; Sigma Aldrich, St. Louis, USA), mouse monoclonal anti-complex II subunit SDHA (ab14715, 1 : 3000; Abcam, Cambridge, UK), mouse monoclonal anti-complex III subunit core 2 (UQCRC2; ab14745, 1 : 2000; Abcam, Cambridge, UK), mouse monoclonal anti-complex IV subunit I (MT-CO1; ab14705, 1 : 1000; Abcam, Cambridge, UK), mouse monoclonal anti-complex V subunit alpha (ATP5F1A; ab14748, 1 : 2000; Abcam, Cambridge, UK), and mouse monoclonal porin antibody subunit VDAC1 (ab14734, 1 : 2000; Abcam, Cambridge, UK). All primary antibodies were diluted in Dako antibody diluent with background-reducing components (Dako, Glostrup, Denmark). Digital micrographs were taken

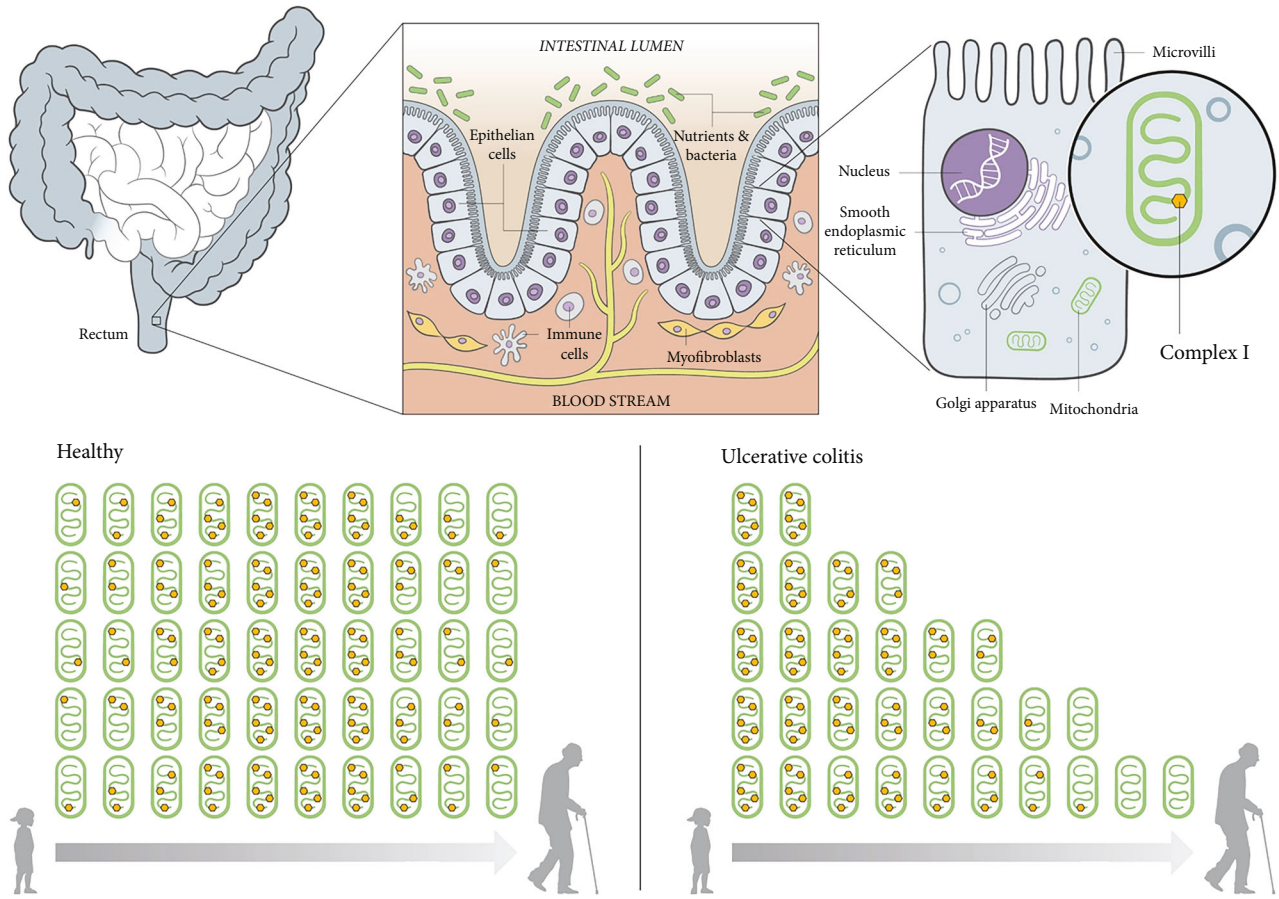

Figure 1: Overview and results of complex I in ulcerative colitis. The rectum, which is one of the main affected sites in ulcerative colitis, is located in the last part of the large intestine (a). The luminal surface of the intestine is formed by an epithelial layer, which is composed of simple columnar epithelial cells separating the intestinal lumen from the blood stream. It is responsible for the absorption of useful substances and acts as a barrier in preventing harmful substances migrating from the gut to other parts of the body (b). The epithelium is composed of simple columnar epithelial cells, which contain numerous mitochondria and other organelles. The mitochondria are composed of inner and outer membranes. Proteins in the latter, like VDAC1, represent the mitochondrial mass. The inner membrane harbors the respiratory chain with its complexes and is responsible for producing energy via oxidative phosphorylation (c). In a healthy state, mitochondrial mass stays stable across the life span and the average protein expression levels of the respiratory chain subunits, here represented by complex I, increase continuously from childhood onward, peak in middle age, and decline thereafter (d). In ulcerative colitis, a trend of continuous deterioration of mitochondrial mass and complex I is seen from childhood onward (e).

with a Moticam 5+ camera using Motic Images Plus 2.0 software (Motic, Wetzlar, Germany).

2.3. Evaluation and Statistics. The staining intensity and overall protein expression (percentage of cells staining positive) of OXPHOS complexes I-V and VDAC1 (porin) for each sample were assessed by two independent examiners blinded to each other and to information regarding the diagnosis or patient's age. A scoring system (0: no staining; 1: weak staining; 2: moderate staining; and 3: strong staining) was used to quantify the levels of staining intensity (Figure 2). The intensities were multiplied by the percentage of positive cells present in the specimen to yield score values, as semiquantitative indicators for expression level [27].

2.4. Statistical Analysis. Epidemiological data were analyzed descriptively. Due to the ordinal data level, expression scores were compared by median and interquartile range (IQR), and graphical representation was done by boxplots and scatterplots. Expression levels were compared in multivariate models per intestinal section by the nonparametric method of Dobler et al., including disease (CD, UC) vs. controls, age (pediatric vs. adults), and the interaction in all models [28]. p values of these three models were corrected using the Bonferroni method.

In a next step, expression levels were analyzed separately for each complex to examine complex-specific differences [29]. This was done first for all IBD patients vs. controls (CD in the terminal ileum, UC in the rectum and CD and UC in the ascending colon). In a second step, samples were stratified by age. As healthy controls have already been compared through their lifespan [25], only IBD patients were included in this study. Nonparametric ANOVA-type statistics were used to examine variable effects. Due to the exploratory style

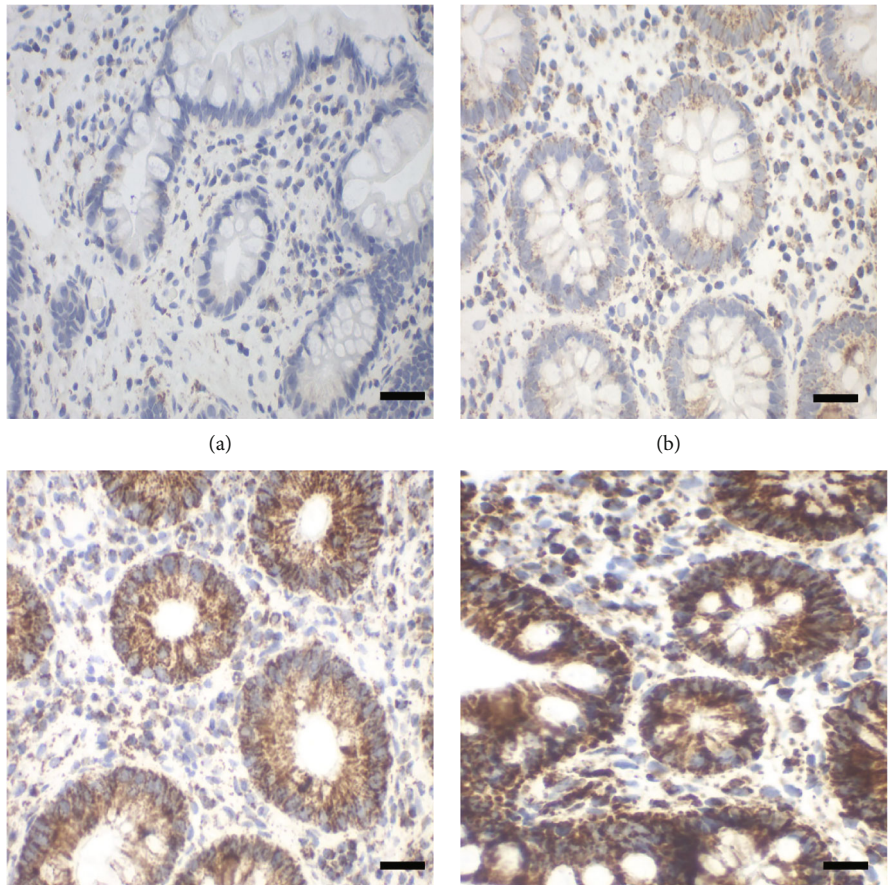

(a) (b) (c) (d)

Figure 2: Assessment of staining intensities (0 to 3) with complex I antibody (subunit NDUFS4). Staining intensity 0: no staining, due to no primary antibody control (a, case number 7229); 1: weak staining (b, case number 41197); 2: moderate staining (c, case number 33837); and 3: strong staining (d, case number 5905). Scale bar 100 μm.

of this further analysis, no p value correction was applied. For the ascending colon, post hoc analysis was done when results were significant so as to distinguish exactly between the three groups.

In a final step, expression levels were stratified by degree of inflammation level (HSS), and correlation analysis for age and stage was done. By definition, the control group had HSS levels less than 1, whereas CD and UC patients had scores from 1 to 3.

All tests were carried out at the 5% significance level. All calculations were performed using R software (version, 4.0.2).

3. Results

3.1. Patient Characteristics. In total, 286 samples from 124 probands (34 CD, 33 UC, and 57 controls) were stained immunohistochemically for all five OXPHOS complexes and VDAC1 (Table 1). 19 samples had to be excluded due to low quality of the sample or no crypts on the sample. The mean age was 38 years, and 46 patients were below 18 years of age, 58% being female and 42% male. The patients were divided into 4 subgroups: pediatric patients with IBD (p-IBD), adult patients with IBD (a-IBD), children and adolescents without IBD or any inflammation (pediatric controls), and adults without IBD or any inflammation (adult controls).

Table 1: Patient characteristics.

Group	Number of patients	Age, mean (range) (years)	Sex, female (%)
p-IBD	28 (CD = 15, CU = 13)	12.6 (3-17)	16 (57)
a-IBD	39 (CD = 19, CU = 20)	52.7 (27-89)	22 (51)
Pediatric controls	18	12.5 (3-17)	10 (59)
Adult controls	39	53.6 (20-82)	26 (65)
Total	124		

p-IBD: children and adolescents with inflammatory bowel disease (IBD); a-IBD: adults with IBD; pediatric controls and adult controls; CD: Crohn's disease; UC: ulcerative colitis.

Regarding evaluation, the average interobserver variability between the two examiners was 0.24 points within the intensity of the staining and 6.31% regarding the percentage of positive cells.

For further statistical analysis, multivariate models per intestinal segment examined all complexes and VDAC1

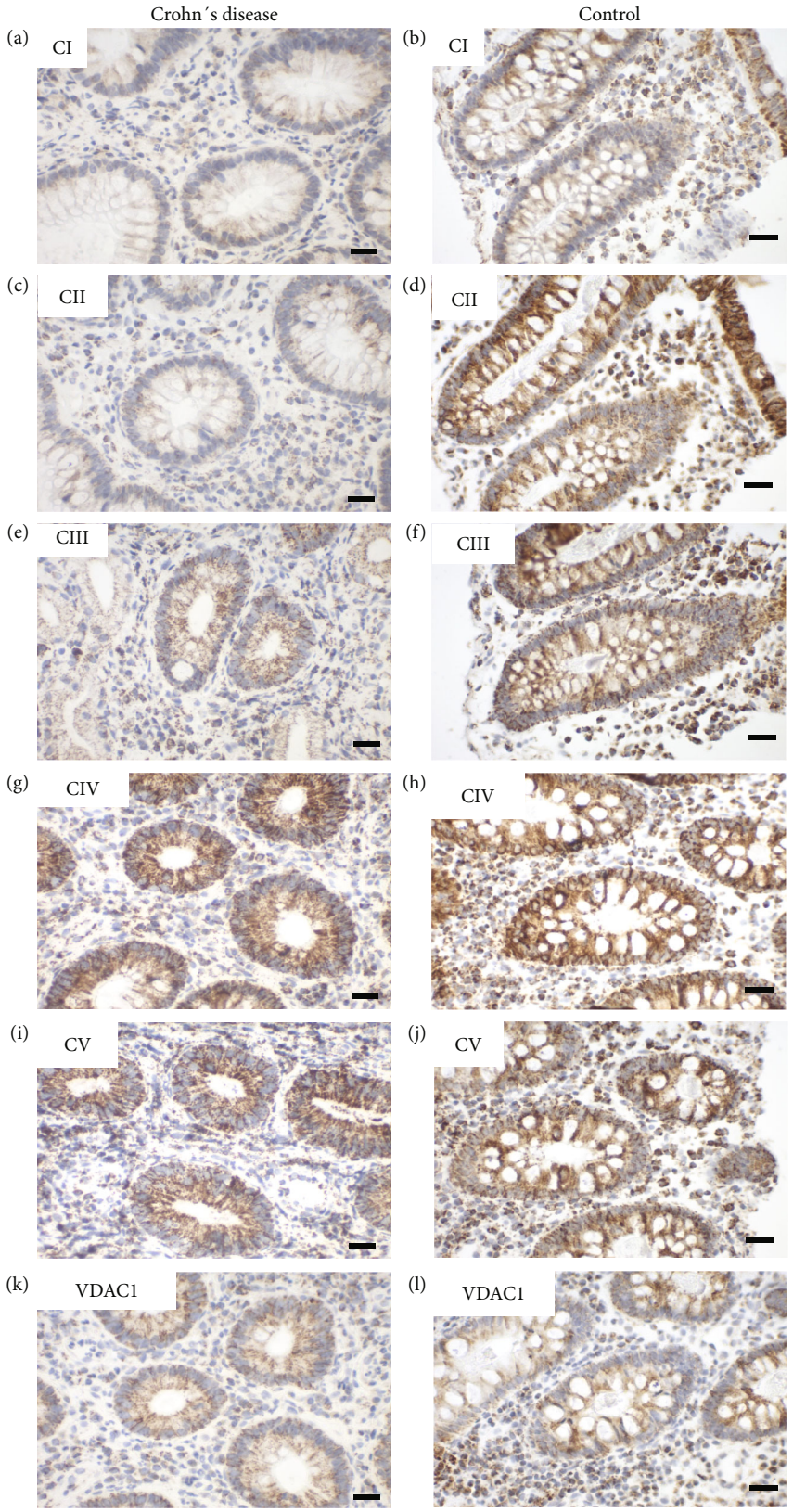

Figure 3: Representative images of immunohistochemical staining of complex I-V and VDAC 1 in the terminal ileum in pediatric Crohn's disease (CD) (case number 11760) and a control (case number 18642). (a, b) Complex I, (c, d) complex II, (e, f) complex III, (g, h) complex IV, (i, j) complex V, and (k, l) VDAC1 (porin). Weaker staining is present in complex I and II and VDAC1 in CD. Scale bar 100 μm.

Table 2: Expression levels of OXPHOS complexes I to V and VDAC1 (porin) in the terminal ileum in Crohn's disease (CD).

	CI	CII	CIII	CIV	CV	VDAC1
Expression level, mean (SD)						
CD	138 (68)	115 (63)	166 (61)	206 (50)	168 (68)	139 (44)
Controls	175 (65)	156 (62)	177 (48)	233 (44)	178 (51)	150 (43)
Reduction controls- CD	37 (21%)	41 (26%)	11 (6%)	27 (12%)	10 (6%)	11 (7%)
p value	0.053	0.030*	0.895	0.081	0.850	0.442

It is shown as mean with standard deviation (SD) and reduction of expression level in CD patients compared to the control group. *$p < 0.05$.

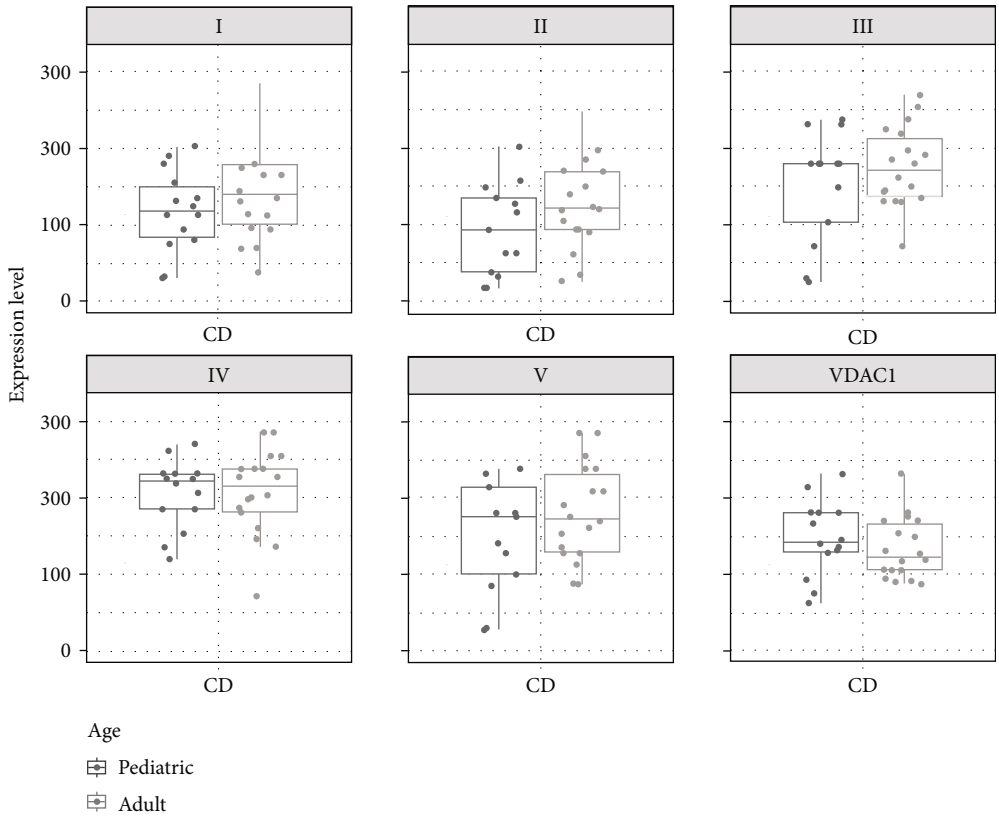

Figure 4: Boxplots and scatterplots showing expression levels of OXPHOS complexes I-V and VDAC1 (porin) in the terminal ileum in Crohn's disease (CD) in pediatric and adult patients.

simultaneously, with group (CD, UC, and controls) and age (pediatric and adult) as covariates first.

3.2. Crohn's Disease (Terminal Ileum). To elucidate whether there are differences in the expression of subunits of the OXPHOS complexes I to V and VDAC1 samples of the terminal ileum of CD patients and age-matched controls were investigated (Figure 3).

VDAC1 levels were moderately diminished by 7% compared to controls. Consistently, levels of subunits of the OXPHOS complexes were diminished by 10-26% with exception of complex III subunit UQCRC2 in CD (Table 2). Across all age groups, CD patients have a reduction of almost 30% in complex II levels compared to that of age-matched controls. The magnitude of the reduction of the NDUFS4 subunit of complex I was equal (21% reduction). However, it was not significant because of a higher standard deviation.

When CD patients were stratified by age, no significant differences in the expression levels of all complexes were seen between pediatric and adult patients. However, minor trends to higher levels were present for all subunits of the OXPHOS complexes. In contrast mitochondrial mass (VDAC1) tended to be lower with increasing age (Figure 4).

To evaluate a potential connection between mitochondrial expression and inflammation, score values of expression levels were stratified by degree of inflammation (HSS). The control group showed high mitochondrial expression levels, comparable to those of CD patients with higher inflammation, while the lowest expression levels were found in the moderate inflammation group of CD patients (HSS 1.5). Adults tended

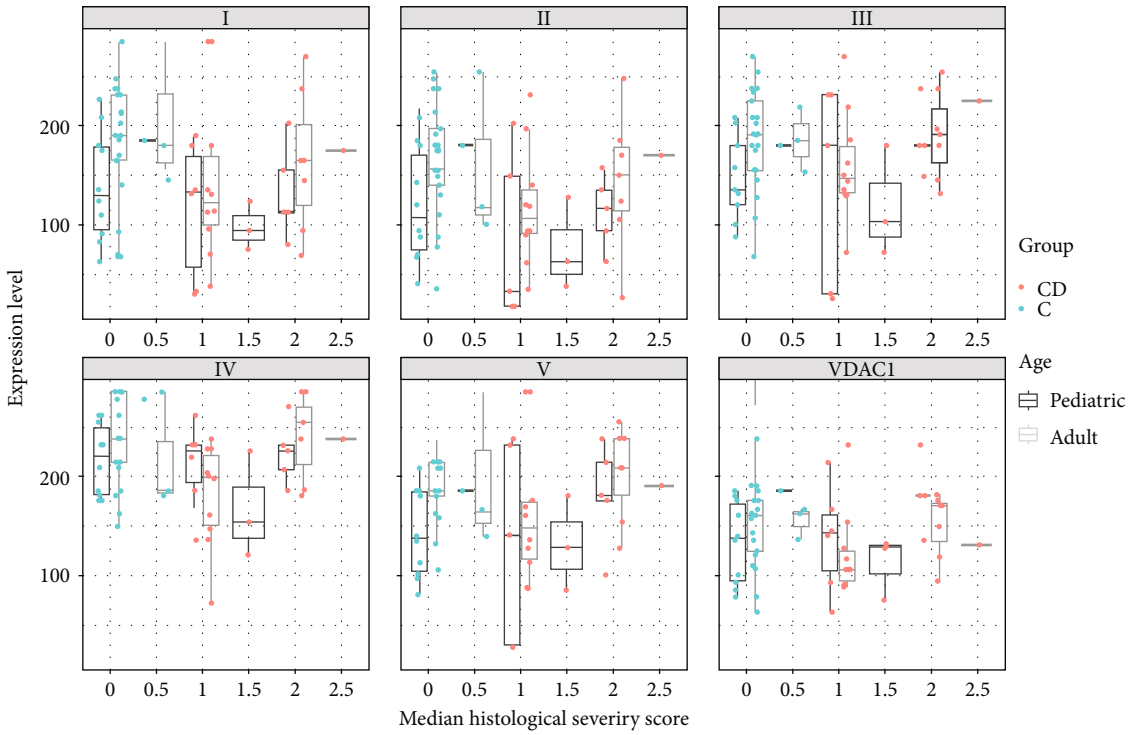

Figure 5: Boxplots and scatterplots of expression levels of OXPHOS complexes I-V and VDAC1 (porin) stratified by age and histological severity score (HSS) in the terminal ileum in Crohn's disease (CD) and controls (C). 0 indicates no histological abnormalities, 2.5 severe signs of inflammation.

to have a higher correlation of inflammation and mitochondrial expression level, while children showed a weaker correlation (spearman correlation 0.312 vs. 0.154; Figure 5).

3.3. Ulcerative Colitis (Rectum). IHC staining of subunits of the complexes I to V and VDAC1 in the rectum was done in tissue samples from UC patients and age-matched controls (Figure 6). VDAC1 was significantly reduced in UC patients compared to controls ($p = 0.009$; reduction by 24%). Consistently, all chosen subunits of the OXPHOS complexes were diminished by 12-43% compared to controls (Table 3). Subunits of complex I, complex II, and complex IV were significantly lower, whereas complex III and V only showed a trend to lower levels.

Stratification of UC patients by age revealed a trend to lower expression for complexes I and IV and VDAC1 in adults, whereas higher expression with increasing age was seen for complex II, III, and V (Figure 7).

Score values of expression levels stratified by degree of inflammation showed an undulating course of expression levels for different degrees of inflammation, but like in CD, patients with the highest HSS inflammatory scores exhibited higher mitochondrial expression levels compared to patients with only moderate degrees of inflammation. Children showed a trend for higher correlation of inflammation and expression level, whereas adults tended to have a weak correlation (Spearman correlation 0.419 vs. 0.165, Figure 8).

3.4. Comparison of IBD Patients and Controls in the Ascending Colon. In the ascending colon, all IBD patients (CD and UC) exhibited lower levels of complexes I, II, and V and VDAC1 compared to age-matched controls. Complex II was most affected, showing a reduction of 51%, followed by complex I, which was reduced by 36%, VDAC1 reduced by 34%, and complex V reduced by 23% compared to the expression levels of the control group. No difference was identified between the groups in the expression of complexes IV and V (Table 4).

A reduction in VDAC1 was found for pediatric IBD patients versus adult IBD patients ($p < 0.05$). Stratified by disease subtype, adult CD patients showed higher expression levels of complexes II, III, and V, and a trend in complex I and IV, but lower expression of VDAC1 compared to pediatric patients. In the UC-subgroup, expression in adults tended to be lower for complex IV and VDAC1 and higher for all other complexes, but no significant differences were found (Figure 9).

4. Discussion

The present study characterized OXPHOS expression and mitochondrial mass in the intestinal mucosa of children and adults with IBD compared to controls. The expression levels of OXPHOS complexes in healthy individuals were recently shown to increase from childhood onward and then decline in older subjects [25]. These data suggest that reductions in the levels of mitochondrial OXPHOS complexes in intestinal crypts might be transiently compensated in adulthood, but that, ultimately, reduced expression occurs in persons aged 60 years and older.

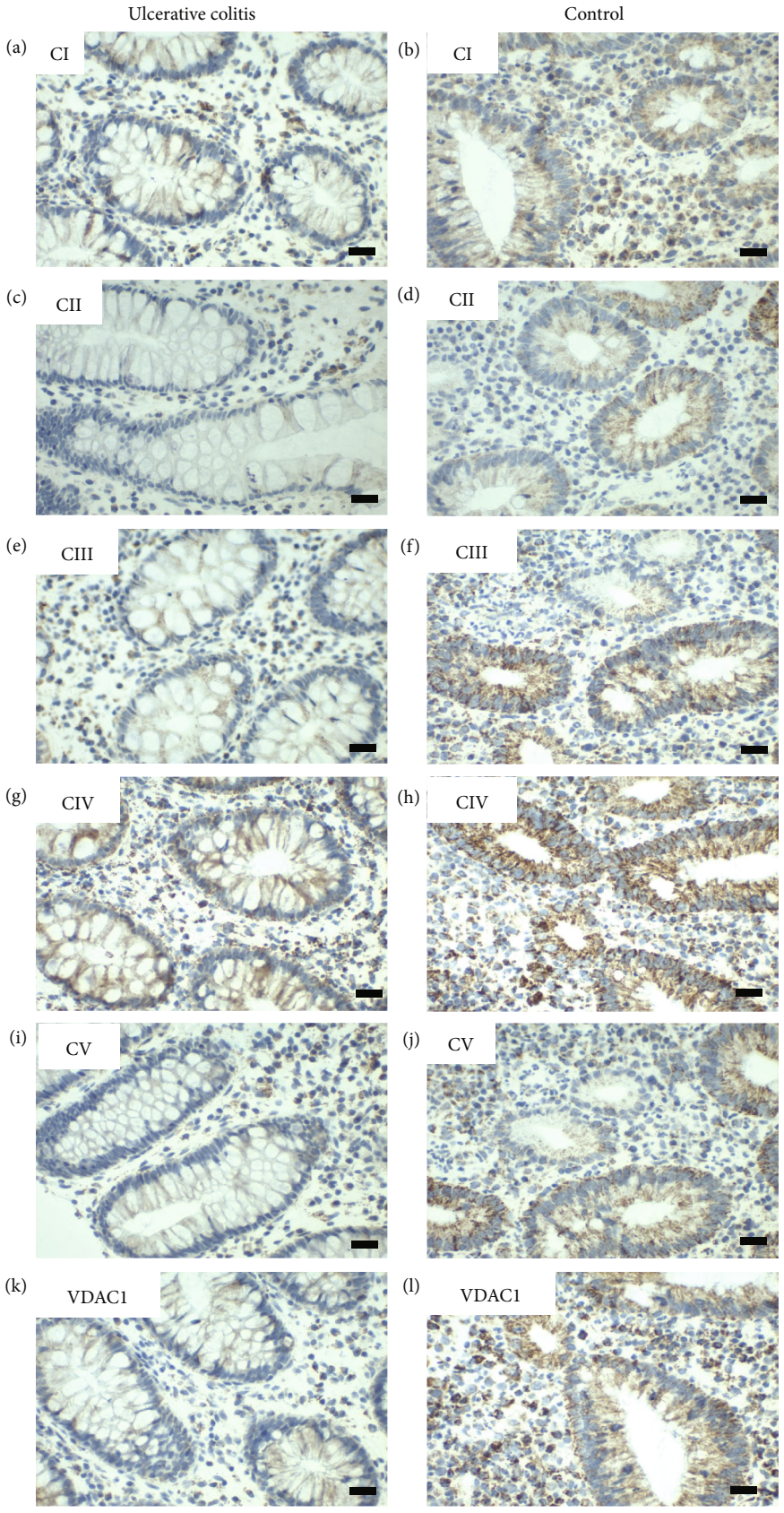

Figure 6: Representative images of immunohistochemical staining of complex I-V and VDAC 1 in the rectum in pediatric ulcerative colitis (UC) (case number 18385) and a control (case number 1867). (a, b) Complex I, (c, d) complex II, (e, f) complex III, (g, h) complex IV, (i, j) complex V, and (k, l) VDAC 1 (porin). Weaker staining is seen in all complexes of the UC patient. Scale bar 100 μm.

Table 3: Expression levels of OXPHOS complexes I to V and VDAC 1 (porin) in the rectum in ulcerative colitis (UC).

	CI	CII	CIII	CIV	CV	VDAC1
Expression level, mean (SD)						
UC	114 (69)	110 (70)	166 (65)	202 (42)	151 (54)	113 (48)
Controls	200 (75)	151 (73)	192 (67)	229 (65)	180 (54)	149 (50)
Reduction controls- UC	86 (43%)	41 (27%)	26 (14%)	27 (12%)	29 (16%)	36 (24%)
p value	<0.001*	0.024*	0.182	0.013*	0.182	0.009*

It is shown as mean with standard deviation (SD) and reduction of expression level in CD patients compared to control group. *$p < 0.05$.

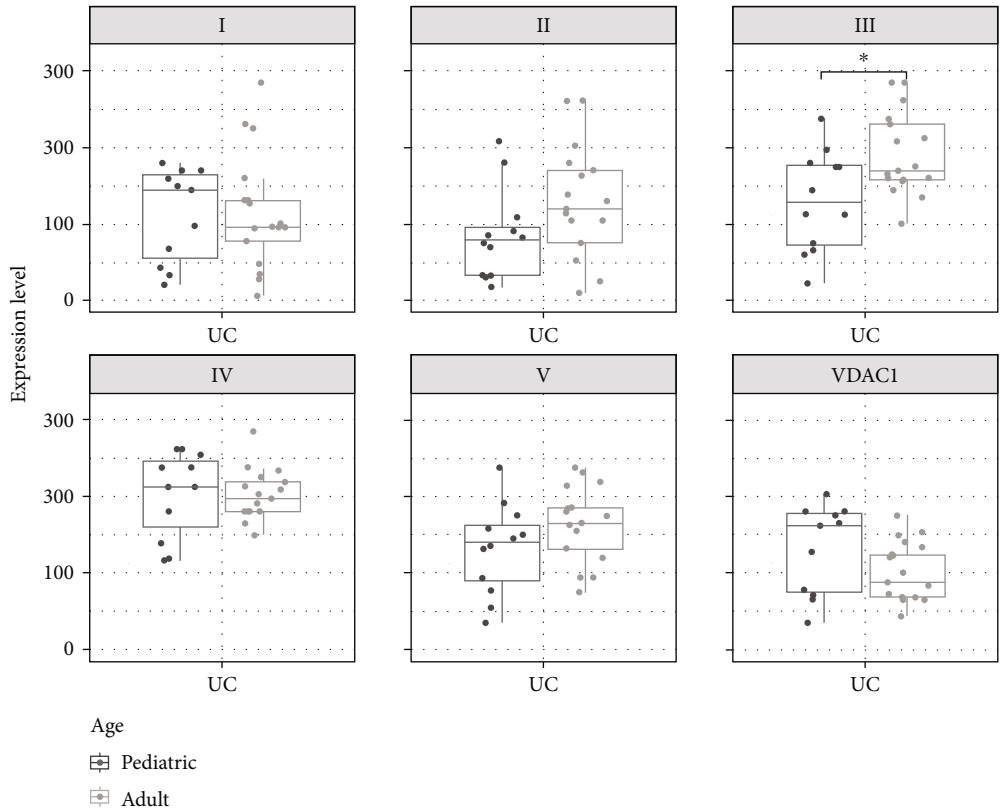

Figure 7: Boxplots and scatterplots showing expression levels of OXPHOS complexes I-V and VDAC1 (porin) in the rectum of pediatric and adult ulcerative colitis (UC) patients. *Significance ($p < 0.05$).

In IBD, the levels of OXPHOS subunits were reduced across all age groups. The defects were more frequent in adult than in pediatric patients and more prominent in UC than in CD (Figure 1). A significant reduction of VDAC1 was present in UC compared to controls, and there was a trend to lower levels in CD. VDAC1 is the gold standard marker protein for mitochondrial mass [30, 31].

Whether the reduction in mitochondrial mass is a consequence of lower mitochondrial biogenesis or higher mitophagy (or both mechanisms) remains to be elucidated. PGC-1α is a master regulator of mitochondrial biogenesis [32, 33]. Deletion of the PGC-1α gene causes spontaneous colitis and increases susceptibility to experimental colitis, and also PPAR-γ, the target of PGC-1α, was reported to be downregulated in UC [34]. Nitric oxide (NO), a well-known effector molecule with diverse functions, has been reported to be a stimulator of mitochondrial biogenesis [35]. NO has also been associated with the initiation and maintenance of inflammation in human IBD [36].

The second principal mechanism to explain the reduction in mitochondrial mass is an increase in autophagy or more specifically mitophagy, a process which removes damaged mitochondria. Indeed, a plethora of proteins associated with autophagy contribute to the pathogenesis of IBD [37–39]. We found normal amounts of the UQCRC2 subunit of complex III in our patient cohort. This might reflect compensatory upregulation in response to the reduced mitochondrial mass present in IBD. Notably, it was very recently proposed that complex III is a tuner of autophagy [40]. Usually, mitochondrial dysfunction causes a reduction of autophagy because

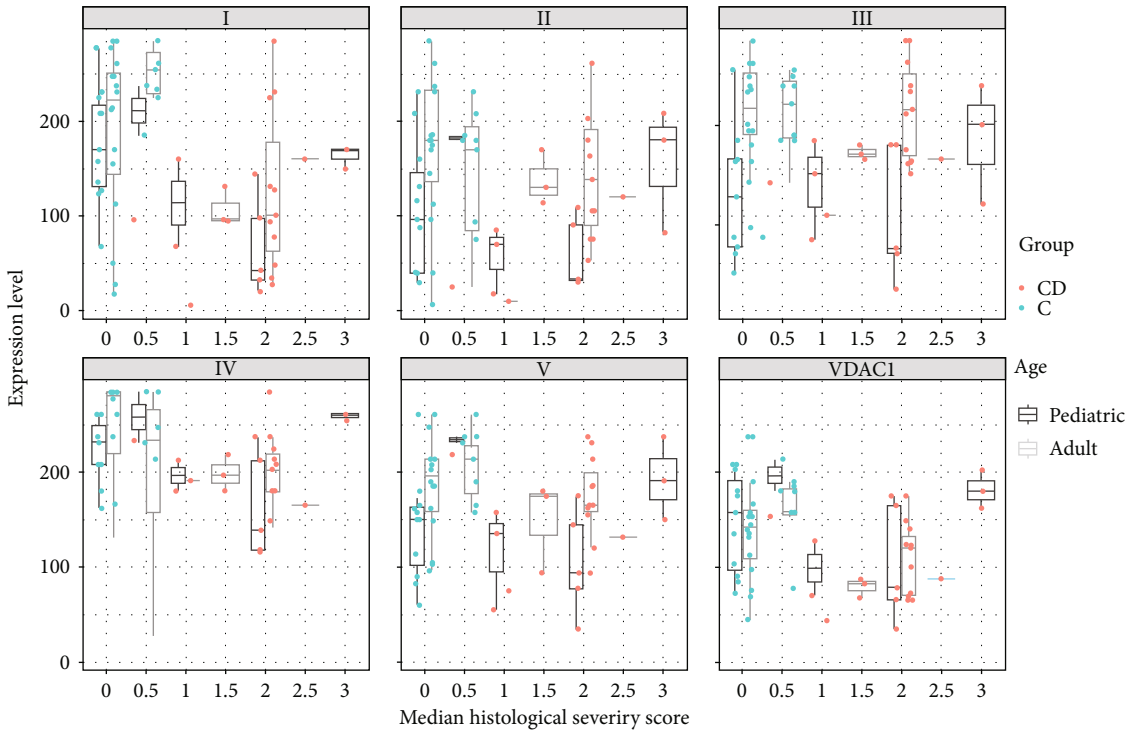

Figure 8: Boxplots and scatterplots of expression levels of OXPHOS complexes I-V and VDAC1 (porin) stratified by age and histological severity score (HSS) in the rectum in ulcerative colitis (UC) patients and controls (C). 0 indicates no histological abnormalities, 3 severe signs of inflammation.

Table 4: Expression levels of OXPHOS complexes I to V and VDAC1 (porin) in Crohn's disease (CD), ulcerative colitis (UC), and controls in the ascending colon.

	CI	CII	CIII	CIV	CV	VDAC1
Expression level, mean (SD)						
CD ($n = 34$)	126 (69)	100 (65)	155 (66)	212 (48)	152 (72)	143 (45)
UC ($n = 33$)	130 (80)	105 (66)	150 (58)	195 (58)	143 (62)	113 (48)
Control ($n = 57$)	195 (73)	160 (75)	181 (59)	227 (54)	192 (60)	153 (42)
Reduction controls- IBD	67 (34%)	58 (36%)	29 (16%)	23 (10%)	45 (23%)	24 (16%)
p value	<.001*	0.002*	0.207	0.079	0.020*	0.005*

It is shown as mean with standard deviation (SD) and reduction of expression level in IBD patients (CD and UC) compared to the control group. *$p < 0.05$.

autophagy is an ATP-consuming process. It would be very interesting if high complex III levels are a signal for the removal of damaged mitochondria. Antimycin A and myxothiazol reduce autophagy via complex III. Inhibition of the other OXPHOS complexes had no effect on autophagy. ATG16L1 is a component of a large protein complex essential for autophagy. In genome-wide association studies, variants in ATG16L1 have been linked to IBD (OMIM#610767) [41, 42]. ATG16L1 regulates mitochondrial antiviral signaling- (MAVS-) dependent type I interferon (IFN-I) production [43]. ATG16L1 deficiency causes mitochondrial defects in human macrophages. Furthermore, the authors reported a reduced number of mitochondria in ATP16L1-deficient cells [44].

Complex I and complex II subunits were more severely reduced than those of the other OXPHOS complexes and VDAC1 in both CD and UC patients. Therefore, an additional dysfunction causing this more pronounced complex I and II reduction might be present in IBD. Complex II is exclusively encoded by the nuclear DNA. Therefore, the combined reduction of complex I and II indicates the multifactorial cause of IBD. It is also known that complex I and complex II do not form respiratory chain supercomplexes together [45]. Our data are in line with those of Haberman et al., who demonstrated reduced complex I expression in UC [24]. In contrast, Sifroni et al. reported diminished complex II, III, and IV in UC patients but normal complex I activity [18]. Complex I is the largest OXPHOS complex, consisting of 44 different subunits encoded by both mitochondrial and nuclear DNA [46]. Therefore, it was previously proposed that complex I is the complex most prone to damage, simply because of its size. In addition, complex I is a multifunctional protein involved in several pathways fundamental for IBD pathogenesis, such as apoptosis. Caspase 3 cleaves the NDUFS1 subunit of complex I to induce

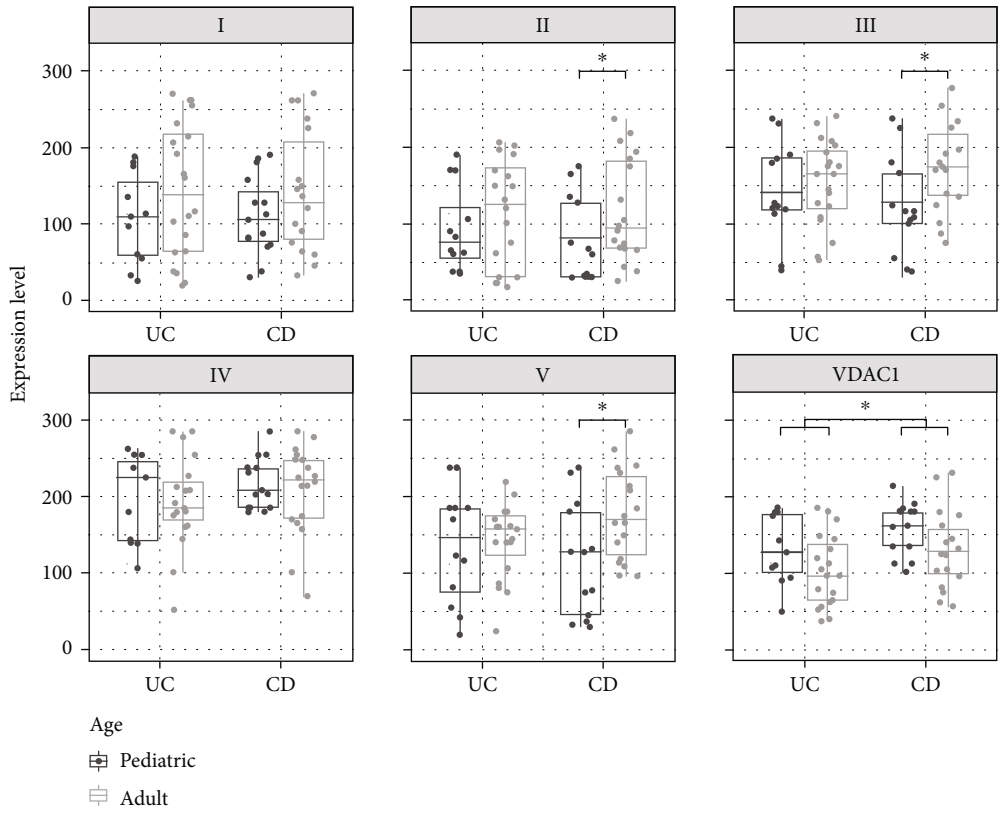

Figure 9: Boxplots and scatterplots showing expression levels of OXPHOS complexes I-V and VDAC1 (porin) in the ascending colon in Crohn's disease (CD) and ulcerative colitis (UC) pediatric and adult patients. *Significance ($p < 0.05$).

apoptosis [47, 48]. In a UC model, granzyme A was increased prior to macroscopic disease manifestation [49]. Granzyme A is another protein able to cleave complex I and induce apoptosis [50]. Stamp et al. showed that a reduction in complex I is associated with an increased rate of stem cell cycle reentry in the mouse colon, suggesting that these changes in stem cell homeostasis could have an impact on age-associated pathologies of the colon [51]. Methylation-controlled J protein (MCJ) acts as a natural inhibitor of complex I. Loss of MCJ results in aggravated disease with a change in microbiota composition and altered intestinal permeability, suggesting that MCJ plays a protective function during intestinal inflammation [52]. Importantly, both of the main entry points for electrons, complex I and complex II ($FADH_2$), are downregulated in IBD, indicating that OXPHOS is indeed reduced in IBD and not compensated via complex II. Santhanam et al. stated that a reduction in complex II activity appears to be a specific change in UC [17]. In a recent study, a marked decrease in MT-CO1 staining in the supranuclear region of the superficial epithelium relative to the subnuclear region was reported in 56% of patients with CD and 60% patients with UC [53]. However, the study did not analyze subunits of the other OXPHOS complexes. The authors further found that mitochondrial dysfunction alters intestinal epithelial metabolism of hepatic acylcarnitine species. NDUFAB1, also termed acyl carrier protein, is a subunit of complex I. Furthermore, NDUFAB1 is involved in Fe-S cluster biogenesis and protein lipoylation [54]. Therefore, it is possible in principle that low levels of NDUFAB1/complex I might influence complex II, which carries a [2Fe-2S] and a [4Fe-4S] cluster [55, 56].

In general, a trend to higher levels of OXPHOS complex subunits was present in adult patients with UC (rectum; ascending colon) and CD (terminal ileum; ascending colon) compared to pediatric patients, whereas VDAC1 showed a trend to lower amounts in adults. In adults, complex I was reduced in the rectum of UC patients and complex IV in the ascending colon of CD patients.

We hypothesize that an altered inner/outer membrane ratio might at least be partially responsible for the observed age-dependent phenotype. Altered mitochondrial (cristae) morphology as well as changes in proteins involved in fission/fusion was reported for IBD. A reduction of all OXPHOS complexes can be a consequence of reduced inner membrane folding [57–59]. MFN1, MFN2, OPA1, and p-DRP1 levels increased in a model of DSS-induced colitis [60, 61]. A mitochondrial fission inhibitor ameliorated DSS- and DNBS-induced murine colitis [62]. Whether a therapeutic intervention that shifts mitochondrial turnover to either fission or fusion would be beneficial remains to be elucidated. Interestingly, it was proposed that mitochondrial fusion of healthy and damaged mitochondria helps to maintain a functional mitochondrial compartment [63].

Studies have shown that the mitochondrial network of aged animals is often more heterogeneous, fragmented, and comprised of large, swollen mitochondria that cannot be

eliminated by mitophagy [63]. We hypothesize that mitochondrial swelling might be present in IBD of adult patients. Swelling would cause a decrease in VDAC1 because the outer membrane fraction would decline. However, it was also reported that fragmentation and swelling induce a loss of OXPHOS complexes, which is in contrast to our findings.

By stratifying the expression levels according to severity of inflammation, lower expression levels in IBD patients were seen, but more severe inflammation did not correlate with a reduction of mitochondrial mass and/or expression level of the OXPHOS complexes. Patients with the highest HSS values exhibited higher expression levels than those with only moderate degrees of inflammation. A possible mechanism could be that the mitochondrial mass increases as a compensatory mechanism due to dysfunctionality within the respiratory chain.

Another possible explanation is that ROS, produced by the respiratory chain, activate the NLRP3 inflammasome, which is a known activator of excessive inflammatory responses. Under physiologic conditions there is only a low leakage of ROS, but damage to the respiratory chain produces higher amounts of ROS and stronger activation of the NLRP3 inflammasome [64]. Since it is not known, if there is an increased production of ROS within the given samples, this is only speculative.

The inflammation by using the HSS score in adults was not more severe than in pediatric patients. The HSS score was 2 (mild-moderate inflammation) in most of the cases and balanced between adults and children (data not shown). However, due to the low case numbers in the higher HSS classes and the heterogeneous results in the subgroups, the results should be interpreted carefully.

Limitations of our study include the lack of enzyme measurements. We cannot exclude defects in the activity of respiratory chain enzymes. We employed IHC staining since it enables reliable analysis of OXPHOS respiratory chain defects at the level of the single cell, thus providing a major advantage over enzymatic measurements, which do not allow discrimination between different cell types [27, 65, 66]. In addition, we cannot provide clinical data, including fecal calprotectin measurements. However, an HSS methodology was chosen, as this is the gold standard for evaluating the degree of inflammation. Low case numbers in the higher HSS classes only allowed for descriptive analysis. However, to our knowledge, this is the most comprehensive study evaluating all complexes and mitochondrial mass in pediatric and adult IBD.

5. Conclusion

Reduced mitochondrial mass is present in UC and CD compared to controls. This is potentially a result of alterations of mitochondrial biogenesis or mitophagy. Reductions were more pronounced in older patients compared to pediatric patients and more prominent in UC than CD. Complex I and II are more severely compromised than the other OXPHOS complexes. This has potential therapeutic implications, since treatments boosting biogenesis or influencing mitophagy could be beneficial for IBD treatment. Additionally, substances specifically stimulating complex I activity should be tested in IBD treatment.

Data Availability

The data used to support the findings of this study are included within the article.

Disclosure

This work was presented as an abstract at the annual conference of the Austrian Society for Children and Adolescent Medicine in September 2021 in Salzburg, Austria [67]. (https://link.springer.com/content/pdf/10.1007/s00112-021-01292-9.pdf).

Conflicts of Interest

The authors declare that they have no conflicts of interest.

References

[1] K. Conrad, D. Roggenbuck, and M. W. Laass, "Diagnosis and classification of ulcerative colitis," *Autoimmunity Reviews*, vol. 13, no. 4-5, pp. 463–466, 2014.

[2] B. Khor, A. Gardet, and R. J. Xavier, "Genetics and pathogenesis of inflammatory bowel disease," *Nature*, vol. 474, no. 7351, pp. 307–317, 2011.

[3] W. T. Uniken Venema, M. D. Voskuil, G. Dijkstra, R. K. Weersma, and E. A. Festen, "The genetic background of inflammatory bowel disease: from correlation to causality," *The Journal of Pathology*, vol. 241, no. 2, pp. 146–158, 2017.

[4] D. C. Baumgart and S. R. Carding, "Inflammatory bowel disease: cause and immunobiology," *Lancet*, vol. 369, no. 9573, pp. 1627–1640, 2007.

[5] C. Gunther, C. Josenhans, and J. Wehkamp, "Crosstalk between microbiota, pathogens and the innate immune responses," *International Journal of Medical Microbiology*, vol. 306, no. 5, pp. 257–265, 2016.

[6] K. J. Maloy and F. Powrie, "Intestinal homeostasis and its breakdown in inflammatory bowel disease," *Nature*, vol. 474, no. 7351, pp. 298–306, 2011.

[7] C. G. Sauer and S. Kugathasan, "Pediatric inflammatory bowel disease: highlighting pediatric differences in IBD," *The Medical Clinics of North America*, vol. 94, no. 1, pp. 35–52, 2010.

[8] M. Aloi, P. Lionetti, A. Barabino et al., "Phenotype and disease course of early-onset pediatric inflammatory bowel disease," *Inflammatory Bowel Diseases*, vol. 20, no. 4, pp. 597–605, 2014.

[9] J. van Limbergen, R. K. Russell, H. E. Drummond et al., "Definition of phenotypic characteristics of childhood-onset inflammatory bowel disease," *Gastroenterology*, vol. 135, no. 4, pp. 1114–1122, 2008.

[10] H. M. McBride, M. Neuspiel, and S. Wasiak, "Mitochondria: more than just a powerhouse," *Current Biology*, vol. 16, no. 14, pp. R551–R560, 2006.

[11] B. Beltrán, P. Nos, F. Dasí et al., "Mitochondrial dysfunction, persistent oxidative damage, and catalase inhibition in immune cells of naïve and treated Crohn's disease," *Inflammatory Bowel Diseases*, vol. 16, no. 1, pp. 76–86, 2010.

[12] K. P. Pavlick, F. S. Laroux, J. Fuseler et al., "Role of reactive metabolites of oxygen and nitrogen in inflammatory bowel disease1, 2," *Free Radical Biology & Medicine*, vol. 33, no. 3, pp. 311–322, 2002.

[13] A. Wang, Å. V. Keita, V. Phan et al., "Targeting mitochondria-derived reactive oxygen species to reduce epithelial barrier dysfunction and colitis," *The American Journal of Pathology*, vol. 184, no. 9, pp. 2516–2527, 2014.

[14] A. Matondo and S. S. Kim, "Targeted-mitochondria antioxidants therapeutic implications in inflammatory bowel disease," *Journal of Drug Targeting*, vol. 26, no. 1, pp. 1–8, 2018.

[15] L. Lih-Brody, S. R. Powell, K. P. Collier et al., "Increased oxidative stress and decreased antioxidant defenses in mucosa of inflammatory bowel disease," *Digestive Diseases and Sciences*, vol. 41, no. 10, pp. 2078–2086, 1996.

[16] F. Bär, W. Bochmann, A. Widok et al., "Mitochondrial gene polymorphisms that protect mice from colitis," *Gastroenterology*, vol. 145, no. 5, pp. 1055–1063.e3, 2013.

[17] S. Santhanam, S. Rajamanickam, A. Motamarry et al., "Mitochondrial electron transport chain complex dysfunction in the colonic mucosa in ulcerative colitis," *Inflammatory Bowel Diseases*, vol. 18, no. 11, pp. 2158–2168, 2012.

[18] K. G. Sifroni, C. R. Damiani, C. Stoffel et al., "Mitochondrial respiratory chain in the colonic mucosal of patients with ulcerative colitis," *Molecular and Cellular Biochemistry*, vol. 342, no. 1-2, pp. 111–115, 2010.

[19] R. K. Boyapati, D. A. Dorward, A. Tamborska et al., "Mitochondrial DNA is a pro-inflammatory damage-associated molecular pattern released during active IBD," *Inflammatory Bowel Diseases*, vol. 24, no. 10, pp. 2113–2122, 2018.

[20] C. H. Ussakli, A. Ebaee, J. Binkley et al., "Mitochondria and tumor progression in ulcerative colitis," *Journal of the National Cancer Institute*, vol. 105, no. 16, pp. 1239–1248, 2013.

[21] N. L. Restivo, M. D. Srivastava, I. A. Schafer, and C. L. Hoppel, "Mitochondrial dysfunction in a patient with Crohn disease: possible role in pathogenesis," *Journal of Pediatric Gastroenterology and Nutrition*, vol. 38, no. 5, pp. 534–538, 2004.

[22] M. Vanderborght, M. C. Nassogne, D. Hermans et al., "Intractable ulcerative colitis of infancy in a child with mitochondrial respiratory chain disorder," *Journal of Pediatric Gastroenterology and Nutrition*, vol. 38, no. 3, pp. 355–357, 2004.

[23] W. Mottawea, C. K. Chiang, M. Mühlbauer et al., "Altered intestinal microbiota-host mitochondria crosstalk in new onset Crohn's disease," *Nature Communications*, vol. 7, no. 1, p. 13419, 2016.

[24] Y. Haberman, R. Karns, P. J. Dexheimer et al., "Ulcerative colitis mucosal transcriptomes reveal mitochondriopathy and personalized mechanisms underlying disease severity and treatment response," *Nature Communications*, vol. 10, no. 1, p. 38, 2019.

[25] M. Özsoy, F. A. Zimmermann, R. G. Feichtinger et al., "Changes in the expression of oxidative phosphorylation complexes in the aging intestinal mucosa," *Experimental Gerontology*, vol. 135, article 110924, 2020.

[26] F. A. Zimmermann, D. Neureiter, R. G. Feichtinger et al., "Deficiency of respiratory chain complex I in Hashimoto thyroiditis," *Mitochondrion*, vol. 26, pp. 1–6, 2016.

[27] F. A. Zimmermann, J. A. Mayr, D. Neureiter et al., "Lack of complex I is associated with oncocytic thyroid tumours," *British Journal of Cancer*, vol. 100, no. 9, pp. 1434–1437, 2009.

[28] D. Dobler, S. Friedrich, and M. Pauly, "Nonparametric MANOVA in Mann-Whitney effects," 2018, https://arxiv.org/abs/1712.06983.

[29] M. Happ, G. Zimmermann, E. Brunner, and A. C. Bathke, "Pseudo-ranks: how to calculate them efficiently inR," *Journal of Statistical Software*, vol. 95, no. Code Snippet 1, pp. 1–22, 2020.

[30] C. L. Alston, M. T. Veling, J. Heidler et al., "Pathogenic Biallelic Mutations in _NDUFAF8_ Cause Leigh Syndrome with an Isolated Complex I Deficiency," *American Journal of Human Genetics*, vol. 106, no. 1, pp. 92–101, 2020.

[31] Y. S. Ng, K. Thompson, D. Loher et al., "Novel MT-ND gene variants causing adult-onset mitochondrial disease and isolated complex I deficiency," *Frontiers in Genetics*, vol. 11, p. 24, 2020.

[32] G. T. Ho, R. E. Aird, B. Liu et al., "MDR1 deficiency impairs mitochondrial homeostasis and promotes intestinal inflammation," *Mucosal Immunology*, vol. 11, no. 1, pp. 120–130, 2018.

[33] R. C. Scarpulla, "Metabolic control of mitochondrial biogenesis through the PGC-1 family regulatory network," *Biochimica et Biophysica Acta*, vol. 1813, no. 7, pp. 1269–1278, 2011.

[34] X. DOU, J. XIAO, Z. JIN, and P. ZHENG, "Peroxisome proliferator-activated receptor-γ is downregulated in ulcerative colitis and is involved in experimental colitis-associated neoplasia," *Oncology Letters*, vol. 10, no. 3, pp. 1259–1266, 2015.

[35] L. Litvinova, D. N. Atochin, N. Fattakhov, M. Vasilenko, P. Zatolokin, and E. Kirienkova, "Nitric oxide and mitochondria in metabolic syndrome," *Frontiers in Physiology*, vol. 6, p. 20, 2015.

[36] G. Kolios, V. Valatas, and S. G. Ward, "Nitric oxide in inflammatory bowel disease: a universal messenger in an unsolved puzzle," *Immunology*, vol. 113, no. 4, pp. 427–437, 2004.

[37] K. G. Lassen and R. J. Xavier, "Genetic control of autophagy underlies pathogenesis of inflammatory bowel disease," *Mucosal Immunology*, vol. 10, no. 3, pp. 589–597, 2017.

[38] C. Ma, C. E. Storer, U. Chandran et al., "Crohn's disease-associated ATG16L1 T300A genotype is associated with improved survival in gastric cancer," *eBioMedicine*, vol. 67, article 103347, 2021.

[39] B. Z. Shao, Y. Yao, J. S. Zhai, J. H. Zhu, J. P. Li, and K. Wu, "The role of autophagy in inflammatory bowel disease," *Frontiers in Physiology*, vol. 12, article 621132, 2021.

[40] S. Jin, "Mitochondrial complex III: tuner of autophagy," *Chemistry & Biology*, vol. 18, no. 11, pp. 1348-1349, 2011.

[41] S. Lavoie, K. L. Conway, K. G. Lassen et al., "The Crohn's disease polymorphism, ATG16L1 T300A, alters the gut microbiota and enhances the local Th1/Th17 response," *eLife*, vol. 8, 2019.

[42] M. Salem, M. Ammitzboell, K. Nys, J. B. Seidelin, and O. H. Nielsen, "ATG16L1: a multifunctional susceptibility factor in Crohn disease," *Autophagy*, vol. 11, no. 4, pp. 585–594, 2015.

[43] W. A. Grimm, J. S. Messer, S. F. Murphy et al., "The Thr300Ala variant in ATG16L1 is associated with improved survival in human colorectal cancer and enhanced production of type I interferon," *Gut*, vol. 65, no. 3, pp. 456–464, 2016.

[44] D. Shih, Y. Kanazawa, A. Hamill, D. McGovern, M. Fukata, and S. Targan, "P-189 ATG16L1 deficiency leads to mitochondria defect and increased oxidative state in mice and human macrophages," *Inflammatory Bowel Diseases*, vol. 22, suppl_1, pp. S66–S67, 2016.

[45] G. V. Novack, P. Galeano, E. M. Castaño, and L. Morelli, "Mitochondrial Supercomplexes: physiological organization and dysregulation in age-related neurodegenerative disorders," *Front Endocrinol (Lausanne)*, vol. 11, p. 600, 2020.

[46] K. Fiedorczuk, J. A. Letts, G. Degliesposti, K. Kaszuba, M. Skehel, and L. A. Sazanov, "Atomic structure of the entire mammalian mitochondrial complex I," *Nature*, vol. 538, no. 7625, pp. 406–410, 2016.

[47] T. Nunes, C. Bernardazzi, and H. S. de Souza, "Cell death and inflammatory bowel diseases: apoptosis, necrosis, and autophagy in the intestinal epithelium," *BioMed Research International*, vol. 2014, Article ID 218493, 2014.

[48] J. E. Ricci, C. Muñoz-Pinedo, P. Fitzgerald et al., "Disruption of mitochondrial function during apoptosis is mediated by caspase cleavage of the p75 subunit of complex I of the electron transport chain," *Cell*, vol. 117, no. 6, pp. 773–786, 2004.

[49] H. HIRAYASU, Y. YOSHIKAWA, S. TSUZUKI, and T. FUSHIKI, "A role of a lymphocyte tryptase, granzyme A, in experimental ulcerative colitis," *Bioscience, Biotechnology, and Biochemistry*, vol. 71, no. 1, pp. 234–237, 2007.

[50] D. Martinvalet, D. M. Dykxhoorn, R. Ferrini, and J. Lieberman, "Granzyme A Cleaves a Mitochondrial Complex I Protein to Initiate Caspase- Independent Cell Death," *Cell*, vol. 133, no. 4, pp. 681–692, 2008.

[51] C. Stamp, J. C. Whitehall, A. L. M. Smith et al., "Age-associated mitochondrial complex I deficiency is linked to increased stem cell proliferation rates in the mouse colon," *Aging Cell*, vol. 20, no. 3, article e13321, 2021.

[52] M. A. Pascual-Itoiz, A. Peña-Cearra, I. Martín-Ruiz et al., "The mitochondrial negative regulator MCJ modulates the interplay between microbiota and the host during ulcerative colitis," *Scientific Reports*, vol. 10, no. 1, p. 572, 2020.

[53] S. A. Smith, S. A. Ogawa, L. Chau et al., "Mitochondrial dysfunction in inflammatory bowel disease alters intestinal epithelial metabolism of hepatic acylcarnitines," *The Journal of Clinical Investigation*, vol. 131, no. 1, 2021.

[54] A. J. Masud, A. J. Kastaniotis, M. T. Rahman, K. J. Autio, and J. K. Hiltunen, "Mitochondrial acyl carrier protein (ACP) at the interface of metabolic state sensing and mitochondrial function," *Biochimica et Biophysica Acta, Molecular Cell Research*, vol. 1866, no. 12, article 118540, 2019.

[55] S. P. Albracht, "The prosthetic groups in succinate dehydrogenase Number and stoichiometry," *Biochimica et biophysica acta Reviews on cancer*, vol. 612, no. 1, pp. 11–28, 1980.

[56] U. Na, W. Yu, J. Cox et al., "The LYR factors SDHAF1 and SDHAF3 mediate maturation of the iron-sulfur subunit of succinate dehydrogenase," *Cell Metabolism*, vol. 20, no. 2, pp. 253–266, 2014.

[57] A. M. Bou-Fersen, J. T. Anim, and I. Khan, "Experimental colitis is associated with ultrastructural changes in inflamed and uninflamed regions of the gastrointestinal tract," *Medical Principles and Practice*, vol. 17, no. 3, pp. 190–196, 2008.

[58] J. S. Modica-Napolitano, G. D. Steele Jr., and L. B. Chen, "Aberrant mitochondria in two human colon carcinoma cell lines," *Cancer Research*, vol. 49, no. 12, pp. 3369–3373, 1989.

[59] P. D. Wilson and L. M. Franks, "The effect of age on mitochondrial ultrastructure and enzymes," *Advances in Experimental Medicine and Biology*, vol. 53, pp. 171–183, 1975.

[60] S. Cipolat, O. M. de Brito, B. Dal Zilio, and L. Scorrano, "OPA1 requires mitofusin 1 to promote mitochondrial fusion," *Proceedings of the National Academy of Sciences of the United States of America*, vol. 101, no. 45, pp. 15927–15932, 2004.

[61] N. L. Mancini, L. Goudie, W. Xu et al., "Perturbed mitochondrial dynamics is a novel feature of colitis that can be targeted to lessen disease," *Cellular and Molecular Gastroenterology and Hepatology*, vol. 10, no. 2, pp. 287–307, 2020.

[62] L. J. L. Goudie, N. Mancini, K. R. Blote, A. Wang, D. M. McKay, and J. Shearer, "A novel mitochondrial fission inhibitor ameliorates DSS and DNBS Induced Murine Colitis," *Induced Murine Colitis.*, vol. 32, no. S1, p. 871.4, 2018.

[63] A. Sharma, H. J. Smith, P. Yao, and W. B. Mair, "Causal roles of mitochondrial dynamics in longevity and healthy aging," *EMBO Reports*, vol. 20, no. 12, article e48395, 2019.

[64] T. Zhang, S. Ding, and R. Wang, "Research progress of mitochondrial mechanism in NLRP3 inflammasome activation and exercise regulation of NLRP3 Inflammasome," *International Journal of Molecular Sciences*, vol. 22, no. 19, p. 10866, 2021.

[65] R. G. Feichtinger, D. Neureiter, T. Skaria et al., "Oxidative phosphorylation system in gastric carcinomas and gastritis," *Oxidative Medicine and Cellular Longevity*, vol. 2017, Article ID 1320241, 14 pages, 2017.

[66] R. G. Feichtinger, F. A. Zimmermann, J. A. Mayr et al., "Alterations of respiratory chain complexes in sporadic pheochromocytoma," *Frontiers in Bioscience (Elite Edition)*, vol. 3, pp. 194–200, 2011.

[67] A. Schneider, "Expression of oxidative phosphorylation complexes and mitochondrial mass in pediatric and adult infammatory bowel disease- abstract," *Monatsschrift Kinderheilkunde*, vol. 169, Suppl 2, pp. S43–S90, 2021.

Hindawi
Oxidative Medicine and Cellular Longevity
Volume 2021, Article ID 4993452, 21 pages
https://doi.org/10.1155/2021/4993452

Review Article

The Oxidative Stress and Chronic Inflammatory Process in Chagas Disease: Role of Exosomes and Contributing Genetic Factors

Edio Maldonado,[1] **Diego A. Rojas**,[2] **Fabiola Urbina**,[1] **and Aldo Solari**[1]

[1]*Programa Biología Celular y Molecular, Instituto de Ciencias Biomédicas, Facultad de Medicina, Universidad de Chile, Santiago, Chile*
[2]*Instituto de Ciencias Biomédicas, Facultad de Ciencias de la Salud, Universidad Autónoma de Chile, Santiago, Chile*

Correspondence should be addressed to Edio Maldonado; emaldona@med.uchile.cl and Aldo Solari; asolari@uchile.cl

Received 20 September 2021; Revised 27 November 2021; Accepted 6 December 2021; Published 23 December 2021

Academic Editor: Daniela Ribeiro

Chagas disease is a neglected tropical disease caused by the flagellated protozoa *Trypanosoma cruzi* that affects several million people mainly in Latin American countries. Chagas disease has two phases, which are acute and chronic, both separated by an indeterminate time period in which the infected individual is relatively asymptomatic. The acute phase extends for 40-60 days with atypical and mild symptoms; however, about 30% of the infected patients will develop a symptomatic chronic phase, which is characterized by either cardiac, digestive, neurological, or endocrine problems. Cardiomyopathy is the most important and severe result of Chagas disease, which leads to left ventricular systolic dysfunction, heart failure, and sudden cardiac death. Most deaths are due to heart failure (70%) and sudden death (30%) resulting from cardiomyopathy. During the chronic phase, *T. cruzi*-infected macrophages respond with the production of proinflammatory cytokines and production of superoxide and nitric oxide by the NADPH oxidase 2 (NOX2) and inducible nitric oxide synthase (iNOS) enzymes, respectively. During the chronic phase, myocardial changes are produced as a result of chronic inflammation, oxidative stress, fibrosis, and cell death. The cellular inflammatory response is mainly the result of activation of the NF-κB-dependent pathway, which activates gene expression of inflammatory cytokines, leading to progressive tissue damage. The persisting production of reactive oxygen species (ROS) is the result of mitochondrial dysfunction in the cardiomyocytes. In this review, we will discuss inflammation and oxidative damage which is produced in the heart during the chronic phase of Chagas disease and recent evidence on the role of macrophages and the production of proinflammatory cytokines during the acute phase and the origin of macrophages/monocytes during the chronic phase of Chagas disease. We will also discuss the contributing factors and mechanisms leading to the chronic inflammation of the cardiac tissue during the chronic phase of the disease as well as the innate and adaptive host immune response. The contribution of genetic factors to the progression of the chronic inflammatory cardiomyopathy of chronic Chagas disease is also discussed. The secreted extracellular vesicles (exosomes) produced for both *T. cruzi* and infected host cells can play key roles in the host immune response, and those roles are described. Lastly, we describe potential treatments to attenuate the chronic inflammation of the cardiac tissue, designed to improve heart function in chagasic patients.

1. Introduction

Chagas disease or American trypanosomiasis is a tropical vector-borne disease, and its etiologic agent is the protozoan parasite *Trypanosoma cruzi*. It was discovered in 1909 by the Brazilian researcher Carlos Chagas and is endemic to South and Central America, including Mexico, however is not endemic in the Caribbean islands and Puerto Rico [1]. A Pan American Health Organization (PAHO) estimate indicates that 8-12 million people are infected in endemic areas and another 100 million people are at risk of infection. In the past two decades, the disease has been spread to other areas, namely, the United States, Europe, and Western Pacific areas, due to human immigration [2–7]; therefore, Chagas disease is a worldwide concern. In the United States, it is estimated that there are over 300.000 infected people by *T.*

cruzi; meanwhile, in Europe, it is estimated to be around 80.000 infected people [1, 3, 7]. In endemic areas, Bolivia has the highest incidence and prevalence rates; however, Brazil, Argentina, and Colombia have a higher number of infected people, due to their larger population and also due to the fact that a large population lives in rural areas, where the vector triatomine bugs are present. The distribution of the triatomine bugs has been changing, and now, Chagas disease is spreading to periurban and urban regions of those countries [1, 3].

Currently, vaccines are not available to prevent infection, although many South American countries have applied programs of interrupting vectorial transmission, which has led to significantly reduced new infections [5]. Also, public health guidelines, such as education of risky populations and serological screening of blood donors, have reduced the transmission of Chagas disease [1, 3, 6]. Despite all those efforts, it is estimated that approximately 60.000 new infections are produced each year and around 15.000 people can die each year from Chagas disease [1, 3, 7].

The disease is transmitted by several species of blood-sucking triatomine insects (invertebrate host), and one of the most common vectors in South America is *Triatoma infestans* [3, 5]. The insects get *T. cruzi* as the infective trypomastigote by sucking the blood of wild or domestic mammals, which act as reservoirs of the parasites; then, the trypomastigotes differentiate to the replicative epimastigotes and multiply in the insect midgut and finally are excreted as metacyclic trypomastigotes in the feces/urine during or immediately after a blood meal [1, 3]. The trypomastigotes enter the vertebrate host bloodstream through the bite wound or can enter through mucosal membranes and proliferate inside the host cells as amastigotes. Chagas disease has two phases, and each of them presents different clinical syndromes. The initial acute phase can last approximately 6-8 weeks and often is asymptomatic or unrecognized due to the mild symptoms; however, around 5% of the infected people can present a severe acute phase, mainly children under 5 years old, elderly, and immunosuppressed patients [3]. This severe form of the disease can cause fulminant myocarditis, which can produce patient death due to heart failure [2]. During the acute phase, there is a high detectable parasitemia level. This acute phase usually resolves spontaneously, and the patients remain infected if they are left untreated. This indeterminate form of Chagas disease has a good prognosis, and most of the infected people never develop symptoms of cardiac or digestive failure, despite being seropositive for *T. cruzi* [2, 3]. However, a decade or up to three decades after the initial infection, around 30-40% of the chronically infected people can progress to a chronic phase and develop organ damage, mainly cardiomyopathy and megaviscera (megaesophagus, megacolon, or both of them) [2, 3]. The most serious and frequent complication of Chagas disease is chronic cardiomyopathy, which is characterized by fibrosis and chronic inflammation resulting in heart failure [2].

Heart tissue inflammation is the hallmark of chronic Chagas disease; however, the pathogenesis of chronic chagasic cardiomyopathy is not completely understood yet. Until recently, the consequences of the chronic disease are considered to be autoimmune, but later, it became clear that autoimmune reaction is a consequence of parasite persistence. However, other factors must be considered to explain chagasic cardiomyopathy. In this article, we will review recent findings on the pathogenesis of the disease, role of reactive oxygen species (ROS) in keeping on the chronic heart inflammation of Chagas disease, the host immune response, the role of exosomes in Chagas disease, and new perspectives on patient treatments.

1.1. Pathophysiology of Chagas Disease. As stated, the most frequent complications of Chagas disease are syndromes affecting cardiac, digestive, and neurological systems of the patients. The late manifestations of the chronic phase of the disease are disturbances in the heart, such as cardiomyopathy and cardiac arrhythmias, esophageal or colon motility, and neurological damage. These late manifestations typically present as cardiac arrhythmias, cardiomyopathy, or disturbances in esophageal and colon motility involving hypertrophy and dilatation of the organ. The underlying anatomical abnormalities in Chagas disease patients with cardiac damage are an enlarged heart with parasympathetic denervation and reduced ganglion cell numbers in the myenteric plexuses [8]. This reduction in ganglion cell numbers is assumed to occur in the acute phase of the infection, as it has been demonstrated through comparative studies [9–12]. The cardiac system is the most compromised and affects about 30% of chagasic patients, while megaesophagus and megacolon are less frequent (5-20%) [2, 3]. A mixed form of chronic Chagas disease (cardiac and digestive) affects only 5-10% of the chagasic patients [3]. Death from chronic Chagas disease is the result of congestive heart failure that follows the development of myocardial dysfunction, caused by a chronic inflammatory response that might progress to fibrosis and cell death; however, intestinal denervation also occurs as a result of *T. cruzi* infection [3, 13, 14]. At least three factors are involved in the pathogenesis of Chagas disease, namely, (i) the induction of autoimmune response, (ii) the cellular inflammatory response, and (iii) oxidative stress generated as a consequence of *T. cruzi* infection [15–19].

The pathophysiology of the acute and chronic phases of Chagas disease is quite different. The acute phase presents high parasitemia and tissue parasitism, but with a preference for the heart, esophagus, colon, and central nervous system. The presence of *T. cruzi* elicits a strong immune/inflammatory response against the parasite. In the heart, diffuse myocarditis is present together with myocyte necrosis, cell infiltration (mononuclear and polymorphonuclear), and interstitial edema [2, 3, 19]. On the other hand, chronic Chagas disease presents persistent inflammation, which results in diffuse myocytolysis and appearance of reparative fibrosis [2, 3, 19]. Subsequently, a ventricular dysfunction appears together with reduced myocardial function, heart remodeling, and neurohumoral activation [19]. Together, the effect of all those factors results in a cycle of disease progression, which can lead to heart failure. Cellular injuries and the strong immune/inflammatory response are the main

sources of reactive oxygen species (ROS), and the mitochondria are the major source of ROS during the chronic phase of Chagas disease [19, 20]. Oxidative stress produced by mitochondrial ROS (mtROS) contributes to tissue damage and sustains oxidative stress in the myocardium [19, 20]. In the following section, the new evidence on the role of oxidative stress on myocardium damage will be described.

2. Inflammation and Oxidative Damage in Chagas Disease

Chronic inflammation and oxidative stress are hallmarks of chronic cardiomyopathy in Chagas disease. When a host is infected by *T. cruzi*, there is an attempt to control the infection by elevating the levels of ROS and NO, which leads to oxidative stress at both the acute and chronic phases of Chagas disease [20]. There are two main ROS sources relevant to this disease which are NOX2 and mitochondria (mtROS), and a proposed mechanism of mitochondrial dysfunction caused by ROS is described in Figure 1. Several studies have demonstrated that NOX2 locates at the plasma membrane of peritoneal mouse macrophages upon interaction with the parasite [20, 21], and it has been also demonstrated that *T. cruzi*-activated macrophages can produce high levels of ROS and NO both in *in vitro* and *in vivo* models [20, 21]. Also, it has been shown that splenocytes from infected mice and *in vitro* cultured macrophages can respond to *T. cruzi* infection by activating NOX2, which results in increased levels of ROS [20]. The heart is a target organ for *T. cruzi* infection, and infiltrating neutrophils and macrophages are the main sources of NOX2- and myeloperoxidase-dependent ROS in the acute phase of the Chagas disease, although it has been also observed that mitochondria can produce ROS from infected cardiomyocytes [20]. Both ROS and NO can react and form peroxynitrite, which is able to kill *T. cruzi* inside the macrophages; however, peroxynitrite can be harmful to the host cell as well. ROS can also act as key regulators of parasite control by means of regulating cytokine responses and also splenic inflammatory cell proliferation during the infection [20]. However, recent evidence indicates that ROS can provide a positive signal for *T. cruzi* cell proliferation [22].

Signaling lymphocyte activation molecule family 1 (SLAMF1 or CD150) of cell-surface receptors is broadly expressed in the hematopoietic system [23]. SLAMF1 can be considered a phenotypic marker of activated T cells, dendritic cells, B cells, and monocytes. It has been shown that it is a key player in innate and adaptive immunity and serves as a bacterial sensor and as a receptor for *Morbilliviruses* [23]. It has been reported that interaction between OmpC/F+ *E. coli* and SLAMF1 is required for macrophage phagocytosis and phagosome localization where it can enhance PI3P production, NOX2 activation, and superoxide production [24]. Superoxide has antimicrobial activity and also is involved in regulating cell motility and phagocytosis; therefore, the phagocytosis of Gram- bacteria can be compromised in the absence of superoxide [25]. In the context of *T. cruzi* infection, SLAMF1 controls the susceptibility of infection by the virulent Y strain, since *Slamf1*−/− mice, lacking the SLAMF1 receptor, are resistant to a lethal *T. cruzi* Y strain challenge [26]. Moreover, Slamf1-defIcient myeloid cells are impaired in their ability to replicate the parasite, and they display an altered pattern of cytokine production. Recent studies by Poveda et al. [27] have shown that the interaction of SLAMF1 with *T. cruzi* is strain-dependent and affects NOX2 expression and ROS production, since five out of six strains tested showed a decrease in parasite load in *Slamf1*−/− infected macrophages compared to wild-type macrophages. Also, NOX2 expression and ROS production were increased in *Slamf1*−/− infected macrophages when compared to wild-type macrophages [27]. Those results indicate that SLAMF1 increases parasite infection and controls ROS production through NOX2.

When ROS are produced in excess or for long and sustained periods, they exert toxic effects that damage cells and tissues, since ROS can oxidize lipids, proteins, and DNA [20, 28]. These effects produce cell membrane damage, which leads to membrane integrity loss and membrane protein function defects. The main damage on molecules produced by ROS is lipid peroxidation, a direct attack on Thr, Pro, Lys, and Arg residues of proteins that can derivatize the polypeptides and lead to the formation of protein carbonyls [20, 28–31]. DNA can be oxidized and damaged to produce 8-oxo-deoxyguanosine (8-oxo-G) lesions, which might exceed the capacity of the cellular DNA repair mechanisms, leading to mutations and transcription mistakes [31]. The ROS in chagasic hearts is produced by dysfunctional mitochondria, since it has demonstrated a decline in complex I (CI) and complex III (CIII) activities, which are associated with excessive electron leakage to produce superoxide and sustained ROS production in the myocardium of chagasic mice [31–33].

ROS play a pivotal role as signaling intermediates to link the innate and adaptive immune responses by generating proinflammatory cytokine production (TNF-α, IL-1β, and IFN-γ) from dendritic cells and macrophages, which are components of the innate immune system [20]. Studies in which the NOX2/ROS axis was inhibited in primary and cultured macrophages have demonstrated that NOX2/ROS is a key regulator of cytokine production in response to *T. cruzi* infection [34]. Subsequent studies using splenocytes from infected mice in vitro stimulated with *T. cruzi* antigens have confirmed those observations and demonstrated that inhibition of NOX2 by apocynin or by using ROS scavengers greatly blocked the phagocyte cell proliferation and production of inflammatory mediators such as IL-1, IL-6, TNF-α, and IFN-γ [34–36]. Most importantly, a genetic deficiency of a subunit of NOX2 (p47phox) resulted in an augmented susceptibility to *T. cruzi* infection in those mice lacking the p47phox gene, suggesting that the redox state plays a key role in immune system activation and control of the *T. cruzi* infection [20, 29, 37].

3. Diseased Heart and Mitochondrial Biogenesis

The heart consumes enormous amounts of energy, and it is highly dependent on the mitochondria for the energy

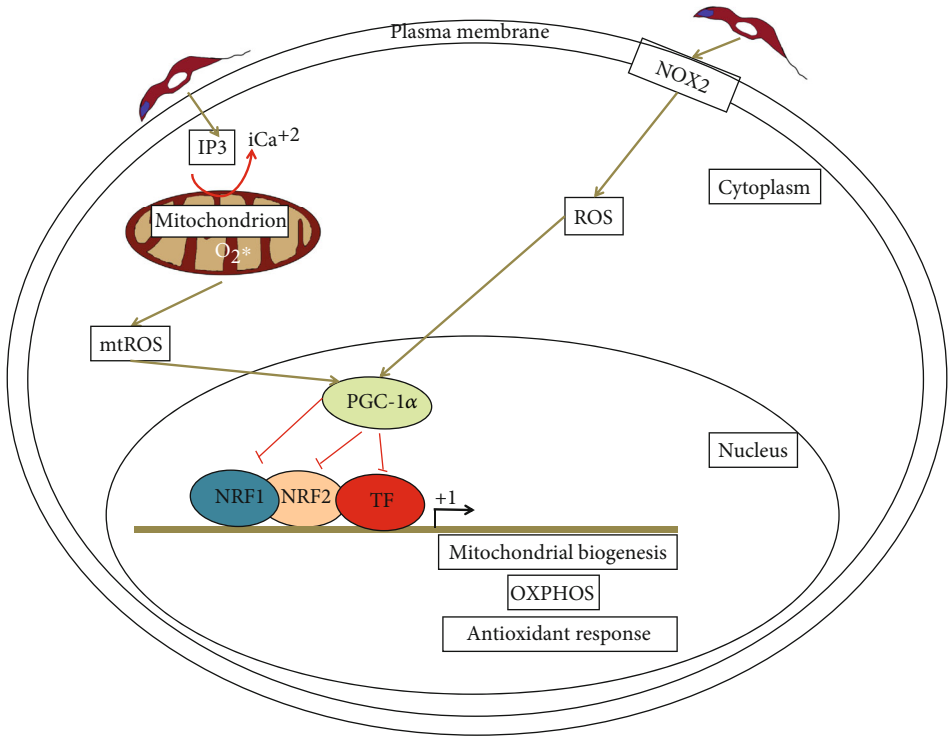

Figure 1: A mechanism to explain the mitochondrial dysfunction in Chagas disease. NOX2 is activated in *T. cruzi*-infected monocytes and macrophages, which can produce ROS. On the other hand, *T. cruzi* infection can induce an intracellular calcium flux (iCa^{2+}), which in turn causes mitochondrial membrane permeability, respiratory complex malfunction, and electron leakage from the electron transport chain to oxygen, which results in increased mtROS production. Most likely, the iCa^{2+} is associated with changes in the inositol 1,4,5 trisphosphate (IP3) signaling pathway, which can cause Ca^{2+} release from the sarcoplasmic reticulum and the nuclear envelope. Both NOX2-produced ROS and mtROS can inhibit the activity of the transcriptional coactivator PGC-1α, a coactivator of NRF1, NRF2, and other transcription factors (TF) involved in mitochondrial biogenesis, OXPHOS, mtDNA replication, and transcription, altering the redox homeostasis of the mitochondria. Additionally, ROS could directly inhibit the activity of NRF1 and NRF2, leading to mitochondrial dysfunction as well. +1 represents the transcription start site of the genes.

required for its contractile and other metabolic activities. In the cardiomyocytes, mitochondria represent around 30% of the total cell volume and provide 90% of the cellular ATP energy through the oxidative phosphorylation (OXPHOS) pathway [38]. Creatine kinase reaction serves as the heart primary energy reserve, and the creatine phosphate shuttle system delivers the high-energy phosphate groups from their production site in the mitochondria to the myofibrils to regenerate the ATP consumed during heart contraction [38]. This ATP flux is reduced in heart failure.

Heart development occurs mainly during perinatal and postnatal periods, when a series of maturation events start including mitophagy, fusion, and fission of the mitochondria [38]. This process allows the redistribution and dense packing of mature mitochondria along the myofibrils and also allows fatty acid oxidation (FAO), which are the predominant fuel substrate for the adult heart. The biogenic machinery can coordinate the nuclear and mitochondrial genomes during development and also in response to the source of fuel substrate utilization or energy demands [38]. Mitochondrial biogenesis, maturation, and function are controlled at the transcriptional level by a master regulator, which is the transcriptional coactivator named peroxisome proliferator-activated receptor γ (PPARγ) coactivator-1α (PGC-1α) [39]. This coactivator is strongly activated by conditions causing energy limitation, such as cold, exercise, and fasting, and is particularly highly expressed in organs demanding large energy consumption, such as the heart [40, 41]. PGC-1α binds to and activates PPARs, which are key regulators of genes involved in FAO, such as PPARs, hepatocyte nuclear factor 4, and SIRT1 [40, 41]. It also functions as a transcriptional coactivator for the nuclear respiratory factors 1 and 2 (NRF1 and NRF2) and triggers the expression of genes involved in mitochondrial biogenesis, OXPHOS, transcription, and replication of the mitochondrial genome [40, 41]. PGC-1α also serves as a transcriptional coactivator for estrogen-related receptors (ERRs), which can act as amplifiers for PGC-1α activation of PPARs and NRFs [36, 42]. PGC-1α is also a coactivator for the transcription factor nuclear factor-erythroid-derived 2-like 2 (NFE2L2, also known as NRF2, however is different from nuclear respiratory factor 2), which plays a key role in inducible expression of several detoxification and cytoprotective genes involved in response to oxidative and electrophilic stresses. SIRT1 is the main regulator of PGC-1α and activates PGC-1α through a NAD^+-dependent deacetylation at specific lysine residues of PGC-1α, and since NAD^+ levels are regulated by AMPK during fasting, the activation of PGC-1α through

deacetylation potentially creates a link between energy status, redox status, and mitochondrial function [42, 43].

Heart failure and cardiac hypertrophy in nonchagasic individuals are characterized by an increase of gene expression of many genes normally expressed in the fetal heart along with a decreased expression of those genes usually expressed in the adult heart [44]. This organ can meet its energy requirements from the oxidation of fatty acids, glucose, lactate, and other oxidizable substrates. However, the heart can function better when it uses both fatty acids and glucose simultaneously [45]. During heart failure, the heart switches from fatty acids to glucose utilization with a downregulation of the enzymes involved in FAO, which implies a reversion to the fetal energy substrate preference [45, 46]. The expression of genes involved in FAO, which are PGC-1α-coactivated, is downregulated during cardiac hypertrophy, and this is even prior to a clear cardiac dysfunction [47]. Cardiac hypertrophy is associated with reduced myocardial fatty acid utilization, and this observation indicates that mitochondria are remodeled to a phenotype with a reduced capacity to perform FAO during cardiac hypertrophy development and heart failure [44]. The loss of PGC-1α accelerates cardiac dysfunction following pressure overload stress [48]. Moreover, germline deletion of PGC-1α evokes perinatal lethal heart failure, which is caused by a lack of cardiac mitochondrial biogenesis [44, 49]. Interestingly, a subset of mitochondria in adult PGC-1α-knockout mice displays ultrastructural cristae abnormalities, which resembles those observed in the Bart syndrome, a congenital disease caused by altered phospholipid biosynthesis [44, 50]. PGC-1α as a transcriptional coactivator can interact directly with members of the nuclear receptor superfamily of transcriptional activators via LXXL recognition motifs, recruiting molecules that mediate chromatin remodeling by histone acetylation and interactions with the mediator complex to recruit the RNA polymerase II transcription machinery [51]. Effector transcriptional factors within this cascade include members of the PPAR, ERR, NRF1, and NRF2 and factors involved in the transcription and replication of the mitochondrial genome.

In the context of Chagas disease, *T. cruzi*-infected cardiomyocytes and human chagasic hearts show increased mRNA levels, but a decreased nuclear localization of PGC-1α-coactivated transcription factors such as NRF1, NRF2, and NFE2L2 [52]. However, there was an enhancement of gene expression of genes involved in PPARγ-regulated FAO, NRF1- and NRF2-activated mtDNA replication, and transcription machinery gene such as the mitochondrial transcription factor A (TFAM) [52]. Mitochondrial DNA content and mtDNA replication decrease by 65% and 83%, respectively. ROS, oxidative stress, and mtDNA oxidation are significantly increased, and the NFE2L2-antioxidant gene expression was severely compromised in infected cardiomyocytes and in human chagasic hearts [52]. The impairment of mitochondrial biogenesis by the decrease of the mtDNA content caused by the defect in the mtDNA replication results in a significant loss of mitochondrial-encoded proteins of the OXPHOS pathway [52]. It is most likely that the oxidated mtDNA is not a template to support replication and gene expression. The mtDNA replication defects increase ROS generation and a functional incapacity of NFE2L2 to activate genes of the antioxidant response leading to oxidative stress in the cardiomyocytes [52]. However, the PGC-1α-coactivated NRF1 and NRF2 transcriptional activities in the expression of genes involved in mtDNA replication and transcription were not compromised; rather, the defects in cardiomyocyte mitochondrial function can be attributed to a loss of function of NFE2L2 [52].

4. Mitochondrial Dysfunction and ROS Production in Chagas Disease

Mitochondrial ROS can be produced from infected cardiomyocytes as a consequence of mitochondrial dysfunction and contributes to increased oxidative stress in the heart of chagasic individuals. Usually, in the mitochondria occurs a low, but constant, ROS production [31]. The main sites for electron leakage are CI and CIII, which leads to increased ROS generation in the mitochondria [53, 54]. Wen and colleagues [14, 33] have demonstrated that in chagasic mice, there is a decline in CI and CIII activities in the myocardium, and this was associated with excessive electron leakage to O_2 and increased superoxide formation, resulting in a sustained ROS production in chagasic mice. In those mice, there was a significant decline in the content of mtDNA, and mitochondria-encoded transcripts were also diminished; therefore, quantitative deficiencies in the respiratory chain activity are produced in chagasic mice [33]. As a consequence of the mitochondrial dysfunction, OXPHOS-mediated ATP synthesis capacity of the myocyte mitochondria is reduced. This is extremely important since the heart is highly dependent on mitochondria for energy requirement for its contractile activity and the mitochondria provide more than 90% of the cellular ATP energy through OXPHOS. Importantly, the mitochondria are targets of several insults, which include inflammatory mediators produced during Chagas disease. Further studies by the same group [33] have identified that CIII is the main source of ROS production in the infected myocardium of chagasic mice. Electron leakage is produced as a consequence of defects in CIII proximal to the Qo site in cardiac mitochondria of *T. cruzi*-infected mice [33]. The excessive electron leakage can be reduced by the treatment of infected mice with the antioxidant phenyl-a-tert-butyl-nitrone (PBN), which is a spin-trapping antioxidant [33]. PBN can improve the respiratory chain function by preventing the excessive mtROS production in myocyte mitochondria and reduce electron leakage. Mitochondrial defects at CIII have been also observed in the heart of chronic Chagas patients [55], indicating that mitochondria are the main source of ROS production and oxidative stress during the chronic phase of Chagas disease. Moreover, the ROS-induced oxidative adducts can conduce to proinflammatory macrophage activation, which in turn can damage the mitochondria, leading to an increase in mtROS production [55].

Mitochondrial ROS has a profound impact on cytokine gene expression in cardiac myocytes infected with *T. cruzi*.

Garg and colleagues have demonstrated that mtROS augmented the nuclear translocation of the v-rel avian reticuloendotheliosis viral oncogene homolog A (RelA or p65), therefore activating the NF-κB-dependent gene expression of inflammatory cytokines such as TNF-α, IL-1β, and IFN-γ [56]. Also, mtROS can cause 8-oxo-G lesions and DNA fragmentation, which can signal poly-ADP ribose polymerase 1 (PARP1) to get modified by poly-ADP-ribose (PAR) together with other proteins in infected cardiomyocytes [20, 57–59]. PARP1 can signal other proteins, such as histones, by PARylation; however, the hyperactivation might have negative effects, such as catalytic activation of inflammatory proteins, enhanced cytokine gene expression activation, NAD^+ depletion, and cell death [20, 57–59]. Importantly, inhibition of PARP1 expression by RNAi, chemical inhibition by PJ34, or removing mtROS by an antioxidant was beneficial to block mtROS formation and DNA damage [20, 56, 59]. Interestingly, PARP1 can also regulate cytokine gene expression by a different mechanism, which is the PAR modification of RelA (p65)-interacting nuclear proteins and the assembly of a NF-κB transcription-dependent complex [20]. All those studies indicate that the ROS-PARP1-RelA signaling pathway can contribute to the proinflammatory cytokine gene expression in *T. cruzi*-infected cardiomyocytes. Those results are summarized in Figure 2.

The mechanisms underlying the progression to the chronic phase of Chagas disease in humans are still under study. It is noteworthy to state that even in the absence of *T. cruzi*, the individual can develop a chronic disease as evidenced by the BENEFIT trial [60, 61]. The mechanisms that trigger the progression to the chronic phase of Chagas disease are not completely known yet. During the chronic phase of the disease, there is a high production of mtROS by the cardiomyocytes as a consequence of changes in the mitochondrial membrane potential ($\Delta\Psi$) due to lipid peroxidation and/or formation of protein carbonyls and a decline in the activities of the respiratory complexes, especially CIII [20, 33]. The persisting ROS release leads to mitochondrial dysfunction, inflammation, and heart tissue damage. Cellular components such as lipids, proteins, and DNA are damaged which can lead to proinflammatory macrophage activation causing cellular injury [55]. The high ROS levels produce exhaustion of the antioxidant defense of the organism, which is mainly the superoxide dismutase (MnSOD), glutathione peroxidase, catalase, and glutathione [37, 61–64]. Therefore, the use of antioxidant compounds, stimulation of mitochondrial biogenesis, and enhancement of antioxidant defenses or ROS scavengers could have benefits in the treatment of chronic Chagas disease. Recently, it has been found that TNF-α+monocytes/macrophages are associated with the inflammatory process in chronic Chagas disease. There is an increase in the maturation of bone marrow hematopoietic stem cell-derived monocytes of proinflammatory and anti-inflammatory phenotypes in chronic *T. cruzi*-infected mice [65]. On the other hand, yolk sac-derived monocytes/macrophages of the CD11b+ F4/80+ phenotype were augmented in sinusoidal compartments of chagasic mice [65]. The splenic monocytes/macrophages of that phenotype displayed augmented mRNA, protein, and surface expression of proinflammatory markers, such as CD80+/CD64+, which are associated with cytokine response (TNF-α, IL-6), and those cells are also detected in the myocardium of chagasic mice [65]. Taken all together, those results indicate that proinflammatory yolk sac-derived monocytes/macrophages trigger the splenic and myocardium inflammatory response.

5. Innate Immune Response in Chagas Disease

ROS are important mediators that participate in the immune response by triggering the production of cytokines by immune cells. This section will analyze the main aspects of the innate immune response mounted by the host during *T. cruzi* infection.

When invading a vertebrate host, *T. cruzi* must face the first defense line with the innate immunity composed of phagocytes, especially macrophages, neutrophils, and dendritic cells [66]. Those cells have two main features that are key to their functions, which are (i) recognition of the pathogen-associated molecular patterns (PAMPs) and the damage-associated molecular patterns (DAMPs) by membrane receptors, such as the Toll-like receptors (TLR). This enables the cells to recognize and phagocyte foreign microorganisms and cellular debris to destroy those invading microorganisms. (ii) Secretion of cytokines which promote inflammation and activate other cells involved in defense at the site of infection. Pattern recognition receptors (PRR) can recognize several shared motifs in different microorganisms, such as the classical lipopolysaccharides present in the cell wall of bacteria, which are able to activate the expression of genes involved in inflammation and antimicrobial responses. *T. cruzi* is also recognized by the nucleotide-binding oligomerization domain-like receptors or Nod-like receptors (NLRs), which are intracellular sensors of PAMPs that can enter the cells via phagocytosis or pores and also of DAMPs, which are associated with cell stress [67]. On the other hand, TLR is a family composed of 10 different members in humans [68]. Some of them are at the cell surface and others into the cell. TLR2 and TLR4 are surface receptors, while TLR7 and TLR9 are located at the endosome. For example, glycosyl phosphatidylinositol- (GPI-) anchors, which are derived from *T. cruzi* mucin-like glycoproteins (GPI-mucins), are ligands of TLR2 and 6 [69], while glycol-inositol-phospholipids (GIPLs) are ligands of TLR4 [70]. Meanwhile, DNA (rich in unmethylated CpG motifs) and RNA are potent activators of TLR9 and 7, respectively [71, 72].

All those recognition signals regulate the expression of proinflammatory cytokines from macrophages, such as IL-1, IL-12, TNF-α, and IL-10 [73]. Those proinflammatory cytokines, together with IFN-γ, which is produced by natural killer (NK) and T cells upon *T. cruzi* infection, are able to prime macrophages, which leads to the induction of the iNOS system that can produce high amounts of NO for 24 hours. The NO can diffuse to the phagosome where it can react with O_2 to produce ONOO-, a powerful oxidant able to kill *T. cruzi* [73]. Dendritic cells, like macrophages and neutrophils, also become activated in the presence of PAMPs and DAMPs to produce costimulatory molecules

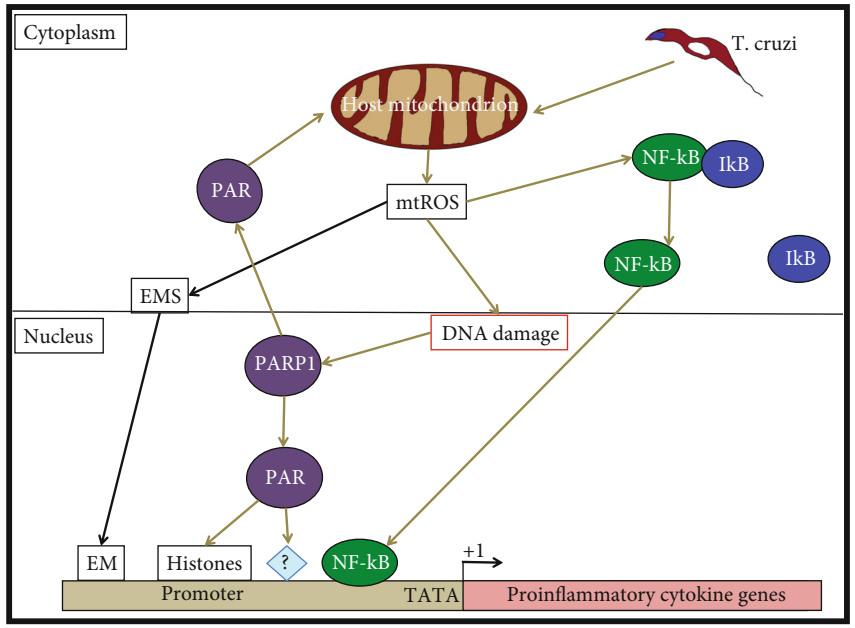

Figure 2: The persisting ROS signal activates proinflammatory gene expression. *T. cruzi*-infected cardiomyocytes are able to produce mtROS, which induces the dissociation of NF-κB transcription factor from IκB in the cytoplasm and translocate to the nucleus to bind target sequences in the gene promoter of proinflammatory cytokine genes, which leads to the high production of proinflammatory cytokines, which in turn can produce tissue damage. Mitochondrial ROS can produce DNA damage and activate PARP1 to produce PAR, which signals transcriptional coactivators to induce proinflammatory cytokine gene expression and modify histones at the gene promoter regions. Alternatively, ROS could activate an epigenetic modification system (EMS) that might be able to produce an epigenetic modification (EM) at the promoter regions of proinflammatory cytokine genes to keep them in an active transcribing state, even though in the absence of *T. cruzi*. +1 represents the transcription start site of the genes.

and cytokines that are necessary, together with the antigen itself, to activate T cells [74]. The profile of the produced cytokines by the dendritic cells will depend on the nature of the invading pathogen and can direct the differentiation of naive T cells towards different functional roles. Experiments with human dendritic cells have shown that their functions are affected by factors secreted by *T. cruzi* that can induce tolerance (no response) by inhibiting TNF-α and IL-12 production, even though the parasite was internalized into the cytoplasm of the dendritic cell [75]. Furthermore, a decrease in molecules of classes I and II of the major histocompatibility complex (MHC) and CD-40 coreceptor expression was observed [75]. Those decreases are induced by *T. cruzi* soluble factors, interfering with the antigen presentation ability of dendritic cells. Despite the fact that the parasite is internalized by the dendritic cell, there are different degrees of infectivity, which is dependent upon the *T. cruzi* strain, however is not dependent on the *T. cruzi* discrete typing units (DTUs) and neither dependent on the biological characteristics of the dendritic cells [76].

Also, NK cells play a key role in innate immunity against intracellular pathogens and in contrast to T and B lymphocytes do not require clonal expansion or differentiation to carry out their functions [66]. NK cells can signal T cell differentiation towards an inflammatory pathway and also can secrete IFN-γ to activate macrophages when viable *T. cruzi* infecting cells are present [66]. For example, it has been shown that a peak of IFN-γ is produced soon after infection by *T. cruzi*, in a process which requires adherent cells in the thymus and viable parasites, however is independent of T cells [77]. This IFN-γ peak might be key in the control of the infection during the acute phase of Chagas disease, as the depletion of NK cells from those mice causes an abrogation in IFN-γ production and an increase in IL-10 levels, which probably leads to tolerance of the parasite and allows infection progression [77]. In addition, NK cells can directly eliminate extracellular parasites by forming intercellular contacts with the pathogen cell, which results in the loss of motility and damage in the cell membrane of the parasite [66, 78, 79]. This killing activity of the NK cells depends on activation by IL-12 and results in the exocytosis of cytotoxic granules, which can damage the cell membrane of the parasite [66, 78, 79]. It is believed that NK cell primary function is the direct killing of the parasite, more than the elimination of *T. cruzi*-infected cells [66, 79]. It is noteworthy to mention that expression of genes related to NK cell's function is upregulated in PCR-positive asymptomatic patients with Chagas disease, while they are downregulated in those patients with severe cardiomyopathy [80].

The complement cascade system is another component of innate immunity. It consists of several plasmatic proteins, which are able to opsonize pathogens, recruit phagocytes to the infection site, and also directly destroy the invading pathogen [66]. It functions as a cascade of proteolytic enzymes, in which a precursor (zymogen) is activated turning it up in an active proteolytic enzyme able to cleave and activate the following component [66, 79]. The complement system works by amplifying the signal generated by the

presence of the pathogen to allow the clearance of the invading pathogen. It can be activated by three different vias, which are the classical, the alternative, and the lectin pathway, but all of them converge in the component C3 convertase and its subsequent split in C3a and C3b [81]. Neutrophils and macrophages have receptors for C3b and promote phagocytosis of the pathogen, whereas C3a acts as a proinflammatory factor. C3b also acts on C5 to produce C5a, a potent proinflammatory factor, and also is able to generate pores in the pathogen cellular membrane [81]. However, despite the power of the complement system to control initial infections, *T. cruzi* has evolved a myriad of molecules to escape or subvert the complement system, by either inactivation or blocking the activation of its components. For example, calreticulin (TcCRT) is a *T. cruzi* endoplasmic reticulum protein, which is translocated to the surface upon infection, and it has been demonstrated that it can bind to several molecular pattern sensors, such as C1q, mannose binding lectin, and L-ficolin [66, 79, 82], thereby affecting the first step on the classical and lectin complement system pathway. Several other examples of complement system inactivation by *T. cruzi* molecules can be found in Reference [66, 79]. Figure 3 shows that a C3 convertase binding protein is contained in *T. cruzi* exosomes, and it is able to block its activity. We believe that TcCRT can also be contained into the *T. cruzi* released exosomes.

6. Adaptive Immune Response in Chagas Disease

B lymphocytes play a fundamental role in adaptive humoral immune response since they are able to produce and secrete antibodies. Moreover, B cells can secrete cytokines and are involved in antigen presentation to other immune cells, thereby acting as a nexus between innate and adaptive immune responses [66, 79]. B cells and their antibodies were one of the first components studied in the context of Chagas disease; however, several aspects of their roles are not well understood yet. The focus of interest during the early days of the field was the specificity of the elicited antibodies generated upon infection [66, 79]. Today, the immune epitope database (IEDB) has more than 90 *T. cruzi* molecules entries and several others marked as "other *T. cruzi* proteins" displaying more than 2.000 different epitopes, which can be bound by antibodies from human patients and animal models. Some of those antibodies are lytic since they can bind to the parasite and activate the complement system for parasite lysis [83]. Therefore, those epitopes bound by neutralizing antibodies might be good candidates to generate vaccines against the parasite. Those antibodies are mostly directed against surface antigens on *T. cruzi*, and a description of several of the antigenic molecules can be found in [66, 79]. The advances of the high throughput technologies and bioinformatics have considerably expanded the possibility to analyze the complete repertory of antibodies after infection, and moreover, a database of antigen binding regions of the antibodies could be built to serve as tools for the study of the humoral response in Chagas disease [84].

The importance of the humoral immune response to control the *T. cruzi* infection has been studied in the mouse infection model, and it has been shown that mutant mice, unable to produce antibodies, cannot control the *T. cruzi* growth and die during the acute phase of the disease [85]. Those results indicate the importance of the B cells to control the infection at the beginning of Chagas disease. However, antibodies produced against *T. cruzi* seem to not effectively control and completely eliminate the parasite, providing the opportunity for the parasite to establish a permanent infection [66, 79]. This inefficient humoral immune response could be due to three main factors: (i) antigenic variability on the surface antigens, which are encoded by multigene families and the high diversity of molecules expressed at the same time, delays the activation of specific B cell clones that impedes the production and maturation of high-affinity specific antibodies with lytic and neutralizing activities; (ii) reduced number of immature B cells in the bone marrow, most likely as a consequence of increased apoptosis in the bone marrow, due to *T. cruzi* infection. By affecting the bone marrow, *T. cruzi* compromises the entire humoral response, causing the decrease of mature B cells in the periphery; and (iii) nonspecific polyclonal B cell activation, since some parasite antigens have been demonstrated that can cause a nonspecific T cell-independent activation of B cells in mouse models of infection. That activation of the B cells can cause splenomegaly and hypergammaglobulinemia with production of antibodies that are unspecific for *T. cruzi* [86]. This could in part explain the pathogenesis of chronic Chagas disease, since those antibodies could react with host antigens, and evidence of molecular mimicry has been found between host and parasite antigens [66, 79, 87].

The B cell-deficient murine model has been used to study, during the acute phase of Chagas disease, the role of B cells in the function of T cells. In those mice, a deficient expansion of CD4+ and CD8+ T cells was observed, especially within the memory T cell subset, and also a decrease in TH1, TH17, and regulatory T cell populations [88, 89]. This indicates that B cells are important for the establishment of memory T cells, which are essential to control *T. cruzi* infection. Moreover, in the absence of mature B cells, the number of IFN-γ CD4+ T cells decreases, while the number of TNF+ CD4+ T cells increases with a concomitant augment of the cytokine levels in plasma [66, 88, 89]. Additionally, the frequency of CD4+ T cells expressing inhibitory receptors is lower than that in wild-type infected mice, indicating that the regulation of those cell populations has been hampered. All of those defects can contribute to the deleterious and proinflammatory state of those mutant mice [88, 89].

T lymphocytes or T cells play a key role in adaptive cellular immune response. A T cell response is initiated by signals, which are produced by a recognition of peptide-MHC complexes presented on the surface of antigen-presenting cells (APC), by the T cell receptors [66, 79, 90]. The consequence of this activation is the generation of a large number of effector and pathogen-specific activated T cells from a relatively small population of naive T (Tn) cells with different specificities and roles. Tn cell activation triggers their clonal expansion, along with changes in the

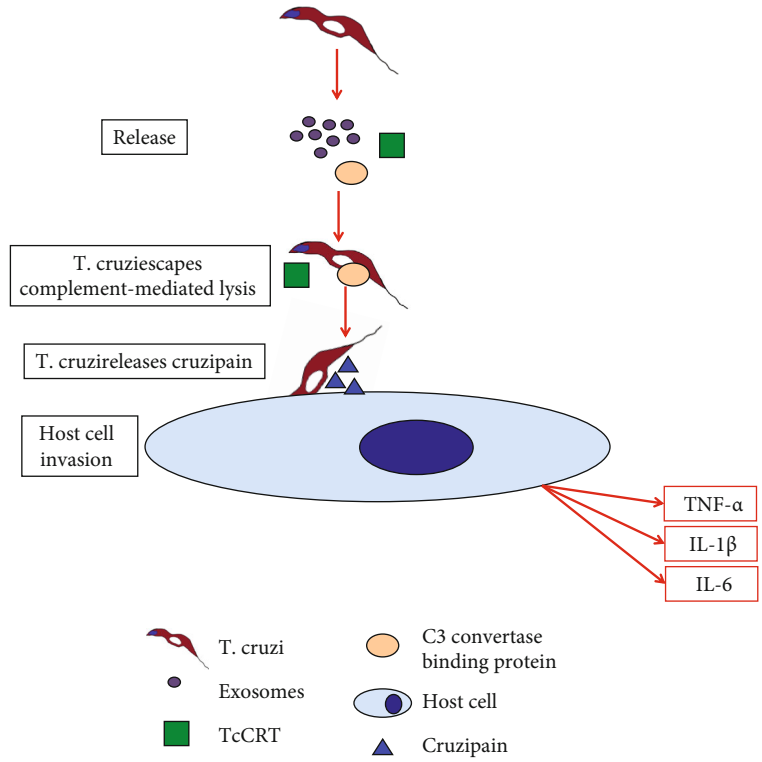

Figure 3: Cellular and molecular mechanisms performed by exosomes during *T. cruzi* infection. *T. cruzi* releases exosomes during infection, which contain C3 convertase binding protein and most likely contains TcCRT as well. C3 binds to the *T. cruzi* surface, but its cleavage is inhibited by C3 convertase binding protein, therefore inhibiting the complement pathway and escaping complement-mediated lysis. On the other hand, TcCRT binds C1q and mannose-binding proteins and ficolins, inhibiting the classical and lectin complement pathways. The parasite also releases cruzipain, which helps *T. cruzi* to invade the host cell. Infected host cells can release cytokines such as TNF-α, IL-1β, and IL-6. Symbols associated with each molecule or cells are indicated in the box.

molecular expression, especially membrane-anchored receptors, and cytokine production, which can enable the T cell effector capabilities [66, 79, 90]. In the context of an acute infection, such as *T. cruzi* infection, the T cell response can be divided into three phases: (i) priming and expansion, (ii) resolution and contraction, and (iii) memory acquisition [66, 79, 90]. During the first phase, the Tn cells proliferate and differentiate in effector T (TE) cells, which increase the expression of several molecules, such as surface receptors and chemokine receptors, which favor activation and migration to lymphoid organs to be retained there [66, 79, 90]. Those changes upon activation promote a rapid amplification of that cell population for a specific response, generation of effector and memory cell populations, enhancement of the APC, and a response within nonpathological levels. There are two types of TE; those monofunctional produce only one cytokine, whereas those polyfunctional simultaneously produce more than one cytokine. In the context of infection and vaccination, the production of polyfunctional cells is considered a good correlate of protection [91, 92]. After the elimination of the antigen source (pathogen), although this is not exactly the case with Chagas disease, the clonal contraction step takes place. Most of the activated TE die for apoptosis, and the immune system goes back to its homeostatic state [93]. However, the process of activation of Tn cells not only produces specific TE cells but also gives rise to memory T cells that can remain after the contraction phase is finished [92]. Those can self-renew by proliferation and can be perpetuated in the long term, being remarkably efficient to acquire effector functions when a new challenge with the antigen occurs [66, 79, 93]. As stated earlier, *T. cruzi* infection can bypass the innate and humoral immunity, and the disease can progress to a chronic state. In chronic Chagas patients, it has been demonstrated that there are an increased number of circulating activated T cells, which can secrete pro- and anti-inflammatory cytokines [94]. However, there is a hampered T cell proliferative response in Chagas disease patients, when cells are exposed to a strong nonspecific mitogen, and there is also a decreased expression of T cell receptors involved in activation [95, 96]. Moreover, T cell activation from noninfected individuals is inhibited by *T. cruzi* antigens [95, 96]. T cell response must be important to maintain a low parasitemia during the chronic phase of Chagas disease, and whether impaired by coinfections (e.g., VIH) could lead to a rapid clinical onset of the disease. On the contrary, whether this response is exacerbated could lead to a pathological state, which must be controlled to impede disease progression and tissue damage. During the host adaptive immune response and Chagas disease progression, the exosomes produced by the parasite play a pivotal role, which is described below.

7. Genetic Variants Associated with Mitochondrial Dysfunction and Inflammation in Cardiomyopathies in Chagas Disease

Chronic Chagas disease cardiomyopathy is an inflammatory cardiomyopathy which is prevalent in Latin America and is present in 30% of the six million individuals infected with *T. cruzi*; however, 70% of the infected individuals remain asymptomatic or free of heart disease. As mentioned earlier, IFN-γ and mitochondrial dysfunction play a main pathogenic role in this disease. Very little is known about the genetic contribution to the progression of chronic inflammatory cardiomyopathy in chronic Chagas disease and the factors that increase cardiomyocyte susceptibility to inflammatory damage. A recent and interesting exome sequencing analysis was performed to study nuclear families containing multiple cases with chronic Chagas inflammatory cardiomyopathy and chronic-infected asymptomatic siblings and in unrelated but infected asymptomatic individuals [97]. Heterozygous pathogenic variants are linked to chronic Chagas disease in all tested families on twenty-two distinct genes; twenty were mitochondrial or inflammation-related, with most of them involved in proinflammatory cytokine production [97]. It has been suggested by the authors that chronic Chagas cardiomyopathy-linked genetic variants can increase mitochondrial susceptibility to IFN-γ-induced damage to the myocardium, which leads to the observed phenotype of chronic inflammatory cardiomyopathy [97]. This was only found in individuals that were both seropositive and carriers of the heterozygous pathogenic variants which developed chronic Chagas cardiomyopathy, but not those seropositive patients carrying the wild-type sequences, neither seronegative siblings carrying the pathogenic variant. The finding that only a single family carried a variant in a gene previously associated with familiar cardiomyopathy indicates that the genetic landscape and pathogenesis of chronic Chagas disease cardiomyopathy is distinct from that of familial cardiomyopathy [97]. Among the nine mitochondrial genes showing chronic Chagas disease cardiomyopathy-specific pathogenic variants, eight are involved in mitochondrial ATP synthesis (biogenesis, translation, FAO, and OXPHOS). Previous studies have shown that patients carrying mutations or animals genetically deficient in six mitochondrial genes (described in 97) can develop cardiac phenotypes [98–101]. Notably, up to 30% of mitochondriopathy patients develop cardiomyopathy, heart conduction defects, ventricular arrhythmia or sudden cardiac death, and autonomic nervous system imbalance [102], while up to 15% develop gastrointestinal motility disorders including achalasia/megaesophagus and megacolon [103]. There is a striking similarity between the clinical presentation and the proportion of cardiac and digestive disorders in mitochondriopathies and the clinical spectrum of chronic Chagas disease, which suggests that the pathogenesis of Chagas disease might be the consequence of mitochondrial dysfunction as well. Chronic Chagas disease cardiomyopathy displays signs of reduced mitochondrial respiratory chain activity [32, 104], energy production [105], decreased rRNA [106], rDNA [107], and decreased ATP production [104]. There is a loss of $\Delta\Psi$ in cardiomyocytes with a concomitant increase in ROS production [108]. In exome sequencing analysis, another eleven pathogenic variants were located in ten inflammation-associated genes. Eight out of these genes are involved in proinflammatory cytokine production via activation of NF-κB and MAP kinase pathways, which leads to an increase in proinflammatory cytokine production, which could lead to further mitochondrial dysfunction in cardiomyocytes. This mitochondrial damage can be further enhanced by IFN-γ. Dysfunctional mitochondria have an increased ROS production, which can produce oxidative stress, further damaging the mitochondria. Interestingly, patients carrying heterozygous gene variants had a normal childhood and reported not to have a debilitating disease before developing chronic Chagas cardiomyopathy as adults, and it is inferred that the genetic variants alone by themselves were not able to induce childhood-onset mitochondriopathy [97]. Finally, the authors support the notion of a two-hit mechanism where IFN-γ and proinflammatory cytokines induced by chronic *T. cruzi* infection trigger mitochondrial dysfunction and clinical disease in carriers of heterozygous mitochondrial gene variants [97].

8. Role of Exosomes in Chagas Disease

The exosomes are membrane-bound extracellular vesicles secreted into the extracellular space by endothelial cells (ECs) and several other cells such as immunocytes, platelets, and smooth muscle cells [109–111]. They play key roles in cell-to-cell signaling, and they are present in almost all biological fluids [112, 113]. There is a continuously extracellular exchange of exosomes, containing bioactive molecules, in between organelles to promote communication during homeostasis and diseased states of the organism [113]. Several studies have suggested the participation of exosomes in cellular communication associated with physiological and pathological states due to their ability to modify the recipient cell phenotype [114, 115]. The process of exosome generation begins with the internalization of the cellular membrane through endocytosis to form an endosome [116]. Afterwards, an invagination occurs on the endosomal membrane to end up with the maturation of multivesicular bodies (MVBs). These MVBs can either be degraded by internal lysosomes or transported to the cell membrane to undertake transcytosis or fusion and release of the contents into the extracellular space as exosomes [116]. Exosomes can then target cells through specific receptors binding to activate cell-to-cell signaling pathways such as horizontal gene transfer, inflammation, antigen presentation, tumor progression, and mediation of the immune response during pathogenic states [117, 118]. The contents of the exosomes consist of several metabolites, proteins, lipids, RNA, and DNA, which can be interchanged in between exosomes and their target cells. Exosomes have been isolated from protozoa, bacteria, viruses, and fungi; however, each exosome has different compositions [119]. As in the case of protozoan parasites, those can modulate host cell responses by producing exosomes with virulence factors and effector molecules and this way can modulate host gene expression, immune response,

and factors to favor parasite growth, survival, and pathogenesis [120]. On the other hand, exosomes released during *T. cruzi* infection might also make possible a host immune response [121].

As in the context of Chagas disease, the parasite and host cell exosomes play a fundamental role in the pathogenesis of Chagas disease. *T. cruzi* infection induces blood cells to release exosomes by a Ca^{2+}-mediated mechanism [122]. The released exosomes are essential to host-parasite interactions, intercellular communications, and increased parasite survival. As an example, exosomes can protect extracellular trypomastigotes from the action of the complement through the binding of C3 convertase on the parasite surface, inhibiting C3 cleavage [123, 124]. Also, exosomes released by *T. cruzi* promote cell invasion and parasite survival by modulating the innate immune system and producing several virulence factors including glycoprotein 85 (gp85), trans-sialidase, phosphatase, and other soluble proteins [124–126]. Therefore, the released parasite and cell host exosomes are able to play a key role during parasite invasion of the host innate immune system, parasite survival, and infection establishment in Chagas disease [127]. Figure 3 shows that *T. cruzi* released exosomes can contain molecules to escape complement-mediated lysis.

Under pathological states, the stimulus that activates exosome formation can regulate their selective arrangement of constituents and composition, thereby regulating the biological information that can transfer. It has been recently demonstrated that exosomes produced by *T. cruzi* trypomastigotes can be fused to host cell membranes and promote exosome release from THP-1 macrophages [128, 129]. Also, it has been found that human peripheral blood mononuclear cells incubated with *T. cruzi* can secrete exosomes, and those exosomes elicit a proinflammatory gene expression response in human THP-1 macrophages. Similarly, a proinflammatory cytokine response was observed in THP-1 macrophages when incubated with exosomes isolated from peripheral blood of Chagas disease patients [130]. Thus, those findings indicate that exposure to *T. cruzi* can influence exosome release, and those have a deep impact on the surrounding infected or injured tissue. The mechanisms of exosome-dependent macrophage activation by *T. cruzi* are not well understood yet. In a recent study, Choudhuri and colleagues [131] have studied the role of exosomes in producing the macrophage response in progressive Chagas disease. It was found that cultured and bone marrow-derived macrophages can respond to exosomes produced from axenic parasite cultures, *T. cruzi*-induced exosomes produced by infected cells, and exosomes derived from plasma of acutely or chronically infected mice [131]. All of those can induce a profound increase in expression and release of cytokines such as TNF-α, IL-6, and IL-1β. Exosomes produced by immune cells (macrophages) and nonimmune cells (muscle) were proinflammatory. However, exosomes derived from plasma of mutant PARP1-/- significantly reduced the exosome-induced transcriptional and translational activation of proinflammatory macrophage response. Interestingly, oxidized DNA contained into the exosomes was necessary for PARP1-dependent proinflammatory response, and the studies suggested that DNA-sensing immune receptor cyclic GMP-AMP synthase (cGAS), a PRR, synergized with PARP1 to signal and activate the NF-κB pathway [131]. Inhibition of both PARP1 and cGAS resulted in more than 80% inhibition of the exosome-induced NF-κB pathway activity. In chagasic mice, a severe inflammatory infiltrate was found, which was associated with an intense increase in CD11b+CD68+TNF-α+ macrophages [131]. In contrast, mutant PARP1-/- chagasic mice showed a low-to-moderate tissue inflammation and more than 80% diminution of myocardial infiltration by TNF-α+ macrophages, and there was no change in immunoregulatory IL-10 macrophages [131]. A schematic representation and the results obtained from those experiments are shown in Figure 4.

Although macrophages are the principal immune cells that can exert trypanocidal effects, since they produce ROS and NO, it has been found that nonimmune cells, such as skeletal muscle cells and cardiomyocytes, can produce high levels of ROS in response to *T. cruzi* infection [77, 132]. ROS can exert cytotoxic effects by oxidizing cellular components including proteins, lipids, and DNA and cannot discriminate between parasite or host cellular components. Indeed, it has been shown that 8-oxo-G, which is a marker for oxidative DNA damage, is augmented in *T. cruzi*-infected cardiomyocytes and in the myocardium of chagasic mice and in chronic Chagas disease patients [59]. Those damaged encapsulated DNA molecules serve as a stimulus for proinflammatory activation of macrophages [131]. The authors proposed that genomic damaged DNA from both host and parasite, which is into the exosomes, provides the primary stimulus in engaging DNA sensing innate immune receptors and macrophage activation in the context of Chagas disease progression [131]. However, it is unknown whether the damaged DNA are random sequences, or it has some sequence preference. Thus, there is an axis PARP1-cGAS-NF-κB, which activates the proinflammatory macrophage activation by exosomes released during *T. cruzi* infection and during the progression of Chagas disease.

9. Omics Studies of *T. cruzi*-Host Cell Interactions

Chagas disease is a clinical consequence of *T. cruzi* infection, and cardiomyopathy is the most severe consequence of the chronic phase of the disease, which cannot be reversed only by reducing the parasite load in the patient. The interaction of *T. cruzi* with host cells is able to trigger several molecular signaling cascades, and the response will be dependent on the cell type, *T. cruzi* strain, and also experimental variables. The global responses of host cells can be effectively studied by -omics technologies, especially transcriptomics and proteomics to assess the gene expression state of *T.cruzi*-infected cells. Even though total gene expression levels can provide useful information, it should be remembered that many important signaling pathways are mediated by post-transcriptional modifications of a particular polypeptide, with minimal variation in protein levels. In particular, posttranscriptional modifications such as phosphorylation, acetylation, and glycosylation are important modifications

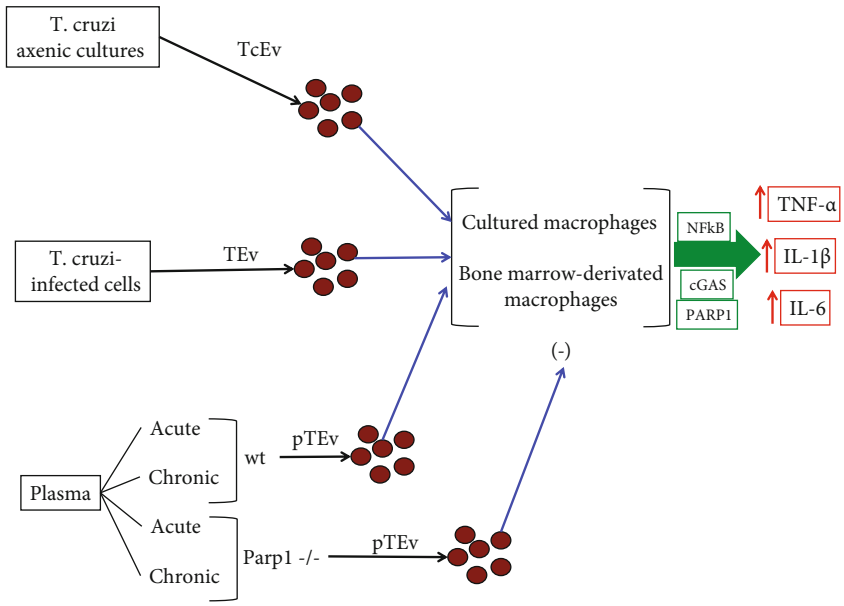

Figure 4: *T. cruzi* extracellular vesicles can activate macrophages to release cytokines. Extracellular vesicles from *T. cruzi* axenic cultures (TcEv), infected cells (TEv), or cultured cells of both acutely or chronically infected mice (pTEv) can stimulate both cultured and bone marrow-derived macrophages to secrete TNF-α, IL-1β, and IL-6. However, plasma-derived TEv from mutant Parp1-/- mice cannot induce cytokine production in macrophages, and it was determined that induction of cytokine production is through the PARP1-cGAS-NF-κB axis.

to regulate the activity of proteins. Therefore, total gene expression levels should be complemented with proteomic approaches that could be combined with phosphoproteomic studies to dissect precisely the signaling pathways involved in chronic *T. cruzi* infection.

It is well known that different *T. cruzi* strains present biological differences including virulence, pathogenicity, and infectivity. To understand the variability, the different strains are classified into six main groups, which are known as discrete typing units (DTUs, from TcI to TcVI). However, there exists a high genetic and biological difference even between strains at the intra-DTU level that can impact the host response to *T. cruzi* infection. Therefore, we would like to highlight that the specific strain impacts *T. cruzi* host cell interactions, and studies with one strain could be not comparable with another different strain, even though they belong to the same DTU.

Transcriptomic studies focused on the changes in the respiratory chain and OXPHOS of host cells, in response to *T. cruzi* infection, have found an upregulation of energy-related metabolism pathways in human primary cardiomyocytes at early times using the Dm28c strain (TcI) [133]. However, when the Tulahuen strain (TcVI) is used, those changes were not observed. In the context of mouse primary cardiomyocytes and at early time postinfection with the Dm28c strain, there were no significant changes in the pathways related to energy metabolism [134], although in other similar studies, but using the Brazil strain (TcI), a downregulation of the electron transport activity was observed, though this study was done on late time postinfection [135]. All these studies indicate that the transcriptomic results are dependent on the *T. cruzi* strain, origin of the infected cell, and the experimental conditions used to perform the study. In the context of in vivo transcriptomics, it has been shown that mouse hearts infected with the Sylvio strain (TcI), Brazil strain (TcI) and Y strain (TcII), Col1.7G2 strain (TcI), and JG strain (TcII) showed a decrease in the expression of genes related to energy metabolism (reviewed in [136] and references therein). Regarding chronic Chagas patients, the cardiac gene expression profile showed an increase in genes related to energy metabolism (reviewed in [136] and references therein). Again, those studies suggest that in vivo transcriptomic results depend on the origin of the infected cell.

Studies that evaluated the changes of both the transcriptional level and the functional response of the components related to cellular respiration have been performed by several groups (reviewed in [135]). In human primary cardiomyocytes with the Dm28c strain, an increase in respiration and mitochondrial biogenesis was found [133], and also, Shah-Simpson et al. [137] found that *T. cruzi*-infected human dermal fibroblasts had increased respiration and mitochondrial biogenesis. Human-infected macrophages with Sylvio strain had also an increase in respiration [138]. Opposite results have been found using murine-infected cells. A decrease in respiration has been found in murine-infected cardiomyocytes with the CLBr strain (TcVI) at similar analyzed times as it was done with human cells [139]. Also, a decrease in the respiration complexes CI and CIII was found in infected murine cardiomyocytes with Sylvio strain [99]. Those studies indicate that the results are related to the specific origin of the cells (mouse or human). In the context of *in vivo* infections, when evaluating the protein expression of different respiratory complexes, a decreased

expression in the complexes CI-CV in cardiac mitochondria of Sylvio-infected mice was found [32]. It has also been found to have a decreased mitochondrial function in the heart, skeletal muscle, colon, and stomach of acute infected mice and in hearts and stomach of chronic *T. cruzi*-infected mice [62]. There are few studies analyzing the cellular respiration in tissues or cells derived from chronic Chagas patients. As an example, in an analysis of hearts from a group of five patients, Teixeira et al. [140] found that there was a small decrease in the expression levels of the alpha subunit of the ATP synthase enzyme (CV). In a similar work done by Wan et al. [52], analyzing the heart of eight chronic Chagas disease patients has shown a decrease in the mitochondrial Cyt B complex protein (CIII) and ND1 protein (CI). Considering that there are several cell types present in the heart (fibroblasts, endothelial cells, and cardiomyocytes) and additional infiltrating macrophages and T cells in the heart of chagasic patients, it might be important to carry out studies in a larger number of chagasic heart samples with isolated cardiomyocytes as long as possible.

Multiplexed proteomic studies in the heart of a Chagas disease mouse model, at the chronic phase of the disease, have revealed an increase in the immune response and strong repression in the expression of several mitochondrial proteins [141]. Concomitantly, the phosphoproteomic analysis showed abundance in phosphosites in plasma membrane and cytoskeletal proteins. The analysis of kinase activity evidenced an activation of the JNK/p38 MAP kinases and also activation of the DYRK2 and AMPKA2 kinases. However, the casein kinase family was inhibited in the host response to *T. cruzi* infection. As it was expected, there was an increase of the IFN-γ-mediated signaling pathways [89] and repression of the mitochondrial function [21, 29, 142].

Significantly, new players that might be important for disease progression were identified in the study [141], such as Immunity-Related GTPase M (IRGM) 1 and 2 and also the immune-associated guanylate binding proteins (GBPs). Additionally, to changes in total protein abundance, it was uncovered a vast signaling network of plasma membranes and intermediate filament proteins with altered phosphorylation status after *T. cruzi* infection. Those include proteins such as Striated Muscle Enriched Protein Kinase (SPEG), Tensin 1, Sorbin and SH3 domain-containing protein (SORBS) 1/2, BCL2 Associated Athanogene (BAG3), and proteins from the myosin family. In those studies, the authors highlighted signaling pathways that can be further studied and validated for their contribution to the disease progression and also could be potential drug targets.

Finally, caution should be taken to interpret and extrapolate results from the murine model to humans, since as mentioned above, an increase in the respiration of *T. cruzi*-infected human cells is found; however, a decrease in infected cells of murine origin is usually found. Libisch and colleagues [136] have proposed that mice have a lower ability to maintain adequate cellular homeostasis against different types of stress, such as oxidative stress by ROS, since mice have a metabolic rate per gram of body weight approximately seven times higher compared with humans [136]. ROS is normally generated [143] but is highly increased in *T. cruzi*-infected cardiomyocytes (mtROS) and macrophages [99, 144]. Perhaps, this is the main reason to explain why cells of human or murine origin do not present the same response against *T. cruzi* infection, at least respecting pathways related to energy metabolism. It is also likely that differences in the immune systems between humans and mice could have an impact on mitochondrial respiration, since a relationship has been established between the immune system and energy metabolism [136, 145].

10. Chagas Disease Treatments

The main therapy for Chagas disease treatment is benznidazole (BZN); however, this drug is highly toxic for patient treatments at the chronic phase and is more effective at the acute phase of the disease [146]. New therapies propose the reduction of BZN doses for chemotherapeutic treatment combined with other drugs to slow the progress of the disease. One example is the combination of the trypanolytic BZN combined with simvastatin to prevent endothelial cell activation induced by *T. cruzi* infection [147]. In this study, the anti-inflammatory effect of simvastatin is mediated by the inhibition of NF-κB. Another study in mice with the antioxidant resveratrol in chronic *T. cruzi* infection improved cardiac function, activating the AMPK pathway without altering the heart inflammatory infiltrates or vascularization [148]. Similar results were observed in a study using carvedilol alone or combined with vitamins E and C to treat patients with chronic chagasic cardiomyopathy. The combined use resulted more efficiently in reducing the oxidative damage, but both treatments were unable to control the inflammatory process, as evaluated by the increase of the inflammatory markers, such as adenosine deaminase and myeloperoxidase [149]. However, when an anti-inflammatory therapy using ibuprofen was compared with an antioxidant therapy using vitamins E and C in *T. cruzi*-infected mice, the first resulted more efficient in the attenuation of oxidative stress and cardiac damage, without altering cardiac parasitism [150]. The use of the anti-inflammatory administration of aspirin does not alter the parasitological course of *T. cruzi* infection in mice, however reduced cardiac inflammatory infiltrates and thromboxane levels [151]. Another type of drug being developed to treat Chagas disease is the so-called target-based drugs to interfere with specific pathways of *T. cruzi* [152]. There are several of those; however, the most important are drugs that can target the ergosterol biosynthesis pathway, trypanothione reductase, cruzipain, enolase, ribose-5-phosphate isomerase, sterol 14-α-demethylase, pteridine reductase, farnesyl diphosphate synthase, isocitrate dehydrogenase 2, dihydrofolate reductase-thymidylate synthase, and the sirtuins [152]. A schematic view of those approaches can be found in Figure 5. On the other hand, new drug candidates with trypanocidal activities have been recently developed, and details can be found in Reference [153]. Sirtuins are deacetylase enzymes of eukaryotic origin, which can regulate several cellular processes, and they have been described as potential targets for Chagas disease treatment [154]. Both *T. cruzi* and the mammalian host have sirtuins. Mammalian

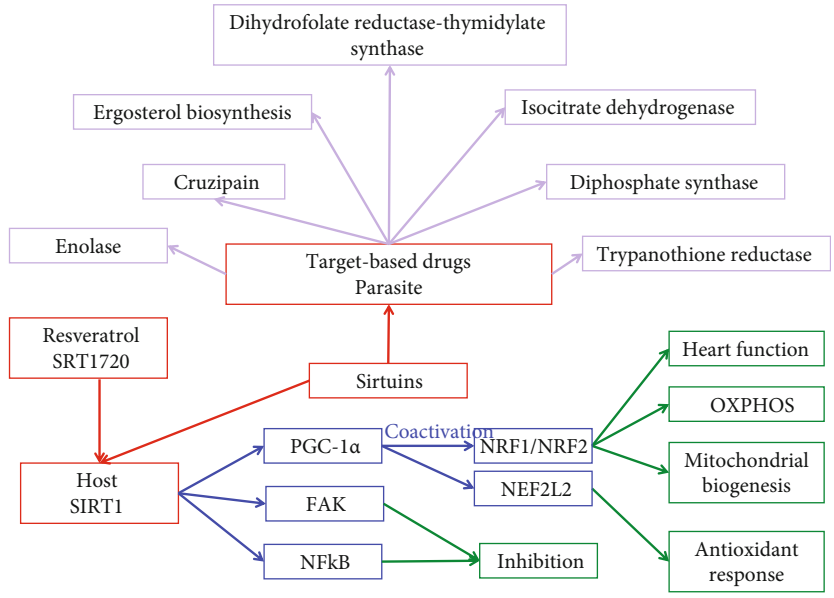

Figure 5: Target-based drugs against *T. cruzi* and SIRT1 therapy. Drugs are being developed against specific *T. cruzi* pathways, and they are shown in the figure. Both the parasite and the mammalian host possess sirtuins; therefore, target-based drugs have been tested against the parasite sirtuins, and antioxidant therapies have been developed to improve the activity of mammalian SIRT1, either by using resveratrol antioxidant or the SRT1720 agonist, which is able to activate SIRT1, which in turn can activate PGC-1α to promote mitochondrial biogenesis and OXPHOS function and improve heart function through the transcription factors NRF1 and NRF2. Also, PGC-1α is a coactivator for NFE2L2, which can activate the antioxidant system. On the other hand, activated SIRT1 can inhibit the activity of transcription factor NF-κB, which leads to a decrease of proinflammatory cytokine production, and also can inhibit the activity of FAK.

SIRT1 is one of the main sirtuins and one of the most studied. SIRT1 therapy is one of the most promising potential new therapies to treat Chagas disease at the chronic phase and deserves a brief analysis. The antioxidant resveratrol, which activates SIRT1, which in turn can deacetylase PGC-1α to activate it and increase the mitochondrial number, stimulates the gene expression of genes involved in oxidative phosphorylation (OXPHOS) function and activates the antioxidant defenses through the NRF factors [155]. SRT1720 is a small selective molecule that can activate SIRT1 by binding to the SIRT1-substrate complex. This small SIRT1 activator is 1,000-fold more potent than resveratrol and can improve OXPHOS function and attenuate aging-related cardiomyocyte dysfunction [156–158]. Its use during the chronic phase of Chagas disease can restore the heart left ventricular function, and PGC-1α was in an active state in chagasic mice, although mitochondrial biogenesis was not improved [155]. SRT1720 treatment of *T. cruzi*-infected mice can decrease splenic expansion and infiltration of proinflammatory monocytes/macrophages in the chagasic mice; however, the capabilities of those cells to respond to *T. cruzi* stimulus are not altered. SRT1720 decreases the *T. cruzi*-induced augment of expression and/or phosphorylation activity of focal adhesion kinase (FAK) and downstream target transcription factors such as Pu.1, c-Myb, and Runx1, involved in macrophage proliferation and migration and Notch1 involved in functional cell activation [55, 65]. Studies using cultured macrophages confirmed that SRT1720 can control the *T. cruzi*-induced FAK-dependent expression of those transcription factors and demonstrated that SRT1720 and a FAK specific inhibitor [55, 65] can inhibit the NF-κB transcriptional activity and in turn inflammatory cytokine gene expression in *T. cruzi*-infected macrophages. Taken altogether, those results indicate that STR1720 can reprogram the *T. cruzi*-induced FAK-dependent transcription factors needed for proliferation and proinflammatory activation in Chagas disease.

SRT1720 treatment can reduce ROS, nitrosative stress, and inflammatory response in the chagasic myocardium through the inhibition of the NF-κB transcriptional pathway, with the subsequent inhibition of the production of proinflammatory cytokines [155]. The main mechanism by which SIRT1 inhibits NF-κB is by a direct deacetylation of p65/RelA preventing the release and nuclear translocation of NF-κB, although other mechanisms can also contribute to the SIRT1 activity [155, 157]. The authors also concluded that *T. cruzi*-induced inhibition of the SIRT1/PGC-1α regulatory axis is not a key mechanism in mitochondrial biogenesis defects observed in Chagas disease [155, 157]. Combined treatment of BZN and SRT1720 could be beneficial during the acute phase of Chagas disease to avoid disease progression and also during the chronic phase of the disease to improve heart function. In this context, we suggest that treatment with activators or agonists of SIRT3 might be another option for the treatment of Chagas disease.

11. Concluding Remarks and Future Directions

It seems clear that chronic cardiomyopathy in Chagas disease is the result of several factors such as the parasite itself, host adaptive immune response, oxidative stress, inflammatory stress, and mitochondrial dysfunction. However, the megaviscera and neurological disorders are another

manifestation of chronic Chagas disease and have not been studied as well as chronic cardiomyopathy, and it is an area that also deserves attention. Mitochondrial dysfunction in cardiomyocytes leads to the production of mtROS, which can induce DNA damage and signal PARP1 to produce PAR, which can help to activate the expression of proinflammatory cytokine genes. Also, mtROS can activate the NF-κB transcription factor, which acts as a transcriptional activator on proinflammatory cytokine genes increasing its expression, which leads to inflammatory stress with sustained ROS production and therefore produces oxidative damage of the cardiac cellular components during the chronic Chagas disease. At the acute phase of the disease, the host innate and the adaptive immune can control the parasitic invasion; however, in around 30% of the patients, the infection is able to progress, and it produces a chronic phase of the disease that can be manifested decades later of the initial infection. The parasite can escape the innate and adaptive immune response by a series of mechanisms such as blocking the complement pathway by producing molecules that can inhibit the complement components or by producing a nonspecific immune response. Secreted extracellular vesicles (exosomes) from both the parasite itself and from the infected host cells play a key role in the immune response. The parasite secretes exosomes containing molecules that can inhibit the complement components and exosomes carrying molecules which can induce cytokine production and a host immune response.

Future studies should be focused to investigate the nature of the mitochondrial dysfunction which produces the mtROS and the persisting ROS signal that produces the inflammatory and oxidative stress states in the cardiac tissue, which is responsible for the cardiac tissue damage. It is likely that epigenetic mechanisms triggered by mtROS could be able to maintain the proinflammatory cytokine gene expression, either by modifying their promoters to keep them on or by activating the gene expression or activity of the NF-κB transcription factor or the transcriptional coactivators necessary for the expression of the proinflammatory cytokine genes. The exosome molecular contents should also be identified, and their contribution to the host immune response has to be studied. Since there is not an available vaccine yet, drugs to treat chronic Chagas disease should be developed and those able to target specific metabolic pathways in *T. cruzi* are especially promising, and also, those drugs able to improve heart function in chagasic patients will be extremely valuable.

Abbreviations

APC: Antigen-presenting cell
BZN: Benznidazole
CI, CII, CIII, CIV: Respiratory chain complexes
cGAS: GMP-AMP synthase
DAMPs: Damage-associated molecular patterns
ΔMIT: Membrane potential
DTU: Discrete typing unit
ERR: Estrogen-related receptor
FAK: Focal adhesion kinase
FAO: Fatty acid oxidation
GPI: Glycosyl phosphatidylinositol
IFN: Interferon
IL: Interleukin
iNOS: Inducible nitric oxide synthase
MHC: Major histocompatibility complex
MnSOD: Manganese-dependent superoxide dismutase
mtROS: Mitochondrial ROS
MVBs: Multivesicular bodies
NAD^+: Nicotinamide adenine dinucleotide
NFE2L2: Nuclear factor erythroid 2-related factor 2
NF-κB: Nuclear factor kappa-light-chain-enhancer of activated B cells
NLR: Nod-like receptor
NOX2: NADPH oxidase 2
NO: Nitric oxide
NRF: Nuclear respiratory factor
OXPHOS: Oxidative phosphorylation
PAMPs: Pathogen-associated molecular patterns
PAR: Poly-ADP-ribose
PARP1: Poly-ADP-ribose polymerase 1
PGC1α: Peroxisome proliferator-activated receptor γ coactivator 1α
PPAR: Peroxisome proliferator-activated receptor γ
PRR: Pattern recognition receptors
RelA: v-rel avian reticuloendotheliosis viral oncogene homolog A
ROS: Reactive oxygen species
SIRT1: Sirtuin 1
SLAMF1: Signaling lymphocytic activation molecule 1
TE: Effector T cell
TcCRT: Calreticulin
TLR: Toll-like receptors
Tn: Naive T cell
TNF: Tumor necrosis factor.

Conflicts of Interest

The authors declare that they have no conflicts of interest.

Authors' Contributions

Edio Maldonado and Diego A. Rojas are the first authors.

Acknowledgments

This work was supported by the Fondo Nacional de Desarrollo Científico y Tecnológico (FONDECYT) Grant #1190392 to A.S. and a Grant from the ICBM to E.M.

References

[1] N. G. Echavarría, L. E. Echeverría, M. Stewart, C. Gallego, and C. Saldarriaga, "Chagas disease: chronic Chagas cardiomyopathy," *Current Problems in Cardiology*, vol. 46, no. 3, article 100507, 2021.

[2] E. A. Bocchi, R. B. Bestetti, M. I. Scanavacca, E. Cunha Neto, and V. S. Issa, "Chronic Chagas heart disease management: from etiology to cardiomyopathy treatment," *Journal of the American College of Cardiology*, vol. 70, no. 12, pp. 1510–1524, 2017.

[3] J. A. Pérez-Molina and I. Molina, "Chagas disease," *The Lancet*, vol. 391, no. 10115, pp. 82–94, 2018.

[4] L. E. Echeverría, R. Marcus, G. Novick et al., "WHF IASC roadmap on Chagas disease," *Global Heart*, vol. 15, no. 1, p. 26, 2020.

[5] R. E. Gürtler and M. C. Cecere, "Chagas disease vector control," in *Triatominae-The biology of chagas disease vectors*, pp. 491–535, Springer, Cham, 2021.

[6] R. Y. Dodd, J. A. Groves, R. L. Townsend et al., "Impact of one-time testing for Trypanosoma cruzi antibodies among blood donors in the United States," *Transfusion*, vol. 59, no. 3, pp. 1016–1023, 2019.

[7] K. C. F. Lidani, F. A. Andrade, L. Bavia et al., "Chagas disease: from discovery to a worldwide health problem," *Frontiers in Public Health*, vol. 7, p. 166, 2019.

[8] J. S. Oliveira, "A natural human model of intrinsic heart nervous system denervation: Chagas' cardiopathy," *American Heart Journal*, vol. 110, no. 5, pp. 1092–1098, 1985.

[9] F. Köberle, "Chagas' disease and Chagas' syndromes: the pathology of American trypanosomiasis," *Advances in Parasitology*, vol. 6, pp. 63–116, 1968.

[10] F. Köberle, "The causation and importance of nervous lesions in American trypanosomiasis," *Bulletin of the World Health Organization*, vol. 42, no. 5, pp. 739–743, 1970.

[11] F. Köberle, "Pathogenesis of Chagas' disease," in *Ciba foundation symposium*, p. 137, Elsevier, 1974.

[12] C. F. Campos, S. D. Cangussú, A. L. C. Duz et al., "Enteric neuronal damage, intramuscular denervation and smooth muscle phenotype changes as mechanisms of chagasic megacolon: evidence from a long-term murine model of Trypanosoma cruzi infection," *PLoS One*, vol. 11, no. 4, article e0153038, 2016.

[13] J. A. Marin-Neto, A. Rassi Jr., A. Avezum Jr. et al., "The BENEFIT trial: testing the hypothesis that trypanocidal therapy is beneficial for patients with chronic Chagas heart disease," *Memórias do Instituto Oswaldo Cruz*, vol. 104, suppl 1, pp. 319–324, 2009.

[14] R. M. E. Arantes, H. H. F. Marche, M. T. Bahia, F. Q. Cunha, M. A. Rossi, and J. S. Silva, "Interferon-γ-Induced Nitric Oxide Causes Intrinsic Intestinal Denervation in _Trypanosoma cruzi_ -Infected Mice," *The American Journal of Pathology*, vol. 164, no. 4, pp. 1361–1368, 2004.

[15] C. N. Paiva, D. F. Feijó, F. F. Dutra et al., "Oxidative stress fuels Trypanosoma cruzi infection in mice," *The Journal of Clinical Investigation*, vol. 122, no. 7, pp. 2531–2542, 2012.

[16] G. R. Goes, P. S. Rocha, A. R. S. Diniz, P. H. N. Aguiar, C. R. Machado, and L. Q. Vieira, "Trypanosoma cruzi needs a signal provided by reactive oxygen species to infect macrophages," *PLoS Neglected Tropical Diseases*, vol. 10, no. 4, article e0004555, 2016.

[17] T. Yoshikawa, A. Baba, and Y. Nagatomo, "Autoimmune mechanisms underlying dilated cardiomyopathy," *Circulation Journal*, vol. 73, no. 4, pp. 602–607, 2009.

[18] E. Cunha-Neto and C. Chevillard, "Chagas disease cardiomyopathy: immunopathology and genetics," *Mediators of Inflammation*, vol. 2014, Article ID 683230, 11 pages, 2014.

[19] K. M. Bonney, D. J. Luthringer, S. A. Kim, N. J. Garg, and D. M. Engman, "Pathology and pathogenesis of Chagas heart Disease," *Mechanisms of Disease*, vol. 14, no. 1, pp. 421–447, 2019.

[20] H. B. Tanowitz, J. J. Wen, F. S. Machado, M. S. Desruisseaux, C. Robello, and N. J. Garg, "Trypanosoma cruzi and Chagas disease: innate immunity, ROS, and cardiovascular system," in *Vascular responses to pathogens*, pp. 183–193, Academic Press, 2016.

[21] S. Gupta, M. Dhiman, J. J. Wen, and N. J. Garg, "ROS Signalling of Inflammatory Cytokines During _*Trypanosoma cruzi*_ Infection," *Advances in Parasitology*, vol. 76, pp. 153–170, 2011.

[22] G. P. Dos Santos, F. M. Abukawa, N. Souza-Melo et al., "Cyclophilin 19 secreted in the host cell cytosol by Trypanosoma cruzi promotes ROS production required for parasite growth," *Cellular Microbiology*, vol. 23, no. 4, article e13295, 2021.

[23] I. Gordiienko, L. Shlapatska, L. Kovalevska, and S. P. Sidorenko, "SLAMF1/CD150 in hematologic malignancies: silent marker or active player?," *Clinical Immunology*, vol. 204, pp. 14–22, 2019.

[24] A. Panday, M. K. Sahoo, D. Osorio, and S. Batra, "NADPH oxidases: an overview from structure to innate immunity-associated pathologies," *Cellular & Molecular Immunology*, vol. 12, no. 1, pp. 5–23, 2015.

[25] B. J. van Driel, G. Liao, P. Engel, and C. Terhorst, "Responses to microbial challenges by SLAMF receptors," *Frontiers in Immunology*, vol. 7, p. 4, 2016.

[26] J. Calderón, E. Maganto-Garcia, C. Punzón, J. Carrión, C. Terhorst, and M. Fresno, "The receptor Slamf1 on the surface of myeloid lineage cells controls susceptibility to infection by Trypanosoma cruzi," *PLoS Pathogens*, vol. 8, no. 7, article e1002799, 2012.

[27] C. Poveda, A. Herreros-Cabello, F. Callejas-Hernández et al., "Interaction of signaling lymphocytic activation molecule family 1 (SLAMF1) receptor with Trypanosoma cruzi is strain-dependent and affects NADPH oxidase expression and activity," *PLoS Neglected Tropical Diseases*, vol. 14, no. 9, article e0008608, 2020.

[28] D. A. Butterfield, T. Koppal, B. Howard et al., "Structural and functional changes in proteins induced by free radical-mediated oxidative stress and protective action of the antioxidants N-tert-Butyl-alpha-phenylnitrone and vitamin Ea," *Annals of the New York Academy of Sciences*, vol. 854, no. 1 TOWARDS PROLO, pp. 448–462, 1998.

[29] M. Lopez, H. B. Tanowitz, and N. J. Garg, "Pathogenesis of chronic Chagas disease: macrophages, mitochondria, and oxidative stress," *Current clinical microbiology reports*, vol. 5, no. 1, pp. 45–54, 2018.

[30] M. Chevion, E. Berenshtein, and E. R. Stadtman, "Human studies related to protein oxidation: protein carbonyl content as a marker of damage," *Free Radical Research*, vol. 33 Suppl, pp. S99–108, 2000.

[31] S. Gupta, J.-J. Wen, and N. J. Garg, "Oxidative stress in Chagas disease," *Interdisciplinary perspectives on infectious diseases*, vol. 2009, Article ID 190354, 8 pages, 2009.

[32] G. Vyatkina, V. Bhatia, A. Gerstner, J. Papaconstantinou, and N. Garg, "Impaired mitochondrial respiratory chain and bioenergetics during chagasic cardiomyopathy development," *Biochimica et Biophysica Acta (BBA) - Molecular Basis of Disease*, vol. 1689, no. 2, pp. 162–173, 2004.

[33] J.-J. Wen and N. J. Garg, "Mitochondrial generation of reactive oxygen species is enhanced at the Q o site of the complex III in the myocardium of Trypanosoma cruzi-infected mice: beneficial effects of an antioxidant," *Journal of Bioenergetics and Biomembranes*, vol. 40, no. 6, pp. 587–598, 2008.

[34] M. Dhiman and N. J. Garg, "NADPH oxidase inhibition ameliorates Trypanosoma cruzi-induced myocarditis during Chagas disease," *The Journal of Pathology*, vol. 225, no. 4, pp. 583–596, 2011.

[35] F. S. Machado, H. B. Tanowitz, and A. L. Ribeiro, "Pathogenesis of Chagas cardiomyopathy: role of inflammation and oxidative stress," *Journal of the American Heart Association*, vol. 2, no. 5, article e000539, 2013.

[36] E. Maldonado, D. A. Rojas, F. Urbina, and A. Solari, "The use of antioxidants as potential co-adjuvants to treat chronic chagas disease," *Antioxidants*, vol. 10, no. 7, p. 1022, 2021.

[37] M. Dhiman and N. J. Garg, "P47phox−/− mice are compromised in expansion and activation of CD8+ T cells and susceptible to Trypanosoma cruzi infection," *PLoS Pathogens*, vol. 10, no. 12, article e1004516, 2014.

[38] J. Hom and S.-S. Sheu, "Morphological dynamics of mitochondria – A special emphasis on cardiac muscle cells," *Journal of Molecular and Cellular Cardiology*, vol. 46, no. 6, pp. 811–820, 2009.

[39] P. Puigserver, Z. Wu, C. W. Park, R. Graves, M. Wright, and B. M. Spiegelman, "A cold-inducible coactivator of nuclear receptors linked to adaptive thermogenesis," *Cell*, vol. 92, no. 6, pp. 829–839, 1998.

[40] K. N. Miller, J. P. Clark, and R. M. Anderson, "Mitochondrial regulator PGC-1a–Modulating the modulator," *Current opinion in endocrine and metabolic research*, vol. 5, pp. 37–44, 2019.

[41] K. N. Miller, J. P. Clark, S. A. Martin et al., "PGC-1a integrates a metabolism and growth network linked to caloric restriction," *Aging Cell*, vol. 18, no. 5, article e12999, 2019.

[42] R. Ventura-Clapier, A. Garnier, and V. Veksler, "Transcriptional control of mitochondrial biogenesis: the central role of PGC-1," *Cardiovascular Research*, vol. 79, no. 2, pp. 208–217, 2008.

[43] B. L. Tang, "Sirt1 and the mitochondria," *Molecules and Cells*, vol. 39, no. 2, pp. 87–95, 2016.

[44] G. W. Dorn, R. B. Vega, and D. P. Kelly, "Mitochondrial biogenesis and dynamics in the developing and diseased heart," *Genes & Development*, vol. 29, no. 19, pp. 1981–1991, 2015.

[45] H. Taegtmeyer, *Switching metabolic genes to build a better heart.*, vol. 106, no. 16, pp. 2043–2045, 2002.

[46] R. Ventura-Clapier, A. Garnier, and V. Veksler, "Energy metabolism in heart failure," *The Journal of Physiology*, vol. 555, no. 1, pp. 1–13, 2004.

[47] L. Lai, T. C. Leone, M. P. Keller et al., "Energy metabolic reprogramming in the hypertrophied and early stage failing heart: a multisystems approach," *Circulation: Heart Failure*, vol. 7, no. 6, pp. 1022–1031, 2014.

[48] Z. Arany, M. Novikov, S. Chin, Y. Ma, A. Rosenzweig, and B. M. Spiegelman, "Transverse aortic constriction leads to accelerated heart failure in mice lacking PPAR- coactivator 1," *Proceedings of the National Academy of Sciences*, vol. 103, no. 26, pp. 10086–10091, 2006.

[49] L. Lai, T. C. Leone, C. Zechner et al., "Transcriptional coactivators PGC-1α and PGC-lβ control overlapping programs required for perinatal maturation of the heart," *Genes & Development*, vol. 22, no. 14, pp. 1948–1961, 2008.

[50] L. Lai, M. Wang, O. J. Martin et al., "A Role for Peroxisome Proliferator-activated Receptor γ Coactivator 1 (PGC-1) in the Regulation of Cardiac Mitochondrial Phospholipid Biosynthesis," *Journal of Biological Chemistry*, vol. 289, no. 4, pp. 2250–2259, 2014.

[51] K. Ge, M. Guermah, C. X. Yuan et al., "Transcription coactivator TRAP220 is required for PPARγ2-stimulated adipogenesis," *Nature*, vol. 417, no. 6888, pp. 563–567, 2002.

[52] X. Wan, S. Gupta, M. P. Zago et al., "Defects of mtDNA replication impaired mitochondrial biogenesis DuringTrypanosoma cruziInfection in human cardiomyocytes and chagasic patients: the role of Nrf1/2 and antioxidant response," *Journal of the American Heart Association*, vol. 1, no. 6, article e003855, 2012.

[53] T. Ide, H. Tsutsui, S. Kinugawa et al., "Mitochondrial electron transport complex I is a potential source of oxygen free radicals in the failing myocardium," *Circulation Research*, vol. 85, no. 4, pp. 357–363, 1999.

[54] Q. Chen, E. J. Vazquez, S. Moghaddas, C. L. Hoppel, and E. J. Lesnefsky, "Production of Reactive Oxygen Species by Mitochondria:," *Journal of Biological Chemistry*, vol. 278, no. 38, pp. 36027–36031, 2003.

[55] X. Wan and N. J. Garg, "Sirtuin control of mitochondrial dysfunction, oxidative stress, and inflammation in Chagas disease models," *Frontiers in Cellular and Infection Microbiology*, vol. 11, p. 693051, 2021.

[56] X. Ba, S. Gupta, M. Davidson, and N. J. Garg, "*Trypanosoma cruzi* Induces the Reactive Oxygen Species-PARP-1-RelA Pathway for Up-regulation of Cytokine Expression in Cardiomyocytes," *Journal of Biological Chemistry*, vol. 285, no. 15, pp. 11596–11606, 2010.

[57] P. Balakumar and M. Singh, "Possible role of poly (ADP-ribose) polymerase in pathological and physiological cardiac hypertrophy," *Methods and Findings in Experimental and Clinical Pharmacology*, vol. 28, no. 10, pp. 683–689, 2006.

[58] P. Pacher and C. Szabo, "Role of the Peroxynitrite-Poly(-ADP-Ribose) Polymerase Pathway in Human Disease," *The American Journal of Pathology*, vol. 173, no. 1, pp. 2–13, 2008.

[59] X. Ba and N. J. Garg, "Signaling Mechanism of Poly(ADP-Ribose) Polymerase-1 (PARP-1) in Inflammatory Diseases," *The American Journal of Pathology*, vol. 178, no. 3, pp. 946–955, 2011.

[60] B. Pecoul, C. Batista, E. Stobbaerts et al., "The BENEFIT trial: where do we go from here?," *PLoS Neglected Tropical Diseases*, vol. 10, no. 2, article e0004343, 2016.

[61] E. Maldonado, D. A. Rojas, S. Morales, V. Miralles, and A. Solari, "Dual and opposite roles of reactive oxygen species (ROS) in Chagas disease: beneficial on the pathogen and harmful on the host," *Oxidative Medicine and Cellular Longevity*, vol. 2020, Article ID 8867701, 17 pages, 2020.

[62] J. Wen, M. Dhiman, E. Whorton, and N. Garg, "Tissue-specific oxidative imbalance and mitochondrial dysfunction during _*Trypanosoma cruzi*_ infection in mice," *Microbes and Infection*, vol. 10, no. 10-11, pp. 1201–1209, 2008.

[63] M. Dhiman, Y. A. Coronado, C. K. Vallejo et al., "Innate immune responses and antioxidant/oxidant imbalance are major determinants of human Chagas disease," *PLoS Neglected Tropical Diseases*, vol. 7, no. 8, article e2364, 2013.

[64] J. P. Sánchez-Villamil, P. K. Bautista-Niño, N. C. Serrano, M. Y. Rincon, and N. J. Garg, "Potential role of antioxidants as adjunctive therapy in Chagas disease," *Oxidative Medicine and Cellular Longevity*, vol. 2020, Article ID 9081813, 13 pages, 2020.

[65] X. Wan, I. H. Chowdhury, Z. Jie, S. Choudhuri, and N. J. Garg, "Origin of monocytes/macrophages contributing to chronic inflammation in Chagas disease: SIRT1 inhibition of FAK-NFκB-dependent proliferation and proinflammatory activation of macrophages," *Cell*, vol. 9, no. 1, p. 80, 2020.

[66] G. R. Acevedo, M. C. Girard, and K. A. Gómez, "The unsolved jigsaw puzzle of the immune response in Chagas disease," *Frontiers in Immunology*, vol. 9, p. 1929, 2018.

[67] P. Gurung and T.-D. Kanneganti, "Immune responses against protozoan parasites: a focus on the emerging role of Nod-like receptors," *Cellular and Molecular Life Sciences*, vol. 73, no. 16, pp. 3035–3051, 2016.

[68] K. Dolasia, M. K. Bisht, G. Pradhan, A. Udgata, and S. Mukhopadhyay, "TLRs/NLRs: Shaping the landscape of host immunity," *International Reviews of Immunology*, vol. 37, no. 1, pp. 3–19, 2018.

[69] M. A. S. Campos, I. C. Almeida, O. Takeuchi et al., "Activation of Toll-like receptor-2 by glycosylphosphatidylinositol anchors from a protozoan parasite," *The Journal of Immunology*, vol. 167, no. 1, pp. 416–423, 2001.

[70] A. C. Oliveira, J. R. Peixoto, L. B. de Arruda et al., "Expression of functional TLR4 confers proinflammatory responsiveness to Trypanosoma cruzi glycoinositolphospholipids and higher resistance to infection with T. cruzi," *The Journal of Immunology*, vol. 173, no. 9, pp. 5688–5696, 2004.

[71] A. Bafica, H. C. Santiago, R. Goldszmid, C. Ropert, R. T. Gazzinelli, and A. Sher, "Cutting edge: TLR9 and TLR2 signaling together account for MyD88-dependent control of parasitemia in Trypanosoma cruzi infection," *The Journal of Immunology*, vol. 177, no. 6, pp. 3515–3519, 2006.

[72] B. C. Caetano, B. B. Carmo, M. B. Melo et al., "Requirement of UNC93B1 reveals a critical role for TLR7 in host resistance to primary infection with Trypanosoma cruzi," *The Journal of Immunology*, vol. 187, no. 4, pp. 1903–1911, 2011.

[73] J. S. Silva, F. S. Machado, and G. A. Martins, "The role of nitric oxide in the pathogenesis of Chagas disease," *Frontiers in Bioscience*, vol. 8, no. 6, pp. s314–s325, 2003.

[74] R. L. Tarleton, "CD8+ T cells in Trypanosoma cruzi infection," in *Seminars in immunopathology*, pp. 233–238, Springer, Berlin Heidelberg, 2015.

[75] L. van Overtvelt, N. Vanderheyde, V. Verhasselt et al., "Trypanosoma cruzi infects human dendritic cells and prevents their maturation: inhibition of cytokines, HLA-DR, and costimulatory molecules," *Infection and Immunity*, vol. 67, no. 8, pp. 4033–4040, 1999.

[76] T. A. da Costa, M. V. Silva, M. T. Mendes et al., "Immunomodulation by Trypanosoma cruzi: toward understanding the association of dendritic cells with infecting TcI and TcII populations," *Journal of Immunology Research*, vol. 2014, Article ID 962047, 12 pages, 2014.

[77] F. Cardillo, J. C. Voltarelli, S. G. Reed, and J. S. Silva, "Regulation of Trypanosoma cruzi infection in mice by gamma interferon and interleukin 10: role of NK cells," *Infection and Immunity*, vol. 64, no. 1, pp. 128–134, 1996.

[78] T. Lieke, S. E. B. Graefe, U. Klauenberg, B. Fleischer, and T. Jacobs, "NK cells contribute to the control of Trypanosoma cruzi infection by killing free parasites by perforin-independent mechanisms," *Infection and Immunity*, vol. 72, no. 12, pp. 6817–6825, 2004.

[79] G. R. Acevedo, M. C. Girard, and K. A. Gómez, "A panoramic view of the immune response to Trypanosoma cruzi infection," in *Chagas Disease*, pp. 61–88, Springer, Cham, 2019.

[80] L. R. P. Ferreira, F. M. Ferreira, H. I. Nakaya et al., "Blood gene signatures of Chagas cardiomyopathy with or without ventricular dysfunction," *The Journal of Infectious Diseases*, vol. 215, no. 3, pp. 387–395, 2017.

[81] K. C. F. Lidani, L. Bavia, A. R. Ambrosio, and I. J. de Messias-Reason, "The complement system: a prey of Trypanosoma cruzi," *Frontiers in Microbiology*, vol. 8, p. 607, 2017.

[82] G. Ramírez-Toloza and A. Ferreira, "Trypanosoma cruzi evades the complement system as an efficient strategy to survive in the mammalian host: the specific roles of host/parasite molecules and Trypanosoma cruzi calreticulin," *Frontiers in Microbiology*, vol. 8, p. 1667, 2017.

[83] G. M. Krautz, J. C. Kissinger, and A. U. Krettli, "The Targets of the Lytic Antibody Response against _*Trypanosoma cruzi*," *Parasitology Today*, vol. 16, no. 1, pp. 31–34, 2000.

[84] T. A. d. O. Mendes, J. L. Reis Cunha, R. de Almeida Lourdes et al., "Identification of strain-specific B-cell epitopes in Trypanosoma cruzi using genome-scale epitope prediction and high-throughput immunoscreening with peptide arrays," *PLoS Neglected Tropical Diseases*, vol. 7, no. 10, article e2524, 2013.

[85] S. Kumar and R. L. Tarleton, "The relative contribution of antibody production and CD8+ T cell function to immune control of Trypanosoma cruzi," *Parasite Immunology*, vol. 20, no. 5, pp. 207–216, 1998.

[86] D. A. Bermejo, M. C. Amezcua Vesely, M. Khan et al., "Trypanosoma cruzi infection induces a massive extrafollicular and follicular splenic B-cell response which is a high source of non-parasite-specific antibodies," *Immunology*, vol. 132, no. 1, pp. 123–133, 2011.

[87] K. M. Bonney and D. M. Engman, "Autoimmune pathogenesis of Chagas heart disease: looking back, looking ahead," *The American Journal of Pathology*, vol. 185, no. 6, pp. 1537–1547, 2015.

[88] M. Gorosito Serrán, J. Tosello Boari, F. Fiocca Vernengo et al., "Unconventional pro-inflammatory CD4+ T cell response in B Cell-deficient mice infected with Trypanosoma cruzi," *Frontiers in Immunology*, vol. 8, p. 1548, 2017.

[89] N. L. Sullivan, C. S. Eickhoff, J. Sagartz, and D. F. Hoft, "Deficiency of antigen-specific B cells results in decreased Trypanosoma cruzi systemic but not mucosal immunity due to CD8 T cell exhaustion," *The Journal of Immunology*, vol. 194, no. 4, pp. 1806–1818, 2015.

[90] B. J. Laidlaw, J. E. Craft, and S. M. Kaech, "The multifaceted role of $CD4^+$ T cells in $CD8^+$ T cell memory," *Nature Reviews Immunology*, vol. 16, no. 2, pp. 102–111, 2016.

[91] D. A. Lewinsohn, D. M. Lewinsohn, and T. J. Scriba, "Polyfunctional CD4+ T cells as targets for tuberculosis vaccination," *Frontiers in Immunology*, vol. 8, p. 1262, 2017.

[92] A. Thakur, L. E. Pedersen, and G. Jungersen, "Immune markers and correlates of protection for vaccine induced immune responses," *Vaccine*, vol. 30, no. 33, pp. 4907–4920, 2012.

[93] B. Pulendran and R. Ahmed, "Translating innate immunity into immunological memory: implications for vaccine development," *Cell*, vol. 124, no. 4, pp. 849–863, 2006.

[94] W. O. Dutra and K. J. Gollob, "Current concepts in immunoregulation and pathology of human Chagas disease," *Current Opinion in Infectious Diseases*, vol. 21, no. 3, pp. 287–292, 2008.

[95] G. R. Acevedo, S. A. Longhi, A. Bunying et al., "Methodological approach to the ex vivo expansion and detection of T. cruzi-specific T cells from chronic Chagas disease patients," *PLoS One*, vol. 12, no. 5, article e0178380, 2017.

[96] N. A. Giraldo, N. I. Bolaños, A. Cuellar et al., "T lymphocytes from chagasic patients are activated but lack proliferative capacity and down-regulate CD28 and CD3ζ," *PLoS Neglected Tropical Diseases*, vol. 7, no. 1, 2013.

[97] M. Ouarhache, S. Marquet, A. F. Frade et al., "Rare pathogenic variants in mitochondrial and inflammation-associated genes may lead to inflammatory cardiomyopathy in Chagas disease," *Journal of Clinical Immunology*, vol. 41, no. 5, pp. 1048–1063, 2021.

[98] J. X. Fang, T. Uchiumi, M. Yagi et al., "Dihydro-orotate dehydrogenase is physically associated with the respiratory complex and its loss leads to mitochondrial dysfunction," *Bioscience Reports*, vol. 33, no. 2, article e00021, 2013.

[99] J. Pang, X. Xu, M. R. Getman et al., "G protein coupled receptor kinase 2 interacting protein 1 (GIT1) is a novel regulator of mitochondrial biogenesis in heart," *Journal of Molecular and Cellular Cardiology*, vol. 51, no. 5, pp. 769–776, 2011.

[100] M. Shoko, F. Shuichi, and H. Takashi, "Reduction of β-oxidation capacity of rat liver mitochondria by feeding orotic acid," *Biochimica et Biophysica Acta (BBA)-Lipids and Lipid Metabolism*, vol. 711, no. 3, pp. 494–502, 1982.

[101] M. Kohda, Y. Tokuzawa, Y. Kishita et al., "A comprehensive genomic analysis reveals the genetic landscape of mitochondrial respiratory chain complex deficiencies," *PLoS Genetics*, vol. 12, no. 1, article e1005679, 2016.

[102] J. Finsterer and S. Kothari, "Cardiac manifestations of primary mitochondrial disorders," *International Journal of Cardiology*, vol. 177, no. 3, pp. 754–763, 2014.

[103] J. Finsterer and M. Frank, "Gastrointestinal manifestations of mitochondrial disorders: a systematic review," *Therapeutic Advances in Gastroenterology*, vol. 10, no. 1, pp. 142–154, 2017.

[104] J.-J. Wen and N. J. Garg, "Mitochondrial complex III defects contribute to inefficient respiration and ATP synthesis in the myocardium of Trypanosoma cruzi–infected mice," *Antioxidants & Redox Signaling*, vol. 12, no. 1, pp. 27–37, 2010.

[105] A. M. Leme, V. M. C. Salemi, J. R. Parga et al., "Evaluation of the metabolism of high energy phosphates in patients with Chagas' disease," *Arquivos Brasileiros de Cardiologia*, vol. 95, no. 2, pp. 264–273, 2010.

[106] E. Cunha-Neto, J. Dzau Victor, D. Allen Paul et al., "Cardiac gene expression profiling provides evidence for cytokinopathy as a molecular mechanism in Chagas' disease cardiomyopathy," *American Journal of Pathology*, vol. 167, no. 2, pp. 305–313, 2005.

[107] X. Wan, S. Gupta, M. P. Zago et al., "Defects of mtDNA replication impaired mitochondrial biogenesis during Trypanosoma cruzi infection in human cardiomyocytes and chagasic patients: the role of Nrf 1/2 and antioxidant response," *Journal of the American Heart Association*, vol. 1, no. 6, article e003855, 2012.

[108] S. Gupta, V. Bhatia, J.-j. Wen, Y. Wu, M.-H. Huang, and N. J. Garg, "*Trypanosoma cruzi* infection disturbs mitochondrial membrane potential and ROS production rate in cardiomyocytes," *Free Radical Biology and Medicine*, vol. 47, no. 10, pp. 1414–1421, 2009.

[109] R. M. Johnstone, "Exosomes biological significance: a concise review," *Blood Cells, Molecules, and Diseases*, vol. 36, no. 2, pp. 315–321, 2006.

[110] E. Wieckowski and T. L. Whiteside, "Human tumor-derived vs dendritic cell-derived exosomes have distinct biologic roles and molecular profiles," *Immunologic Research*, vol. 36, no. 1-3, pp. 247–254, 2006.

[111] S. C. Saunderson, A. C. Dunn, P. R. Crocker, and A. D. McLellan, "CD169 mediates the capture of exosomes in spleen and lymph node," *Blood*, vol. 123, no. 2, pp. 208–216, 2014.

[112] J. Zhang, S. Li, L. Li et al., "Exosome and exosomal microRNA: trafficking, sorting, and function," *Genomics, Proteomics & Bioinformatics*, vol. 13, no. 1, pp. 17–24, 2015.

[113] S. Gurunathan, M.-H. Kang, and J.-H. Kim, "A comprehensive review on factors influences biogenesis, functions, therapeutic and clinical implications of exosomes," *International Journal of Nanomedicine*, vol. 16, pp. 1281–1312, 2021.

[114] M. Simons and G. Raposo, "Exosomes - vesicular carriers for intercellular communication," *Current Opinion in Cell Biology*, vol. 21, no. 4, pp. 575–581, 2009.

[115] J. Liao, R. Liu, L. Yin, and Y. Pu, "Expression profiling of exosomal miRNAs derived from human esophageal cancer cells by Solexa high-throughput sequencing," *International Journal of Molecular Sciences*, vol. 15, no. 9, pp. 15530–15551, 2014.

[116] N. P. Hessvik and A. Llorente, "Current knowledge on exosome biogenesis and release," *Cellular and Molecular Life Sciences*, vol. 75, no. 2, pp. 193–208, 2018.

[117] M. Mathieu, L. Martin-Jaular, G. Lavieu, and C. Théry, "Specificities of secretion and uptake of exosomes and other extracellular vesicles for cell-to-cell communication," *Nature Cell Biology*, vol. 21, no. 1, pp. 9–17, 2019.

[118] A. Bobrie, M. Colombo, G. Raposo, and C. Théry, "Exosome secretion: molecular mechanisms and roles in immune responses," *Traffic*, vol. 12, no. 12, pp. 1659–1668, 2011.

[119] J. S. Schorey, Y. Cheng, P. P. Singh, and V. L. Smith, "Exosomes and other extracellular vesicles in host–pathogen interactions," *EMBO Reports*, vol. 16, no. 1, pp. 24–43, 2015.

[120] P.-Y. Mantel and M. Marti, "The role of extracellular vesicles inPlasmodiumand other protozoan parasites," *Cellular Microbiology*, vol. 16, no. 3, pp. 344–354, 2014.

[121] E. Bayer-Santos, C. Aguilar-Bonavides, S. P. Rodrigues et al., "Proteomic analysis of Trypanosoma cruzi secretome: characterization of two populations of extracellular vesicles and soluble proteins," *Journal of Proteome Research*, vol. 12, no. 2, pp. 883–897, 2013.

[122] I. Cestari, E. Ansa-Addo, P. Deolindo, J. M. Inal, and M. I. Ramirez, "Trypanosoma cruzi immune evasion mediated by host cell-derived microvesicles," *The Journal of Immunology*, vol. 188, no. 4, pp. 1942–1952, 2012.

[123] M. P. Wyllie and M. I. Ramirez, "Microvesicles released during the interaction between Trypanosoma cruzi TcI and TcII strains and host blood cells inhibit complement system and increase the infectivity of metacyclic forms of host cells in a strain-independent process," *Pathogens and Disease*, vol. 75, no. 7, p. 7, 2017.

[124] I. Cestari and M. I. Ramirez, "Inefficient complement system clearance of Trypanosoma cruzi metacyclic trypomastigotes enables resistant strains to invade eukaryotic cells," *PLoS One*, vol. 5, no. 3, article e9721, 2010.

[125] A. Trocolitorrecilhas, R. Tonelli, W. Pavanelli et al., "Trypanosoma cruzi: parasite shed vesicles increase heart parasitism and generate an intense inflammatory response," *Microbes and Infection*, vol. 11, no. 1, pp. 29–39, 2009.

[126] L. M. De Pablos Torró, L. Retana Moreira, and A. Osuna, "Extracellular vesicles in Chagas disease: a new passenger for an old disease," *Frontiers in Microbiology*, vol. 9, p. 1190, 2018.

[127] S. Varikuti, B. Kumar Jha, E. A. Holcomb et al., "The role of vascular endothelium and exosomes in human protozoan parasitic diseases," *Vessel plus*, vol. 2020, 2020.

[128] I. H. Chowdhury, S.-j. Koo, S. Gupta et al., "Gene expression profiling and functional characterization of macrophages in response to circulatory microparticles produced during Trypanosoma cruzi infection and Chagas disease," *Journal of Innate Immunity*, vol. 9, no. 2, pp. 203–216, 2017.

[129] A. Cronemberger-Andrade, P. Xander, R. P. Soares et al., "Trypanosoma cruzi-Infected Human Macrophages Shed Proinflammatory Extracellular Vesicles That Enhance Host-Cell Invasion via Toll-Like Receptor 2," *Frontiers in Cellular and Infection Microbiology*, vol. 10, p. 99, 2020.

[130] N. J. Garg, K. V. Soman, M. P. Zago et al., "Changes in proteome profile of peripheral blood mononuclear cells in chronic Chagas disease," *PLoS Neglected Tropical Diseases*, vol. 10, no. 2, article e0004490, 2016.

[131] S. Choudhuri and N. J. Garg, "PARP1-cGAS-NF-κB pathway of proinflammatory macrophage activation by extracellular vesicles released during Trypanosoma cruzi infection and Chagas disease," *PLoS Pathogens*, vol. 16, no. 4, article e1008474, 2020.

[132] P. P. Dias, R. F. Capila, N. F. do Couto et al., "Cardiomyocyte oxidants production may signal to T. cruzi intracellular development," *PLoS Neglected Tropical Diseases*, vol. 11, no. 8, article e0005852, 2017.

[133] M. G. Libisch, P. Faral-Tello, N. J. Garg, R. Radi, L. Piacenza, and C. Robello, "Early Trypanosoma cruzi infection triggers mTORC1-mediated respiration increase and mitochondrial biogenesis in human primary cardiomyocytes," *Frontiers in Microbiology*, vol. 9, p. 1889, 2018.

[134] P. A. Manque, C. Probst, M. C. S. Pereira et al., "Trypanosoma cruzi infection induces a global host cell response in cardiomyocytes," *Infection and Immunity*, vol. 79, no. 5, pp. 1855–1862, 2011.

[135] R. C. S. Goldenberg, D. A. Iacobas, S. Iacobas et al., "Transcriptomic alterations in _*Trypanosoma cruzi*_ -infected cardiac myocytes," *Microbes and Infection*, vol. 11, no. 14-15, pp. 1140–1149, 2009.

[136] M. G. Libisch, N. Rego, and C. Robello, "Transcriptional studies on Trypanosoma cruzi–host cell interactions: a complex puzzle of variables," *Frontiers in Cellular and Infection Microbiology*, vol. 11, p. 521, 2021.

[137] S. Shah-Simpson, G. Lentini, P. C. Dumoulin, and B. A. Burleigh, "Modulation of host central carbon metabolism and in situ glucose uptake by intracellular Trypanosoma cruzi amastigotes," *PLoS Pathogens*, vol. 13, no. 11, article e1006747, 2017.

[138] S. J. Koo, I. H. Chowdhury, B. Szczesny, X. Wan, and N. J. Garg, "Macrophages promote oxidative metabolism to drive nitric oxide generation in response to Trypanosoma cruzi," *Infection and Immunity*, vol. 84, no. 12, pp. 3527–3541, 2016.

[139] D. Estrada, G. Specker, A. Martínez et al., "Cardiomyocyte diffusible redox mediators controlTrypanosoma cruziinfection: role of parasite mitochondrial iron superoxide dismutase," *Biochemical Journal*, vol. 475, no. 7, pp. 1235–1251, 2018.

[140] P. C. Teixeira, R. H. B. Santos, A. I. Fiorelli et al., "Selective decrease of components of the creatine kinase system and ATP synthase complex in chronic Chagas disease cardiomyopathy," *PLoS Neglected Tropical Diseases*, vol. 5, no. 6, article e1205, 2011.

[141] J. M. Wozniak, T. A. Silva, D. Thomas et al., "Molecular dissection of Chagas induced cardiomyopathy reveals central disease associated and druggable signaling pathways," *PLoS Neglected Tropical Diseases*, vol. 14, no. 5, article e0007980, 2020.

[142] A. L. Báez, M. N. Reynoso, M. S. Lo Presti et al., "Mitochondrial dysfunction in skeletal muscle during experimental Chagas disease," *Experimental and Molecular Pathology*, vol. 98, no. 3, pp. 467–475, 2015.

[143] M. Scheibye-Knudsen, E. F. Fang, D. L. Croteau, D. M. Wilson III, and V. A. Bohr, "Protecting the mitochondrial powerhouse," *Trends in Cell Biology*, vol. 25, no. 3, pp. 158–170, 2015.

[144] M. N. Alvarez, G. Peluffo, L. Piacenza, and R. Radi, "Intraphagosomal Peroxynitrite as a Macrophage-derived Cytotoxin against Internalized *Trypanosoma cruzi*," *Journal of Biological Chemistry*, vol. 286, no. 8, pp. 6627–6640, 2011.

[145] C. N. S. Breda, G. G. Davanzo, P. J. Basso, N. O. Saraiva Câmara, and P. M. M. Moraes-Vieira, "Mitochondria as central hub of the immune system," *Redox Biology*, vol. 26, article 101255, 2019.

[146] Ḿ. J́. Pinazo, J́. Muñoz, E. Posada et al., "Tolerance of benznidazole in treatment of Chagas' disease in adults," *Antimicrobial Agents and Chemotherapy*, vol. 54, no. 11, pp. 4896–4899, 2010.

[147] C. Campos-Estrada, A. Liempi, F. González-Herrera et al., "Simvastatin and benznidazole-mediated prevention of Trypanosoma cruzi-induced endothelial activation: role of 15-epi-lipoxin A4 in the action of simvastatin," *PLoS Neglected Tropical Diseases*, vol. 9, no. 5, article e0003770, 2015.

[148] G. Vilar-Pereira, V. C. Carneiro, H. Mata-Santos et al., "Resveratrol reverses functional Chagas heart disease in mice," *PLoS Pathogens*, vol. 12, no. 10, article e1005947, 2016.

[149] P. Budni, R. C. Pedrosa, E. M. Dalmarco, J. B. Dalmarco, T. S. Frode, and D. Wilhelm Filho, "Carvedilol enhances the antioxidant effect of vitamins E and C in chronic Chagas heart disease," *Arquivos Brasileiros de Cardiologia*, vol. 101, pp. 304–310, 2013.

[150] R. D. Novaes, E. C. Santos, M. D. C. Q. Fialho et al., "Nonsteroidal anti-inflammatory is more effective than anti-oxidant therapy in counteracting oxidative/nitrosative stress and heart disease inT. cruzi-infected mice," *Parasitology*, vol. 144, no. 7, pp. 904–916, 2017.

[151] A. Molina-Berríos, C. Campos-Estrada, M. Lapier et al., "Protection of vascular endothelium by aspirin in a murine model of chronic Chagas' disease," *Parasitology Research*, vol. 112, no. 7, pp. 2731–2739, 2013.

[152] V. Kourbeli, E. Chontzopoulou, K. Moschovou, D. Pavlos, T. Mavromoustakos, and I. P. Papanastasiou, "An overview on target-based drug design against kinetoplastid protozoan infections: human African trypanosomiasis, Chagas disease and leishmaniases," *Molecules*, vol. 26, no. 15, p. 4629, 2021.

[153] A. B. Vermelho, G. C. Rodrigues, and C. T. Supuran, "Why hasn't there been more progress in new Chagas disease drug discovery?," *Expert Opinion on Drug Discovery*, vol. 15, no. 2, pp. 145–158, 2020.

[154] N. S. Moretti, L. da Silva Augusto, T. M. Clemente et al., "Characterization of Trypanosoma cruzi sirtuins as possible drug targets for Chagas disease," *Antimicrobial Agents and Chemotherapy*, vol. 59, no. 8, pp. 4669–4679, 2015.

[155] X. Wan, J. J. Wen, S. J. Koo, L. Y. Liang, and N. J. Garg, "SIRT1-PGC1α-NFκB pathway of oxidative and inflammatory stress during Trypanosoma cruzi infection: benefits of SIRT1-targeted therapy in improving heart function in Chagas disease," *PLoS Pathogens*, vol. 12, no. 10, article e1005954, 2016.

[156] Y. J. Hsu, S. C. Hsu, C. P. Hsu et al., "Sirtuin 1 protects the aging heart from contractile dysfunction mediated through the inhibition of endoplasmic reticulum stress-mediated apoptosis in cardiac-specific Sirtuin 1 knockout mouse model," *International Journal of Cardiology*, vol. 228, pp. 543–552, 2017.

[157] A. Prola, J. Pires da Silva, A. Guilbert et al., "SIRT1 protects the heart from ER stress-induced cell death through eIF2 _α_ deacetylation," *Cell Death and Differentiation*, vol. 24, no. 2, pp. 343–356, 2017.

[158] W. Zhang, Q. Huang, Z. Zeng, J. Wu, Y. Zhang, and Z. Chen, "Sirt1 inhibits oxidative stress in vascular endothelial cells," *Oxidative Medicine and Cellular Longevity*, vol. 2017, Article ID 7543973, 8 pages, 2017.

Hindawi
Oxidative Medicine and Cellular Longevity
Volume 2021, Article ID 2105406, 12 pages
https://doi.org/10.1155/2021/2105406

Research Article

The Differences in the Levels of Oxidative Status Marker and Soluble CD95 in Patients with Moderate to Severe COPD during an Exacerbation and a Stable Period

Svetlana Soodaeva,[1] **Nailya Kubysheva**,[2] **Igor Klimanov**,[1] **Alexey Shutov**,[1] **Tatyana Eliseeva**,[3] **Viktor Novikov**,[4,5] **Klavdiya Kontorshchikova**,[3] **Dmitry Novikov**,[4,5] **and Ildar Batyrshin**[6]

[1]*Pulmonology Scientific Research Institute under FMBA of Russia, Orekhovyy Bul'var 28, Moscow 115682, Russia*
[2]*Kazan Federal University, Kremlyovskaya St, 18, Kazan 420000, Russia*
[3]*Federal State Budgetary Educational Institution of Higher Education Privolzhsky Research Medical University, Minin and Pozharsky Square 10/1, Nizhny Novgorod 603005, Russia*
[4]*N.I.Lobachevsky Nizhny Novgorod National Research State University, Gagarina Avenue 23, Nizhny Novgorod 603950, Russia*
[5]*I.N. Blokhina Research Institute of Epidemiology and Microbiology, Malaya Yamskaya St., 71, Nizhny Novgorod 603950, Russia*
[6]*Instituto Politécnico Nacional, Centro de Investigación en Computación (CIC-IPN), Av. Juan de Dios Bátiz, Esq. Miguel Othón de Mendizábal S/N, Gustavo A. Madero, 07738 Mexico City, Mexico*

Correspondence should be addressed to Nailya Kubysheva; aibolit70@mail.ru

Received 7 June 2021; Revised 13 September 2021; Accepted 25 November 2021; Published 9 December 2021

Academic Editor: Daniela Ribeiro

Studying the features of changes in markers of oxidative stress (OS) and inflammation indicators in COPD patients depending on the degree of bronchial obstruction is one of the priority directions for improving the prognosis and monitoring of the course of this pathology. We conducted a comparative investigation of changes in markers of OS and apoptosis at the systemic and local levels in patients with moderate to severe COPD during exacerbation and stable phase. 105 patients with COPD aged 46-67 and 21 healthy nonsmoking volunteers comparable in age were examined. COPD patients were divided into four groups: moderate COPD (GOLDII) during the exacerbation (GOLDIIex, $n = 25$) and in the stable phase (GOLDIIst, $n = 27$), severe COPD (GOLDIII) during the exacerbation (GOLDIIIex, $n = 29$), and in the stable phase (GOLDIIIst, $n = 24$). We studied the levels of such lipid peroxidation (LPO) products as diene conjugates (DC) and Schiff bases (SB) and parameters of induced chemiluminescence (Imax, total light sum-S, Imax/S) in blood serum, as well as sCD95 concentration in blood and exhaled breath condensate (EBC). The relationship between the values of the OS system indicators with sCD95, as well as with the parameters of lung function, was investigated. Multidirectional changes in OS indicator levels in COPD patients depending on the severity of obstructive airway disorders have been established. The maximum values of DC (0.26 ± 0.046 RU), Imax (0.265 ± 0.19 RLU), and Imax/S (0.13 ± 0.05) were typical for patients with moderate COPD, while the highest SB level (5.7 ± 2.3 RU) was observed in severe COPD during an exacerbation. The exacerbation of the disease was characterized by an increase in DC concentration in both GOLDIIex (0.26 ± 0.046 RU) and GOLDIIIex (0.209 ± 0.02 RU) compared to the stable moderate and severe COPD (0.202 ± 0.028 RU and 0.19 ± 0.03 RU, respectively, $p < 0.05$). The established decrease in high values of DC, Imax, Imax/S, and sCD95 and an increase in SB concentration in GOLD III can serve as quantitative indicators of the prognosis of the severity of the disease. The serum concentration of sCD95 in GOLDIIex (366.4 ± 70.5 U/ml) and GOLDIIst (361.4 ± 72.8 U/ml) did not differ from the control group (393.7 ± 80.9 U/ml, $p > 0.05$). In patients with FEV1 < 49% during the exacerbation and stable phase, the serum levels of Imax/S (0.058 ± 0.01 and 0.062 ± 0.01) and sCD95 (318.2 ± 66.3 U/ml and 321.4 ± 42.5 U/ml) were lower than the values of healthy volunteers (0.08 ± 0.01 and 393.7 ± 80.9 U/ml, respectively, $p < 0.05$). A positive correlation between sCD95 concentration and airway obstruction degree in all examined COPD patients was established. The revealed numerous associations between sCD95 and OS marker levels in GOLDIII indicate a relationship

between systemic radical stress and apoptosis processes both in the respiratory tract and the whole body under conditions of severe inflammation. The established correlations between the values of DC, Imax, and sCD95 in the blood serum and the lung function parameters in all studied patients allow us to consider these indicators as additional prognostic indicators of disease intensification. Our work results help clarify the participation and detail of FRO and apoptosis processes in developing pathophysiological features in moderate to severe COPD in different periods and, accordingly, improve the efficiency of diagnosis and treatment of the disease.

1. Introduction

Local and systemic inflammation in COPD is closely related to the intensification of free radical oxidation (FRO) processes and the development of oxidative and nitrosative stress [1–5]. The leading role of oxidative (OS) and nitrosative stress (NS) in the damaging effect on almost all lung structures, especially in the formation of lung tissue remodeling, is well known [1, 5].

Several studies have shown an increase in OS and NS marker concentration in various biological environments in COPD patients [1, 2, 4]. An increase in H2O2 concentration and the total oxidative status (TOS) in the EBC was revealed in this disease [6–8]. In some works, an increase in Fe2+ level in the respiratory tract was noted [9]. The interaction of hydrogen peroxide and divalent iron in the Fenton reaction can lead to the overproduction of extremely reactive hydroxyl radicals, which initiate the processes of FRO and lipid peroxidation (LPO). An increase in lipid peroxidation products such as MDA, 4-Hydroxy2-nonenal, and 8-isoprostane has also been found in serum, EBC, and sputum in COPD [8, 10–13].

Along with an increase in FRO indices, it was found that in patients with this disease, the activity of antioxidant enzymes, such as SOD, catalase, and glutathione peroxidase, as well as nonenzymatic antioxidant concentration (vitamins A and C, glutathione, etc.) decreases [14, 15]. However, several other studies have obtained opposite data on OS indicators in COPD. For example, an increase in enzymatic antioxidant activity, the absence of an increase in the level of lipid peroxidation products in patients with this disease has been shown [16, 17].

A significant proportion of OS and NS studies in COPD are devoted to investigating biomarkers reflecting the intensity of FRO directly in the respiratory tract: exhaled breath condensate (EBC), sputum, and BAL fluid [10–12, 18–20].

Currently, information is accumulating on circulating systemic OS markers associated with various pathophysiological disorders in COPD patients [21]. However, the feature changes in the systemic indicators of radical stress in COPD depending on the severity and period of the disease have not been sufficiently studied. The activity of OS processes is often researched by the lipid peroxidation indicators, such as MDA and isoprostanes. At the same time, it is important to study the intensification of lipoperoxidation reactions by the values of the initial and end products of LPO—diene conjugates (DC) and Schiff bases (SB). It is also relevant to determine the DC to SB (DC/SB) ratio, which allows you to define the direction and expressive of lipoperoxidation processes stages. There are few studies of these molecular products in patients with COPD, depending on the severity and period of the disease. There are few studies of these molecular product concentrations in COPD patients depending on the severity and period of the disease.

It should be noted that one of the most significant ways to investigate FRO reactions is to determine the potential ability of lipid substrates to form free radicals, which can be detected using chemiluminescence (CL) analysis. This method allows us to comprehensively evaluate both the prooxidant and antioxidant properties of the biosubstrate [22–24]. Given that there has been a growing interest in a complex assessment of the oxidant/antioxidant system in COPD, using this integral method to determine OS markers in developing this disease is essential.

In addition to the study of FRO, to identify the mechanisms of pathophysiological processes in COPD, special attention is paid to investigating the relationship between OS indicators and inflammation markers, such as cytokines and soluble differentiation molecules (sCD). Earlier in our works, we showed the role of several soluble forms of membrane molecules in the mechanisms of development of systemic and local inflammation in patients with this disease [3, 4, 25, 26]. In particular, changes in soluble CD95 (sCD95) concentration in serum and EBC were detected in moderate and severe COPD patients during an exacerbation [3]. The sCD95 molecules are one of the apoptosis-specific markers and play an essential role in developing and regulating inflammatory processes in the airways and at the systemic level [3, 27]. For a more detailed study of the pathogenetic mechanisms of COPD progression, it is necessary to comparatively research changes in FRO markers and sCD95 levels in the blood and airways in patients with COPD, depending on the stage and period of the disease.

The study is aimed at investigating changes in the concentrations of DC, SB, and CL parameters in the blood serum and the level of sCD95 in the circulation and exhaled breath condensate in moderate to severe COPD patients during the exacerbation and stable phase.

Analysis of the relationship between OS and sCD95 markers, as well as these indicators and lung function parameters, will help clarify the involvement of FRO and apoptosis processes in the development of pathophysiological features of COPD and improve the diagnosis efficiency and therapy of the disease.

2. Materials and Methods

The study included 126 people: patients with COPD ($n = 105$) and healthy nonsmoking volunteers ($n = 21$).

The diagnosis of COPD was defined and classified according to the criteria of the Global Initiative on Chronic Obstructive Pulmonary Disease (GOLD) [28]. The COPD

diagnosis was established based on largely irreversible airway obstruction with an improvement in FEV1 < 12% after inhalation of 400 μg salbutamol. Lung function was measured again 15-20 minutes after inhalation of the bronchodilator to assess bronchodilator-induced bronchospasm reversibility.

COPD patients ($n = 105$) were divided into four groups: patients with moderate COPD (GOLDII) during the exacerbation (GOLDIIex, $n = 25$), patients with moderate COPD in the stable phase (GOLDIIst, $n = 27$), patients with severe COPD (GOLDIII) during the exacerbation (GOLDIIIex, $n = 29$), and patients with severe COPD in the stable phase (GOLDIIIst, $n = 24$).

The presented study is a pilot, so we did not use traditional approaches to calculating the sample size [29]. Currently, there are several practical rules according to which the group size in the pilot study is from 15 to 35 people [30, 31].

The study was implemented based on the principles of the Helsinki Declaration. Written informed consent was obtained from all participants. The study was approved by the Ethics Committee of the Pulmonology Research Institute, Moscow, Russia (the protocol number N 05-19 от 16.10.2019).

The study included COPD patients meeting the following inclusion criteria: age over 40 years, active or ex-smokers (smoking index (IC) ≥ 10 pack-years), exacerbation of COPD and stable period, and evidence of obstructed lung function (postbronchodilator FEV1 < 80% and FEV1/FVC < 70%) according to the GOLD [28]. An exacerbation was defined as a change in the symptoms of a cough, expectoration, and dyspnea beyond the daily variation and required changes in therapy in COPD patients.

The exclusion criteria were the following: asthma and other allergic diseases, pneumonia, history of congestive heart failure, severe arterial hypertension, diabetes, and conditions requiring the long-term use of systemic corticosteroids.

The control group included healthy nonsmokers with similar gender and age indicators who did not take any medications. Healthy subjects underwent a medical examination at the clinic and were randomly selected as a control group. The participants in the healthy group had no diagnosed respiratory diseases, diabetes, coronary heart disease, malignancies, or connective tissue diseases.

A pulmonary function study was carried out on a computer Spirograph "SpiroLab III" (Italy) for the evaluation of the FEV1, FEV1/FVC, and the parameters of inspiratory capacity (IC).

2.1. Serum and Exhaled Breath Condensate Preparation. Blood samples were obtained in the morning on an empty stomach from the middle cubital vein, immediately centrifuged at 3000 rpm for 10 minutes, and then extracted. Serum samples were frozen at -40°C.

EBC was collected using the RTube and following the guidelines for EBC by the ERS/ATS Task Force [32]. All patients were asked to refrain from drinking any liquid (except water) for 2 hours before the collection of EBC. To avoid oral or nasal contamination, the patients were asked to rinse their mouths with freshwater before collection and to wear a nose clamp during collection. The donors were asked to use tidal breathing into the mouthpiece for 10 minutes. After the 10-minute period of breathing is over, the samples were immediately stored and cooled to -40°C.

2.2. Measurement of the Diene Conjugates and Schiff Base Concentrations. The concentrations of DC and SB were determined as described in [33, 34] spectrophotometrically on a PerkinElmer LS-50 spectrophotometer. The levels of these LPO products were expressed in relative units (RU).

2.3. Chemiluminescence Analysis. To determine the intensity of free radical processes in blood serum, we used the CL method induced by hydrogen peroxide with ferrous sulfate. The measurements were carried out on a Dynatech chemiluminometer (Germany).

The following CL indicators were analyzed:

Imax (relative light units (RLU)) is the maximum value of the CL outbreak intensity, reflecting the biological system's potential ability to develop FRO processes.

S (total light sum) is the area under the CL response curve, which characterizes the FRO activity and is inversely proportional to the antioxidant activity (AOA).

Imax/S is the ratio that characterizes antioxidant activity (AOA) of the reaction system.

2.4. Measurement of sCD95 Concentration. The levels of soluble CD95 molecules in the serum and the EBC were determined by enzyme-linked immunosorbent assay (ELISA) using an ELISA reader (Multiskan MS, Labsystems, Finland) wavelength of 405 nm. In determining the content of soluble CD95 molecules, we used goat polyclonal antibodies against PBMC superficial antigens and mouse monoclonal antibodies ICO-160 against the CD95 antigen conjugated with horseradish peroxidase. The results were expressed in conventional units (U/ml).

2.5. Statistical Analysis. The statistical analysis was carried out using the Statgraphics Centurion software package, v.9. The data were presented as the mean ± SD. To determine the distribution normality, the Shapiro-Wilk test was used. The student's t-test performed further analysis. To calculate the correlation coefficient (r), the Pearson correlation test was used. The statistical significance level was considered to be $p < 0.05$.

3. Results

Figure 1 shows a block diagram of patient recruitment. A total of 258 people have successfully passed spirometry. Out of 258 patients, 153 people did not participate in this study according to the exclusion criteria. Therefore, 105 patients were recommended for further examination.

The demographic and clinical characteristics of individuals are shown in Table 1. There was no significant difference between the groups by age. In all groups, the majority of subjects were men. Spirometric values such as FEV1%, FEV1/FVC ratio, and IC were significantly lower in COPD patients compared to the control group ($p < 0.01$). Lung

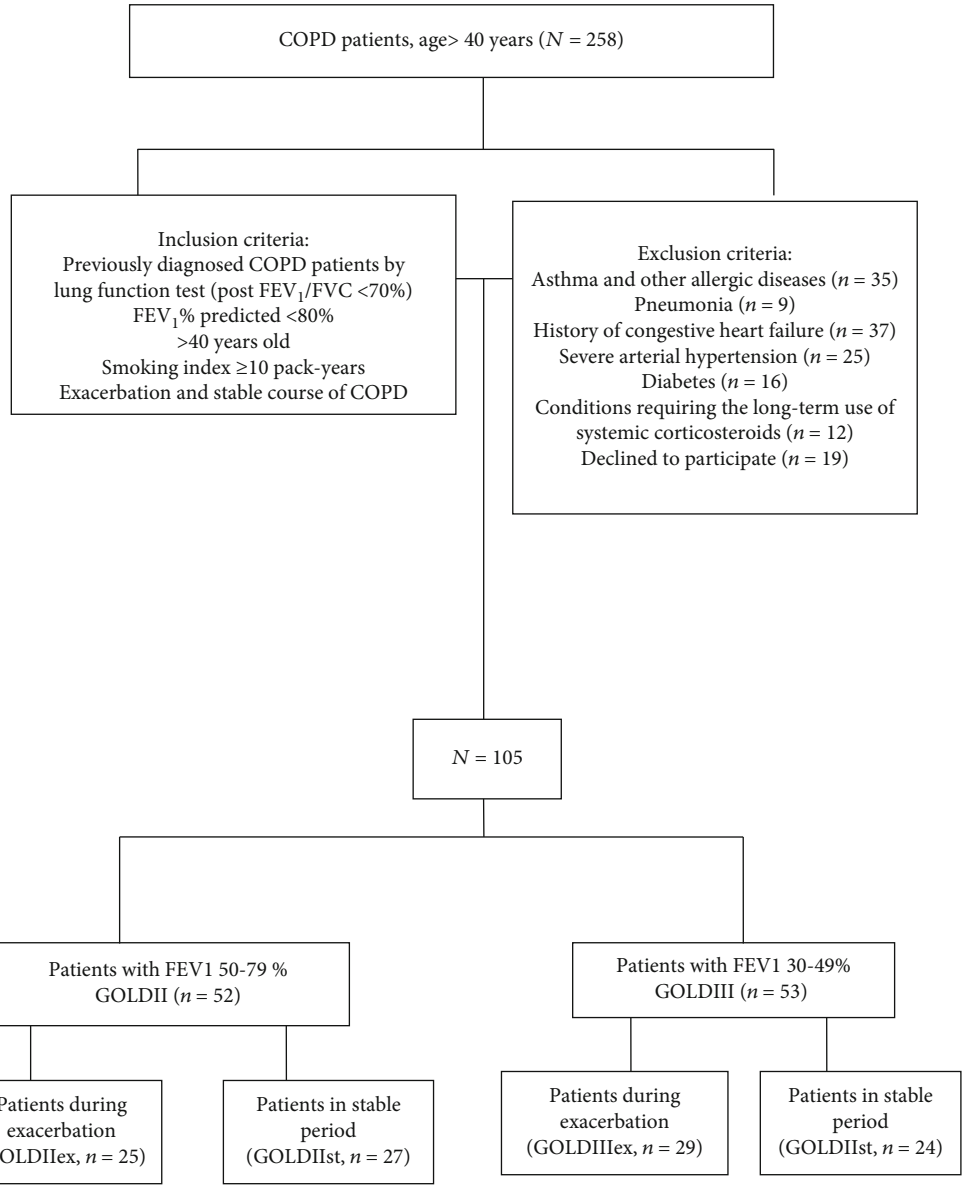

Figure 1: The flowchart of the study population. COPD: chronic obstructive pulmonary disease; FEV1: forced expiratory volume in 1 s; FVC: forced vital capacity.

function parameters in GOLDII exceeded similar values in patients with severe COPD ($p < 0.01$). The exacerbation of the disease was characterized by a decrease in the values of the studied spirometric parameters compared to the stable phase in both GOLDII and GOLDIII ($p < 0.05$).

3.1. The Serum Concentration of Diene Conjugates in COPD Patients. The DC level was increased in all COPD patients compared to the control ($p < 0.01$) (Table 2). The maximum value of these LPO products was observed in GOLDIIex relative to all the examined patients. The stable period of the disease was characterized by a decrease in DC level compared to during exacerbation in both moderate and severe COPD ($p < 0.05$).

3.2. Schiff Base Concentration in COPD Patients. The SB concentration in all the examined patients exceeded the values of the control ($p < 0.05$) (Table 2). The highest SB level was found in GOLDIIIex relative to controls and patients with moderate COPD ($p < 0.05$). The concentration of these LPO end products in patients during the exacerbation did not differ from analogous values in the stable phase in both moderate and severe COPD ($p > 0.05$).

3.3. Index of DC/SB in COPD Patients. To identify the expressive of the initial or final stages of LPO, the DC/SB ratio was determined. The value of the DC/SB index in patients with moderate COPD was significantly higher compared to the control ($p < 0.05$) (Table 2). At the same time,

Table 1: Characteristics of COPD patients and healthy nonsmokers included in the study.

	Healthy nonsmokers	COPD			
		Moderate		Severe	
	1	2	3	4	5
Subjects (n)	21	Exacerbation ($n = 25$)	Stable ($n = 27$)	Exacerbation ($n = 29$)	Stable ($n = 24$)
Sex, male/female	15 (71%)/6 (29%)	18 (72%)/7 (28%)	22 (81%)/5 (19%)	26 (90%)/3 (10%)	20 (83%)/4 (17%)
Age (years)	50.4 ± 9.7	52.6 ± 7.9	49.5 ± 5.6	58.3 ± 4.2	55.2 ± 6.5
Smoking pack-years	0	36.5 ± 4.8	34.3 ± 5.3	42.6 ± 3.9	39.6 ± 5.1
FEV_1 % pred	101.3 ± 5.3	59.1 ± 7.1 $p_1 = 0.001$	65.4 ± 8.2 $p_1 = 0.001$ $p_2 = 0.01$	36.5 ± 5.2 $p_1 = 0.001$ $p_2 = 0.001$ $p_3 = 0.001$	42.5 ± 9.8 $p_1 = 0.001$ $p_2 = 0.001$ $p_3 = 0.001$ $p_4 = 0.02$
FEV_1/FVC %	104.2 ± 3.7	55.7 ± 9.2 $p_1 = 0.001$	63.8 ± 11.3 $p_1 = 0.001$ $p_2 = 0.01$	46.5 ± 8.2 $p_1 = 0.001$ $p_2 = 0.001$ $p_3 = 0.001$	51.9 ± 10.5 $p_1 = 0.001$ $p_2 = 0.001$ $p_3 = 0.001$ $p_4 = 0.04$
Inspiratory capacity IC (%)	108.3 ± 3.5	64.5 ± 6.1 $p_1 = 0.001$	70.8 ± 9.1 $p_1 = 0.001$ $p_2 = 0.01$	59.6 ± 12.6 $p_1 = 0.001$ $p_2 = 0.001$ $p_3 = 0.001$	68.5 ± 14.1 $p_1 = 0.001$ $p_2 = 0.001$ $p_3 = 0.001$ $p_4 = 0.01$
COPD medication	—				
LAMA		2 (8%)	4 (14.8%)	—	—
LAMA+LABA		7 (28%)	13 (48.1%)	8 (27.6%)	6 (25%)
ICS+LABA+LAMA		16 (64%)	10 (37%)	21 (77.8%)	18 (75%)
SCS		9 (36%)	—	29 (100%)	—

Data were presented as mean ± SD. COPD: chronic obstructive pulmonary disease; pack-years: number of cigarette packs per day multiplied by the number of smoking years; FEV_1: forced expiratory volume in one second; % pred: % predicted; FVC: forced vital capacity; IC: inspiratory capacity (%); LAMA: long-acting muscarinic antagonists; LABA: long-acting β agonists; ICS: inhaled corticosteroids; SCS: systemic corticosteroids.

there was a decrease in DC/SB values in severe COPD both during exacerbation and stable periods relative to healthy volunteers and GOLDII patients ($p < 0.05$). There were no differences in DC/SB level depending on the periods of the disease in the examined individuals.

3.4. Chemiluminescent Parameters in the Blood Serum in COPD Patients. The Imax and S values were increased in all examined COPD patients in comparison with healthy volunteers ($p < 0.05$) (Table 2). At the same time, the high Imax level gradually decreased as the severity of the disease increased. The maximum CL intensity in the serum was recorded in GOLDIIex and was higher than in severe COPD patients during exacerbation ($p = 0.01$) and in the stable phase ($p = 0.01$).

The highest light sum (S) values were found in GOLDIIIex patients. This indicator's value was lower in all examined COPD patients in the stable phase than during exacerbation ($p < 0.05$).

The ratio Imax/S (AOA) was higher in moderate COPD compared to control ($p > 0.05$) (Table 2). The level of Imax/S (AOA) in severe COPD was lower than in healthy volunteers and all GOLDII patients ($p < 0.05$). There were no differences in Imax/S (AOA) value depending on the period of the disease.

3.5. sCD95 Concentration in Blood Serum and Exhaled Breath Condensate in COPD during Exacerbation and Stable Periods. The serum level of sCD95 in patients with moderate COPD did not differ from the level of healthy nonsmoking volunteers (393.7 ± 80.9 U/ml, $p > 0.05$) (Figure 2). However, the concentration of these molecules in severe COPD during the exacerbation (318.2 ± 55.4 U/ml) and stable period (321.4 ± 42.5 U/ml) was statistically lower than in healthy nonsmokers ($p < 0.001$), GOLDIIex (366.4 ± 70.5 U/ml), and GOLDIIst (361.4 ± 65.4 U/ml, $p < 0.001$).

The level of sCD95 in EBC was higher in patients with moderate COPD both during the exacerbation (204.5 ± 41.5 U/ml) and the stable period (198.5 ± 38.3 U/ml) than in healthy volunteers (139.6 ± 31.2 U/ml, $p = 0.001$). The endobronchial concentrations of sCD95 in GOLDIIIex (145.5 ± 19.5 U/ml) and GOLDIIIst (150.6 ± 23.3 U/ml) were significantly lower compared to the GOLDII patients ($p < 0.001$). They did not differ from the levels in the control group ($p > 0.05$).

3.6. The Correlations between Oxidative Stress Indicators, sCD95 Levels, and Lung Function Parameters. We found correlations between the values of spirometric indicators and the studied OS markers in COPD patients (Table 3). A negative association between DC level and FEV1 and

Table 2: Changes in indicators of oxidative stress in patients with moderate to severe COPD in different periods of the disease.

	Healthy nonsmoking volunteers 1	GOLDIIex 2	GOLDIIst 3	GOLDIIIex 4	GOLDIIIst 5
Schiff bases (RU)	3.2 ± 0.25	4.3 ± 1.2 $p_{2-1} = 0.01$	3.8 ± 0.8 $p_{3-1} = 0.03$ $p_{3-2} > 0.05$	5.7 ± 2.3 $p_{4-1} = 0.01$ $p_{4-2} = 0.04$ $p_{4-3} = 0.001$	4.7 ± 1.7 $p_{5-1} = 0.01$ $p_{5-2} > 0.05$ $p_{5-3} = 0.001$ $p_{5-4} > 0.05$
Diene conjugates (RU)	0.165 ± 0.01	0.26 ± 0.046 $p_{2-1} = 0.001$	0.202 ± 0.028 $p_{3-1} = 0.001$ $p_{3-2} = 0.048$	0.209 ± 0.02 $p_{4-1} = 0.001$ $p_{4-2} = 0.042$ $p_{4-3} = 0.385$	0.19 ± 0.03 $p_{5-1} = 0.001$ $p_{5-2} = 0.001$ $p_{5-3} > 0.05$ $p_{5-4} = 0.026$
Diene conjugates/Schiff base	0.0515 ± 0.02	0.06 ± 0.015 $p_{2-1} = 0.032$	0.0664 ± 0.035 $p_{3-1} = 0.035$ $p_{3-2} > 0.05$	0.0368 ± 0.008 $p_{4-1} = 0.001$ $p_{4-2} = 0.001$ $p_{4-3} = 0.001$	0.04 ± 0.017 $p_{5-1} = 0.001$ $p_{5-2} = 0.003$ $p_{5-3} = 0.001$ $p_{5-4} > 0.05$
Imax (RLU)	0.061 ± 0.029	0.265 ± 0.19 $p_{2-1} = 0.001$	0.23 ± 0.13 $p_{3-1} = 0.01$ $p_{3-2} > 0.05$	0.18 ± 0.1 $p_{4-1} = 0.001$ $p_{4-2} = 0.01$ $p_{4-3} > 0.05$	0.13 ± 0.07 $p_{5-1} = 0.01$ $p_{5-2} = 0.01$ $p_{5-3} = 0.031$ $p_{5-4} > 0.05$
S	0.75 ± 0.18	2.13 ± 0.48 $p_{2-1} = 0.016$	1.75 ± 0.23 $p_{3-1} = 0.002$ $p_{3-2} = 0.01$	3.1 ± 0.46 $p_{4-1} = 0.001$ $p_{4-2} = 0.001$ $p_{4-3} = 0.001$	2.09 ± 0.34 $p_{5-1} = 0.047$ $p_{5-2} > 0.05$ $p_{5-3} = 0.001$ $p_{5-4} = 0.001$
Imax/S	0.08 ± 0.01	0.12 ± 0.05 $p_{2-1} = 0.041$	0.13 ± 0.05 $p_{3-1} = 0.046$ $p_{3-2} > 0.05$	0.058 ± 0.01 $p_{4-1} = 0.034$ $p_{4-2} = 0.01$ $p_{4-3} = 0.01$	0.062 ± 0.01 $p_{5-1} = 0.049$ $p_{5-2} = 0.01$ $p_{5-3} = 0.01$ $p_{5-4} > 0.05$

Data were presented as mean ± SD.

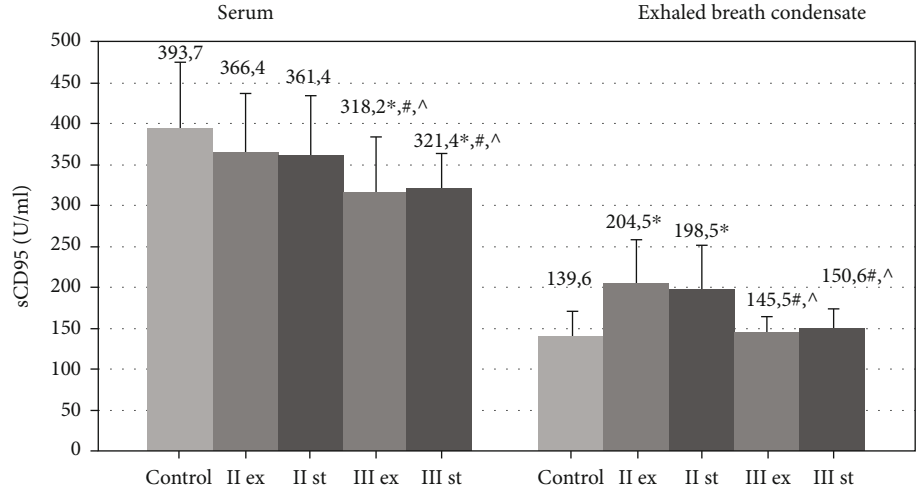

Figure 2: The concentration of sCD95 molecules in blood serum and exhaled breath condensate in COPD patients during the exacerbation and the stable period. Data are presented as mean ± SD; control: healthy nonsmoking volunteers; II: moderate COPD; III: severe COPD; ex: exacerbation; st: stable phase. $^{*}p < 0.05$ versus healthy nonsmokers; $\#p < 0.05$ versus patients with moderate COPD during the exacerbation; $\wedge p < 0.05$ versus patients with moderate COPD in the stable period.

Table 3: Correlations between oxidative stress markers and lung function parameters in patients with moderate to severe COPD.

	GOLDII			GOLDIII		
	FEV_1 (%)	FEV_1/FVC (%)	IC	FEV_1 (%)	FEV_1/FVC (%)	IC
Diene conjugates	$r = -0.47$ $p = 0.026$	$r = -0.43$ $p = 0.045$	$r = -0.33$ $p = 0.18$	$r = -0.45$ $p = 0.01$	$r = -0.43$ $p = 0.03$	$r = -0.41$ $p = 0.09$
Schiff base	$r = 0.08$ $p = 0.68$	$r = 0.32$ $p = 0.18$	$r = -0.39$ $p = 0.11$	$r = -0.3$ $p = 0.18$	$r = -0.42$ $p = 0.03$	$r = -0.5$ $p = 0.04$
Imax	$r = -0.54$ $p = 0.02$	$r = -0.6$ $p = 0.01$	$r = 0.103$ $p = 0.69$	$r = 0.36$ $p = 0.04$	$r = 0.5$ $p = 0.03$	$r = 0.13$ $p = 0.57$
Imax/S	$r = 0.32$ $p = 0.11$	$r = 0.27$ $p = 0.19$	$r = 0.63$ $p = 0.01$	$r = 0.47$ $p = 0.04$	$r = 0.72$ $p = 0.01$	$r = 0.52$ $p = 0.02$
sCD95 (serum)	$r = 0.61$ $p = 0.01$	$r = 0.5$ $p = 0.02$	$r = 0.62$ $p = 0.01$	$r = 0.43$ $p = 0.02$	$r = 0.45$ $p = 0.02$	$r = 0.6$ $p = 0.002$
sCD95 (EBC)	$r = 0.28$ $p = 0.24$	$r = 0.64$ $p = 0.01$	$r = 0.58$ $p = 0.04$	$r = 0.65$ $p = 0.001$	$r = 0.46$ $p = 0.04$	$r = 0.53$ $p = 0.03$

r: correlation coefficient; FEV_1: forced expiratory volume in 1 second; % pred: % predicted; FVC: forced vital capacity; IC: inspiratory capacity (%); EBC: exhaled breath condensate.

FEV1/FVC was revealed in all COPD patients. The inverse correlation was established between SB concentration and FEV1/FVC (%), IC in severe disease. The multidirectional nature of the relationship of the Imax values and lung function parameters was revealed. The negative correlation between these indicators was established in moderate COPD; a positive relationship was found in severe disease.

A positive relationship between the AOA value and all the studied lung function parameters in patients with severe COPD was established. The increase in Imax/S (AOA) values occurred against the background of an increase in the IC level in GOLD II.

3.7. Analysis of Correlation between Oxidative Stress Indicators. The results of the association analysis between the concentration of LPO products and the studied CL were the following:

(i) The negative correlations between the values of Imax/S (AOA) and levels of SB and DC ($r = -0.45$ $p = 0.001$ and $r = -0.43p = 0.001$, respectively)

(ii) The negative relationship between the Imax value and the SB level ($r = -0.38p = 0.002$)

(iii) The positive association of the DC concentration and the value of light sum ($r = 0.41p = 0.001$)

3.8. Associations between sCD95 Levels and Lung Function Parameters. An analysis of associations showed a positive correlation between serum and endobronchial sCD95 levels and the studied lung function parameters in all examined patients (Table 3).

3.9. The Relationship between the Studied Markers of Oxidative Stress and the Level of sCD95 in COPD Patients. The relationship between the sCD95 level and the studied OS indicators was revealed only in patients with severe airway obstructive disorders (Table 4). In this group of patients, a decrease in the concentration of sCD95 both in the bloodstream and in the EBC occurs against the background of an increase in the SB level, as well as a decrease in DC concentration and Imax and Imax/S (AOA) values.

4. Discussion

In our work, we established a change in the concentration of the studied molecular products of lipid peroxidation (SB, DC) and CL indicators (Imax, S, Imax/S) in the blood serum of patients with COPD depending on the severity and period of the disease.

Increased DC and SB levels were found in all examined COPD patients compared with healthy nonsmoking volunteers. The established negative correlations between DC concentration and FEV1 and FEV1/FVC values in all studied patients may indicate the relationship between the activity of the initial processes of lipoperoxidation and the degree of airway obstruction violation. It is generally accepted that diene conjugates (DCs) are formed at the initiation stage of LPO reaction chain. At the final stage of lipid peroxidation, the resulting malondialdehyde (MDA) interacts with free amino groups to form the fat-soluble fluorescent and end product LPO—Schiff's base (SB) [35]. Quantifying the levels of initial and end products (DC and SB) allows assessing the activity and direction of LPO processes. The obtained high rates of diene conjugates and Schiff bases indicate an intensification of LPO processes in moderate and severe COPD. Our results are consistent with research data, which found an increase in the serum concentration of lipid peroxidation products such as MDA in COPD patients [6–8, 21].

The present work revealed that the maximum concentration of DCs was typical for patients with moderate COPD during the exacerbation period. Based on the results obtained, it can be assumed that activation of the initial lipid peroxidation stage predominates at this disease stage. The high concentration of DCs decreased with the increasing severity of COPD. The decline in these molecules level may be associated with the subsequent transformation of diene conjugates into secondary and end LPO products,

Table 4: Correlations between the studied system markers of oxidative stress and sCD95 levels in serum and EBC in patients with moderate to severe COPD.

	sCD95 (serum) GOLDII	sCD95 (EBC) GOLDII	sCD95 (serum) GOLDIII	sCD95 (EBC) GOLDDIII
Schiff base	$r = 0.27$ $p = 0.22$	$r = -0.27$ $p = 0.24$	$r = -0.39$ $p = 0.038$	$r = -0.46$ $p = 0.02$
Diene conjugates	$r = -0.3$ $p = 0.25$	$r = 0.25$ $p = 0.27$	$r = 0.37$ $p = 0.046$	$r = 0.23$ $p = 0.35$
Imax	$r = -0.13$ $p = 0.54$	$r = -0.06$ $p = 0.79$	$r = 0.37$ $p = 0.046$	$r = 0.58$ $p = 0.001$
Imax/S	$r = 0.3$ $p = 0.25$	$r = 0.3$ $p = 0.25$	$r = 0.38$ $p = 0.045$	$r = 0.42$ $p = 0.02$

r: correlation coefficient; EBC: exhaled breath condensate.

depletion of oxidized substrates, and/or a decrease in the intensity of free radical processes against the background of chronic inflammation progression and under conditions of increasing hypoxia. This assumption is confirmed by results demonstrating an increase in SB concentration and a decrease in the DC/SB ratio in COPD patients with severe obstructive airway disorders. These results may indicate the predominance of the final stage of lipid peroxidation processes and the accumulation of end LPO products in GOLDIII. Under physiological conditions, SB transfers toxic and unstable products of lipid peroxidation metabolism (aldehydes, etc.) to the path of further utilization. However, in high concentrations, SB can modify serum lipoproteins and have a destructive effect on cells due to the destruction of intermolecular cross-links of biopolymers and damage to membranes [36]. In this case, the accumulation of these end products of LPO can be one of the reasons for the dysregulation of reparative processes, the formation of lung tissue remodeling, and the intensification of chronic inflammatory processes [37].

The revealed negative relationship between Schiff base level and FEV1/FVC values in GOLDIII indicates the mutual influence of the intensity of systemic oxidative stress and the functional capacity of the lungs under conditions of increasing chronic inflammation severity. The results obtained make it possible to consider the excessive accumulation of Schiff bases as an additional diagnostic criterion for an unfavorable course of COPD.

The CL parameters (Imax, S) also exceeded the control group's values and depended on disease severity. The intensity of induced CL (Imax) in the blood serum reflects the potential ability of lipid substrates to form highly active electron-excited products [22, 23]. Accordingly, the registered increased Imax values confirm the activation of free radical reactions in all examined COPD patients. At the same time, the inhibition of CL intensity was revealed in COLDIII compared to patients with moderate COPD. The established decrease in the CL response against the background of increased violations of airway obstruction is confirmed by a positive correlation between Imax and FEV1 and FEV1/FVC in GOPDII. The recorded decline in Imax values with a growth in the severity of the disease may be associated with an increasing deficiency of lipid substrates for oxidation due to prolonged activation of free radical reactions. This assumption is confirmed by the increased formation and accumulation of end products (SB) of LPO, which are not capable of oxidation, as well as a decrease in the concentration of DCs in severe COPD compared with GOLDII patients.

The revealed negative correlation between the SB and Imax levels also indicates a decrease in the CL intensity against the background of an increase in the concentration of lipid peroxidation end products. Thus, lower Imax values in GOLDIII relative to patients with moderate COPD may indicate an unfavorable course of inflammation in patients with this disease.

The value of the light sum (S) increased with the progression of COPD severity. It should be noted that in the examined patients GOLDII and GOLDIII, the S level and DC concentration were significantly higher during the exacerbation than in the stable period. In this case, the results obtained allow us to consider the DC and light sum values as prognostic markers of an intensification in the inflammatory process in COPD.

The light sum value reflects the concentration of free radicals and is inversely proportional to the activity of the antioxidant system. Accordingly, the assessment of antioxidant activity (AOA) in the blood serum was determined by the Imax/S ratio. The observed increase in Imax/S (AOA) level against the background of high values of the intensity of CL in the GOLDII group is probably a response of the protective mechanism of antioxidant protection to the activation of FRO processes in patients with moderate obstructive airway disorders. At the same time, a decrease in Imax/S (AOA) values in GOLD III may indicate a depletion of the components of the general antioxidant defense under the condition of systemic chronic inflammation progression. The revealed positive correlations between Imax/S and FEV1 and FEV1/FVC in severe COPD confirm the association between a decrease in antioxidant potential and the formation of persistent ventilation restrictions in the growth of disease severity.

Thus, the detected increase in SB concentration, as well as a decrease in the level of DC, Imax, and Imax/S (AOA) in GOLDIII patients, may indicate a violation of the feedback principle in the proantioxidant system and dysregulation of FRO processes in severe inflammation.

It is known that OS has a wide range of biochemical and pathophysiological effects that affect the regulatory processes

of inflammation in COPD, including apoptosis [38]. In this regard, we considered it expedient to study the features of changes in sCD95 concentrations depending on the stages and period of COPD as well as and the relationship of the studied FRO parameters with this apoptosis marker level. Previously, it was shown that an increase in the severity in patients with exacerbation of COPD is accompanied by a decrease in the level of sCD95 in the blood serum and EBC [3]. In the present work, we evaluated the change in this apoptosis marker level compared to the exacerbation and the stable phase at different disease stages. As a result, we did not find differences in sCD95 concentration in studied COPD patients depending on the disease period. In addition, the decrease in this apoptosis marker concentration was established in the tested biological fluids with the progression of inflammation, which was confirmed by a positive correlation between spirometric parameters and concentrations of these molecules in both moderate and severe COPD. Functionally, sCD95 competes with the CD95 membrane-localized receptor for Fas ligand binding and thus can inhibit CD95-mediated apoptosis [39]. Thus, the soluble form of this apoptotic marker can participate in the preservation of cellular homeostasis during the normally developing process of programmed cell death. In this case, the decrease in sCD95 level in patients with severe COPD creates conditions for more effective implementation of Fas-dependent apoptosis. This change in sCD95 concentration can increase the apoptosis progression of pathogenetically significant cells and promote the development of destructive processes in the lung tissue and the whole body in GOLDIII patients.

Association analysis showed multiple correlations between serum and endobronchial sCD95 levels and the studied OS markers values in patients with severe COPD. The revealed relationships may indicate indirect participation of the tested OS indicators in activating programmed cell death processes through Fas-mediated mechanisms. These mechanisms may underlie the development of reparative disorders and, as a result, the lung fibrosis formation and pathophysiological manifestations, severe inflammation in GOLDIII patients.

In our work, we also established the positive correlations between the levels of sCD95, Imax/S (AOA), and such a spirometric indicator as to the inspiratory capacity (IC) in all examined COPD patients. Also, the decline in IC values was accompanied by an increase in SB concentration in severe disease. The decrease in IC level is associated with pulmonary hyperinflation development, increased hypoxia, and loss of elasticity of the lung tissue in COPD.

Thus, the obtained data may indicate that a decrease in the antioxidant potential, a violation of the regulation of LPO processes, and an intensification in apoptotic reactions contribute to structural and functional changes in the respiratory tract, as well as the formation of hypoxemia and impaired gas exchange in severe inflammation in COPD patients.

A limitation of the presented results in this work may be the approaches to the interpretation of the obtained data in EBC. To date, there are various methodological approaches for the determination of analytes in exhaled breath condensate. EBC is a liquid formed as a result of cooling and subsequent condensation of exhaled breath. From a physical point of view, the exhaled breath is an aerosol or an aerodisperse system consisting of a gaseous dispersion medium and a liquid dispersed phase suspended in it (aerosol particles). In other words, EBC is a suspension of liquid particles in a gas [40]. One of the main components of exhaled breath is water vapor. The concentration of water vapor in exhaled breath is a fairly constant value, little dependent on environmental parameters [41]. The levels of nonvolatile components of exhaled air can vary depending on a number of factors, such as the exhalation rate, the state (diameter) of the airways, and pathophysiological processes in airway lining fluid (ALF) [40–46]. In several works, attempts have been made to standardize the assessment of nonvolatile compounds in EBC, by taking into account the degree of dilution of EBC. So, the dilution of the EBC was estimated based on the measurement of its conductivity [47, 48]. In the works [49, 50], the level of urea in EBC was used as a marker of dilution. In another study [51], the assessment of the degree of dilution was studied by the concentrations of K+, Na+, Mg2+, Ca2+, the total level of cations, urea level, and the EBC conductivity. However, until now, a unified approach to standardizing the assessment of nonvolatile compounds in EBC has not been found. In our opinion, the concentrations of the analytes considered in these studies may vary depending on the pathophysiological processes in the airway lining fluid, especially in lung diseases. Accordingly, these approaches may incorrectly display the dilution rate of the EBC and require further study. Earlier, in our work, a methodology was proposed for standardizing the procedure for collecting EBC and evaluating nonvolatile components in ALF based on taking into account the concentration of aerosol particles in exhaled breath [52]. Therefore, in this work, we proceeded from the assumption that the concentrations of nonvolatile components in the EBC are indicators reflecting the pathophysiological processes in the airway lining fluid of patients.

5. Conclusion

The findings indicate not only the participation of OS in the development of COPD but also show the importance of determining the degree of FRO activity and antioxidant potential, taking into account the severity of impaired ventilation function of the lungs. A complex evaluation of OS indicators in COPD patients, including the determination of the concentration of DC and SB, the values of CL parameters in the blood serum, allowed us to clarify the activity of systemic FRO reactions depending on the severity of airway obstruction degree and disease periods.

Combining an increase in SB concentration, a decrease in DC, Imax, Imax/S (AOA), and sCD95 levels in GOLDIII patients allows us to consider these indicators as additional quantitative indicators for predicting the disease severity.

The exacerbation of the disease was characterized by the most significant increase in DC level in the blood serum compared to the stable period of the disease, which makes

it possible to use the concentration of this LPO product as potential monitoring markers of inflammation intensification in COPD.

The established numerous associations between the levels of the studied LPO products, the CL, sCD95, and spirometric parameter values in COPD patients indicate the mutual influence of the intensity of systemic oxidative stress, the processes of apoptosis, and the functional capacity of the lungs. Also, the obtained correlations make it possible to consider the studied indicators of OS and apoptosis as laboratory-diagnostic and prognostic markers of systemic and local chronic inflammation progression in COPD.

The revealed relationship between the values of sCD95 and OS markers in GOLD III patients may indicate the possible participation of LPO products and FRO processes in the forming soluble CD95 and apoptosis processes activity both in the respiratory tract and whole body in severe obstructive airway violation.

The results obtained make it possible to clarify and supplement the influence of systemic oxidative stress and apoptosis processes on the development of pathophysiological features in moderate and severe forms of COPD and, accordingly, to improve the efficiency of diagnosis and treatment of the disease.

Data Availability

The data used to support the findings of this study are available from the corresponding author upon request.

Conflicts of Interest

The authors declare that there is no potential conflict of interest associated with this manuscript.

Authors' Contributions

Each of the authors contributed equally to the manuscript writing.

Acknowledgments

This paper has been supported by the Kazan Federal University Strategic Academic Leadership Program.

References

[1] A. J. A. McGuinness and E. Sapey, "Oxidative stress in COPD: sources, markers, and potential mechanisms," *Journal of Clinical Medicine*, vol. 6, no. 2, p. 21, 2017.

[2] S. Soodaeva, N. Kubysheva, I. Klimanov, L. Nikitina, and I. Batyrshin, "Features of oxidative and nitrosative metabolism in lung diseases," *Oxidative Medicine and Cellular Longevity*, vol. 2019, 12 pages, 2019.

[3] N. Kubysheva, S. Soodaeva, L. Postnikova, V. Novikov, A. Maksimova, and A. Chuchalin, "Associations between indicators of nitrosative stress and levels of soluble HLA-I, CD95 molecules in patients with COPD," *COPD: Journal of Chronic Obstructive Pulmonary Disease*, vol. 11, no. 6, pp. 639–644, 2014.

[4] N. I. Kubysheva, L. B. Postnikova, S. K. Soodaeva et al., "The significance of soluble molecules of cellular adhesion, nitric oxide metabolites, and endothelin-1 and their associations as markers of progression of inflammation in COPD," *Sovremennye Tehnologii v Medicine*, vol. 9, no. 2, pp. 105–117, 2017.

[5] P. A. Kirkham and P. J. Barnes, "Oxidative stress in COPD," *Chest*, vol. 144, no. 1, pp. 266–273, 2013.

[6] A. Koutsokera, T. S. Kiropoulos, D. J. Nikoulis et al., "Clinical, functional and biochemical changes during recovery from COPD exacerbations," *Respiratory Medicine*, vol. 103, no. 6, pp. 919–926, 2009.

[7] I. Rahman, D. Morrison, K. Donaldson, and W. MacNee, "Systemic oxidative stress in asthma, COPD, and smokers," *American Journal of Respiratory and Critical Care Medicine*, vol. 154, no. 4, pp. 1055–1060, 1996.

[8] M. Calikoğlu, A. Unlü, L. Tamer, B. Ercan, R. Buğdayci, and U. Atik, "The levels of serum vitamin C, malonyldialdehyde and erythrocyte reduced glutathione in chronic obstructive pulmonary disease and in healthy smokers," *Clinical Chemistry and Laboratory Medicine*, vol. 40, no. 10, pp. 1028–1031, 2002.

[9] W. Z. Zhang, C. Oromendia, S. A. Kikkers et al., "Increased airway iron parameters and risk for exacerbation in COPD: an analysis from SPIROMICS," *Scientific Reports*, vol. 10, no. 1, pp. 1–13, 2020.

[10] M. L. Bartoli, F. Novelli, F. Costa et al., "Malondialdehyde in exhaled breath condensate as a marker of oxidative stress in different pulmonary diseases," *Mediators of Inflammation*, vol. 2011, 7 pages, 2011.

[11] I. Rahman, A. A. van Schadewijk, A. J. L. Crowther et al., "4-Hydroxy-2-nonenal, a specific lipid peroxidation product, is elevated in lungs of patients with chronic obstructive pulmonary disease," *American Journal of Respiratory and Critical Care Medicine*, vol. 166, no. 4, pp. 490–495, 2002.

[12] P. Paredi, S. A. Kharitonov, and P. J. Barnes, "Analysis of expired air for oxidation products," *American Journal of Respiratory and Critical Care Medicine*, vol. 166, supplement_1, pp. S31–S37, 2002.

[13] P. Montuschi, "Exhaled breath condensate analysis in patients with COPD," *Clinica Chimica Acta*, vol. 356, no. 1-2, pp. 22–34, 2005.

[14] M. Zeng, Y. Li, Y. Jiang, G. Lu, X. Huang, and K. Guan, "Local and systemic oxidative stress and glucocorticoid receptor levels in chronic obstructive pulmonary disease patients," *Canadian Respiratory Journal*, vol. 20, no. 1, 41 pages, 2013.

[15] B. Antus, C. Paska, B. Simon, and I. Barta, "Monitoring antioxidant enzyme activity during exacerbations of chronic obstructive pulmonary disease," *COPD*, vol. 15, no. 5, pp. 496–502, 2018.

[16] I. Hanta, A. Kocabas, N. Canacankatan, S. Kuleci, and G. Seydaoglu, "Oxidant-antioxidant balance in patients with COPD," *Lung*, vol. 184, no. 2, pp. 51–55, 2006.

[17] T. Tug, F. Karatas, and S. M. Terzi, "Antioxidant vitamins (A, C and E) and malondialdehyde levels in acute exacerbation and stable periods of patients with chronic obstructive pulmonary disease," *Clinical and investigative medicine*, vol. 27, pp. 123–128, 2004.

[18] S. A. Kharitonov and P. J. Barnes, "Exhaled markers of pulmonary disease," *American Journal of Respiratory and Critical Care Medicine*, vol. 163, no. 7, pp. 1693–1722, 2001.

[19] Z. Kluchová, D. Petrášová, P. Joppa, Z. Dorková, and R. Tkáčová, "The association between oxidative stress and obstructive lung impairment in patients with COPD," *Physiological Research*, vol. 56, no. 1, pp. 51–56, 2007.

[20] P. PAREDI, S. . A. KHARITONOV, D. LEAK, S. WARD, D. CRAMER, and P. . J. BARNES, "Exhaled ethane, a marker of lipid peroxidation, is elevated in chronic obstructive pulmonary disease," *American Journal of Respiratory and Critical Care Medicine*, vol. 162, no. 2, pp. 369–373, 2000.

[21] E. Zinellu, A. Zinellu, A. G. Fois, C. Carru, and P. Pirina, "Circulating biomarkers of oxidative stress in chronic obstructive pulmonary disease: a systematic review," *Respiratory research*, vol. 17, no. 1, p. 150, 2016.

[22] Y. A. Vladimirov, E. V. Proskurnina, and D. Y. Izmailov, "Chemiluminescence as a method for detection and study of free radicals in biological systems," *Bulletin of Experimental Biology and Medicine*, vol. 144, no. 3, pp. 390–396, 2007.

[23] M. M. Sozarukova, A. M. Polimova, E. V. Proskurnina, and Y. A. Vladimirov, "Changes in kinetics of chemiluminescence of plasma as a measure of systemic oxidative stress in humans," *Biofizika*, vol. 61, no. 2, pp. 337–344, 2016.

[24] Y. A. Vladimirov and E. V. Proskurnina, "Free radicals and cell chemiluminescence," *Biochemistry*, vol. 74, no. 13, pp. 1545–1566, 2009.

[25] N. Kubysheva, L. Postnikova, S. Soodaeva et al., "Relationship of the content of systemic and endobronchial soluble molecules of CD25, CD38, CD8, and HLA-I-CD8 and lung function parameters in COPD patients," *Disease markers*, vol. 2017, 2017.

[26] N. Kubysheva, S. Soodaeva, V. Novikov et al., "Soluble HLA-I and HLA-II molecules are potential prognostic markers of progression of systemic and local inflammation in patients with COPD," *Disease Markers*, vol. 2018, 7 pages, 2018.

[27] M. Plataki, E. Tzortzaki, P. Rytila, M. Demosthenes, A. Koutsopoulos, and N. M. Siafakas, "Apoptotic mechanisms in the pathogenesis of COPD," *International Journal of Chronic Obstructive Pulmonary Disease*, vol. 1, no. 2, pp. 161–171, 2006.

[28] Global Initiative Chronic Obstructive Pulmonary Disease, "Global strategy for diagnosis, management, and prevention of chronic obstructive pulmonary disease," 2018, https://goldcopd.org/wp-content/uploads/2017/11/GOLD-2018-v6.0-FINAL-revised-20-Nov_WMS.pdf.

[29] M. L. Bell, A. L. Whitehead, and S. A. Julious, "Guidance for using pilot studies to inform the design of intervention trials with continuous outcomes," *Clinical Epidemiology*, vol. 10, no. 10, pp. 153–157, 2018.

[30] K. Cocks and D. J. Torgerson, "Sample size calculations for pilot randomized trials: a confidence interval approach," *Journal of Clinical Epidemiology*, vol. 66, no. 2, pp. 197–201, 2013.

[31] A. Whitehead, S. Julious, C. Cooper, and M. J. Campbell, "Estimating the sample size for a pilot randomised trial to minimise the overall trial sample size for the external pilot and main trial for a continuous outcome variable," *Statistical Methods in Medical Research*, vol. 25, no. 3, pp. 1057–1073, 2016.

[32] J. H. Horvath and P. J. Barnes, "Exhaled breath condensate: methodological recommendations and unresolved questions," *The European Respiratory Journal*, vol. 26, no. 3, pp. 523–548, 2005.

[33] R. O. Recknagel and E. A. Glende Jr., "Spectrophotometric Detection of Lipid Conjugated Dienes," in *Methods in Enzymology*, vol. 105, pp. 331–337, Academic Press, 1984.

[34] I. A. Volchegorskii, A. G. Nalimov, R. I. Lifshits, and B. G. Iarovinskii, "Comparison of various approaches to the determination of the products of lipid peroxidation in heptane-isopropanol extracts of blood," *Voprosy meditsinskoi khimii*, vol. 35, no. 1, pp. 127–131, 1989.

[35] S. A. Negre, C. Coatrieux, C. Ingueneau, and R. Salvayre, "Advanced lipid peroxidation end products in oxidative damage to proteins. Potential role in diseases and therapeutic prospects for the inhibitors," *British Journal of Pharmacology*, vol. 153, no. 1, pp. 6–20, 2008.

[36] A. L. Tappel, "Lipid peroxidation and fluorescent molecular damage to membranes," *Pathobiology of cell membranes*, vol. 1, pp. 145–170, 1975.

[37] G. L. Ignatova, I. A. Volchegorskii, E. G. Volkova, E. L. Kazachkov, and O. L. Kolesnikov, "Lipid peroxidation processes in chronic bronchitis," *Terapevticheskiĭ Arkhiv*, vol. 70, no. 3, pp. 36-37, 1998.

[38] I. Rahman, "Oxidative stress in pathogenesis of chronic obstructive pulmonary disease: cellular and molecular mechanisms," *Cell Biochemistry and Biophysics*, vol. 43, no. 1, pp. 167–188, 2005.

[39] J. Cheng, T. Zhou, C. Liu et al., "Protection from Fas-mediated apoptosis by a soluble form of the Fas molecule," *Science*, vol. 263, no. 5154, pp. 1759–1762, 1994.

[40] I. A. Klimanov and S. K. Soodaeva, "Механизмы формирования конденсата выдыхаемого воздуха и маркеры оксидативного стресса при патологиях респираторного тракта," *Pulmonology*, no. 2, pp. 113–119, 2009.

[41] W. S. Snyder, M. J. Cook, E. S. Nasset, L. R. Karhausen, G. P. Howells, and I. H. Tripton, *Report of the Task Group on Reference Man. A Report Prepared by a Task Group of Committee 2 of the International Commission on Radiological Protection*, Pergamon Press, Oxford, 1975.

[42] E. Zaprudnova, S. Soodaeva, I. Klimanov et al., "FEV1 dynamics and total NO3-/NO2-level in exhaled breath condensate of current smokers," *European Respiratory Journal*, vol. 44, Supplement 58, 2014.

[43] I. Klimanov, S. Soodaeva, M. Glukhova, N. Nikitina, T. Li, and N. Popova, "Assessment of exhaled breath condensate contamination during measurement of nitric oxide metabolites," *European Respiratory Journal*, vol. 46, article PA3995, Supplement 59, 2015.

[44] S. Soodaeva, I. Klimanov, T. Eliseeva, and N. Kubysheva, "Concentrations of nitric oxide metabolites in the exhaled breath condensate in children with different bronchial asthma control," *European Respiratory Journal*, vol. 40, Supplement 56, p. P2206, 2012.

[45] S. Soodaeva, I. Klimanov, T. Eliseeva, N. Kubysheva, L. Nikitina, and S. Bolevich, "Dynamics of the nitric oxide metabolites in the exhaled breath condensate (EBC) in atopic asthma (BA) children receiving various treatment options," *European Respiratory Journal*, vol. 42, Supplement 57, p. P1116, 2013.

[46] I. Klimanov, S. Soodaeva, T. Li et al., "Level of soluble molecules of major histocompatibility complex CLASS II in serum, sputum and exhaled breath condensate in COPD of patients with an exacerbation of COPD," *European Respiratory Journal*, vol. 48, article PA885, Supplement 60, 2016.

[47] A. Bikov, G. Galffy, L. Tamasi, Z. Lazar, G. Losonczy, and I. Horvath, "Exhaled breath condensate pH is influenced by respiratory droplet dilution," *Journal of Breath Research*, vol. 6, no. 4, article 046002, 2012.

[48] Z. Lázár, E. Huszár, T. Kullmann et al., "Adenosine triphosphate in exhaled breath condensate of healthy subjects and patients with chronic obstructive pulmonary disease," *Inflammation Research*, vol. 57, no. 8, pp. 367–373, 2008.

[49] C. R. Esther Jr., H. M. Jasin, L. B. Collins, J. A. Swenberg, and G. Boysen, "A mass spectrometric method to simultaneously measure a biomarker and dilution marker in exhaled breath condensate," *Rapid Communications in Mass Spectrometry: An International Journal Devoted to the Rapid Dissemination of Up-to-the-Minute Research in Mass Spectrometry*, vol. 22, no. 5, pp. 701–705, 2008.

[50] T. M. Dwyer, "Sampling airway surface liquid: non-volatiles in the exhaled breath condensate," *Lung*, vol. 182, no. 4, pp. 241–250, 2004.

[51] R. M. Effros, B. Peterson, R. Casaburi et al., "Epithelial lining fluid solute concentrations in chronic obstructive lung disease patients and normal subjects," *Journal of Applied Physiology*, vol. 99, no. 4, pp. 1286–1292, 2005.

[52] I. A. Klimanov, S. K. Soodaeva, A. V. Lisitsa, V. B. Kudryavtsev, and A. G. Chuchalin, "Standardizing of preanalytic evaluation of exhaled breath condensate," *Pulmonology*, pp. 53–55, 2006.

Hindawi
Oxidative Medicine and Cellular Longevity
Volume 2021, Article ID 7138800, 10 pages
https://doi.org/10.1155/2021/7138800

Research Article

The Association of Nephroblastoma Overexpressed (NOV) and Endothelial Progenitor Cells with Oxidative Stress in Obstructive Sleep Apnea

Eddie W. Fakhouri,[1] Jeremy A. Weingarten,[1,2] Shailendra P. Singh,[3] Purvi Shah,[1,2] and Stephen J. Peterson[1,2]

[1]*New York-Presbyterian Brooklyn Methodist Hospital, Brooklyn, NY 11215, USA*
[2]*Department of Medicine, Weill Cornell Medicine, New York, NY 10065, USA*
[3]*Department of Pharmacology, New York Medical College, Valhalla, New York 10595, USA*

Correspondence should be addressed to Jeremy A. Weingarten; jaw9031@nyp.org

Received 30 July 2021; Revised 30 October 2021; Accepted 13 November 2021; Published 24 November 2021

Academic Editor: Daniela Ribeiro

Objective. Obstructive sleep apnea (OSA) is a sleep disorder characterized by intermittent hypoxia, chronic inflammation, and oxidative stress and is associated with cardiometabolic disease. Several biological substrates have been associated with OSA such as nephroblastoma overexpressed (NOV), endothelial progenitor cells (EPC), and circulating endothelial cells (CEC). Few studies have looked at the association of NOV with OSA while the EPC/CEC relationships with OSA are unclear. In this study, we hypothesize that (1) NOV is associated with the severity of OSA independent of BMI, identifying a protein that may play a role in the biogenesis of OSA complications, and (2) EPCs and CECs are also associated with the severity of OSA and are biomarkers of endothelial dysfunction in OSA. *Methods*. 61 subjects underwent overnight polysomnography (PSG), clinical evaluation, and blood analysis for NOV, EPC, CEC, interleukin 6 (IL-6), and other potential biomarkers. *Results*. NOV and EPCs were independently associated with the oxygen desaturation index (ODI) after adjusting for potential confounders including body mass index (BMI), age, and sex (NOV $p = 0.032$; EPC $p = 0.001$). EPC was also independently associated with AHI after adjusting for BMI, age, and sex ($p = 0.017$). IL-6 was independently associated with AHI, but not with ODI. *Conclusion*. NOV and EPC levels correlate with the degree of OSA independent of BMI, indicating that these biomarkers could potentially further elucidate the relationship between OSA patients and their risk of the subsequent development of cardiovascular disease.

1. Introduction

Obstructive sleep apnea (OSA) is a highly prevalent disorder, ranging from 3% to 17% in the general population depending on age and gender [1]. OSA is characterized by repetitive episodes of upper airway closure resulting in a reduction or complete cessation of airflow and intermittent hypoxia; obstructive respiratory events are terminated with an arousal state accompanied by sympathetic surges [2]. The result of poor alveolar ventilation associated with apnea/hypopnea events reduces arterial oxygen saturation and increases arterial pressure of carbon dioxide causing intermittent hypoxia. This leads to oxidative imbalance and increased inflammatory cytokines, lipid peroxidation, and cell-free DNA [3]. The severity of OSA is quantified by overnight sleep studies which measure the apnea-hypopnea index (AHI) and oxygen desaturation index (ODI). Risk factors for OSA include high body mass index, male gender, and age, resulting in a patient population already at risk for cardiometabolic disease. Indeed, OSA has been associated with prevalent and incident hypertension [4, 5], coronary artery disease, and cerebrovascular events [6], likely via inflammatory processes from oxidative stress with increased reactive oxygen species (ROS) formation and proinflammatory cytokines [7].

However, studies associating nephroblastoma overexpressed (NOV), endothelial progenitor cells (EPC), and circulating endothelial cells (CEC) with OSA and as a potential measure of vascular inflammation to determine the risk for cardiovascular disease (CVD) in OSA patients are minimal (NOV) or discrepant (EPC/CEC). A recent meta-analysis showed a linear correlation between AHI severity and olfactory dysfunction, but statistical differences between mild-moderate-severe were not seen [8]. Other recent findings include the apelin ligand of G protein-coupled receptor APJ; the apelin/APJ system appears to be closely related to the development of respiratory diseases, including OSA, that may well be an attractive target for therapeutic intervention [9].

NOV is a multifunctional protein that plays a role in inflammation, cancer, and fibrosis through its involvement in adhesion and mitosis pathways [10] and has been associated with multiple disorders either directly or indirectly linked to cardiovascular disease. Previously, we demonstrated a novel association between OSA and NOV in a clinical sample of obese and nonobese subjects [**11**].

CECs and EPCs are involved with vascular injury and repair. CECs are essentially "sloughed endothelial cells" resulting from systemic inflammation, which are replaced by EPCs that are expected to increase as inflammation-induced CECs sloughing increase [12]. When the EPC can no longer sustain the replacement of sloughed CECs, this denuded area is now ripe for plaque formation [13]. In a prior study, we found that CECs in morbidly obese women at increased risk of cardiovascular disease were elevated and EPCs were altered in obesity, suggestive of early inflammation [12]. Another study has also shown CEC elevation in a population of type 2 diabetics, showing that inflammation induced by diabetes was independent of HgbA1C levels [14]. Although these studies do not involve OSA patients, due to the strong association of OSA with both morbid obesity and diabetes, similar associations with OSA are likely present.

In the current study, we sought to demonstrate that in a sample of well-characterized OSA subjects at increased risk for cardiovascular disease, baseline inflammation in OSA, as demonstrated by changes in known and novel inflammatory biomarkers, may help to risk stratify this population and further elucidate a pathogenic link between OSA and cardiovascular disease. This manuscript is a follow-up study to our previous work [11] with a larger sample of subjects and further blood analysis including EPC, CEC, and cytokines. Specifically, we hypothesized that NOV and other inflammatory adipokines, CECs, and EPCs would independently correlate with increasing OSA severity and provide further evidence to support novel pathways leading to endothelial damage and cardiovascular disease.

2. Methods

2.1. Study Design and Sample. Study subjects and controls were enrolled at New York-Presbyterian Brooklyn Methodist Hospital (NYPBMH), and laboratory analysis of blood samples was analyzed at New York Medical College (NYMC). Subjects were drawn from individuals presenting to the Center for Sleep Disorders at NYPBMH for evaluation of possible OSA and from faculty and staff of NYMBMH who were not at risk for OSA to serve as controls. Subjects were considered for enrollment only in the absence of a known history (chart review) of coronary artery disease, atherosclerosis, or congestive heart failure. Only adults (age > 18 years old) were recruited. All subjects provided informed consent. A total of 61 subjects were enrolled. IRB approval at the clinical site (NYPBMH) was obtained prior to enrollment. All data were collected prospectively.

2.2. Clinical Parameters. All recruited patients had a complete history and physical examination. Patient demographics were collected including age, gender, and race. Patients underwent measurement of systolic and diastolic blood pressure, height and weight for BMI determination, neck circumference, and waist and hip circumference for waist-hip ratio determination by standard methods. Patients were also queried, and medication lists were evaluated to determine the presence of comorbid medical conditions (hypertension, diabetes, hyperlipidemia, chronic obstructive pulmonary disease, and asthma).

2.3. Polysomnography. All patients underwent nocturnal polysomnography (PSG) either by (1) conventional full-montage in-laboratory PSG or (2) home sleep testing; studies were performed in accordance with American Academy of Sleep Medicine (AASM) guidelines. Conventional full-montage in-laboratory PSG was performed using Compumedics (Victoria, Australia) software: standard 10-20 electroencephalography (EEG), electrocardiography (ECG), electromyography (EMG) of the chin and anterior tibialis muscle, electrooculography (EOG), snore, and pulse oximetry monitoring were utilized. Oral and nasal airflow were measured by pressure transducer and thermocouple. Respiratory effort was measured with respiratory impedance plethysmography bands at the chest and the abdomen including summation channel. Home sleep testing was performed using ResMed ApneaLink Air (San Diego, California). An apnea was defined as a reduction in peak thermal sensor (or nasal pressure signal in the case of home sleep testing) excursion by ≥90% of baseline, in which there is continued or increased inspiratory effort throughout the entire period of absent airflow lasting at least 10 seconds. Desaturation and/or arousal were not required. A hypopnea was defined as an abnormal respiratory event lasting at least 10 seconds with at least a ≥30% reduction in the nasal pressure signal excursion (or alternate sensor) accompanied by a ≥4% oxyhemoglobin desaturation. The AHI is a measure of OSA severity and derived from the number of apneas and hypopneas per hour of sleep (in-lab determination) or per hour of recording time (home sleep testing). OSA was defined as AHI ≥ 5/hr for analysis purposed. Further analysis with AHI ≥ 15/hr was also explored.

2.4. Laboratory Measurement. Venous blood was drawn from antecubital vein into a serum separator tube and a tube containing EDTA. Each SST sample was centrifuged at a force of 1600 g for 10 minutes after blood draw. The tubes were placed in an insulated container with dry ice until analysis.

2.5. Plasma NOV Protein Levels. Subjects frozen plasma was suspended in buffer (mmol/l: 10 phosphate buffer, 250 sucrose, 1.0 EDTA, 0.1 PMSF, and 0.1% v/v tergitol, pH 7.5). Immunoblotting for NOV was performed as previously described [15]. NOV levels were based on densitometry fold-increase from a single control sample.

2.6. Blood Samples and Cytokine Measurements. After overnight fasting, venous blood was drawn from an antecubital vein to measure serum levels of inflammatory cytokines, Leptin, and EPC testing (blood was drawn in heparinized tubes). Serum samples were frozen at -80°C before analysis. IL-6 was determined using ELISA.

2.7. Isolation of Circulating Endothelial Cells. A 10 ml sample of peripheral blood was obtained and used for CEC and EPC experiments. One ml of blood was incubated with 100 μl of anti-CD146 coated 45 μm Dynabeads (1.4×108 beads/ml) overnight at 4°C in a Dynal mixer (Dynal, Lake Success, New York) at 50 rpm. Cells bound to anti-CD146 coupled beads were separated from blood in a Dynal magnet, washed (3 washings using phosphate-buffered saline and 0.1% bovine serum albumin and repetitive mixing for 5 minutes in the Dynal mixer at 4°C), and dissolved in 100 μl buffer. Side-by-side assays were performed with Dynabeads coated with human antibodies against mouse IgG but without an antiendothelial antibody to check for nonspecific binding to the Dynabeads. The cells were mixed with acridine and visualized by light and fluorescence microscopy.

2.8. Isolation of Mononuclear Cells and EPC Colony Formation. Peripheral mononuclear cells (PMNCs) were fractionated using Ficoll density-gradient centrifugation. Isolated PMNCs were resuspended in CFU-Hill Medium (Stem Cell Technologies, Vancouver, Canada) and plated on 6-well plates, coated with human fibronectin at a concentration of 5×10^6 cells per well. After 48 hours, the nonadherent cells were collected and replated onto fibronectin-coated 24-well plates. EPC colonies were counted using an inverted microscope 7 days after plating. An EPC colony was defined as a cluster of at least 100 flat cells surrounding a cluster of rounded cells, as previously described [12]. Results are expressed as the mean number of colony-forming units (CFUs) per well.

2.9. Statistical Analysis. We summarized continuous variables using means and standard deviations and summarized categorical variables as frequencies and percentages. Continuous variables were compared with Student's t-test or Mann–Whitney/Wilcoxon paired test as appropriate. Categorical variables were compared with the chi-square test for independence. The relationship between NOV and OSA was compared in several different categories including ODI quartiles, AHI quartiles, and categories of OSA (no OSA, mild OSA, moderate OSA, and severe OSA) as defined by the AASM; these relationships were determined both between groups and overall trends. Due to nonnormal distribution of dependent variables, the cube-root transformation of NOV (and ODI/AHI when dependent variables), which approximated normality, was used in both multivariable models and between group comparisons (Student's t-test) to ensure validity of the model. All analyses were performed in Stata 15.1.

3. Results

61 subjects were recruited for enrollment. 3 subjects did not complete sleep studies following blood draw. In the overall group, the mean age was 42.6 years. Patients with OSA were significantly older than those without OSA. Women predominated the study population (57%). There was a similar proportion of OSA among men and women (66%). Black race accounted for 54% of the study population, while white race accounted for 31%. Among comorbid conditions, hypertension was the most common at 31%; hypertension was seen more frequently in OSA vs. no OSA subjects (41% vs. 11%, $p = 0.018$). BMI was greater in OSA vs. no OSA subjects (42.9 ± 10.4 vs. 32.1 ± 11.8 kg/m^2; $p = 0.007$). 67% of subjects demonstrated OSA on sleep testing with an AHI $\geq$ 5/hr while 41% of subjects had OSA under more stringent criteria of AHI $\geq$ 15/hr (Table 1).

NOV levels were greater among those with OSA (3.3 ± 2.9 vs. 2.2 ± 2-fold increase in OSA vs. no OSA ($p = 0.02$) (Figure 1)). NOV levels increase as quartiles of ODI ($p = 0.002$) and AHI ($p = 0.039$) increase. Within group differences were observed (Figure 2): NOV was different among ODI quartiles 1 and 3 ($p = 0.028$), quartiles 1 and 4 ($p = 0.009$), and quartiles 2 and 4 ($p = 0.033$), while NOV was different among AHI quartiles 2 and 4 ($p = 0.033$). NOV levels increase as OSA severity categories (clinical severity of no OSA, mild, moderate, and severe OSA) increase ($p = 0.013$); within group differences in NOV were only seen comparing mild and severe OSA ($p = 0.011$).

EPC and CEC were not significantly different when comparing OSA vs. no OSA (Figure 3), while leptin and IL-6 were (leptin: 70.5 ± 54 vs. 40.3 ± 45.5 ng/mL, $p = 0.015$; IL-6 4.4 ± 2.7 vs. 2.5 ± 2.7 ng/mL, $p = 0.006$; Figure 4). EPC levels increased as quartiles of ODI increased ($p = 0.017$) but not with AHI quartiles or by OSA severity categories. In exploratory analysis, EPC levels were higher in OSA when OSA was classified as AHI $\geq$ 15 hr (39.3 ± 29.8 vs. 22 ± 16.1 number/mL, $p = 0.021$) (Figure 3(a)). These results support that more severe disease has an association with higher EPC levels.

In multivariable analysis (Table 2), after adjusting for age, gender, and BMI, NOV was independently associated with ODI ($p = 0.032$). NOV was not independently associated with AHI. EPCs were independently associated with both ODI ($p = 0.001$) and AHI ($p = 0.017$). Leptin was independently associated with both ODI and AHI in model 2; however, when BMI was added, leptin was no longer associated with either parameter indicative that BMI is a strong confounding variable. IL-6 was independently associated with ODI ($p < 0.0001$) and AHI ($p < 0.0001$) in model 2; however, when BMI was added, it was no longer associated with ODI but maintained significance with AHI ($p = 0.049$), which supports that BMI confounded IL-6 as well.

Table 1: Baseline characteristics*.

	Total ($n = 61$)	No OSA ($n = 19$)	OSA ($n = 39$)	p value
Age (mean)	42.6 ± 13.8	34.6 ± 8.7	45.4 ± 12.8	$p = 0.0016$
Gender (%)				NS
Men	26 (43)	8 (42)	16 (41)	
Women	35 (57)	11 (58)	23 (59)	
Race (%)				NS
White	19 (31)	7 (37)	10 (36)	
Black	33 (54)	7 (37)	25 (64)	
Hispanic	3 (5)	0	3 (8)	
Asian	6 (10)	5 (26)	1 (3)	
Comorbidities (%)				
Hypertension	19 (31)	2 (11)	16 (41)	$p = 0.018$
Diabetes	13 (21)	2 (11)	10 (26)	NS
Hyperlipidemia	10 (16)	1 (5)	8 (21)	NS
BMI (kg/m^2)	39 ± 11.9	32.1 ± 11.8	42.9 ± 10.4	$p = 0.0007$
AHI (events/hr)	21.4 ± 30	2.4 ± 1.3	30.6 ± 32.9	$p = 0.0004$
ODI (desat/hr)	17.3 ± 24.7	2.3 ± 2.0	24.6 ± 27.3	$p = 0.0008$
OSA (≥5/hr) (%)	39 (67)			
OSA (≥15/hr) (%)	24 (41)			

Abbreviations: OSA: obstructive sleep apnea; BMI: body mass index; AHI: apnea hypopnea index; ODI: oxygen desaturation index; NS: not significant ($p > 0.05$). *Note: 3 subjects did not complete sleep study, accounting for the discrepancy between total and subgroup frequency.

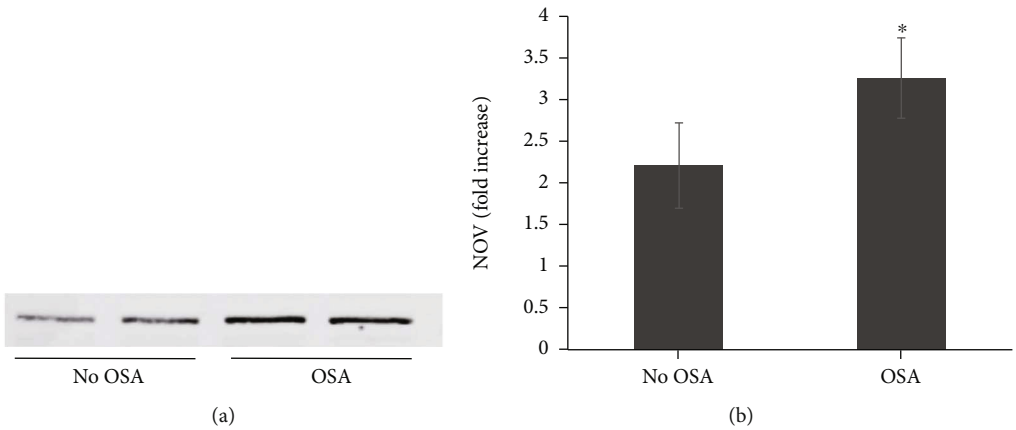

Figure 1: (a) Representative serum immunoblotting analysis for NOV in no OSA vs. OSA subjects. Subjects with OSA displayed an increase in NOV proteins on western blot when compared to those without OSA. (b) Fold change in NOV expression in OSA vs. no OSA subjects. Subjects with OSA displayed greater fold-increase in NOV levels when compared to subjects without OSA ($n = 50$, $^*p = 0.02$). Results are mean ± SE.

4. Discussion

We have shown for the first time that measures of obstructive sleep apnea (OSA) are independently associated with the novel adipokine matricellular protein nephroblastoma overexpressed (NOV) and endothelial progenitor cells (EPC) after adjusting for baseline demographics and BMI. Specifically, NOV levels were higher in those with OSA compared to those without OSA in univariate analysis. Further, multivariable methods showed that NOV is associated with the oxygen desaturation index (ODI) after adjusting for age, gender, and BMI; this finding was not seen in association with the apnea hypopnea index, suggesting that intermittent hypoxia, as specifically measured by the ODI, is central to this relationship, and that the more general measure of sleep-disordered breathing (AHI), which may also include nonhypoxic arousal events, is not. EPCs, in contrast, are independently associated with both the ODI and AHI, suggesting that overall mechanisms of OSA including intermittent hypoxia and other pathophysiologic variables are important in this relationship. Leptin and IL-6 levels related to OSA measures appear to be modified by BMI.

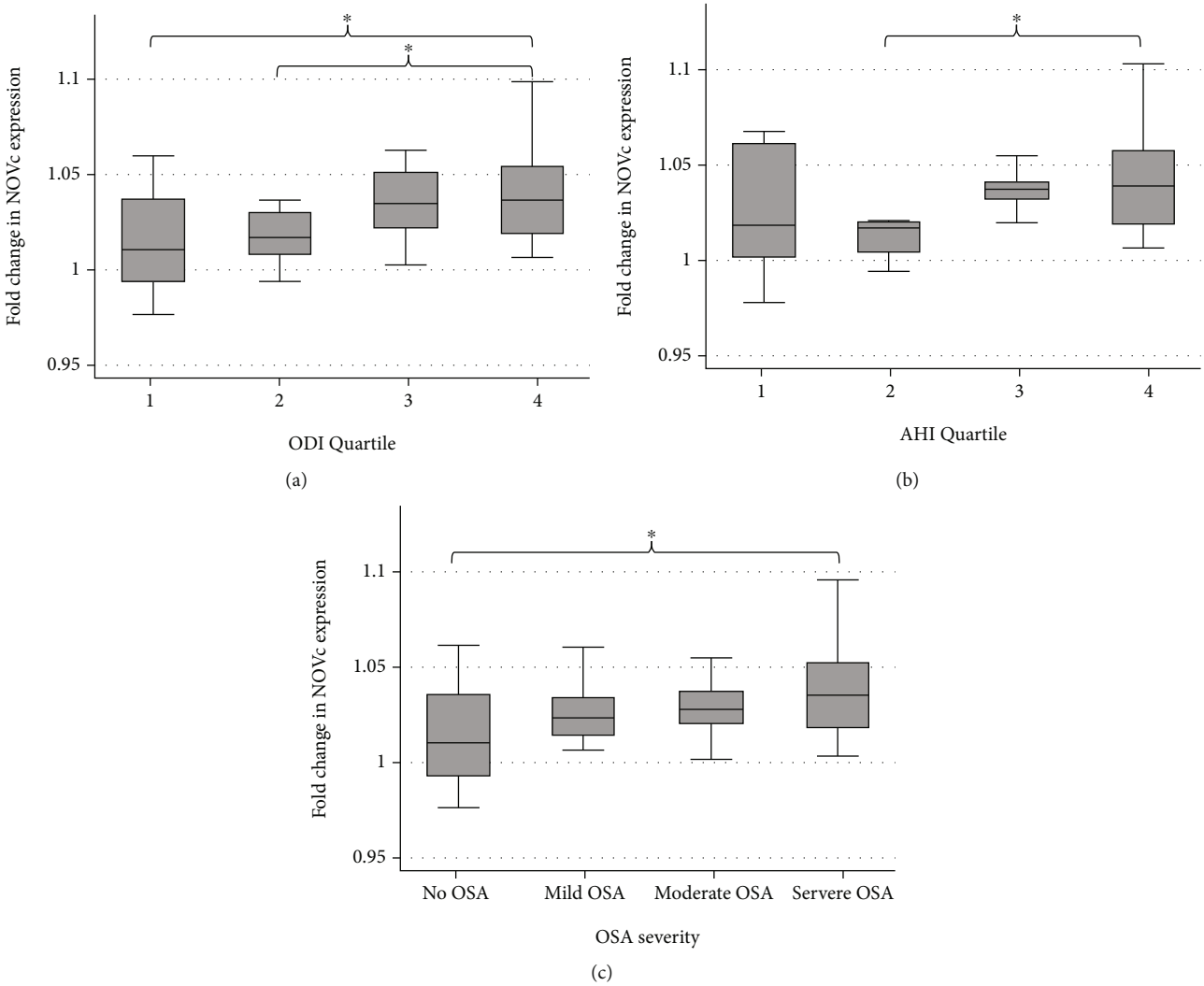

Figure 2: Box plots demonstrating change in cube-root transformed NOV levels (NOVc) as severity of sleep apnea increases. (a) ODI quartiles, overall trend $p = 0.002$; (b) AHI quartiles, overall trend $p = 0.039$; (c) OSA severity, overall trend $p = 0.013$. $^{*}p < 0.05$. These plots were made using cube root transformation of NOV and Student's t-test performed in Stata 15.1. (a) Box plots representing NOV levels in the different ODI quartiles. Subjects in the upper ODI quartiles have increasing levels of NOV. There is statistically significant higher expression of NOV in ODI quartile 4 when compared to ODI quartiles 1 and 2. The overall trend for NOV expression increases as ODI quartile increases. (b) Box plots representing NOV levels in the different AHI quartiles. Subjects in the upper AHI quartiles have increasing levels of NOV. There is statistically significant higher expression of NOV in AHI quartile 4 when compared to AHI quartile 2. The overall trend for NOV expression increases as AHI quartile increases. (c) Box plots representing NOV levels in the different severities of OSA. Subjects in the high severity groups have increasing levels of NOV. There is statistically significant higher expression of NOV in the severe OSA group when compared to the no OSA group. The overall trend for NOV expression increases as AHI quartile increases.

Inflammation in OSA is driven by intermittent hypoxia and fragmented sleep leading to oxidative stress, manifested by increased formation of ROS and elevated adipocytokines [16, 17]. Oxidative imbalance is the result of this intermittent hypoxia with increased inflammatory cytokine production of IL-6, TNF, and lipid peroxidation; literature review has not identified which biomarkers better correlate with the severity of disease [3]. CPAP has been shown to decrease this oxidative stress [3] and normalize ROS, nitric oxide, and 8-isoprostane levels [18]. In contrast, obesity's baseline chronic inflammatory state is due to insulin and leptin resistance resulting in increased inflammatory cytokines released from white adipose tissue (WAT), which has diminished thermogenic capability from mitochondrial dysfunction compared to brown or beige adipose tissue (BBAT) [19–21]. Due to OSA's strong correlation with obesity, the inflammation and associated comorbid conditions of obesity can be seen in OSA patients. Our findings suggest that obesity plays a role in chronic inflammation (as seen in leptin and IL-6 levels modified by BMI) while the additional inflammatory pressure resulting in elevated NOV and EPC levels is likely driven by intermittent hypoxia and inflammation specific to OSA pathophysiology. The development of atherosclerosis is thought to be highly influenced by this

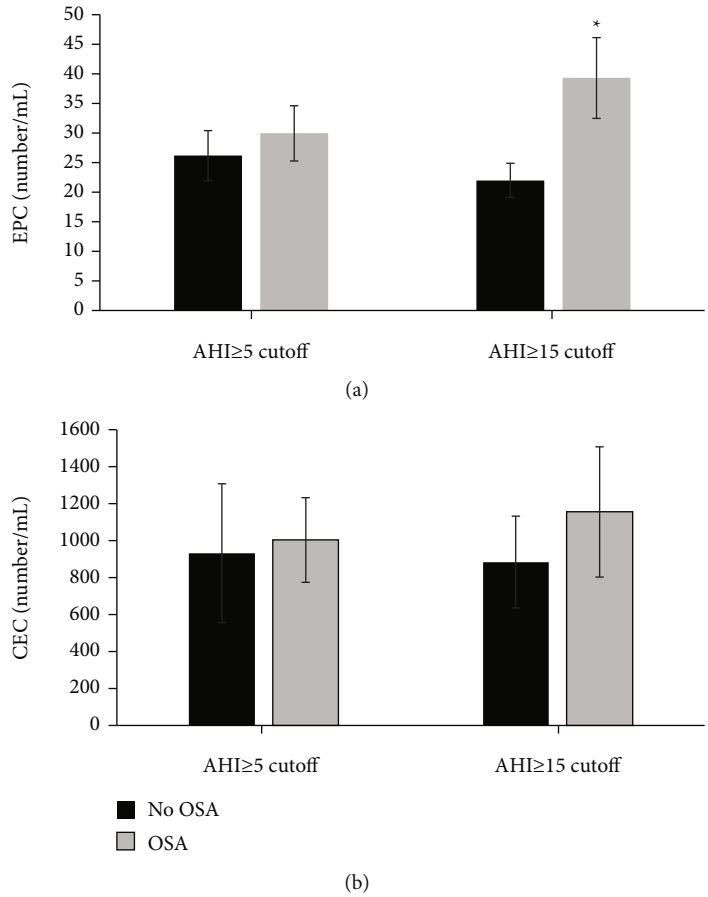

Figure 3: (a) Difference in EPC levels in subjects with OSA vs. no OSA; OSA defined as AHI ≥ 5/hr or AHI ≥ 15/hr. Those with OSA had higher EPC levels when more stringent criteria for OSA diagnosis (i.e., AHI ≥ 15) were used supportive that more severe disease has an association with higher EPC levels ($n = 53$, $^*p = 0.021$). (b) Difference in CEC levels in subjects with OSA vs. no OSA; OSA defined as AHI ≥ 5/hr or AHI ≥ 15/hr. Those with OSA displayed higher levels of CEC, but the association did not reach statistical significance ($n = 44$).

intermittent hypoxia; this involves a complex interaction of multiple factors that include oxidative stress and inflammation, autonomic nervous system dysfunction, and platelet activation [22].

NOV, a member of the CCN multifunctional proteins, plays a role in inflammation, cancer, and fibrosis through its involvement in adhesion and mitosis pathways [10]. It has been associated with multiple disorders either directly or indirectly linked to cardiovascular disease. NOV is an established regulator of and regulated by various cyto/chemokines, including the anti-inflammatory enzyme heme oxygenase-1 (HO-1) [23], [10]. A recent study in humans showed that NOV is strongly correlated with BMI and fat mass, decreases with weight loss, and is associated with elevated hemoglobin A1c levels [24]. Disease states associated with increased inflammation, including endothelial cell dysfunction, obesity, insulin resistance, metabolic syndrome, and interstitial renal fibrosis, have all been associated with increased NOV levels [23–25], [26]. Furthermore, epoxyeicosatrienoic acid (EET), a molecule that inhibits the inflammatory process, improves insulin sensitivity, and decreases NOV was shown to attenuate obesity-induced cardiomyopathy by down regulating NOV, increasing heme oxygenase-1 (HO-1) and Wnt signaling in both cardiac and pericardial fat [15, 27]. This resulted in decreased inflammatory cytokines IL-6 and TNF, as well as an increase in anti-inflammatory molecules and mitochondrial integrity [15, 27]. HO-1 upregulation and EET upregulation both result in marked reductions of IL-6, TNF, and NOV [28]. The knockout mouse model of peroxisome proliferator-activated receptor gamma coactivator-1α (PGC-1 α) reversed these findings and blocking the nuclear coactivator of HO-1 suggested that HO-1 upregulation was the mechanism involved. These findings propose that NOV may play a role in the OSA-related risk of developing cardiac disease and may be a target for potential therapy. This was shown again by administration of an EET agonist that increased PGC-1 α, which induced the HO-1 increase, improved mitochondrial function, and induced a change in the pericardial and epicardial adipocyte phenotype from white to beige; the improved insulin receptor phosphorylation improved insulin sensitivity and resulted in reversal of heart failure [27]. Thymoquinone (TQ) is another molecule that comes from the Nigella sativa plant that has major anti-inflammatory properties; in combination with omega fish oils, they improved insulin sensitivity in obesity and

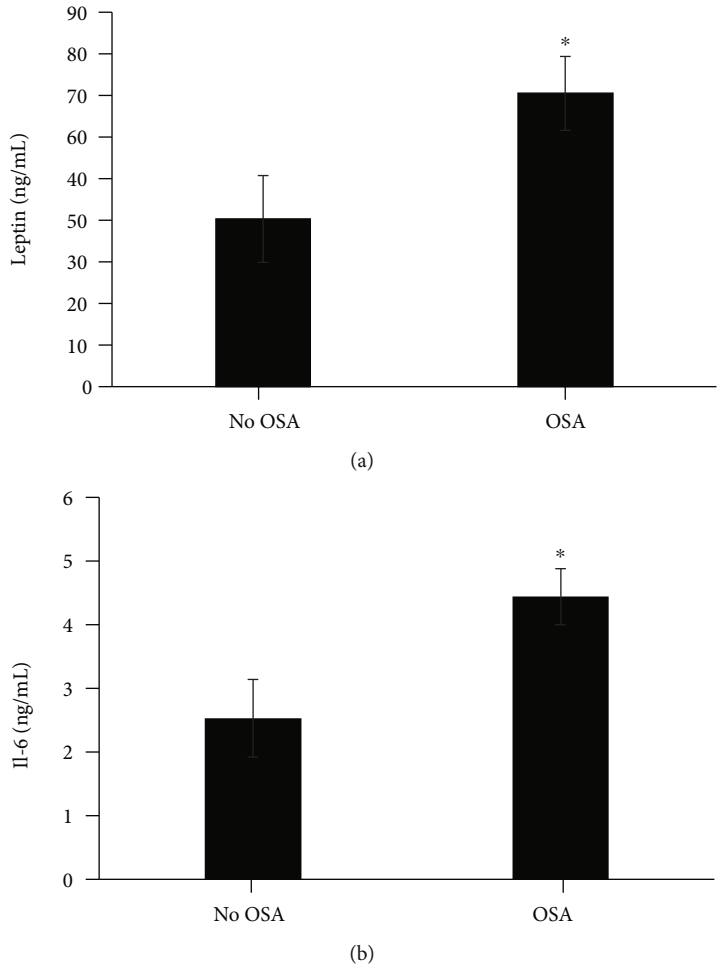

Figure 4: (a) Difference in Leptin levels by OSA vs. no OSA. Those with OSA had higher levels of leptin ($n = 59$, $^{*}p \leq 0.05$) prior to adjusting for age, gender, and BMI. This association was lost when BMI was adjusted for indicating BMI is a strong confounding variable. Results are mean ± SE. (b) Difference in IL-6 levels by OSA vs. no OSA. Those with OSA had higher IL-6 levels ($n = 59$, $^{*}p \leq 0.05$). This association was seen in both ODI and AHI as parameters for diagnosing OSA prior to adjusting for BMI. When BMI was added IL-6 maintained association with AHI only ($p = 0.049$) supportive that BMI is a confounding variable. Results are mean ± SE.

Table 2: Regression model with dependent variables (ODI and AHI) vs. independent variables.

	Model 1	Model 2	Model 3
ODIc			
NOVc	17.1 (4.8, 29.3) ¶	20.0 (7.5, 32.6) ¶	14.4 (1.3, 27.5)*
EPCs	0.16 (0.03, 0.29)*	0.17 (0.04, 0.31)*	0.20 (0.09, 0.31) ¶
Leptins	0.07 (-0.01, 0.16)	0.13 (0.05, 0.22) ¶	0.05 (-0.06, 0.16)
IL-6 s	0.57 (0.22, 0.93) ¶	0.71 (0.35, 1.1)§	0.46 (-0.10, 1.0)
AHIc			
NOVc	11.0 (-1.6, 23.6)	12.9 (-0.1, 25.9)	7.4 (-6.2, 21.1)
EPCs	0.11 (-0.01, 0.24)	0.12 (-0.01, 0.26)	0.14 (0.03, 0.26)*
Leptins	0.05 (-0.04, 0.13)	0.10 (0.01, 0.19)*	0.02 (-0.10, 0.13)
IL-6 s	0.54 (0.19, 0.90)¶	0.68 (0.33, 1.03)§	0.56 (0.002, 1.11)*

Model 1 is before adjustment; model 2: adjustment for age and sex; model 3: adjustment for BMI, age, and sex. $^{*}p < 0.05$; $^{¶}p < 0.01$; $^{§}p < 0.0001$. Abbreviations: ODIc: cube-root transformed oxygen desaturation index; AHIc: cube-root transformed apnea hypopnea index; NOVc: cube-root transformed NOV levels; EPCs: square-root transformed endothelial progenitor cells; Leptins: square-root transformed Leptin; IL-6 s: square-root transformed interleukin-6.

promoted the browning of white fat, with upregulation of mitochondrial enzymes, HO-1 levels, and reduction of the inflammatory adipokine NOV, twist-related protein (TWIST2), and the adipocyte hypoxia inducible factor HIF-1α [29]. NOV induces cytokine formation by increasing adipogenesis, with decreased numbers of mitochondria and diminished mitochondrial function, which is all reversed by EET upregulation [27]. White adipose tissue has higher NOV levels than beige and brown adipose tissue [15]. In addition, the inflammatory state is destructive to mitochondria and contributes to multiorgan dysfunction [30–32]. The ability to generate thermogenesis via mitochondrial electron transport chain (ETC) uncoupling is highest in brown fat, followed by beige, and finally least in white fat [19, 20]. Therefore, lean individuals with a higher brown/beige adipose tissue (BBAT) to WAT ratio have better anti-inflammatory mechanisms to fight severe inflammation due to stable thermogenesis secondary to higher mitochondria concentration, which utilizes HO-1 to promote uncoupling [29, 33].

Other potential predictive markers such as CECs and EPCs are of interest in proinflammatory disease states as well. CECs are accepted and reliable indicators of vascular damage [34]. CECs are a measure of "sloughed cells" from the vascular endothelium that are routinely replaced by bone marrow-derived EPCs as part of the injury-repair mechanism, but EPCs are rarely identified in the peripheral blood of healthy individuals, and when they are, they will be few in number [35]. When the production of EPCs are no longer able to replace the increasing amounts of sloughed CECs, the area of denuded endothelium is now primed for the development of vascular plaques [36]. EPCs have been implicated in plaque "vulnerability to rupture" [12, 37]. As a result, their presence in peripheral blood is a measure of endothelial injury/repair [34]. Endothelial dysfunction is the initial stage of atherosclerotic disease and more need to be done to identify patients at increased risk and intervene [38].

Quantification of CEC and EPC has correlated with cardiovascular disease. Studies show increased levels of CECs in the acute coronary syndrome spectrum, stable angina, ischemic cerebrovascular accident (CVA), and critical limb ischemia [39]. CEC quantification 48 hours after acute coronary syndrome was shown to accurately risk stratify patients for major adverse coronary events and death at both one month and one year [39]. Furthermore, the pathogenesis of atherosclerosis and plaque rupture leading to ischemic events is a proinflammatory process resulting in higher oxidative stress in the endothelium [40]. On the other hand, decreased EPCs have been associated with increased levels of cardiovascular disease [36]. One theory posits that there is a finite supply of EPCs, and once they have been exhausted due to repetitive vascular injury, the evolution of cardiovascular disease is established [41].

Individuals with higher levels of oxidative stress, such as those with OSA and obesity, have higher risk for unstable plaque formation over the damaged endothelium that consists of cholesterol deposits and foam cells [40]. Presumably, those with established cardiovascular disease would demonstrate a reduction in EPCs, and this should be in a dose response manner to the severity of OSA. However, this was not what we found in our study, and the literature in OSA and EPCs is quite variable. Multiple investigators have found that EPCs are reduced in those with OSA [42]; [43]; [44]. Alternatively, other investigators found that EPCs were increased [45] or unchanged [46] [47] in OSA vs. control. Potential reasons for these discrepant results are numerous, including differences in EPC measurement, differences in patient population (i.e., race and age) [48], and differences in the presence and evolution of cardiovascular disease in each individual patient. Those with changes in EPC levels are at risk for a vulnerable thin fibrous cap rupture leading to acute thrombosis placing individuals with OSA at higher risk for cardiovascular disease [12, 37, 40]. Intermittent hypoxia seen in OSA causes increased ROS formation as a result of decreased oxygenation and may subsequently result in higher EPC levels as the endothelium undergoes repair [7, 40]. In our study, EPC levels were found to be independently associated with both ODI ($p = 0.001$) and AHI ($p = 0.017$) (Table 2). There was no statistically significant correlation between OSA and CEC in our data; of note, only 44 subjects had CECs measured in this study which may have resulted in a type 2 error.

The proinflammatory state of OSA was confirmed in our subjects by increased levels of IL-6. There was an overall positive correlation between AHI and IL-6 (Table 2, model 1 $p = 0.003$), but the relationship was weakened when adjusted for BMI (Table 2 model 3 $p = 0.049$), suggesting the inflammatory state of obesity acts as an effect modifier. Similar findings are well established in OSA patients, in which several inflammatory markers are known to be elevated in OSA, including leptin, CRP, TNF-a, and IL-6 [49].

There are several limitations in our study. Although we feel that the findings are generalizable, the fact that we had a large percentage of black subjects makes this less so. Known racial differences in cardiovascular disease [50] may indicate that the pathogenic mechanisms underlying the vascular inflammatory cascade may also be different. Because our study subjects in general did not have established coronary or other cardiovascular diseases, we were unable to differentiate those in whom EPCs may have been decreased due to exhaustion of the bone marrow response from those with an exuberant EPC response. Because we did not collect actigraphy data, we were unable to assess the role that shortened sleep duration and therefore sleep deprivation may have played in our results. Similarly, the lack of arterial blood gas analysis to determine the presence of hypoventilation prevented us from identifying subjects with obesity-hypoventilation syndrome, which may affect the degree of deoxygenation and thus oxidative stress. Finally, the cross-sectional nature of our study prevents any temporality and therefore any causal inference.

5. Conclusion

The subjects of our study demonstrated that OSA is independently correlated with NOV after adjusting for BMI, age, and sex when compared to control. NOV appeared to be driven by intermittent hypoxia rather than general

obstructive episodes as the correlation was with ODI and not AHI. EPCs were independently associated with both ODI and AHI, while CECs did not demonstrate an association with OSA. IL-6 was elevated in OSA subjects based on AHI, but BMI appeared to be a strong modifier of this relationship. Leptin was not associated with OSA after fully adjusting for BMI. In summary, the inflammatory adipokine NOV and EPC represent potential biomarkers that may help identify OSA patients at a current or future increased risk of cardiovascular disease from oxidative stress and may be a potential target to prevent the vascular downstream consequences of this systemic inflammatory cascade.

Data Availability

Access to data is restricted due to legal and ethical concerns.

Additional Points

Study Importance Questions. What is already known about this subject? (i) OSA is associated with oxidative stress of chronic inflammation, elevation of adipocytokines, and endothelial dysfunction. (ii) OSA is associated with cardiometabolic disease. What are the new findings in your manuscript? (i) NOV levels correlate with the degree of OSA independent of BMI. (ii) EPC levels correlate with the degree of OSA independent of BMI. How might your results change the direction of research or the focus of clinical practice? NOV and EPC represent potential biomarkers which may help to identify OSA patients at a current or future increased risk of cardiovascular disease caused by oxidative stress and chronic inflammation and may be a potential target to prevent the vascular downstream consequences of this systemic inflammatory cascade.

Conflicts of Interest

All authors declare no conflict of interest.

Authors' Contributions

Eddie W. Fakhouri and Jeremy A. Weingarten contributed equally to this work.

References

[1] P. E. Peppard, T. Young, J. H. Barnet, M. Palta, E. W. Hagen, and K. M. Hla, "Increased prevalence of sleep-disordered breathing in adults," *American Journal of Epidemiology*, vol. 177, no. 9, pp. 1006–1014, 2013.

[2] A. S. Jordan, D. G. McSharry, and A. Malhotra, "Adult obstructive sleep apnoea," *Lancet*, vol. 383, no. 9918, pp. 736–747, 2014.

[3] A. Maniaci, G. Iannella, S. Cocuzza et al., "Oxidative stress and inflammation biomarker expression in obstructive sleep apnea patients," *Journal of Clinical Medicine*, vol. 10, no. 2, p. 277, 2021.

[4] F. J. Nieto, T. B. Young, B. K. Lind et al., "Association of sleep-disordered breathing, sleep apnea, and hypertension in a large community-based study," *Journal of the American Medical Association*, vol. 283, no. 14, pp. 1829–1836, 2000.

[5] J. M. Marin, A. Agusti, I. Villar et al., "Association between treated and untreated obstructive sleep apnea and risk of hypertension," *Journal of the American Medical Association*, vol. 307, no. 20, pp. 2169–2176, 2012.

[6] J. M. Marin, S. J. Carrizo, E. Vicente, and A. G. Agusti, "Long-term cardiovascular outcomes in men with obstructive sleep apnoea- hypopnoea with or without treatment with continuous positive airway pressure: an observational study," *Lancet*, vol. 365, no. 9464, pp. 1046–1053, 2005.

[7] L. Lavie, "Oxidative stress in obstructive sleep apnea and intermittent hypoxia - Revisited - The bad ugly and good: Implications to the heart and brain," *Sleep Medicine Reviews*, vol. 20, pp. 27–45, 2015.

[8] G. Iannella, G. Magliulo, A. Maniaci et al., "Olfactory function in patients with obstructive sleep apnea: a meta-analysis study," *European Archives of Oto-Rhino-Laryngology*, vol. 278, no. 3, pp. 883–891, 2021.

[9] J. Yan, A. Wang, J. Cao, and L. Chen, "Apelin/APJ system: an emerging therapeutic target for respiratory diseases," *Cellular and Molecular Life Sciences*, vol. 77, no. 15, pp. 2919–2930, 2020.

[10] L. Kular, J. Pakradouni, P. Kitabgi, M. Laurent, and C. Martinerie, "The CCN family: a new class of inflammation modulators?," *Biochimie*, vol. 93, no. 3, pp. 377–388, 2011.

[11] J. A. Weingarten, L. Bellner, S. J. Peterson et al., "The association of NOV/CCN3 with obstructive sleep apnea (OSA): preliminary evidence of a novel biomarker in OSA," *Hormone Molecular Biology and The Clinical Investigator*, vol. 31, no. 2, 2017.

[12] S. J. Peterson, J. I. Shapiro, E. Thompson et al., "Oxidized HDL, adipokines, and endothelial dysfunction: a potential biomarker profile for cardiovascular risk in women with obesity," *Obesity*, vol. 27, no. 1, pp. 87–93, 2019.

[13] J. L. Wilson, F. Bouillaud, A. S. Almeida et al., "Carbon monoxide reverses the metabolic adaptation of microglia cells to an inflammatory stimulus," *Free Radical Biology & Medicine*, vol. 104, pp. 311–323, 2017.

[14] J. A. McClung, N. Naseer, M. Saleem et al., "Circulating endothelial cells are elevated in patients with type 2 diabetes mellitus independently of HbA (1)c," *Diabetologia*, vol. 48, no. 2, pp. 345–350, 2005.

[15] J. Cao, S. P. Singh, J. A. McClung et al., "EET intervention on Wnt1, NOV, and HO-1 signaling prevents obesity-induced cardiomyopathy in obese mice," *American Journal of Physiology. Heart and Circulatory Physiology*, vol. 313, no. 2, pp. H368–H380, 2017.

[16] S. S. Martin, A. Qasim, and M. P. Reilly, "Leptin resistance: a possible interface of inflammation and metabolism in obesity-related cardiovascular disease," *Journal of the American College of Cardiology*, vol. 52, no. 15, pp. 1201–1210, 2008.

[17] A. Stanek, K. Brozyna-Tkaczyk, and W. Myslinski, "Oxidative stress markers among obstructive sleep apnea patients," *Oxidative Medicine and Cellular Longevity*, vol. 2021, Article ID 9681595, 8 pages, 2021.

[18] A. Alonso-Fernandez, F. Garcia-Rio, M. A. Arias et al., "Effects of CPAP on oxidative stress and nitrate efficiency in sleep apnoea: a randomised trial," *Thorax*, vol. 64, no. 7, pp. 581–586, 2009.

[19] E. W. Fakhouri, S. J. Peterson, J. Kothari, R. Alex, J. I. Shapiro, and N. G. Abraham, "Genetic polymorphisms complicate COVID-19 therapy: pivotal role of HO-1 in cytokine storm," *Antioxidants*, vol. 9, no. 7, p. 636, 2020.

[20] S. Demine, P. Renard, and T. Arnould, "Mitochondrial uncoupling: a key controller of biological processes in physiology and diseases," *Cell*, vol. 8, no. 8, p. 795, 2019.

[21] G. H. Goossens, "The metabolic phenotype in obesity: fat mass, body fat distribution, and adipose tissue function," *Obesity Facts*, vol. 10, no. 3, pp. 207–215, 2017.

[22] J. Chen, S. Lin, and Y. Zeng, "An update on obstructive sleep apnea for atherosclerosis: mechanism, diagnosis, and treatment," *Frontiers in Cardiovascular Medicine*, vol. 8, p. 647071, 2021.

[23] C. Martinerie, M. Garcia, T. T. Do et al., "NOV/CCN3: a new adipocytokine involved in obesity-associated insulin resistance," *Diabetes*, vol. 65, no. 9, pp. 2502–2515, 2016.

[24] J. Pakradouni, W. le Goff, C. Calmel et al., "Plasma NOV/CCN3 levels are closely associated with obesity in patients with metabolic disorders," *PLoS One*, vol. 8, no. 6, article e66788, 2013.

[25] D. Sacerdoti, S. P. Singh, J. Schragenheim et al., "Development of NASH in obese mice is confounded by adipose tissue increase in inflammatory NOV and oxidative stress," *International Journal of Hepatology*, vol. 2018, Article ID 3484107, 14 pages, 2018.

[26] P. O. Marchal, P. Kavvadas, A. Abed et al., "Reduced NOV/CCN3 expression limits inflammation and interstitial renal fibrosis after obstructive nephropathy in mice," *PLoS One*, vol. 10, no. 9, article e0137876, 2015.

[27] S. P. Singh, J. A. McClung, L. Bellner et al., "CYP-450 epoxygenase derived epoxyeicosatrienoic acid contribute to reversal of heart failure in obesity-induced diabetic cardiomyopathy via PGC-1 alpha activation," *Cardiovascular Pharmacology: Open Access*, vol. 7, no. 1, article e0137876, 2018.

[28] J. A. McClung, L. Levy, V. Garcia, D. E. Stec, S. J. Peterson, and N. G. Abraham, "Heme-oxygenase and lipid mediators in obesity and associated cardiometabolic diseases: therapeutic implications," *Pharmacology & Therapeutics*, p. 107975, 2021.

[29] H. H. Shen, S. J. Peterson, L. Bellner et al., "Cold-pressed nigella sativa oil standardized to 3% thymoquinone potentiates omega-3 protection against obesity-induced oxidative stress, inflammation, and markers of insulin resistance accompanied with conversion of white to beige fat in mice," *Antioxidants*, vol. 9, no. 6, p. 489, 2020.

[30] A. Sasson, E. Kristoferson, R. Batista, J. A. McClung, N. G. Abraham, and S. J. Peterson, "The pivotal role of heme oxygenase-1 in reversing the pathophysiology and systemic complications of NAFLD," *Archives of Biochemistry and Biophysics*, vol. 697, p. 108679, 2021.

[31] S. J. Peterson, R. Rubinstein, M. Faroqui et al., "Positive effects of heme oxygenase upregulation on adiposity and vascular dysfunction: gene targeting vs. pharmacologic therapy," *International Journal of Molecular Sciences*, vol. 20, no. 10, p. 2514, 2019.

[32] S. J. Peterson, A. Choudhary, A. K. Kalsi, S. Zhao, R. Alex, and N. G. Abraham, "OX-HDL: a starring role in cardiorenal syndrome and the effects of heme oxygenase-1 intervention," *Diagnostics*, vol. 10, no. 11, p. 976, 2020.

[33] M. Raffaele, M. Licari, S. Amin et al., "Cold press pomegranate seed oil attenuates dietary-obesity induced hepatic steatosis and fibrosis through antioxidant and mitochondrial pathways in obese mice," *International Journal of Molecular Sciences*, vol. 21, no. 15, p. 5469, 2020.

[34] U. Erdbruegger, A. Dhaygude, M. Haubitz, and A. Woywodt, "Circulating endothelial cells: markers and mediators of vascular damage," *Current Stem Cell Research & Therapy*, vol. 5, no. 4, pp. 294–302, 2010.

[35] H. Wu, H. Chen, and P. C. Hu, "Circulating endothelial cells and endothelial progenitors as surrogate biomarkers in vascular dysfunction," *Clinical Laboratory*, vol. 53, no. 5-6, pp. 285–295, 2007.

[36] A. Briasoulis, D. Tousoulis, C. Antoniades, N. Papageorgiou, and C. Stefanadis, "The role of endothelial progenitor cells in vascular repair after arterial injury and atherosclerotic plaque development," *Cardiovascular Therapeutics*, vol. 29, 139 pages, 2011.

[37] D. Kashiwazaki, N. Akioka, N. Kuwayama et al., "Involvement of circulating endothelial progenitor cells in carotid plaque growth and vulnerability," *Journal of Neurosurgery*, vol. 125, no. 6, pp. 1549–1556, 2016.

[38] A. Stanek, B. Fazeli, S. Bartus, and E. Sutkowska, "The role of endothelium in physiological and pathological states: new data," *BioMed Research International*, vol. 2018, Article ID 1098039, 3 pages, 2018.

[39] C. J. Boos, G. Y. Lip, and A. D. Blann, "Circulating endothelial cells in cardiovascular disease," *Journal of the American College of Cardiology*, vol. 48, no. 8, pp. 1538–1547, 2006.

[40] P. Libby, J. E. Buring, L. Badimon et al., "Atherosclerosis," *Nature Reviews. Disease Primers*, vol. 5, no. 1, p. 56, 2019.

[41] J. M. Hill, G. Zalos, J. P. J. Halcox et al., "Circulating endothelial progenitor cells, vascular function, and cardiovascular risk," *New England Journal of Medicine*, vol. 348, no. 7, pp. 593–600, 2003.

[42] M. de la Peña, A. Barceló, F. Barbe et al., "Endothelial function and circulating endothelial progenitor cells in patients with sleep apnea syndrome," *Respiration*, vol. 76, no. 1, pp. 28–32, 2008.

[43] S. Jelic, M. Padeletti, S. M. Kawut et al., "Inflammation, oxidative stress, and repair capacity of the vascular endothelium in obstructive sleep apnea," *Circulation*, vol. 117, no. 17, pp. 2270–2278, 2008.

[44] M. Murri, R. Garcia-Delgado, J. Alcazar-Ramirez et al., "Effect of CPAP on oxidative stress and circulating progenitor cell levels in sleep patients with apnea-hypopnea syndrome," *Respiratory Care*, vol. 56, no. 11, pp. 1830–1836, 2011.

[45] T. Kizawa, Y. Nakamura, S. Takahashi, S. Sakurai, K. Yamauchi, and H. Inoue, "Pathogenic role of angiotensin II and oxidised LDL in obstructive sleep apnoea," *The European Respiratory Journal*, vol. 34, no. 6, pp. 1390–1398, 2009.

[46] C. H. Yun, K. H. Jung, K. Chu et al., "Increased circulating endothelial microparticles and carotid atherosclerosis in obstructive sleep apnea," *Journal of Clinical Neurology*, vol. 6, no. 2, pp. 89–98, 2010.

[47] K. Martin, M. Stanchina, N. Kouttab, E. O. Harrington, and S. Rounds, "Circulating endothelial cells and endothelial progenitor cells in obstructive sleep apnea," *Lung*, vol. 186, no. 3, pp. 145–150, 2008.

[48] Q. Wang, Q. Wu, J. Feng, and X. Sun, "Obstructive sleep apnea and endothelial progenitor cells," *Patient Preference and Adherence*, vol. 7, pp. 1077–1090, 2013.

[49] E. S. Arnardottir, M. Mackiewicz, T. Gislason, K. L. Teff, and A. I. Pack, "Molecular signatures of obstructive sleep apnea in adults: a review and perspective," *Sleep*, vol. 32, no. 4, pp. 447–470, 2009.

[50] M. M. Safford, T. M. Brown, P. M. Muntner et al., "Association of race and sex with risk of incident acute coronary heart disease events," *Journal of the American Medical Association*, vol. 308, no. 17, pp. 1768–1774, 2012.

Hindawi
Oxidative Medicine and Cellular Longevity
Volume 2021, Article ID 9970627, 17 pages
https://doi.org/10.1155/2021/9970627

Research Article

Biomarkers of Inflammation and Redox Imbalance in Umbilical Cord in Pregnancies with and without Preeclampsia and Consequent Perinatal Outcomes

Marilene Brandão Tenório Fragoso,[1] **Raphaela Costa Ferreira**,[2] **Micaely Cristina dos Santos Tenório**,[1] **Fabiana Andréa Moura**,[3] **Orlando Roberto Pimentel de Araújo**,[4] **Nassib Bezerra Bueno**,[3] **Marília Oliveira Fonseca Goulart**,[1,2,4] **and Alane Cabral Menezes de Oliveira**[3]

[1]*Instituto de Química e Biotecnologia (IQB/UFAL), Rede Nordeste de Biotecnologia (RENORBIO), Universidade Federal de Alagoas, Campus A. C. Simões, BR 104 Norte, Km. 96.7, Tabuleiro dos Martins, CEP 57.072-970 Maceió, Alagoas, Brazil*
[2]*Programa de Pós-graduação em Ciências da Saúde, ICBS, Universidade Federal de Alagoas, Campus A. C. Simões, BR 104 Norte, Km. 96.7, Tabuleiro dos Martins, CEP 57.072-970 Maceió, Alagoas, Brazil*
[3]*Faculdade de Nutrição, Universidade Federal de Alagoas, Campus A. C. Simões, BR 104 Norte, Km. 96.7, Tabuleiro dos Martins, CEP 57.072-970 Maceió, Alagoas, Brazil*
[4]*Instituto de Química e Biotecnologia (IQB/UFAL), Programa de Pós-graduação Em Química e Biotecnologia, Universidade Federal de Alagoas, Campus A. C. Simões, BR 104 Norte, Km. 96.7, Tabuleiro dos Martins, CEP 57.072-970 Maceió, Alagoas, Brazil*

Correspondence should be addressed to Marília Oliveira Fonseca Goulart; mariliaofg@gmail.com and Alane Cabral Menezes de Oliveira; alanecabral@gmail.com

Received 6 March 2021; Revised 16 July 2021; Accepted 11 October 2021; Published 9 November 2021

Academic Editor: Valentina Pallottini

Objective. To compare redox imbalance and inflammation biomarkers in umbilical cords from pregnancies with and without preeclampsia (PE) and to analyse their relationships with perinatal outcomes. *Methods*. A controlled cross-sectional study was conducted in Maceió, Alagoas, Brazil, that involved pregnant women with PE and a group of women without the disease, through the application of a standardized questionnaire. After delivery, umbilical cord samples were collected to measure antioxidant defense, products from oxidative damage, and inflammation biomarkers such as myeloperoxidase (MPO), interleukin- (IL-) 6, IL-8, IL-10, and tumor necrosis factor-alpha (TNF-α). Statistical analyses were performed using Stata version 13.0 software and IBM Statistical Package for the Social Sciences (SPSS) 20.0, adopting a 95% confidence level ($\alpha = 0.05$), with the chi-square test, the Wilcoxon–Mann–Whitney test, and the multinomial and Poisson regression tests. *Results*. One hundred PE pregnant women and 50 women without the disease were studied. The umbilical cords from PE pregnancies showed higher levels of reduced glutathione (GSH) ($p \leq 0.001$), glutathione peroxidase (GPx) ($p = 0.016$), and malondialdehyde (MDA) ($p = 0.028$) and lower levels of IL-6 ($p = 0.030$) and TNF-α ($p \leq 0.001$) than the other group, with some associations among these biomarkers with perinatal outcomes. *Conclusion*. The higher levels of GSH and GPx, in addition to the lower levels of IL-6 and TNF-α, found in the PE umbilical cord, may result from adaptive mechanisms to maintain the oxidative and inflammatory balance; however, despite these changes, the damage to the cell membranes was not minimized, as the MDA level was higher in women with PE than in women without the disease. This implies that a redox imbalance is present, confirming that other physiological and adaptive mechanisms are being activated to preserve foetal health. Therefore, the present work unveils an important role of the umbilical cord in controlling redox imbalance and inflammation in PE pregnancies. Our results reinforce the necessity for continuous research on GSH as a protective compound for the perinatal outcome, especially in PE women.

1. Introduction

The umbilical cord is a vital structure for foetal development, as it provides the only connection with the placenta. The outer part presents a layer of amniotic epithelium that surrounds a core of mucoid connective tissue, namely, Wharton's jelly (WJ), capable of filling the entire tissue space. WJ does not contain other blood or lymph vessels and is not innervated. As a connective tissue, WJ is suited for producing only mesenchymal cells, which comprise the functional myofibroblasts of the tissue and their precursors. WJ surrounds three vessels, two arteries responsible for transporting nutrients and oxygenated blood to the foetus, and a vein, which conducts deoxygenated blood and waste products back to the placenta. The umbilical vessels are comprised of an intimate tunic and a medium tunic, different from other vessels, which also have an adventitious tunic [1–4].

Scientists have demonstrated that structural and functional changes in the umbilical cord may be associated with pathological conditions. For example, diseases such as gestational diabetes mellitus and preeclampsia (PE), which lead to adverse perinatal outcomes such as intrauterine growth restriction (IUGR) and foetal death, are influenced by the cord length and width, WJ area, type of cord insertion, cord knot, morphometry, and the flow parameters of the umbilical vessels [5–7].

The aetiology of PE is not fully understood, but it is known that a deficient placentation process occurs at the beginning of pregnancy, resulting in inadequate remodeling of the uterine spiral arteries, which compromises the supply of oxygenated blood to the foetoplacental unit. As a consequence, hypoxia/reperfusion occurs in the organ, which leads to high production of reactive oxygen species (ROS), leading to oxidative stress in addition to inflammation and endothelial dysfunction. Such changes culminate in the occurrence of adverse perinatal outcomes, such as IUGR, premature birth, newborns small for gestational age, and other complications, including maternal and foetal deaths [8–12]. It is also important to highlight that redox homeostasis depends on a number of factors, including gender, age, disease, and pregnancy, emphasizing, therefore, that PE is a factor able to interfere in this redox homeostasis [9, 13].

PE is currently considered a public health problem that is associated with high maternal and perinatal morbidity and mortality. Changes occur in the extracellular matrix that lead to increased vascular resistance in the foetoplacental circulation. As a result, changes in umbilical cord morphology and composition occur in PE by reducing the area of the umbilical vein and WJ, with narrower cords evident in early-onset PE [4, 14, 15].

In addition, there is an increase in collagen deposition, a reduction in elastin, a thickening of the vessel walls, and the migration of smooth muscle cells. In the PE umbilical cord artery, a decrease in the levels of collagen-degrading enzymes, such as the matrix metalloproteinases, favours changes in the collagen-elastin relationship. Additionally, there is an increase in the proteoglycan amount associated with the reduction of hyaluronic acid, causing WJ to lose its ability to retain water and resist compression. Therefore, the observed changes in the umbilical cord of pregnant women with PE lead to premature deterioration of these tissues, which can result in or contribute to the haemodynamic changes characteristic of PE, as well as favour ROS passage to the foetus through the umbilical cord [4, 16–18].

Despite not being a frequent target of research related to PE, the umbilical cord constitutes a primary vascular structure, responsible for carrying oxygenated blood and nutrients to the foetoplacental unit, as well as foetal metabolites for excretion. As such, changes in its shape and function reflect complications affecting maternal-foetal health [19]. To date, no articles have been published concerning the role of the umbilical cord in maintaining redox and inflammatory balance in women with PE and its consequences on foetal outcomes, which gives a strong support to the present work. It is necessary to obtain data about the pathophysiology of the disease, the role of oxidative stress and inflammation in the umbilical cord, and possible changes in its function, as a way to further understand its role, aiming at minimizing the damage to foetal health from PE. Therefore, this study is aimed at evaluating the markers of redox imbalance and inflammation in umbilical cords of pregnancies with PE, to compare them with those without the disease and analyse their relationship with perinatal outcomes.

2. Materials and Methods

2.1. Experimental: Reagents and Equipment. A superoxide dismutase (SOD) assay kit-WST® was purchased from Sigma-Aldrich. Cytokine kits were obtained from PeproTech® (PeproTech Brasil FUNPEC, Ribeirão Preto, SP, BR), protease inhibitor cocktail tablets were obtained from Roche® (Germany), and radioimmunoprecipitation assay (RIPA) buffer was obtained from Cell Signaling Technology®. All other chemicals and enzymes were purchased from Sigma-Aldrich® (St. Louis, USA).

The high-performance liquid chromatography system (HPLC) (LC-20 AT-Prominence, Shimadzu) coupled to a UV detector (Shimadzu, Serial no. L201550) was used. A biofreezer from the VIP Series by Sanyo was used. The spectrofluorometer was manufactured by Thermo Fisher Scientific® (Multiskan), who also supplied a Filizola® digital balance, with a capacity of 150 kg and 100 g accuracy and a stadiometer with a 2 m length and 0.1 cm precision.

2.2. Study Design and Ethical Aspects. This was a controlled cross-sectional study carried out in 2017 in the city of Maceió, AL, Brazil. The present work is part of a larger research project financed by the Research Program for the Unified Health System, with approval by the Ethics Committee in Research of the Federal University of Alagoas (process no. 35743614.1.0000.5013). It is important to mention that an article has already been published containing the data referring to the placenta analysis by our research group [12] and that this study used the same PE women, women without the disease, and their newborns [12]. Their umbilical cords are herein analysed for the first time.

With regard to the proportion of the sample size between PE and women without the disease groups, according to Tenny et al. [20] and Munnangi and Boktor [21], there is no standard concerning the number of cases and the comparative group, and this proportion can reach up to 4 : 1. However, groups need to have similar characteristics, such as sex and age, differing only in the disease presence or absence. Therefore, the 1 : 1 ratio is optional, and the 2 : 1 ratio used was considered to be adequate.

2.3. Inclusion and Exclusion Criteria. The study group included pregnant women diagnosed with PE, and their identification was carried out through medical records following the criteria of the American College of Gynecology and Obstetrics (ACOG) [22] and adjusted posteriorly according to Brown et al. [23]. Women with HELLP (hemolysis, elevated liver transaminases, and thrombocytopenia) syndrome [24], eclampsia, severe general conditions, smokers, twin pregnancies, or other conditions capable of influencing pregnancy outcomes, such as preexisting or gestational diabetes mellitus, cardiovascular and autoimmune diseases, and infections, were not included in this study. Additionally, healthy pregnant women were included as a comparative group. They were recruited in the same maternity of the PE cases. The presence of gestational or pregestational diseases and smoking habits were the exclusion criteria for the women without the disease group. The majority of them were already close to childbirth. Thus, they were invited to participate in the study, answered the questionnaire, and were monitored until the moment of delivery, where the umbilical cord samples were collected.

2.4. Data Collection and Classification. The selection of participants took place by an analysis of their medical records to identify pregnant women diagnosed with PE, according to the inclusion criteria previously defined. Then, properly trained researchers approached these women and invited them to participate in the study. After accepting and signing the informed consent form, a standardized questionnaire was used to gather socioeconomic (maternal age, education, and family income) and obstetric (gestational age, presence of complications in the current pregnancy, and information on previous pregnancies) information, in addition to information about the current maternal nutritional status (height, current weight, and calculation of the body mass index (BMI)).

Regarding the socioeconomic data collected, women were classified according to age (≤19 years: adolescents; 20 to 34 years: average age; and ≥35 years: advanced age) [25], level of education (<4 years; ≥4 years of study) [26], monthly family income (<1 minimum wage; ≥1 minimum wage), self-declaration of black race (yes or no), and occupation (at home or work outside the home).

The assessment of maternal nutritional status was carried out using height and current weight, measured with the aid of a digital scale with a stadiometer to calculate BMI, and classified according to Atalah Samur et al. [27].

After delivery, information on the newborns was also obtained from the medical records and the declaration of live births, such as weight and length at birth, gestational age at delivery, type of delivery, the Apgar score in the 1st and 5th minutes of life, sex, head circumference (HC), and chest circumference (CC).

The characterization of the newborns was made based on the weight and length at birth and classified following the method of Villar et al. [28] in percentiles, with those below the 10th percentile considered small for gestational age (SGA), those between the 10th and 90th percentiles considered suitable for gestational age (SUGA), and those above the 90th percentile considered large for gestational age (LGA). The classification of the length at birth followed the same pattern as the weight. Additionally, birth weight was also classified according to the criteria proposed by the World Health Organization (WHO) [29], such as low birth weight (LBW) (<2,500 kg), adequate birth weight (≥2,500 kg-<4,000 kg), and macrosomia (≥4,000 kg). To obtain information on the newborn's nutritional status, the CC/HC ratio was calculated and was considered adequate when the value was equal to 1 [30]. In addition, the Apgar score in the 1st and 5th min of life, when the score is higher than 7, is indicative of the child's vitality at birth [31].

2.5. Umbilical Cord Samples. The samples were obtained from the central region of the umbilical cord immediately after delivery or, at most, within 20 min, to perform analyses to quantify the biomarkers of redox imbalance and inflammation. After carrying out the appropriate washing procedures, the tissues were stored in a biofreezer at -80°C.

2.6. Umbilical Cord Extract Preparation. Extracts of the umbilical cords were prepared using approximately 100 mg of the tissue. Liquid nitrogen was used to promote tissue disintegration, which facilitates maceration. After this step, the product obtained was transferred to microtubes, and RIPA buffer was added in a volume equal to nine times the weight of the tissue. RIPA buffer (radioimmunoprecipitation assay) contains 50 mM Trizma base, 150 mM NaCl (sodium chloride), and 1 mM ethylenediamine tetraacetic acid (EDTA), as well as the detergents Triton X-100 1%, deoxycholate 1%, and sodium dodecyl sulfate (SDS) 0.1%, with protease inhibitors at pH 7.4 (protease inhibitor cocktail tablets were purchased from Sigma-Aldrich). Subsequently, the homogenates were centrifuged at 12,000 rpm for 12 min at 4°C, and the supernatant was collected as the umbilical cord extracts, which were stored in appropriate volumes for subsequent analyses, in a biofreezer at -80°C. This procedure was used for most analyses, except for MDA, MPO, and GPx (Figure 1).

2.7. Protein Quantification. After preparing the extracts, the proteins from the umbilical cord were quantified according to Bradford [32], aiming at normalizing the results of the subsequent analyses by the protein content. For this, 20 μL of the sample, using bovine serum albumin ((BSA) 1 to 5 mg dL^{-1}) as the standard, was pipetted into a microplate in duplicate, followed by the addition of 200 μL of the Bradford reagent. After 5 min in the dark, the reading was performed on a spectrophotometer at 595 nm.

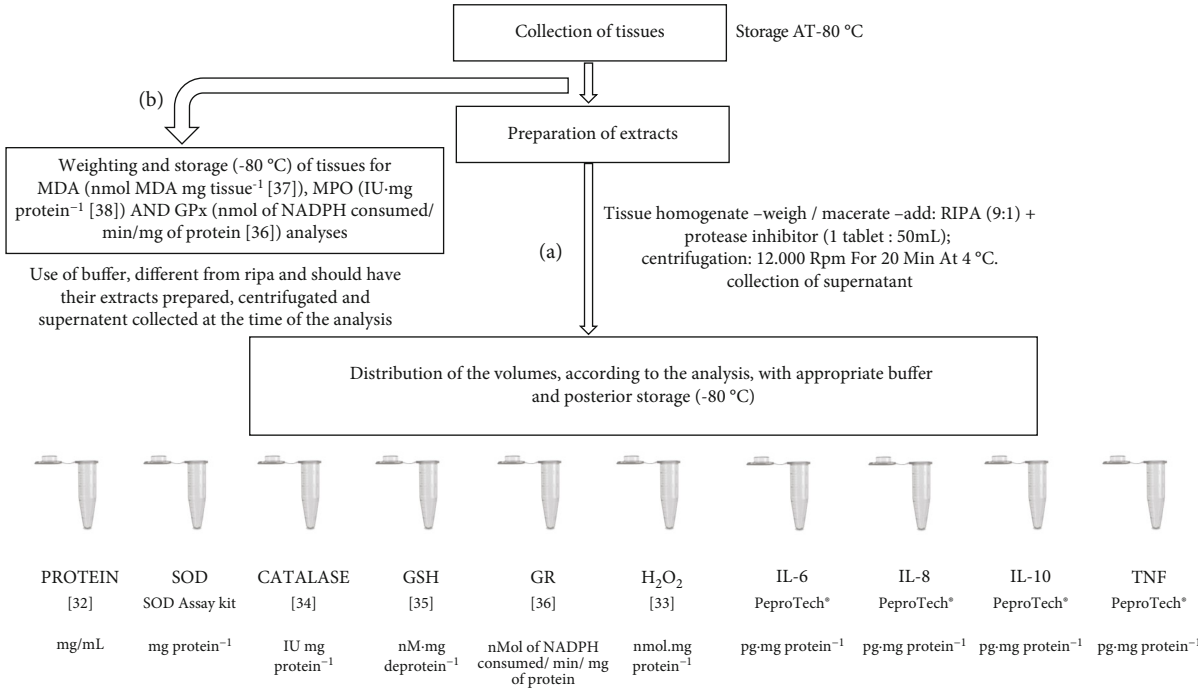

Figure 1: Flowchart representing the steps of collection, preparation and analyses of umbilical cords. Legend: CAT—catalase; GPx—glutathione peroxidase; GR—glutathione reductase; GSH—reduced glutathione; H_2O_2—hydrogen peroxide; IL—interleukin; MDA—malondialdehyde; MPO—myeloperoxidase; SOD—superoxide dismutase; TNF—tumor necrosis factor.

2.8. Redox Imbalance Biomarkers. SOD was analysed using the SOD Sigma Kit-WST®, following the manufacturer's instructions, with the spectrophotometer reading performed at 450 nm and the activity expressed in mg protein^{-1}. Hydrogen peroxide (H_2O_2) was analysed according to the method of Pick and Keisari [33], which is based on the ability of H_2O_2 to oxidize phenol red, a reaction mediated by radish peroxidase, and the concentration was expressed in nmol mg of protein^{-1}. Buffer (phosphate buffer, dextrose, and NaCl, in a proportion of 1 : 25, at pH 7.0) was added to the umbilical cord extracts just before the analyses. Then, 5 μL of phenol red and 4.25 μL of radish peroxidase were added and incubated for 30 min at 37°C. Finally, the samples were transferred to microplates. Then, 25 μL of NaOH was added, and the spectrophotometer reading at 610 nm was obtained. All assays were performed in duplicate.

Catalase (CAT) was evaluated according to Paton et al. [34], as previously described by Aebi [35]. The method consists of monitoring the decomposition rate of H_2O_2 in a spectrophotometer at 240 nm, with readings taken every 15 seconds for 5 min, with the results expressed in U of CAT mg of protein^{-1}. A CAT unit is defined as the amount of enzyme needed to decompose, at 37°C, 1 μmol min^{-1} of H_2O_2. Reduced glutathione (GSH), adapted from Tipple and Rogers [36], uses assay buffer (PBS 0.1 M + 5 mM EDTA, at pH 7.4 and 5% metaphosphoric acid), and the reading is carried out in a spectrophotometer at 412 nm, in 3 min kinetics, with readings every 30 seconds and the results expressed in nM mg of-protein^{-1}.

Glutathione reductase (GR) and glutathione peroxidase (GPx) were analysed according to a protocol adapted from Flohé and Gunzler [37], with GR activity being directly measured by nicotinamide dinucleotide phosphate (NADPH) as a cofactor in the reduction of GSSG (oxidized glutathione) to GSH. For this analysis, umbilical cord extracts and a freshly prepared reaction medium (0.1 M phosphate buffer (pH 7.0) and 1.0 mM EDTA, GSSG, and NADPH) were used. The analyses were performed in duplicate, and the decrease in absorbance at 340 nm was monitored for 10 min, kinetically, with 10 readings taken every 15 seconds. The results are expressed in nmol of NADPH consumed/min/mg of protein.

For the analysis of GPx, considering its ability to convert H_2O_2 into H_2O and O_2, *tert*-butyl hydroperoxide (*t*-BuOOH) was used once its dismutation was performed by GPx, generating 2 GSH molecules through the action of GR based on the oxidation of NADPH. Therefore, this assay assesses the consumption of NADPH. The sample preparation was different from that previously described. In summary, approximately 50 mg of the tissue in assay buffer (0.1 M phosphate buffer with 5 mM EDTA, at pH 7.4) was used. The homogenate was centrifuged at 12,000 rpm for 20 min at 4°C, and the supernatant was collected. GR, GSH, *t*-BuOOH, and NADPH were added at the time of analysis. The experiment was performed in a microplate in duplicate, with incubation at 37°C for 10 min, with subsequent spectrometric monitoring of the absorbance decay at 340 nm per min for 5 min, and the result is expressed in nmol of NADPH consumed/min/mg of protein.

Malondialdehyde (MDA) was evaluated by HPLC, measuring the peak height, following the technique of Vickie et al. [38]. The conditions of the HPLC system were a C18

column, a 259 mm length, and a 4.6 mm internal diameter, with a mobile phase of acetonitrile and Trizma buffer (pH 7.4, in a proportion of 1 : 9). The umbilical cord tissue was homogenized in Trizma, *tert*-butyl-hydroxytoluene (BHT), and acetonitrile buffer. Afterward, these homogenates were centrifuged at 3500 rpm for 10 min at 4°C, and the supernatant was later filtered through a specific HPLC filter (0.22 μm). The flow rate was 1.0 mL min^{-1}, and the MDA level was calculated using a standard curve, which was generated using 1,1,3,3-tetramethoxypropane (TMP), which is a precursor to MDA, and subsequently corrected for the weight of the tissue analysed (in mg), as shown in the following:

$$\text{Tissue MDA} = \text{MDA found} \times \frac{1000}{\text{tissue weight (mg)}}. \quad (1)$$

The results are expressed in nmol MDA mg tissue^{-1}. The retention time was approximately 2 min and 48 seconds, and the UV detector was adjusted to 270 nm.

2.9. Inflammatory Biomarkers. The inflammatory biomarkers interleukin- (IL-) 6, IL-8, IL-10, and tumor necrosis factor-alpha (TNF-α), with duplicate analyses, were evaluated by means of an enzyme-linked immunosorbent assay (ELISA) with a PeproTech® kit (PeproTech Brasil FUNPEC, Ribeirão Preto, SP, BR), following the manufacturer's instructions, with cytokine levels expressed in pg mg protein^{-1}.

Myeloperoxidase (MPO) activity was measured via adaptation of the method proposed by Bradley et al. [39]. For the analysis, approximately 25 mg of tissue in assay buffer (50 mM potassium phosphate buffer, 0.5% hexadecyltrimethylammonium bromide, and 5 mM EDTA (pH 6.0)) was used. This homogenate was centrifuged at 4,000 rpm for 15 min at 4°C. Then, the supernatant was removed and centrifuged again at 12,000 rpm for 15 min, at 4°C. Afterward, in duplicate, 50 μL of the supernatant was transferred to a microplate, and 50 μL of *ortho*-dianisidine solution (0.68 mg/mL) was added. The incubation was carried out at 37°C for 15 min, and then 50 μL of H_2O_2 solution (0.3%) was added. After incubation at the same temperature for 10 min, a spectrophotometer reading was performed at 460 nm. It should be noted that an MPO unit is defined as the amount of H_2O_2 decomposed per min. The results are expressed in U of MPO mg protein$^{-1.}$

2.10. Statistical Analyses. Statistical analyses were performed using Stata version 13.0 software and IBM Statistical Package for the Social Sciences (SPSS) software 20.0 (SPSS Inc., USA), adopting $\alpha = 0.05$. To compare the socioeconomic, obstetric, and nutritional status characteristics of the studied groups, a chi-square test was performed. To evaluate normality, the Lilliefors test was used. Then, a visual graphical analysis was performed with a QQ plot, and it was decided to use nonparametric investigations due to violations of normality. After this, Wilcoxon–Mann–Whitney tests were performed. Finally, the results of the biomarkers evaluated in this study were related to the perinatal variables (birth weight, gestational age, the Apgar scores in the 1st and 5th min, HC, CC/HC, length at birth, and birth complications) through the multinomial and Poisson regression, adjusting for maternal age, origin, education, family income, gestational BMI, black race, primigravida, mode of delivery, and gestational age. In addition, in order to investigate if there were significant interactions between the different redox/inflammatory markers and PE for each of the outcomes, the interaction term biomarkers ∗ PE was also included in each outcome regression model, considering $p < 0.05$ as significant.

3. Results

3.1. Sample Size. In this study, 100 pregnant women with PE (PE group) and 50 pregnant women without the disease were included. As this study is part of a larger study, the achieved sample power was calculated with the G Power program, considering a determination coefficient (R^2) of 0.027 and a sample of 100, with an alpha of 5%, which results in an achieved power of 50.3% in the present study.

3.2. PE and without PE Group Characterization. The mean age of the PE group was 25.5 ± 7.04 years; for the group of women without the disease, it was 24.2 ± 6.53 years ($p = 0.259$). Table 1 summarizes the socioeconomic, obstetric, and nutritional status data of the pregnant women with PE and women without the disease. It is possible to observe that in the PE group, 26% were teenagers, and 13% were older; 8.3% declared themselves to be black; concerning education, 3% had <4 years of study; 24.2% stated that they lived monthly on less than 1 minimum wage per family; in terms of nutritional status, 26.9% and 32.2% were overweight and obese, respectively, and half of them were in their first pregnancy. About folic acid supplementation, 7.8% started before pregnancy and 63.3% started in the first trimester; ferrous supplementation was received by 84.8%. There were no statistically significant differences in these variables between the PE and without PE groups.

Besides, in the PE group, magnesium sulfate supplementation, as an eclampsia-preventive medicine, was used in only 5% of the cases; 78% did not receive this supplementation. About medications, 49% of them used standard hospital medication to control the disease, especially antihypertensive drugs, such as methyldopa and hydralazine.

3.3. Newborn Characterization. Regarding the newborn characterization data from PE pregnancies, 52.5% were female, the predominant mode of delivery was cesarean delivery (70.4%), 22.4% of the neonates were premature, 75.3% had an adequate length at birth, and 8.6% and 1.1% had low vitality on the Apgar score in the 1st and 5th min, respectively. Regarding birth weight, 11.5% were classified as SGA and 13.5% as LGA, and the CC/HC ratio was inadequate in 73% of cases (Table 2).

It is important to mention that Tables 1 and 2 are reproduced from a previously published part of the overall study and are repeated here for the reader's convenience. Permission to duplicate them was obtained.

Table 1: Socioeconomic, obstetric, and nutritional status characteristics of preeclampsia pregnant women and women without preeclampsia in Maceió, Alagoas, Brazil, in 2017.

	Preeclampsia		Without preeclampsia		OR	CI 95%
	n	%	*n*	%		
	100	66.7	50	33.3		
Age (years)						
≤19	26	26.0	16	32.0	0.747	0.355-1.570
20-35	61	61.0	31	62.0	1.084	0.542-2.168
≥35	13	13.0	3	6.0	2.341	0.635-8.629
Self-declaration of black race						
Yes	8	8.3	7	14.0	0.534	0.182-1.568
No	88	91.7	43	86.0		
No information	4		0			
Education (years)						
<4	3	3.0	2	4.0	0.742	0.120-4.529
≥4	97	97.0	48	96.0		
Monthly family income (minimum wage)						
<1	23	24.2	12	26.7	0.878	0.391-1.976
≥1	72	75.8	33	73.3		
No information	5		5			
Primiparous						
Yes	50	50.0	21	42.0	1.381	0.696-2.739
No	50	50.0	29	58.0		
Previous PE						
Yes	23	23.0	1	2.7	10.753	1.397-82.769
No	77	77.0	36	97.3		
Gestational BMI						
Low weight	6	6.5	8	17.4	0.345	0.112-1.060
Eutrophy	32	34.4	17	37.0	0.957	0.461-1.985
Overweight	25	26.9	12	26.1	1.103	0.497-2.450
Obesity	30	32.2	9	19.5	2.063	0.886-5.989
No information	7		4			
Folic acid supplementation before pregnancy						
Yes	7	7.8	4	8.9	0.86	0.23-3.12
No	83	92.2	41	91.1		
No information	10		5			
Folic acid supplementation in the first trimester						
Yes	57	63.3	31	70.5	0.72	0.33-1.57
No	33	36.7	13	29.5		
No information	10		6			
Ferrous sulfate supplementation						
Yes	78	84.8	40	85.1	0.97	0.36-2.60
No	14	15.2	7	14.9		
No information	8		3			

Legend: BMI—body mass index; PE—preeclampsia; CI—confidence interval; OR—odds ratio. Chi-square test, $p < 0.05$. Source: data on preeclampsia was reported by Ferreira et al. [12], with permission.

3.4. Redox Imbalance and Inflammation Biomarker Levels. Figures 2 and 3 show the whiskers charts of redox imbalance and inflammation biomarkers, respectively, between PE and the without PE pregnancies. The umbilical cords of the PE group showed higher levels of GSH ($p \leq 0.001$), GPx ($p = 0.016$), and MDA ($p = 0.028$), and lower levels of IL-6

Table 2: Characteristics of newborns from pregnancies with preeclampsia in Maceió, Alagoas, Brazil, in 2017.

Variables	PE $n = 100$	
	n	%
Sex		
Men	52	52.5
Women	47	47.5
No information	1	
Mode of delivery		
Cesarean	69	70.4
Normal	29	29.6
No information	2	
Gestational age at birth		
Preterm	22	22.4
Term	76	77.6
Postterm	0	0.0
No information	2	
Birth weight		
SGA	11	11.5
SUGA	72	75.0
LGA	13	13.5
No information	4	
Length at birth		
Low	8	9.0
Adequate	67	75.3
High	14	15.7
No information	11	
Apgar 1st minute		
≤6	8	8.6
≥7	85	91.4
No information	7	
Apgar 5th minute		
≤6	1	1.1
≥7	92	98.9
No information	7	
CC/HC ratio		
Adequate	24	27.0
Inadequate	65	73.0
No information	11	

Legend: CC—chest circumference; HC—head circumference; LGA—large for gestational age; PE—preeclampsia; SGA—small for gestational age; SUGA—suitable for gestational age. Source: data reported in Ferreira et al. [12], with permission.

($p = 0.019$), and TNF-α ($p \leq 0.001$), than those of the women without PE group. The other results showed no statistically significant differences.

3.5. Association between Redox Imbalance and Inflammation Biomarkers and Perinatal Variables. Tables 3–6 show the results of the associations between the biomarkers of redox imbalance and inflammation in the umbilical cord of PE and without PE pregnancies, and the perinatal variables (birth weight, gestational age, the Apgar scores in the 1st and 5th min, HC, CC/HC, length at birth, and birth complications), with significant associations identified.

In the PE group, the associations identified by perinatal variables were LBW with TNF-α and MDA; LGA with TNF-α; preterm with TNF-α and MDA; a low Apgar score in the 5th min with TNF-α, SOD, H_2O_2, CAT, GR, GPx, IL-8, and MPO; CC/HC with TNF-α, SOD, H_2O_2, and GR; a low Apgar score in the 1st min with MDA; macrosomia with SOD; low HC with GR and MPO; and birth complications with GSH.

In turn, the group of women without PE shows the following associations: preterm with SOD, CAT, GR, GPx, IL-6, IL-10, and MPO; a low Apgar score in the 1st min with SOD, GR, IL-10, and MDA; low HC with SOD, CAT, GR, GPx, IL-6, IL-10, and MPO; short length with SOD, CAT, GR, GPx, IL-6, IL-8, IL-10, MPO, MDA, GSH, and H_2O_2; birth complications with SOD, GR, GPx, IL-8, MPO, MDA, and GSH; a low Apgar score in the 5th min with CAT, GR, GPx, IL-6, IL-10, and MDA; and CC/HC with CAT and MPO.

Interaction analysis was also performed between the redox imbalance/inflammatory biomarkers and PE (Tables 3–6) for each of the investigated outcomes, where a significant interaction was only seen between the MDA biomarker and LGA newborns ($p = 0.022$) (Table 3, column 11); however, MDA showed a nonsignificant role in the PE group (PR: 0.21; CI: 0.04-1.07) and in the group without PE (PR: 1.02; CI: 0.81-1.27).

4. Discussion

Few studies [40–42] in the literature have evaluated biomarkers of oxidative stress and inflammation in the umbilical cord tissues from pregnancies with PE. To our knowledge, the present work is the only one that evaluated a wide variety of such markers, including antioxidants of an enzymatic and nonenzymatic nature and markers of oxidative damage, and analysed their relationship with perinatal outcomes. Higher levels of the antioxidants GSH and GPx and the oxidative tissue damage marker MDA, as well as lower levels of IL-6 and TNF-α, were observed in the umbilical cords of PE pregnancies.

It is understood that in PE, there is an imbalance between the enzymatic and low-molecular weight antioxidants (superoxide dismutase (SOD), GPx, catalase; biothiols, and others) and prooxidants (with exacerbation of these), based on the inadequacy of the remodeling of the spiral arteries [9, 43]. Given this scenario, placental hypoxia resulting from impaired trophoblastic invasion raises the Th1 immune response characterized by the production of gamma interferon (IFN-γ), TNF-α, and IL-2, when compared to Th2 activity, which is characterized by the production of IL-4, IL-5, IL-6, IL-10, and IL-13, in addition to an increase in the Th17 profile, which secretes the proinflammatory cytokine IL-17 and stimulates the migration of other cytokines that act in cellular communication, and oxidative stress, with the production of ROS and RNS [44].

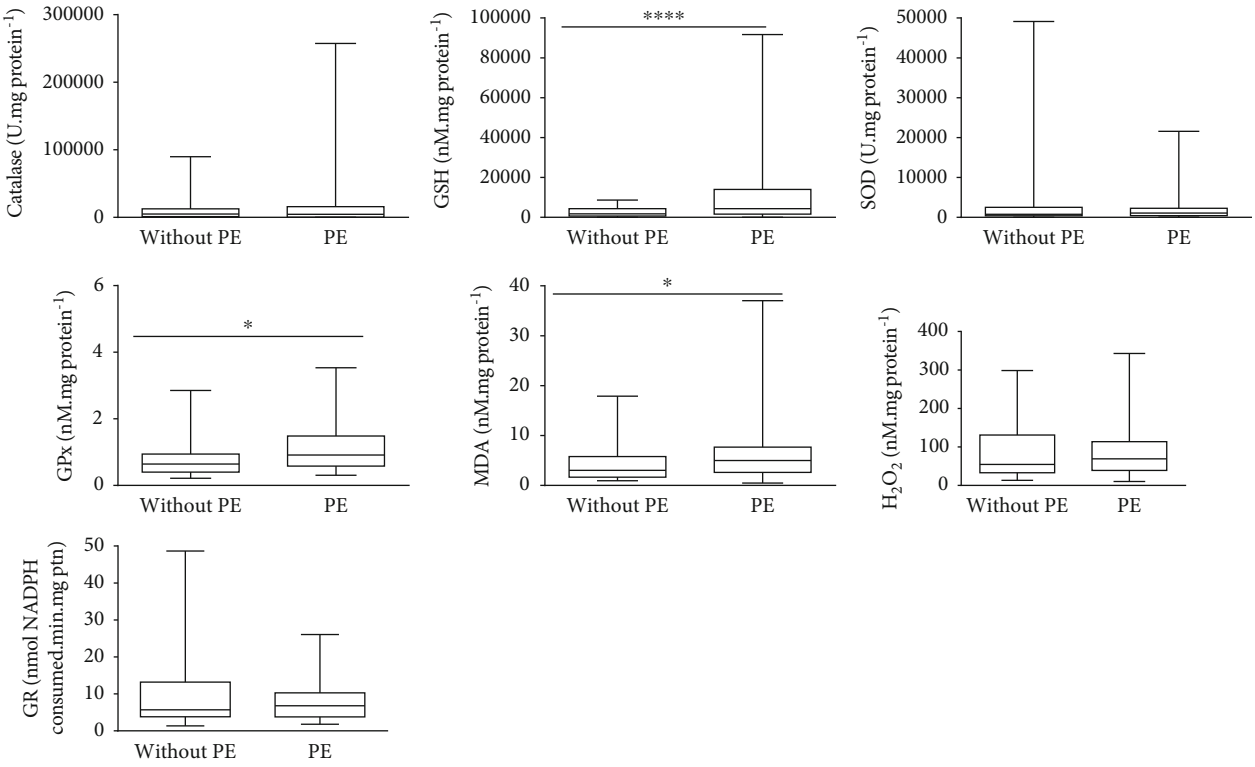

Figure 2: Whisker charts of the biomarkers of redox imbalance between pregnant women with PE and without PE. Legend: CAT—catalase; GPx—glutathione peroxidase; GR—glutathione reductase; GSH—reduced glutathione; H_2O_2—hydrogen peroxide; MDA—malondialdehyde; SOD—superoxide dismutase. Mann–Whitney test: $p < 0.05$.

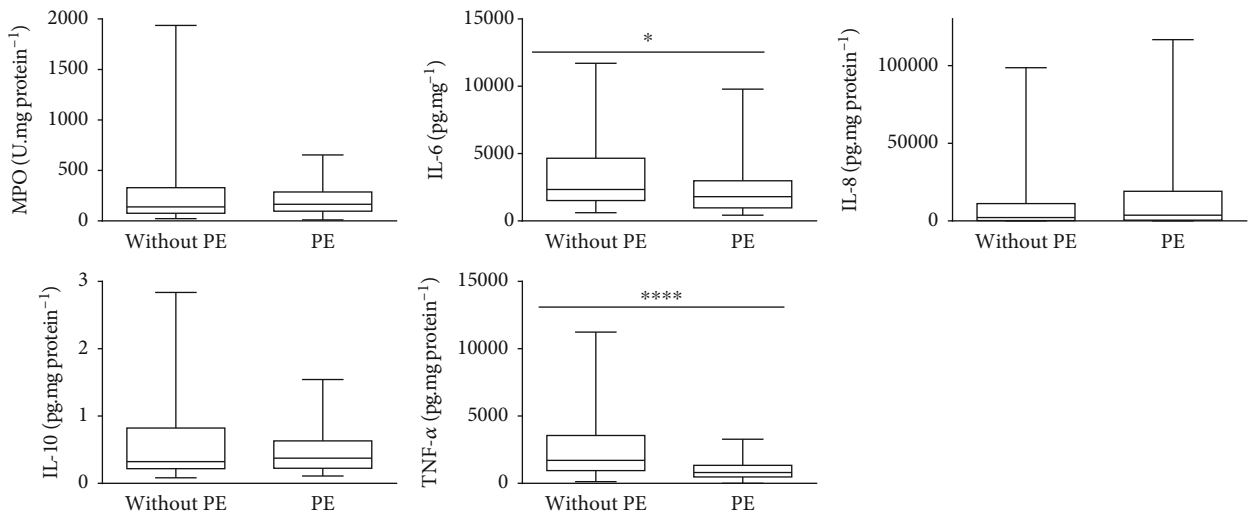

Figure 3: Whisker charts of the biomarkers of inflammation between pregnant women with PE and without PE. Legend: IL—interleukin; MPO—myeloperoxidase; TNF—tumor necrosis factor. Mann–Whitney test: $p < 0.05$.

Therefore, it is important to highlight that in PE, there is an increase in oxidative stress and inflammation in a two-way path, where the hypoxia/reperfusion process during inadequate placentation, which leads to inadequate remodeling of the uterine spiral arteries, maintaining its caliber and high resistance, is responsible for initiating the higher production of ROS and proinflammatory cytokines. It is also known that, in the inflammatory response, there is the involvement of genes related to the increase of oxidative stress, especially by the release of the nuclear factor kappa B (NF-κB), located in the cellular cytoplasm. ROS are able to oxidize the IκB kinase (IKK) complex, leading to the delivery of NF-κB, which is formed by p50 and p65 subunits, and so this factor is able to enter the cell nucleus, promoting the transcription of several proinflammatory cytokines such as IL-6 and TNF-α. This process is exacerbated in PE, but

Table 3: Association between biomarkers of redox imbalance and inflammation in umbilical cords and perinatal outcome birth weight of pregnancies with and without preeclampsia at a university hospital in Maceió, Alagoas, Brazil, in 2017.

(a)

Redox imbalance and inflammatory markers	Birth weight									
	Small for gestational age					Large for gestational age				
	PE		Without PE		*p*-for-interaction	PE		Without PE		*p*-for-interaction
	OR	CI	OR	CI		OR	CI	OR	CI	
SOD	0.99	0.99-1.00	1.00	0.01-81.32	0.483	0.99	0.99-1.00	0.99	0.99-1.00	0.216
H_2O_2	0.99	0.97-1.00	1.02	0	0.771	1.00	0.99-1.01	1.00	0.99-1.02	0.998
CAT	0.99	0.99-1.00	1.00	0.25-3.97	0.411	0.99	0.99-1.00	1.00	0.99-1.00	0.389
GSH	1.00	0.99-1.00	1.00	0.14-6.72	0.382	0.99	0.99-1.00	0.99	0.99-1.00	0.665
GR	0.99	0.85-1.14	0.95	0	0.971	1.05	0.97-1.14	1.00	0.82-1.22	0.913
GPx	3.11	0.60-16.03	8.87	0	0.241	1.33	0.49-3.59	1.03	0.21-4.92	0.897
MDA	1.13	0.91-1.42	0.79	0	0.144	0.21	0.04-1.07	1.02	0.81-1.27	**0.022**
IL-6	1.00	0.99-1.00	1.00	7.25*e*-10–1.38*e* + 09	0.469	1.00	0.99-1.00	1.00	0.99-1.00	0.679
IL-8	0.99	0.99-1.00	0.99	0.14-6.68	0.290	0.99	0.99-1.00	0.99	0.99-1.00	0.167
IL-10	0.73	0.06-8.74	10.86	0	0.987	2.27	0.54-9.53	2.44	0.17-35.19	0.833
TNF-α	0.99	0.99-1.00	1.00	5.22*e*-07–1918116	0.639	1.00	**1.00-1.00**	1.00	0.99-1.00	0.875
MPO	0.99	0.99-1.00	1.00	0.00-60179.64	0.565	1.00	0.99-1.00	0.99	0.99-1.00	0.361

(b)

Redox imbalance and inflammatory markers	Birth weight									
	Low birth weight					Macrosomia				
	PE		Without PE		*p*-for-interaction	PE		Without PE		*p*-for-interaction
	OR	CI	OR	CI		OR	CI	OR	CI	
SOD	0.99	0.99-1.00	0.99	0.99-1.00	0.954	0.99	**0.99-0.99**	—	—	0.994
H_2O_2	0.99	0.98-1.00	1.02	0.99-1.05	0.819	1.00	0.98-1.01	—	—	1.000
CAT	0.99	0.99-1.00	0.98	0	0.522	0.99	0.99-1.00	—	—	1.000
GSH	1.00	0.99-1.00	0.99	0.99-1.00	0.138	0.99	0.99-1.00	—	—	0.999
GR	0.96	0.87-1.05	9.54*e*-13	0	0.347	0.97	0.83-1.13	—	—	1.000
GPx	0.96	0.42-2.17	1.9*e*-164	0	0.306	0.22	0.02-1.87	—	—	1.000
MDA	1.23	**1.02-1.50**	0.62	0.26-1.48	0.068	0.58	0.17-1.92	—	—	0.999
IL-6	0.99	0.99-1.00	0.99	0.99-1.00	0.264	0.99	0.99-1.00	—	—	1.000
IL-8	0.99	0.99-1.00	0.98	0	0.482	0.99	0.99-1.00	—	—	0.999
IL-10	0.50	0.10-2.50	0	0	0.282	0.64	0.04-9.58	—	—	1.000
TNF-α	0.99	**0.99-0.99**	0.66	0	0.196	1.00	0.99-1.00	—	—	1.000
MPO	0.99	0.99-1.00	0.95	0.89-1.01	0.358	1.00	0.99-1.00	—	—	1.000

Legend: CAT—catalase; CI—confidence interval; GPx—glutathione peroxidase; GR—glutathione reductase; GSH—reduced glutathione; H_2O_2—hydrogen peroxide; IL—interleukin; MDA—malondialdehyde; MPO—myeloperoxidase; OR—odds ratio; SOD—superoxide dismutase; TNF—tumor necrosis factor. Multinomial regression: $p < 0.05$. Adjusted for maternal age, origin, education, family income, gestational BMI, black race, primigravida, way of delivery, and gestational age. *Note*. *p*-for-interaction: *p* value for the interaction term between the redox imbalance/inflammatory marker and PE, for each of the investigated outcomes.

occurs naturally during gestation. Furthermore, in PE, there is an overactivation of NF-κB, contributing to induce the expression of proinflammatory and antiangiogenic proteins, further elevating oxidative stress, inflammation, and vascular dysfunction [9, 45, 46].

Besides, during the trophoblastic invasion, the decidua contains a lot of necessary immune system cells to promote this process, such as macrophages, natural killer (NK) cells, T cells, and regulatory T cells (Treg). In PE, a higher secretion of proinflammatory cytokines and a decrease of Treg cells occur as a result of an immunological imbalance, leading to the activation of a chronic inflammatory response in the immune system [9, 47, 48].

Among the components of the nonenzymatic oxidative defense system, GSH has a prominent role. It is the major intracellular antioxidant compound, found in abundance in the cytosol, nucleus, and mitochondria, able to perform biotransformation and elimination of xenobiotics and in

Table 4: Association between biomarkers of redox imbalance and inflammation in umbilical cords and perinatal outcomes such as preterm birth and the low Apgar scores in the 1st min and 5th min of pregnancies with and without preeclampsia at a university hospital in Maceió, Alagoas, Brazil, in 2017.

Redox imbalance and inflammatory markers	Outcomes														
	Preterm birth					Low Apgar score 1st (min)					Low Apgar score 5th (min)				
	PE		Without PE		*p*-for-interaction	PE		Without PE		*p*-for-interaction	PE		Without PE		*p*-for-interaction
	PR	CI	PR	CI		PR	CI	PR	CI		PR	CI	PR	CI	
SOD	0.99	0.99-1.00	**0.99**	**0.99-0.00**	0.756	**0.99**	0.99-1.00	**1.00**	**1.00-1.00**	0.675	**1.00**	**1.00-1.00**	**0.99**	0.99-1.00	—
H_2O_2	**1.00**	0.99-1.00	**1.00**	0.99-.00	0.363	**1.00**	0.99-1.00	**0.99**	0.97-1.01	0.352	**0.97**	**0.95-0.98**	**0.98**	0.95-1.00	—
CAT	**0.99**	0.99-1.00	**0.99**	**0.99-0.99**	0.203	**0.99**	0.99-1.00	**1.00**	0.99-1.00	0.842	**1.00**	**1.00-1.00**	**0.99**	**0.99-0.99**	—
GSH	1.00	0.99-1.00	0.99	0.99-1.00	0.393	**0.99**	0.99-1.00	**0.99**	0.99-1.00	0.416	—	—	**0.99**	0.99-1.00	—
GR	**1.00**	0.95-1.05	**0.88**	**0.81-0.97**	0.414	**1.02**	0.95-1.10	**0.14**	**0.11-0.19**	0.236	**0.76**	**0.76-0.76**	**0.34**	**0.11-0.19**	—
GPx	**1.19**	0.77-1.82	**0.36**	**0.17-0.75**	0.582	**1.09**	0.39-3.05	**0.00**	**0.00-0.00**	0.221	**0.25**	**0.07-0.79**	**0.00**	**0.00-0.00**	—
MDA	**1.15**	**1.07-1.23**	**0.91**	0.81-1.03	0.181	**0.81**	0.68-0.96	**0.56**	**0.52-0.62**	0.451	**0.80**	**0.61-1.05**	**0.43**	**0.43-0.43**	—
IL-6	0.99	0.99-1.00	**0.99**	**0.99-0.99**	0.124	1.00	0.99-1.00	0.99	0.99-1.00	0.151	0.99	0.99-1.00	**0.99**	**0.99-0.99**	—
IL-8	1.00	0.99-1.00	0.99	0.99-1.00	0.366	**1.00**	0.99-1.00	**1.00**	0.99-1.00	0.538	**1.00**	**1.00-1.00**	**0.99**	0.99-1.00	—
IL-10	**1.04**	0.39-2.76	**0.09**	**0.018-0.515**	0.450	**1.49**	0.38-5.77	**4.36*e*-07**	**5.08-0.00**	0.215	**0.05**	0.00-1.80	**4.34*e*-09**	**1.09-1.72**	—
TNF-α	**0.99**	**0.99-0.99**	**0.99**	**0.99-0.99**	0.482	**1.00**	0.99-1.00	**0.99**	0.98-0.99	0.209	**0.99**	**0.99-0.99**	**0.99**	0.98-0.99	0.988
MPO	1.00	0.99-1.00	**0.99**	**0.99-0.99**	0.694	**1.00**	0.99-1.00	**1.00**	0.99-1.00	0.157	**0.99**	**0.99-0.99**	**1.00**	0.99-1.00	—

Legend: CAT—catalase; CC/HC—ratio chest circumference and head circumference; CI—confidence interval; GPx—glutathione peroxidase; GR—glutathione reductase; GSH—reduced glutathione; HC—head circumference; H_2O_2—hydrogen peroxide; IL—interleukin; MDA—malondialdehyde; MPO—myeloperoxidase; PR—prevalence ratio; SOD—superoxide dismutase; TNF—tumor necrosis factor. Poisson regression: $p < 0.05$. Adjusted for maternal age, origin, education, family income, gestational BMI, black race, primigravida, way of delivery, and gestational age. *Note*. *p*-for-interaction: *p* value for the interaction term between the redox imbalance/inflammatory marker and PE, for each of the investigated outcomes.

Table 5: Association between biomarkers of redox imbalance and inflammation in umbilical cords and perinatal outcomes such as low head circumference, CC/HC ratio < 1, and low length at birth of pregnancies with and without preeclampsia at a university hospital in Maceió, Alagoas, Brazil, in 2017.

Redox imbalance and inflammatory markers	Outcomes														
	Low head circumference					CC/HC < 1					Low length at birth				
	PE		Without PE		*p*-for-interaction	PE		Without PE		*p*-for-interaction	PE		Without PE		*p*-for-interaction
	PR	CI	PR	CI		PR	CI	PR	CI		PR	CI	PR	CI	
SOD	0.99	0.99-1.00	**0.99**	**0.99-0.99**	0.085	**0.99**	**0.99-0.99**	**0.99**	0.99-1.00	0.456	0.99	0.99-1.00	**0.99**	**0.99-0.99**	0.652
H_2O_2	**1.00**	0.99-1.00	**0.95**	**0.93-0.98**	0.315	**0.99**	**0.99-0.99**	**1.00**	0.99-1.00	0.092	**0.99**	0.97-1.00	**0.37**	**0.35-0.39**	0.379
CAT	**0.99**	0.99-1.00	**0.99**	**0.99-0.99**	0.208	**0.99**	0.99-1.00	**0.99**	**0.99-0.99**	0.357	0.99	0.99-1.00	**0.99**	**0.99-0.99**	0.447
GSH	**0.99**	0.99-1.00	**0.99**	0.99-1.00	0.221	1.00	0.99-1.00	0.99	0.99-1.00	0.882	1.00	0.99-1.00	**0.99**	**0.99-0.99**	0.730
GR	**1.04**	**1.00-1.08**	**2.9*e*-176**	**8.8*e*-216 – 9.6*e*137**	0.087	**0.96**	**0.94-0.99**	**1.00**	0.97-1.03	0.395	**0.99**	0.86-1.14	**0.68**	**0.55-0.85**	0.834
GPx	1.01	0.47-2.19	**1.70*e*-48**	—	0.184	**1.02**	0.78-1.34	**1.06**	0.86-1.30	0.759	**1.23**	0.48-3.17	**0.23**	**0.07-0.74**	0.543
MDA	**1.01**	0.90-1.12	**0.94**	0.79-1.11	0.264	**1.00**	0.96-1.04	**1.01**	0.99-1.03	0.503	**1.04**	0.96-1.13	**1853.957**	**957.6-3589.0**	0.465
IL-6	0.99	0.99-1.00	**0.99**	**0.98-0.99**	0.251	0.99	0.99-1.00	1.00	0.99-1.00	0.324	0.99	0.99-1.00	**0.99**	**0.99-0.99**	0.620
IL-8	**0.99**	0.99-1.00	**0.99**	**0.99-0.99**	0.395	0.99	0.99-1.00	1.00	0.99-1.00	0.522	0.99	0.99-1.00	**1.00**	**1.00-1.00**	0.220
IL-10	**2.22**	0.95-5.13	**2.7*e*-179**	**1.8*e*-194 – 4.2*e*164**	0.106	**0.62**	0.39-1.00	**1.24**	0.85-1.81	0.143	**0.98**	0.08-11.64	**0.01**	**0.00-0.20**	0.835
TNF-α	**1.00**	0.99-1.00	**0.99**	**0.99-0.99**	0.188	**0.99**	**0.99-0.99**	**1.00**	0.99-1.00	0.163	**0.99**	0.99-1.00	**0.99**	**0.99-0.99**	0.604
MPO	**1.00**	**1.00-1.00**	**0.96**	**0.93-0.98**	0.126	**0.99**	0.99-1.00	**0.99**	**0.99-0.99**	0.114	**1.00**	0.99-1.00	**0.95**	**0.91-0.99**	0.834

Legend: CAT—catalase; CC/HC—ratio chest circumference and head circumference; CI—confidence interval; GPx—glutathione peroxidase; GR—glutathione reductase; GSH—reduced glutathione; HC—head circumference; H_2O_2—hydrogen peroxide; IL—interleukin; MDA—malondialdehyde; MPO—myeloperoxidase; PR—prevalence ratio; SOD—superoxide dismutase; TNF—tumor necrosis factor. Poisson regression: $p < 0.05$. Adjusted for maternal age, origin, education, family income, gestational BMI, black race, primigravida, way of delivery, and gestational age. *Note*. *p*-for-interaction: *p* value for the interaction term between the redox imbalance/inflammatory marker and PE, for each of the investigated outcomes.

Table 6: Association between biomarkers of redox imbalance and inflammation in umbilical cords and perinatal outcome birth complications of pregnancies with and without preeclampsia at a university hospital in Maceió, Alagoas, Brazil, in 2017.

Redox imbalance and inflammatory markers	Outcome Birth complications PE PR	PE CI	Without PE PR	Without PE CI	*p*-for-interaction
SOD	**0.99**	0.99-1.00	**1.00**	**1.00-1.00**	0.260
H_2O_2	**1.00**	0.99-1.01	**0.98**	0.94-1.01	0.579
CAT	0.99	0.99-1.00	1.00	0.99-1.00	0.935
GSH	**0.99**	**0.99-1.00**	**0.99**	**0.99-0.99**	0.318
GR	**1.03**	0.95-1.11	**0.44**	**0.35-0.55**	0.259
GPx	**0.76**	0.18-3.16	**0.00**	**4.45-0.00**	0.278
MDA	**1.12**	0.84-1.51	**0.31**	**0.22-0.43**	0.870
IL-6	1.00	0.99-1.00	0.99	0.99-1.00	0.195
IL-8	0.99	0.99-1.00	**0.99**	**0.99-0.99**	0.223
IL-10	**1.62**	0.39-6.65	**0.00**	—	0.177
TNF-α	1.00	0.99-1.00	0.99	0.99-1.00	0.324
MPO	**1.00**	0.99-1.00	**1.00**	**1.00-1.00**	0.216

Legend: CAT—catalase; CC/HC—ratio chest circumference and head circumference; CI—confidence interval; GPx—glutathione peroxidase; GR—glutathione reductase; GSH—reduced glutathione; HC—head circumference; H_2O_2—hydrogen peroxide; IL—interleukin; MDA—malondialdehyde; MPO—myeloperoxidase; PR—prevalence ratio; SOD—superoxide dismutase; TNF—tumor necrosis factor. Poisson regression. $p < 0.05$. Adjusted for maternal age, origin, education, family income, gestational BMI, black race, primigravida, way of delivery, and gestational age. *Note*. *p*-for-interaction: *p* value for the interaction term between the redox imbalance/inflammatory marker and PE, for each of the investigated outcomes.

defense of cells against oxidative stress, which is very important in PE pathology. It exerts antioxidant action through its oxidation to oxidized glutathione (GSSG), in a reaction catalyzed by GPx. In addition, GSH has important effects on various organs of the human body; it plays a variety of roles in detoxification, redox regulation, and cellular signaling; including biological development, fertilization, implantation, and cellular differentiation [8, 9, 12, 49, 50].

Regarding the placenta, the total GSH and GPx levels are higher in the decidua, although they are increased throughout the organ and reflect the maternal protective capacity of this tissue against toxins and free radicals produced by the maternal-foetal interface or by the placenta in relation to the foetus. Both in healthy pregnant women and in PE ones, where there is an increase in redox imbalance, the protective effect of this antioxidant can be observed, including on foetal outcomes [12, 51]. However, the studies are still controversial. It was also reported in the literature that there may be a reduction in the placental levels of GSH in PE in response to the increase in oxidative stress [52].

The findings of the present study revealed, in comparison with the women without PE, higher levels of GSH in the umbilical cord of PE pregnancies. This result suggests that higher production of this antioxidant may be related to an organic compensatory mechanism, aimed at mitigating the consequences of oxidative stress. The presence of oxidative stress in the umbilical cord during PE was revealed by the increased level of MDA in comparison to the group without PE. GSH plays a beneficial role in the health of the foetus, as demonstrated previously in the placenta, where higher levels of GSH in PE placentas positively influenced birth weight, HC, CC, and gestational age at birth, which might be a compensation mechanism against oxidative stress [12]. However, data on this topic are still controversial. Research with blood and placenta that has evaluated GSH levels has produced conflicting results, with some authors observing higher levels of this antioxidant in PE [51, 53] and others finding reduced levels [8, 52, 54–56].

In addition to catalyzing the conversion of GSH to GSSG, the enzyme GPx also helps transforming H_2O_2 into water [57]. The findings of our study revealed higher levels of GPx in the umbilical cords of PE pregnancies than in women without PE. This may explain the similar levels of H_2O_2 in comparison to normal pregnancies. Therefore, it is possible that the effects of GPx prevented the formation of hydroxyl radicals from H_2O_2; thus, the damage to the membrane, revealed by the increase in MDA levels in the cords of women with PE, may be due to other reactive species.

Ferreira et al. [12], after evaluating biomarkers of oxidative stress in placental PE pregnancies compared to normal pregnancies, reported higher levels of SOD and CAT and a higher GSH/GSSG ratio, suggesting the existence of a compensatory mechanism against oxidative stress and a positive relationship of GSH with perinatal outcomes at birth, indicating an important role of this antioxidant in the health of the foetus.

These findings are partly in line with those of the present study, suggesting that the increase in the levels of this antioxidant in PE umbilical cords has occurred to compensate for the oxidative stress present during PE in order to protect the foetus.

Despite the scarcity of data evaluating oxidative stress markers in umbilical cords from PE pregnancies, a study conducted in Turkey assessed MDA levels in the placenta and umbilical cords in women with PE and their relationships to perinatal outcomes, and higher MDA levels were found in both tissues, in addition to a positive correlation between MDA levels in the umbilical cord and the neonate's asphyxia criteria [40]. Thus, the data in the present study are similar to the previous findings, except for the relationship between MDA levels and perinatal outcomes.

It is known that during pregnancy, PE causes oxidative stress, which simultaneously leads to an increase in the inflammatory response mediated by proinflammatory cytokines, especially TNF-α and IL-6, and activation of the inflammatory process also leads to more significant oxidative stress [9, 58]. Notably, as a consequence of oxidative stress, there is a release into the maternal circulation of a high amount of syncytial material, antiangiogenic factors, and debris, stimulating the activation of systemic leukocytes, which finally leads to a generalized inflammatory response [59]. Given the above, it is interesting to note that the scientific community widely reports that the exacerbated inflammatory response in PE observed in the blood and in the

placenta is an essential determinant of the disease's pathophysiology. However, in this research, lower levels of IL-6 and TNF-α were observed in umbilical cords from pregnancies with PE.

TNF-α is a cytokine with an inflammatory capacity that activates macrophages, regulates the production of other inflammatory cytokines, and increases the production of lipid mediators [60, 61]. IL-6, in general, is responsible for communicating with monocytes, endothelial cells, and fibroblasts [47, 62]. In healthy pregnancies, the IL-6 and TNF-α levels are reduced in placentas and in maternal blood, umbilical cord blood, and the amniotic fluid. As pregnancy progresses and labour begins, their concentrations increase considerably, indicating that the presence of these cytokines in gestational fluids is a maturational event, as they increase with gestational age [63].

In PE, it is proposed that inadequate placentation leads to placental hypoxia, which leads to the expression of higher amounts of proinflammatory cytokines, especially IL-6 and TNF-α, which subsequently favours higher production of ROS, in addition to the release of autoantibodies against the angiotensin II type 1 receptor (AT1-AA) and other antiangiogenic factors, such as sFlt-1, soluble endoglin, and endothelin-1. Therefore, these changes induce endothelial dysfunction and clinically characterize PE. Additionally, the increase in placental levels of these interleukins promotes the excessive activation of macrophages and prevents the recruitment of deciduous natural killer cells, which are essential for the remodeling of the spiral arteries, and they stimulate the activity of matrix metalloproteinases, which further inhibit the trophoblast invasion process by degrading the decidual extracellular matrix [64].

There is little information on the levels of inflammatory markers in umbilical cords in PE. Valencia-Ortega et al. [65] reported higher umbilical serum concentrations of IL-6 and TNF-α in PE than in the control group. Reyes-Aguilar et al. [66], studying the transcription of proinflammatory cytokine genes in umbilical cord blood, identified lower levels of IL-6 transcripts in PE women than in normotensive women. Thus, the authors suggested that the decrease in the release of inflammatory cytokines by umbilical vein endothelial cells in women with PE is an attempt to protect the foetus. This is clinically significant because neonates of mothers with PE have reduced immune activity, a fact supported by their augmented susceptibility to infections [66].

However, a study carried out in Portugal found a correlation between inflammatory markers in the maternal circulation and umbilical cord blood during PE, including IL-6. Therefore, the increase in maternal inflammation during PE is reflected in higher inflammation in the foetal circulation, which leads to early stimulation of the immune system to combat the increase in circulating cytokines. Lower leukocyte and neutrophil levels have also been observed in mothers' umbilical cord blood with PE, which was interpreted by the authors as a physiological response to try to neutralize the inflammatory process [67]. Thus, the present study's findings suggest that the lower levels of IL-6 and TNF-α observed in PE umbilical cords may be the result of an adaptive mechanism to protect the foetus.

The literature is scarce regarding the study of umbilical cord tissues. Therefore, no data related to the specific role of cytokines in this organ could be obtained. However, studies carried out on the placenta emphasize that cytokines play a physiological role in that organ, including modulation of the invasion and differentiation of trophoblasts, placental growth, and metabolic and endocrine homeostasis. In addition, the release of cytokines from placental tissues to the umbilical circulation results in increased concentrations of cytokines in umbilical cord blood and, consequently, in the foetus. It is noteworthy that physiological situations, such as labour, and pathological situations involving hypoxia, as in the case of PE, both lead to greater production of placental cytokines, and both can be reflected in the cord and foetal blood [68–70].

The present study allowed observing some significant associations between biomarkers of redox imbalance and inflammation in umbilical cords and perinatal outcomes. Regarding the biomarkers of redox imbalance in the PE group, a positive association was observed between SOD and a low Apgar score in the 5th min, CAT and a low Apgar score in the 5th min, GR with low HC, and MDA with LBW and preterm birth. A negative association was seen between SOD, macrosomia, and CC/HC ratio < 1; GR with a low Apgar score in the 5^{th} min and CC/HC ratio < 1; GPx with a low Apgar score in the 5th min; GSH with complications at birth; MDA with a low Apgar score in the 1st min of life; and H_2O_2 with a low Apgar score in the 5th min and CC/HC ratio < 1. Therefore, it is possible to note that about enzymatic and nonenzymatic antioxidants, the higher the levels of these, the greater protection over perinatal outcomes, including birth weight and CC/HC ratio < 1, which indicates better nutritional status at birth. On the other hand, the cell damage marker MDA showed a relationship with worse health conditions at birth, such as LBW and prematurity.

Concerning inflammation biomarkers, an inverse association was seen between TNF-α and LBW, preterm birth and a low Apgar score in the 5th min, and MPO with a low Apgar score in the 5th min. On the other hand, the higher the TNF-α level, the greater the occurrence of LGA newborns. IL-8 was directly associated with a low Apgar score in the 5th min. Corroborating with these findings, a direct association was seen between MPO and low HC. Thus, a relationship is observed between higher levels of proinflammatory biomarkers with adverse perinatal outcomes, including a low Apgar score in the 5th min and low HC, reinforcing the existence of an inadequate health condition at birth and insufficient foetal development in PE. Therefore, high levels of proinflammatory mediators are related to adverse perinatal outcomes in PE. As such, once inflammatory biomarkers can negatively influence the proper development of the conceptus and the pregnancy, the inflammation in PE requires an early control and should be the therapeutic target in the clinical monitoring of these pregnant women.

Corroborating with these findings, in a recent study carried out by our group in PE placentas from the same population herein studied, a positive (beneficial) association was

observed between placental GSH levels and birth weight, HC, CC, and gestational age at birth [12]. In other words, the higher the placental GHS levels, the better the perinatal outcomes of conceptuses from pregnancies with PE. Such results are considered to reflect a maternal physiological adaptive process, aimed at allowing adequate passage of nutrients through the cord to the foetus, and in this way, favouring an adequate foetal development. The literature has shown that changes in the umbilical cord structure may be associated with pathological conditions and adverse perinatal outcomes, such as gestational diabetes mellitus, PE, IUGR, and foetal death, and that these changes are related to the umbilical cord length and thickness, WJ area, cord insertion type, cord knot, morphometry, and flow parameters of the umbilical vessels [5–7].

With regard to perinatal outcomes, a study evaluating preterm newborns from a university hospital reported that maternal PE generates an increase in neonatal morbidities in preterm infants without causing significant changes in the levels of cytokines in the umbilical blood, given that the levels of cytokines can be altered by other conditions, causing prematurity [11]. In another study, with pregnant women in Turkey, the authors reported higher maternal and umbilical serum levels of IL-6, IL-8, and TNF-α in PE, in addition to significantly higher levels of IL-8 and TNF-α in newborns with IUGR from PE mothers relative to those who, even with PE, had infants with normal foetal growth [71]. In another cohort study carried out with pregnant women in prenatal care, they observed an increase in the levels of TNF-α in the umbilical blood of newborns of mothers diagnosed with PE, although no differences were observed in the maternal serum levels of this cytokine in the first and second trimesters [72]. In turn, a study produced in a high-risk hospital in Turkey identified a serum elevation of IL-6 and TNF-α in women with PE and a correlation of these markers with birth weight [73].

Regarding the associations between redox imbalance biomarkers and adverse perinatal outcomes in the group of women without PE, it was seen that the enzymes and antioxidant compounds analysed showed an inverse association with unfavorable health conditions at birth and foetal development, such as prematurity, a low Apgar score in the 1st and 5th min of life, short length, low HC, HC/CC ratio < 1, and complications during delivery, showing the antioxidant protective role of these compounds to foetal health. On the other hand, the higher the levels of the damage marker MDA, the lower the Apgar score in the 1st and 5th min, and the greater the occurrence of short length at birth, indicating the possibility of the involvement of this biomarker with impaired foetal development and health conditions at birth.

The relationship between inflammation biomarkers and perinatal outcomes assessed in the group of women without PE indicated the protective role of IL-10 against prematurity, a low Apgar score in the 1st and 5th min of life, low HC, and a short length. On the other hand, increased MPO levels were associated with complications at birth. In turn, the IL-6, IL-8, and TNF-α levels were associated with better perinatal outcomes at birth, including gestational age, weight, length, HC at birth, the Apgar score, and even the complications during childbirth, emphasizing the occurrence of better foetal conditions at birth in women without PE.

After performing the interaction analysis between the PE group and the group without PE, a significant interaction was seen between the MDA biomarker and LGA newborns, as shown in Table 3. So, there was only one significant interaction, but it was an outcome that did not show significance with the groups alone. Thus, although the MDA is higher in the umbilical cords of PE pregnancies, this is not enough to justify an action of this marker that is different from the action it normally exerts in pregnant women without the disease.

In view of the above and comparing the findings of the present study with the previous study carried out by our group on placentas of PE women [12], it is possible to observe that the reduced levels of IL-6 in the umbilical cord of pregnancies with PE, as well as the increase of this cytokine in placentas, indicate the accumulation of IL-6 in the placenta for foetal protection. On the other hand, TNF-α was reduced in the umbilical cord of PE pregnancies; however, in placentas, there were no differences between the PE and without PE groups. With this, we hypothesized that the cord tissue is without protection against inflammation in PE, and more tissues must be researched in this condition since there was low inflammation in the evaluated tissues, and proinflammatory cytokines may have been recruited to another organ.

Given the above, it is possible to identify some limitations in the present study, which include nonassessment of food consumption and the lack of measurement of markers of endothelial damage, such as sFlt-1, soluble endoglin, and endothelin-1, which have been suggested by the literature as possibly involved in PE pathophysiology. We also report that the sample size power calculated at 50.3% is considered low, which can also be a study limitation. Still, we were able to find significant results in some of the analysis, indicating that the low power of the primary analysis was not able to compromise the other analysis in our study.

Despite the appointed limitations, the present study suggests a potential compensation mechanism that protects the newborn of a mother with PE from the stress process experienced in pregnancy, which seems to have an evolutionary advantage in protecting the foetus exposed to oxidative damage during labour, as evidenced in the placenta [12]. In an additional study, not directly related to the placenta/umbilical cord but indirectly related to the health of the foetus, Silberstein et al. [74] reported a significant decrease (approximately 20%) in lipid peroxidation levels (MDA) in the colostrum of women who had PE compared with the control group and an increase in polyphenol concentrations (approximately 33%), an important antioxidant, highlighting a possible compensatory effect where the body activates the defense system, which can be a physiological organic adaptation to prioritize and protect the child.

As such, the results found in this research showed an increase in the levels of GSH, GPx, and MDA, in addition to a reduction in the levels of IL-6 and TNF-α in PE cords

compared to women without PE. They can serve as subsidies to guide clinical management of PE, as well as for future research on pathophysiology and perinatal outcomes resulting from the disease. Furthermore, the importance of the umbilical cord against the oxidative damage and inflammation present in PE is evident, providing protection of the health of the foetus, although an increase in the oxidative damage marker MDA was noted. Therefore, the existence of a compensatory mechanism developed by the umbilical cord is suggested to protect the health of the foetus during PE.

Future perspectives from the present study include a comparison of the present data on PE pregnancy, using similar biomarkers obtained from other biological matrixes, such as urine, saliva, and blood, which may facilitate the clinical routine, once they can be assessed throughout pregnancy. Additionally, the use of the umbilical cord may be considered together with the placenta, in these studies, once they give a real picture of the mother/foetal health at the moment of birth.

5. Conclusion

Higher levels of GSH and GPx, in addition to lower levels of IL-6 and TNF-α, in the PE umbilical cord may result from an adaptive mechanism to maintain the oxidative and inflammatory balance; however, despite these changes, damage to the cell membrane occurred since the MDA content was higher. Besides, it is clear that this redox imbalance does not directly influence the outcome of the pregnancy, confirming that other physiological and adaptive mechanisms may act to preserve foetal health. Therefore, it is suggested that the umbilical cord plays an important role in controlling redox imbalance and inflammation in pregnancies with PE. The present results also reinforce the necessity for continuous research on GSH as a protective compound for the perinatal outcome, favouring a possible supplementation to increase GSH levels, especially in PE women. It will also stimulate research on umbilical cords.

Data Availability

Data are available on request through Prof. Alane Cabral Menezes de Oliveira, Universidade Federal de Alagoas, Faculdade de Nutrição. E-mail: alanecabral@gmail.com. Phone: +55 (82) 999766895. Fax: +55 (11) 55739525.

Conflicts of Interest

The authors declare that they have no conflict of interest.

Acknowledgments

We thank the PPSUS/FAPEAL process 60030 000818/2016 for financial support. We also thank the Brazilian agencies CAPES and CNPq for their financial support and fellowships.

References

[1] F. Vieira Paladino, J. de Moraes Rodrigues, A. da Silva, and A. C. Goldberg, "The immunomodulatory potential of Wharton's jelly mesenchymal stem/stromal cells," *Stem Cells International*, vol. 2019, 7 pages, 2019.

[2] J. E. Davies, J. T. Walker, and A. Keating, "Concise review: Wharton's jelly: the rich, but enigmatic, source of mesenchymal stromal cells," *Stem Cells Translational Medicine*, vol. 6, no. 7, pp. 1620–1630, 2017.

[3] S. Rostamzadeh, M. Kalantari, M. Shahriari, and M. Shakiba, "Sonographic measurement of the umbilical cord and its vessels and their relation with fetal anthropometric measurements," *Iranian Journal of Radiology*, vol. 12, no. 3, article e12230, 2015.

[4] V. L. Ferguson and R. B. Dodson, "Bioengineering aspects of the umbilical cord," *European Journal of Obstetrics & Gynecology and Reproductive Biology*, vol. 144S, no. 2009, pp. S108–S113, 2009.

[5] E. di Naro, F. Ghezzi, L. Raio, M. Franchi, and V. D'Addario, "Umbilical cord morphology and pregnancy outcome," *European Journal of Obstetrics & Gynecology and Reproductive Biology*, vol. 96, no. 2, pp. 150–157, 2001.

[6] K. I. Ismail, A. Hannigan, K. O'Donoghue, and A. Cotter, "Abnormal placental cord insertion and adverse pregnancy outcomes: a systematic review and meta-analysis," *Systematic Reviews*, vol. 6, no. 1, pp. 1–11, 2017.

[7] L. E. Linde, S. Rasmussen, J. Kessler, and C. Ebbing, "Extreme umbilical cord lengths, cord knot and entanglement: risk factors and risk of adverse outcomes, a population-based study," *PLoS One*, vol. 13, no. 3, article e0194814, 2018.

[8] I. M. Ahmad, M. C. Zimmerman, and T. A. Moore, "Oxidative stress in early pregnancy and the risk of preeclampsia," *Pregnancy Hypertension*, vol. 18, pp. 99–102, 2019.

[9] M. B. Tenório, R. C. Ferreira, F. A. Moura, N. B. Bueno, A. C. M. de Oliveira, and M. O. F. Goulart, "Cross-talk between oxidative stress and inflammation in preeclampsia," *Oxidative Medicine and Cellular Longevity*, vol. 2019, 26 pages, 2019.

[10] R. Marin, D. I. Chiarello, C. Abad, D. Rojas, F. Toledo, and L. Sobrevia, "Oxidative stress and mitochondrial dysfunction in early-onset and late-onset preeclampsia," *BBA-Molecular Basis of Disease*, vol. 1866, no. 165961, pp. 1–16, 2020.

[11] S. C. Cakir, B. A. Dorum, N. Koksal, and H. Ozkan, "The effects of maternal preeclampsia on inflammatory cytokines and clinical outcomes in premature infants," *Pakistan Journal of Medical Sciences*, vol. 36, no. 2, pp. 26–31, 2020.

[12] R. C. Ferreira, M. B. T. Fragoso, M. C. S. Tenório et al., "Biomarkers of placental redox imbalance in pregnancies with preeclampsia and consequent perinatal outcomes," *Archives of Biochemistry and Biophysics*, vol. 691, no. 691, article 108464, 2020.

[13] M. Maciejczyk, A. Zalewska, and J. R. Ładny, "Salivary antioxidant barrier, redox status, and oxidative damage to proteins and lipids in healthy children, adults, and the elderly," *Oxidative Medicine and Cellular Longevity*, vol. 2019, Article ID 4393460, 12 pages, 2019.

[14] A. J. Adekanmi, A. Roberts, J. A. Akinmoladun, and A. O. Adeyinka, "Uterine and umbilical artery doppler in women with pre-eclampsia and their pregnancy outcomes," *Nigerian Postgraduate Medical Journal*, vol. 26, no. 2, pp. 106–112, 2019.

[15] L. Raio, F. Ghezzi, E. di Naro, M. Franchi, D. Bolla, and H. Schneider, "Altered sonographic umbilical cord morphometry in early-onset preeclampsia," *Obstetrics & Gynecology*, vol. 100, no. 2, pp. 311–316, 2002.

[16] L. Romanowicz, T. Gogiel, Z. Galewska et al., "Divergent changes in the content and activity of MMP-26 and TIMP-4 in human umbilical cord tissues associated with preeclampsia," *European Journal of Obstetrics & Gynecology and Reproductive Biology*, vol. 231, pp. 48–53, 2018.

[17] T. Gogiel, Z. Galewska, and S. Jaworski, "Pre-eclampsia-associated alterations in Wharton's jelly proteoglycans," *Acta Biochimica Polonica*, vol. 52, pp. 501–507, 2005.

[18] Z. Galewska, E. Bańkowski, L. Romanowicz, and S. Jaworski, "Pre-eclampsia (EPH-gestosis)-induced decrease of MMP-s content in the umbilical cord artery," *Clinica Chimica Acta*, vol. 335, no. 1-2, pp. 109–115, 2003.

[19] M. Olaya-C, J. Salcedo-Betancourt, S. H. Galvis, A. M. Ortiz, S. Gutierrez, and J. E. Bernal, "Umbilical cord and preeclampsia," *Journal of Neonatal-Perinatal Medicine*, vol. 9, no. 1, pp. 49–57, 2016.

[20] S. Tenny, C. C. Kerndt, and M. R. Hoffman, *Case Control Studies*, StatPearls, Treasure Island (FL), 2020, https://pubmed.ncbi.nlm.nih.gov/28846237/.

[21] S. Munnangi and S. W. Boktor, *Epidemiology of Study Design*, StatPearls, Treasure Island (FL), 2020, https://pubmed.ncbi.nlm.nih.gov/29262004/.

[22] The American College of Obstetricians and Gynecologists, "Hypertension in pregnancy. Report of the American College of Obstetricians and Gynecologists' Task Force on Hypertension in Pregnancy," *Obstetrics & Gynecology*, vol. 122, no. 5, pp. 1122–1131, 2013.

[23] M. A. Brown, L. A. Magee, L. C. Kenny et al., "Hypertensive disorders of pregnancy ISSHP classification, diagnosis, and management recommendations for international practice," *Hypertension*, vol. 72, no. 1, pp. 24–43, 2018.

[24] A. L. Tranquilli, G. Dekker, L. Magee et al., "The classification, diagnosis and management of the hypertensive disorders of pregnancy: a revised statement from the ISSHP," *Pregnancy Hypertension*, vol. 4, no. 2, pp. 97–104, 2014.

[25] J. L. C. P. Silva and F. G. C. Surita, "Maternal age: perinatal outcomes and birth routes," *Revista Brasileira de Ginecologia e Obstetrícia*, vol. 3, pp. 1321–1325, 2009.

[26] L. Scliar-Cabral, "Reviewing the "functional illiterate" category," *Revista Crear Mundos*, vol. 3, pp. 1–5, 2003.

[27] E. Atalah Samur, L. C. Castillo, R. Castro, and A. Aldea, "Propuesta de un nuevo estándar de evaluación nutricional en embarazadas/proposal of a new standard for the nutritional assessment of pregnant women," *Revista Médica de Chile*, vol. 125, pp. 1429–1436, 1997.

[28] J. Villar, L. C. Ismail, C. G. Victora et al., "International standards for newborn weight, length, and head circumference by gestational age and sex: the Newborn Cross-Sectional Study of the INTERGROWTH-21st Project," *The Lancet*, vol. 384, no. 9946, pp. 857–868, 2014.

[29] WHO (World Health Organization), *Physical Status: The Use and Interpretation of Anthropometry*, Technical Reports Series, 854, Geneva, 1995.

[30] S. M. Dal Bosco, *Nutritional Therapy in Pediatrics*, Atheneu Editor, 1st edition, 2010.

[31] American Academy Of Pediatrics Committee On Fetus And Newborn, American College Of Obstetricians And Gynecologists Committee On Obstetric Practice, "The Apgar score," *Pediatrics*, vol. 136, no. 4, pp. 819–822, 2015.

[32] M. M. Bradford, "A rapid and sensitive method for the quantitation of microgram quantities of protein utilizing the principle of protein-dye binding," *Analytical Biochemistry*, vol. 72, no. 1-2, pp. 248–254, 1976.

[33] E. Pick and Y. Keisari, "A simple colorimetric method for the measurement of hydrogen peroxide produced by cells in culture," *Journal of Immunological Methods*, vol. 38, no. 1-2, pp. 161–170, 1980.

[34] L. N. Paton, T. J. Mocatta, A. M. Richards, and C. C. Winterbourn, "Increased thrombin-induced polymerization of fibrinogen associated with high protein carbonyl levels in plasma from patients post myocardial infarction," *Free Radical Biology and Medicine*, vol. 48, no. 2, pp. 223–229, 2009.

[35] H. Aebi, "[13] Catalase *in vitro*," *Methods Enzymology*, vol. 105, pp. 121–126, 1984.

[36] T. E. Tipple and L. K. Rogers, "Methods for the determination of plasma or tissue glutathione levels," *Methods in Molecular Biology*, vol. 889, pp. 315–324, 2012.

[37] L. Flohé and W. A. Gunzler, "[12] Assays of glutathione peroxidase," *Methods Enzymology*, vol. 105, pp. 114–121, 1984.

[38] V. L. Tatum, C. Changchit, and C. K. Chow, "Measurement of malondialdehyde by high performance liquid chromatography with fluorescence detection," *Lipids*, vol. 25, no. 4, pp. 226–229, 1990.

[39] P. P. Bradley, D. A. Priebat, R. D. Christensen, and G. Rothstein, "Measurement of cutaneous inflammation: estimation of neutrophil content with an enzyme marker," *Journal of Investigative Dermatology*, vol. 78, no. 3, pp. 206–209, 1982.

[40] S. Zeteroglu, Y. Ustun, and Y. E. Ustun, "Placental and cord malondialdehyde and maternal and perinatal outcomes," *International Journal of Gynecology & Obstetrics*, vol. 85, no. 1, pp. 47–49, 2004.

[41] R. H. M. Salama, M. M. F. Fathalla, A. R. M. Mekki, and B. E. K. M. Elsadek, "Implication of umbilical cord in preeclampsia," *Medical Principles and Practice*, vol. 20, no. 2, pp. 124–128, 2011.

[42] K. Bhavina, J. Radhika, and S. S. Pandian, "VEGF and eNOS expression in umbilical cord from pregnancy complicated by hypertensive disorder with different severity," *BioMed Research International*, vol. 2014, Article ID 982159, 6 pages, 2014.

[43] L. C. Sanchéz-Araguren, C. E. Prada, C. E. Riaño-Medina, and M. Lopez, "Endothelial dysfunction and preeclampsia: role of oxidative stress," *Frontiers in Physiology*, vol. 5, p. 372, 2014.

[44] E. A. Phipps, R. Thadhani, T. Benzing, and S. A. Karumanchi, "Pre-eclampsia: pathogenesis, novel diagnostics and therapies," *Nature Reviews Nephrology*, vol. 15, no. 5, pp. 275–289, 2019.

[45] M. W. Socha, B. Malinowski, O. Puk et al., "The role of NF-κB in uterine spiral arteries remodeling, insight into the cornerstone of preeclampsia," *International Journal of Molecular Sciences*, vol. 22, no. 2, pp. 704–714, 2021.

[46] I. Striz, E. Brabcova, L. Kolesar et al., "Epithelial cells modulate genes associated with NF kappa B activation in co- cultured human macrophages," *Immunobiology*, vol. 216, no. 10, pp. 1110–1116, 2011.

[47] A. C. Harmon, D. C. Cornelius, L. M. Amaral et al., "The role of inflammation in the pathology of preeclampsia," *Clinical Science*, vol. 130, no. 6, pp. 409–419, 2016.

[48] P. Dhillion, K. Wallace, F. Herse et al., "IL-17-mediated oxidative stress is an important stimulator of AT1-AA and hypertension during pregnancy," *American Journal of Physiology-Regulatory, Integrative and Comparative Physiology*, vol. 303, no. 4, pp. R353–R358, 2012.

[49] J. M. Hansen and C. Harris, "Glutathione during embryonic development," *Biochimica*, vol. 1850, pp. 1527–1542, 2015.

[50] S. Taysi, A. S. Tascan, M. G. Ugur, and M. Demir, "Radicals, oxidative/nitrosative stress and preeclampsia," *Mini-Reviews in Medicinal Chemistry*, vol. 19, no. 3, pp. 178–193, 2019.

[51] M. F. C. M. Knapen, W. H. M. Peters, T. P. J. Mulder, H. M. W. M. Merkus, J. B. M. J. Jansen, and E. A. P. Steegers, "Glutathione and glutathione-related enzymes in decidua and placenta of controls and women with pre-eclampsia," *Placenta*, vol. 20, no. 7, pp. 541–546, 1999.

[52] N. Rani, R. Dhingra, D. S. Arya, M. Kalaivani, N. Bhatla, and R. Kumar, "Role of oxidative stress markers and antioxidants in the placenta of preeclamptic patients," *Journal of Obstetrics and Gynaecology Research*, vol. 36, no. 6, pp. 1189–1194, 2010.

[53] J. Neves, A. S. Cruz, I. Azevedo et al., "Reduced and oxidized glutathione of the placenta in pregnancy complicated by pre-eclampsia," *Acta Medica Portuguesa*, vol. 10, no. 5, pp. 357–360, 1997.

[54] V. O. Osunkalu, I. A. Taiwo, C. C. Makwe, O. J. Akinsola, and R. A. Quao, "Methylenetetrahydrofolate reductase enzyme level and antioxidant activity in women with gestational hypertension and pre-eclampsia in Lagos, Nigeria," *The Journal of Obstetrics and Gynecology of India*, vol. 69, no. 4, pp. 317–324, 2019.

[55] Y. Atamer, Y. Koçyigit, B. Yokus, A. Atamer, and A. C. Erden, "Lipid peroxidation, antioxidant defense, status of trace metals and leptin levels in preeclampsia," *European Journal of Obstetrics & Gynecology and Reproductive Biology*, vol. 119, no. 1, pp. 60–66, 2005.

[56] R. Madazli, A. Benian, S. Aydin, H. Uzun, and N. Tolun, "The plasma and placental levels of malondialdehyde, glutathione and superoxide dismutase in pre-eclampsia," *Journal of Obstetrics and Gynaecology*, vol. 22, no. 5, pp. 477–480, 2002.

[57] P. C. Huber, W. P. Almeida, and Â. Fátima, "Glutationa e enzimas relacionadas: papel biológico e importância em processos patológicos," *Química Nova*, vol. 31, no. 5, pp. 1170–1179, 2008.

[58] D. I. Chiarello, C. Abad, D. Rojas et al., "Oxidative stress: normal pregnancy versus preeclampsia," *Biochimica et Biophysica Acta (BBA)-Molecular Basis of Disease*, vol. 1866, no. 2, pp. 1–11, 2020.

[59] R. Aggarwal, A. K. Jain, P. Mittal, M. Kohli, P. Jawanjal, and G. Rath, "Association of pro- and anti-inflammatory cytokines in preeclampsia," *Journal of Clinical Laboratory Analysis*, vol. 33, no. 4, article e22834, 2019.

[60] K. D. Black and J. A. Horowitz, "Inflammatory markers and preeclampsia: a systematic review," *Nursing Research*, vol. 67, no. 3, pp. 242–251, 2018.

[61] D. C. Cornelius, "Preeclampsia: from inflammation to immunoregulation," *Clinical Medicine Insights: Blood Disorders*, vol. 11, 2018.

[62] N. C. Serrano, E. Guio, S. M. Becerra-Bayona et al., "C-reactive protein, interleukin-6 and pre-eclampsia: large-scale evidence from the GenPE case-control study," *Scandinavian Journal of Clinical and Laboratory Investigation*, vol. 80, no. 5, pp. 381–387, 2020.

[63] S. L. Opsjøn, N. C. Wathen, S. Tingulstad et al., "Tumor necrosis factor, interleukin-1, and interleukin-6 in normal human pregnancy," *American Journal of Obstetrics and Gynecology*, vol. 169, no. 2, pp. 397–404, 1993.

[64] I. Bellos, V. Karageorgiou, D. Kapnias, K. E. Karamanli, and C. Siristatidis, "The role of interleukins in preeclampsia: a comprehensive review," *American Journal of Reproductive Immunology*, vol. 80, no. 6, pp. 1–21, 2018.

[65] J. Valencia-Ortega, A. Zárate, R. Saucedo, M. Hernández-Valencia, J. G. Cruz, and E. Puello, "Placental proinflammatory state and maternal endothelial dysfunction in preeclampsia," *Gynecologic and Obstetric Investigation*, vol. 84, no. 1, pp. 12–19, 2019.

[66] S. S. Reyes-Aguilar, I. Poblete-Naredo, Y. Rodríguez-Yáñez et al., "*CYP1A1, GSTT1, IL-6* and *IL-8* transcription and IL-6 secretion on umbilical endothelial cells from hypertensive pregnant women: Preliminary results," *Pregnancy Hypertension*, vol. 18, pp. 63–66, 2019.

[67] C. Catarino, A. Santos-Silva, L. Belo et al., "Inflammatory disturbances in preeclampsia: relationship between maternal and umbilical cord blood," *Journal of Pregnancy*, vol. 2012, Article ID 684384, 10 pages, 2012.

[68] J. M. Bowen, L. Chamley, J. A. Keelan, and M. D. Mitchell, "Cytokines of the placenta and extra-placental membranes: roles and regulation during human pregnancy and parturition," *Placenta*, vol. 23, no. 4, pp. 257–273, 2002.

[69] C. W. Redman and I. L. Sargent, "Latest advances in understanding preeclampsia," *Science*, vol. 308, no. 5728, pp. 1592–1594, 2005.

[70] C. J. Chan, K. L. Summers, N. G. Chan, D. B. Hardy, and B. S. Richardson, "Cytokines in umbilical cord blood and the impact of labor events in low-risk term pregnancies," *Early Human Development*, vol. 89, no. 12, pp. 1005–1010, 2013.

[71] M. Tosun, H. Celik, B. Avci, E. Yavuz, T. Alper, and E. Malatyalioğlu, "Maternal and umbilical serum levels of interleukin-6, interleukin-8, and tumor necrosis factor-α in normal pregnancies and in pregnancies complicated by preeclampsia," *The Journal of Maternal-Fetal & Neonatal Medicine*, vol. 23, no. 8, pp. 880–886, 2010.

[72] L. Guillemette, M. Lacroix, C. Allard et al., "Preeclampsia is associated with an increased pro-inflammatory profile in newborns," *Journal of Reproductive Immunology*, vol. 112, pp. 111–114, 2015.

[73] M. A. Guven, A. Coskun, I. E. Ertas, M. Aral, B. Zencırcı, and H. Oksuz, "Association of maternal serum CRP, IL-6, TNF-α, homocysteine, folic acid and vitamin b12 levels with the severity of preeclampsia and fetal birth weight," *Hypertension in Pregnancy*, vol. 28, no. 2, pp. 190–200, 2009.

[74] T. Silberstein, B. Hamou, S. Cervil, T. Barak, A. Burg, and O. Saphier, "Colostrum of preeclamptic women has a high level of polyphenols and better resistance to oxidative stress in comparison to that of healthy women," *Oxidative Medicine and Cellular Longevity*, vol. 2019, Article ID 1380605, 5 pages, 2019.

Hindawi
Oxidative Medicine and Cellular Longevity
Volume 2021, Article ID 1641717, 16 pages
https://doi.org/10.1155/2021/1641717

Research Article

ALDH2/SIRT1 Contributes to Type 1 and Type 2 Diabetes-Induced Retinopathy through Depressing Oxidative Stress

Mengshan He,[1] **Pan Long**,[2] **Tao Chen**,[3] **Kaifeng Li**,[4] **Dongyu Wei**,[3] **Yufei Zhang**,[5] **Wenjun Wang**,[1] **Yonghe Hu**,[6] **Yi Ding**,[1] **and Aidong Wen**[1]

[1]*Department of Pharmacy, Xijing Hospital, Fourth Military Medical University, Xi'an, 710032 Shaanxi, China*
[2]*Department of Ophthalmology, The General Hospital of Western Theater Command, Chengdu, 610083 Sichuan, China*
[3]*Center of Clinical Aerospace Medicine, Fourth Military Medical University, Xi'an, 710032 Shaanxi, China*
[4]*Experiment Teaching Center, Fourth Military Medical University, Xi'an, 710032 Shaanxi, China*
[5]*The Air Force Hospital from Northern Theater PLA, Shenyang, 110092 Liaoning, China*
[6]*Clinical Medical College & Affiliated Hospital of Chengdu University, Chengdu, 610081 Sichuan, China*

Correspondence should be addressed to Yonghe Hu; huyonghe789@sina.com, Yi Ding; dingyi.007@163.com, and Aidong Wen; adwen-2004@hotmail.com

Received 30 June 2021; Revised 7 September 2021; Accepted 24 September 2021; Published 23 October 2021

Academic Editor: Daniela Ribeiro

Clinical observations found vision-threatening diabetic retinopathy (DR) occurs in both type 1 diabetes mellitus (T1DM) and type 2 diabetes mellitus (T2DM) patients, but T1DM may perform more progressive retinal abnormalities at the same diabetic duration with or without clinical retinopathy. In the present study, T1DM and T2DM patients without manifestations of DR were included in our preliminary clinical retrospective observation study to investigate the differentiated retinal function at the preclinical stage. Then, T1DM and T2DM rat models with 12-week diabetic duration were constructed to explore the potential mechanism of the discrepancy in retinal disorders. Our data demonstrated T1DM patients presented a poor retinal function, a higher allele frequency for ALDH2GA/AA, and a depressed aldehyde dehydrogenase 2 (ALDH2) activity and silent information regulator 1 (SIRT1) level, compared to T2DM individuals. In line with this, higher amplitudes of neurovascular function-related waves of electroretinograms were found in T2DM rats. Furthermore, the retinal outer nuclear layers were reduced in T1DM rats. The levels of retinal oxidative stress biomarkers including total reactive oxygen species, NADPH oxidase 4 and mitochondrial DNA damage, and inflammatory indicators covering inducible/endothelial nitric acid synthase ratio, interleukin-1, and interleukin-6 were obviously elevated. Notably, the level of retinal ALDH2 and SIRT1 in T1DM rats was significantly diminished, while the expression of neovascularization factors was dramatically enhanced compared to T2DM. Together, our data indicated that the ALDH2/SIRT1 deficiency resulted in prominent oxidative stress and was in association with DR progression. Moreover, a differentiating ALDH2/SIRT1 expression may be responsible for the dissimilar severity of DR pathological processes in chronic inflammatory-related T1DM and T2DM.

1. Introduction

Diabetes mellitus (DM) has been a severe health-killer, and how to manage itself and its comorbidities is becoming a global concern [1]. It is estimated that the prevalence of DM will rise sharply from the 464 million cases in 2019 to 700 million by 2045 [2]. Diabetic retinopathy (DR) is a common neurovascular complication of DM and has become one of the most frequent causes of blindness in the working-age population worldwide [3, 4].

In clinical, diabetic retinopathy occurs both in type 1 diabetes mellitus (T1DM) featured with severe insulin deficiency and type 2 diabetes mellitus (T2DM) featured with insulin resistance and/or impaired insulin secretion. Astonishingly, individual lifetime risk of DR is up to 90% in T1DM patients and 50–60% in T2DM patients [5–7]. As

we have known, the frequency of the progression to DR is influenced by multifactors, such as age, persisted hyperglycemia, and duration of diabetes [8]. Interestingly, the severity of DR denoted by various clinical symptoms existed an obvious difference between T1DM and T2DM at the nearly duration point [9]. However, there are few systematic researches about the comparison of DR features at preclinical or clinical stages caused by T1DM and T2DM, respectively. Here, we would like to study preclinical DR patients who suffered from T1DM or T2DM and established two corresponding animal models to determine the different retinal manifestations. Specifically, via exploring the representative retinal structure, function, and biochemical features of T1DM and T2DM animal models at the same duration, we may reconfirm the clinical finding and further uncover the substantial mechanism of different retinal disorders between T1DM and T2DM.

Intricate interconnecting biochemical pathways are implicated in modulating the pathophysiology of diabetic retinopathy [10]. Among those related mechanisms, oxidative stress (OS), as a consequence of hyperglycemia-provoked overproduction of reactive oxygen species (ROS), is believed as the promising pathway to be responsible for DR progression. As we all know, elevated ROS can result in massive cellular structure damage and mitochondrial dysfunction. Moreover, OS has been postulated as the underlying stressor linking other relative mechanisms which could be related to retinal structural, functional, and metabolic abnormalities in DR process [11, 12]. Specifically, NADPH oxidases (NOX4) could induce OS-correlated mitochondrial impairment and lipid peroxidation (4-hydroxynonenal) in neurodegeneration disease [13].

Recently, studies found that diabetic retinal cells possessed an impaired aldehyde detoxifying capacity, making them especially be prone to aldehyde damages [14, 15]. And elevated lipid aldehydes such as 4-hydroxynonenal (4-HNE) can induce carbonyl stress and mitochondrial damage and accumulate advanced glycation end products (AGEs) [16, 17]. Interestingly, aldehyde dehydrogenase 2 (ALDH2), the mitochondrial isoform of aldehyde dehydrogenases, plays vital roles in clearing acetaldehyde and endogenous lipid aldehydes. Furthermore, epidemiological studies suggest that the gene polymorphism of ALDH2 rs671 in the population is related to DR susceptibility and development [18, 19]. Indeed, our previous study verified that ALDH2 could alleviate early stage aged diabetic retinal damage through upregulating silent information regulator 1 (SIRT1) signaling and depressing oxidative stress reaction [20].

SIRT1 wildly expresses throughout the retinal cells' nuclear, which plays a pivotal role in regulating cell metabolism and mitochondrial homeostasis. Moreover, a body of evidences from our group and others demonstrated that SIRT1 showed strongly protective roles against DR development through attenuating oxidative stress, inflammation, and apoptosis [20, 21]. Additionally, SIRT1 is well-recognized as a redox-sensitive enzyme and tightly affected by cellular oxidative stress conditions [21, 22]. To be specific, the disturbance of oxidative stress, including carbonyl stress (induced by lipid aldehydes), can interfere SIRT1 via down-regulating nicotinamide adenine dinucleotide (NAD) levels, decreasing posttranslational modification's ability, and inducing protein-protein interaction disorders [21, 22].

To this regard, ALDH2/SIRT1 may serve as one of the potent molecules to restore the redox homeostasis and mitochondrial health. Lately, our work further revealed that ALDH2 could diminish oxidative stress-related apoptosis and inflammation in naturally aged mouse retinas [23]. In fact, proinflammatory cytokines (interleukin-6), nitric oxide synthase (iNOS), and vascular endothelial growth factor-α (VEGF-α) directly or indirectly stimulated by oxidative stress can be found in varying ocular diseases including age-related macular degeneration, retinitis pigmentosa, and diabetic retinopathy [24–26]. To be specific, VEGF-α is a powerful angiogenic inducer which is not only responsible for ocular neovascularization but also implicated in the increase of macrophage and monocyte chemotaxis [27]. As a result of ROS overabundance and a compromised defense against oxidative stress, aggravated retinal neuron (photoreceptor cells) and capillary disorders can accelerate the development of DR pathogenesis. Accordingly, elucidating the distinction of such typical biomarkers would be conducive to uncover the underlying mechanisms in T1DM/T2DM-related DR and make more targeted therapeutical strategies.

Therefore, the goal of this preliminary clinical retrospective observation study was to determine whether preclinical stage of DR in T1DM and T2DM would exist retinal structural or functional difference. Moreover, rat models, involving single high-dose streptozotocin- (STZ-) induced T1DM and high-calorie diet combined with low-dose STZ-induced T2DM, were applied to investigate the retinal dysfunction characteristics and further explore the potential mechanism in the pathological processes of T1DM and T2DM.

2. Materials and Methods

2.1. Study Subjects. A total of 85 individuals were included in this preliminary clinical retrospective observation study, including 70 cases with diabetes mellitus and 15 healthy individuals as controls (CON). Diabetic patients were classified into two cohorts by the type of diabetes mellitus, and it included 15 type 1 diabetes mellitus (T1DM) and 55 type 2 diabetes mellitus (T2DM). All of the subjects had no clinical manifestations of DR such as microaneurysms, macular edema, or neovascularization, which was confirmed by fundus fluorescein angiography, slit lamp microscope, and optical coherence tomography (OCT) according to certified ophthalmologists, and the best-corrected visual acuity (BCVA) was beyond 20/20. Additionally, the demographic and clinical characteristics of the study participants such as age, sex, body mass index (BMI), fasting blood glucose, diabetic duration, retina thickness, full-field electroretinograms (ERG) test, and therapies for diabetes were recorded. Subjects with uncontrolled hypertension, acute or chronic systematical inflammatory disease, and maturity-onset diabetes of the young were excluded. The cases were collected from the Department of Ophthalmology in the General Hospital of Western Theater Command through

2018.01-2020.02. All participants gave written informed consent prior to study participation, and this retrospective case-control study was approved by the Ethics Committee of the General Hospital of Western Theater Command for human studies.

2.2. Genotyping of ALDH2 Genotypes in Preclinical DR Patients. The blood samples were collected from subjects following a 12-hour fast, and genomic DNA specimens were extracted by using a commercial DNA extraction and purification kit (Shenggong, China) following the manufacturer's protocols. Genotyping was performed on coded genomic DNA samples following a previous study [28]. The ALHD2 rs671, the most well-known functional single nucleotide polymorphism (SNP) acting as a coenzyme binding site [29], was selected as a typical ALDH2 genotyping marker in this study. Individuals carrying wild-type homozygote of the GG (ALDH2∗1/∗1) have a full enzyme activity, whereas participants with mutant heterozygote of the GA (ALDH2∗1/∗2) or mutant homozygote of the AA (ALDH2∗2/∗2) genotype have reduced or little enzyme activity.

2.3. The Determination of Serum ALDH2 Activity and SIRT1 Expression in Preclinical DR Patients. The blood serum samples were collected and assayed for ALDH2 activity using a commercial colorimetric kit (#ab115348; Abcam) according to the manufacturer's protocol. The specific method was accordant with previous study [30]. The SIRT1 level was estimated by enzyme-linked immunosorbent assay (ELISA) according to the manufacturer's protocols. The ELISA kit for human SIRT1 was obtained from Abcam (#ab171573). Plate readings were done on a Multiskan® GO Microplate Reader from Thermo Fisher (Basingstoke, UK). Standard solutions in the kit were used to normalize the ELISA values for each plate.

2.4. Animals and T1DM and T2DM Rats' Model. Male Sprague Dawley (SD) rats were purchased from the Laboratory Animal Center of Fourth Military Medical University in Xi'an, China (license No. 2014270138S). Rats were housed under standard laboratory conditions, and all experiments were performed in compliance with the ARVO Statement for the Use of Animals in Ophthalmic and Vision Research. Studies were approved by the research ethics committee for the care and use of laboratory animals at the Fourth Military Medical University. 40 SD rats (6-8 weeks old, male, 200-240 g) were fed with a high-fat and high-calorie diet (breeding rodent material 54.6%, lard 16.9%, sucrose 14%, casein 10.2%, premix 2.1%, and maltodextrin 2.2%) for 4 weeks, as previously described [20]. Then, the T2DM rats' model was induced by an intraperitoneal injection of streptozotocin (STZ) (45 mg/kg body weight) (Sigma, USA) after a 4-week specific diet. Simultaneously, to construct the T1DM rats' model with the same diabetic duration, 40 age-matched SD rats (10-12 weeks old, male, 320-360 g) were intraperitoneally injected with a single dose of STZ (60 mg/kg body weight). Seventy-two hours post-STZ injection, blood glucose level was measured by ACCU-CHEK Performa (Roche, Germany) and rats showing a blood glucose level above 16.7 mmol/L were considered as DM and selected for the study. Diabetic rats were divided into two groups: T1DM group ($n = 30$) and T2DM group ($n = 30$), both groups treated with a high-fat and high-calorie diet afterwards. And 30 age-matched SD rats (10-12 weeks old, 320-360 g) served as the CON group.

2.5. Full-Field Electroretinograms (ffERG) and Fundus Fluorescein Angiography (FFA) Detection in Diabetic Rats. Full-field electroretinography (ffERG) and fundus fluorescein angiography (FFA) measurements were performed according to the International Society for Clinical Electrophysiology of Vision (ISCEV) guidelines as described earlier [31]. Briefly, dark-adapted (12 h) rats were anesthetized as previously described [20] and scotopic recordings were performed under a dim red-light condition. Electrical responses were recorded with custom-made silver chloride electrodes as previously described [20]. The ERG items, including dark-adaptation 3.0 response and dark-adaptation 3.0 oscillatory potential response, were evaluated. Subsequently, anesthetized rats underwent FFA testing using HRAplusII (Heidelberg, Germany) after intraperitoneal injecting 0.1 mL/100 g 10% fluorescence sodium (Baiyunshan Mingxing Corporation, China). Sodium fluorescein intravenous imaging time was obtained to evaluate retinal vessel function.

2.6. HE Staining Detection in Diabetic Rats. Retinal histological alterations were visualized by HE staining of rat eye sections. Rats were euthanized by a lethal dose of sodium pentobarbital, and the eyeballs were rapidly removed and enucleated. The eyes were kept immersed for at least 48 h at 4°C in a fixative solution containing 4% paraformaldehyde and embedded in paraffin blocks. 4 μm sections were prepared in the standard manner and stained with HE staining. The layers of outer nuclear layer (ONL) and inner nuclear layer (INL) cells and the thickness of inner and outer segment layer (IS/OS) were calculated for morphometric analysis. Color micrographs were photographed under a digital imaging system.

2.7. Detection of Apoptosis in Diabetic Rats. To determine apoptosis in the retina, we performed TdT-mediated dUTP nick-end labeling (TUNEL) assay labeling the nuclear cut ends of DNA fragments in apoptotic (or necrotic) cells. The detection was conducted following the manufacturer's instructions. DAPI (100 ng/mL) was added in the fluorescent staining procedure to label the nuclei of retinal cells. The fluorescence intensity of the apoptotic signal was quantified by ImageJ software.

2.8. Real Time-Quantitative PCR (RT-qPCR) Analysis in Diabetic Rats. Total RNA was isolated from the retinal samples collected at 12-week diabetic duration, using TRIzol reagent. RNA was converted to cDNA by synthesis according to the manufacturer's protocol of the RevertAid M-MuLV cDNA synthesis kit (Thermo Scientific™, EP0733, USA). Real-time polymerase chain reaction (RT-PCR) was performed on the ABI StepOnePlus Real-Time PCR device with FastStart Universal SYBR-Green Master kit (Roche, Germany). GAPDH was used as a housekeeping gene.

Table 1: General characteristics of the included diabetic patients.

Characteristic	T1DM ($n = 15$)	T2DM ($n = 55$)	CON ($n = 15$)	p value
Female (%)	6(40.0%)	28(50.9%)	8(53.3%)	
Age (years)	40.3 ± 10.8	52.5 ± 11.5$^{\#\#}$	45.8 ± 15.3	0.002
BMI (kg/m^2)	24.9 ± 4.0	24.1 ± 3.6	23.5 ± 3.2	ns
Duration of diabetes (years)	11.8 ± 4.5	18.2 ± 6.8$^{\#\#}$		0.001
Systolic blood pressure (mmHg)	124.7 ± 14.3	130.4 ± 16.4	122.2 ± 14.4	ns
Diastolic blood pressure (mmHg)	75.3 ± 7.9	77.3 ± 9.3	76.3 ± 7.4	ns
HbA1c (%)	7.6 ± 1.0**	7.5 ± 1.1**	5.2 ± 0.6	<0.001
Fasting blood glucose (mmol/L)	8.3 ± 1.1**	7.7 ± 1.1**	5.2 ± 0.8	<0.001
Therapy components				
Diet only (%)	0	0		
Insulin (%)	15(100%)	51(92.7%)		
Sulfonylureas (%)	0(0%)	8(14.5%)		
α-Glucosidase inhibitors (%)	11(73.3%)	31(56.4%)		
Biguanides (%)	9(60.0%)	47 (85.5%)		
Retinal thickness (μm)	279.1 ± 19.8	283.6 ± 18.9	288.9 ± 21.9	ns
ERG test				
Amplitude of max b (μv)	288.5 ± 51.4**	337.1 ± 58.9$^{\#\#}$	367.5 ± 47.8	0.001
Amplitude of OPs2 (μv)	86.3 ± 17.8**	114.2 ± 20.6$^{**\#\#}$	136.3 ± 19.4	<0.001

The results are described as mean ± standard deviation (SD) or number (%). ns: no significance. $^{**}p < 0.01$: T1DM cohort and T2DM cohort vs. CON cohort; $^{\#\#}p < 0.01$: T2DM cohort vs. T1DM cohort.

Primers were as follows: 5′-GAGCAACGTCACTATGCAG ATC-3′ (forward) and 5′-TTTCTCCGCTCTGAACAAGG-3′ (reverse) for VEGF-α, 5′-TGGATTTGGACATGGTTCT GA-3′ (forward) and 5′-GCGGGTGTAGCTGAAGAAGT-3′ (reverse) for ALDH2, 5′-GCTCGCCTTGCTGTGGACT TC-3′ (forward) and 5′-GTGACACAGAGATGGCTGG AACTG-3′ (reverse) for SIRT1, and 5′-CAAGTTCAACG GCACAGTCAA-3′ (forward) and 5′-CGCCAGTAGAC TCCACGACA-3′ (reverse) for GAPDH. Quantification of VEGF-α, ALDH2, and SIRT1 mRNA expressions was calculated by normalizing with the GAPDH mRNA expression. Analysis was performed using the $2^{-\Delta\Delta Ct}$ method.

2.9. Immunofluorescence Staining in Diabetic Rats. The immunofluorescence staining and quantitation of VEGF-α, ALDH2, SIRT1, SOD1, eNOS, iNOS, and VEGF Receptor2 in rat retinas were performed as described in our previous study [20]. In brief, after deparaffinization and antigen restoration, eye sections were blocked in 1% bovine serum albumin for 1 h and stained overnight at 4°C with VEGF-α (1 : 200; #GTX102643, GeneTex), ALDH2 (1 : 200; #ab108306, Abcam,), SIRT1 (1 : 200; #ab110304, Abcam), NOX4 (1 : 200; #ab133303, Abcam), SOD1 (1 : 200; #ab51254, Abcam), eNOS (1 : 200; #ab5589, Abcam), iNOS (1 : 200; #18985-1-AP, Proteintech Group, Inc.), and VEGF Receptor2 (1 : 200; #9698, Cell Signaling Technology) primary antibody. Then, the slides were incubated with HRP-IgG (H + L) secondary antibody (#EK022, #EK012, Zhuangzhibio, China) at 1 : 200 dilution for 1 hour, and the nuclei were stained with 4-6-diamidino-2-phenylindole (DAPI). Images were captured by a fluorescence microscope.

2.10. Immunoblotting in Diabetic Rats. The whole retina was dissected, and protein was isolated as described previously [23]. Sodium dodecyl sulfate-polyacrylamide gel electrophoresis (SDS-PAGE) of retinal proteins was performed with Tris-glycine-SDS running buffer (NCM Biotech, China). Next, the proteins from the gels were transferred onto the PVDF membrane (Millipore, US) with electroblotting. After blocking with 5% nonfat milk solution, membranes were incubated with ALDH2 (1 : 1000; #ab108306, Abcam), VEGF-α (1 : 1000; #ab46154, Abcam), SIRT1 (1 : 1000; #ab110304, Abcam), Bax (1 : 1000; #ab32503, Abcam), Bcl-2 (1 : 1000; #ab182858, Abcam), Caspase 3 (1 : 1000; #19677-1-AP, Proteintech Group, Inc.), 4-HNE (1 : 1000; #ab46545, Abcam), hypoxia-inducible factor-1α (HIF-1α) (1 : 1000; #ab1, Abcam), VEGF Receptor2 (1 : 1000; #9698, Cell Signaling Technology), and GAPDH (1 : 1000; #5174, Cell Signaling Technology) overnight at 4°C. Binding of HRP-conjugated secondary antibody (1 : 10000; #EK020, #EK010; Zhuangzhibio, China) was observed using enhanced chemiluminescence (Thermo Fisher Scientific). All blots were quantified by densitometry using ImageJ software (NIH).

2.11. Determination of the Retinal Total ROS and Mitochondrial DNA Damage in Diabetic Rats. The fluorescent probe 2′,7′-dichlorofluorescein diacetate (DCHFDA; Sigma, USA) was applied to quantify total ROS levels of

Table 2: ALDH2 polymorphisms in DM and healthy individuals.

ALDH2 genotype (rs671)	T1DM ($n = 15$)	T2DM ($n = 55$)	CON ($n = 15$)
ALDH2GG (%)	9 (60%)	48 (87.3%)	14 (93.3%)
ALDH2GA (%)	4 (26.7%)	5 (9.1%)	1 (6.7%)
ALDH2AA (%)	2 (13.3%)	2 (3.6%)	0 (0.0%)
ALDH2GA/AA (%)	6 (40.0%)*	7 (12.7%)#	1 (6.7%)

The results are described as number (%). *$p < 0.05$: T1DM cohort and T2DM cohort vs. CON cohort; #$p < 0.05$: T2DM cohort vs. T1DM cohort.

the retina. Specifically, 10 μg protein extracted from the retina was incubated with 2 μmol/L DCHFDA for 10 minutes and the resultant fluorescence intensity was detected at excitation wavelength of 485 nm and emission wavelength of 530 nm [32, 33]. Mitochondria were isolated from retina tissues by using the Mitochondria Isolation kit (Sigma, USA) in compliance with the manufacturer's protocols. Total DNA was isolated with a DNeasy blood and tissue kit (Qiagen, USA), and extended-length PCR was performed by amplification of long and short regions of mitochondrial DNA (mtDNA). Un-Scan-It Gel digitizing software was used to capture the intensity of PCR gel photographs, and then, the ratio of the long (13.4 kb) to short fragment (210 bp) of PCR amplicons was estimated. The primers of mtDNA long were 5′-AAAATCCCGCAAACAATGACC ACCCC-3′ (forward) and 5′-GGCAATTAAGAGTGGG ATGGAGCCAA-3′ (reverse). The primers of mtDNA short were 5′-CCTCCCATTCATTATCGCCGCCCTTGC-3′ (forward) and 5′-GTCTGGGTCTCCTAGTAGGTCTGG GAA-3′ (reverse). The mtDNA damage was denoted by the decreased ratio of long to short amplicons [33].

2.12. Determination of Inflammatory Parameters in Diabetic Rats. Retinal tissues were collected at 12 weeks post diabetic rat model established. Interleukin-1 (IL-1) and interleukin-6 (IL-6) levels in retinas and insulin in serum were assessed using a commercially available enzyme-linked immunosorbent assay (ELISA) kit from Westang Bio-Tech Co., LTD. (Shanghai, China) according to the manufacturer's instructions.

2.13. Statistical Analysis. The statistical software SPSS, version 19.0 (IBM Co., USA), was applied to perform the statistical analysis. Student's t-test was used for two-group comparison, and one-way ANOVA followed by Fisher's Least Significant Difference (LSD) post hoc analysis was performed to examine the statistical differences among multiple groups. The chi-squared test (Fisher's exact test) was used to analyze the distributions of allele and genotype frequencies. Categorical variables were expressed as percentages, and continuous data are presented as mean ± standard deviation (SD). All p values ≤ 0.05 were considered as statistically significant.

3. Results

3.1. The Characteristics of Preclinical DR Patients. The general characteristics of diabetic patients with no clinical manifestation of DR are presented in Table 1. The diabetic patients were classified into two cohorts by type of diabetes, and there were 15 patients with T1DM and 55 patients with T2DM. Moreover, 15 healthy individuals were included as the control (CON). The blood glucose levels exhibited no statistically significant difference (fasting blood glucose level < 10 mmol/L) between T1DM and T2DM patients, because of a well-maintained blood glucose control by insulin therapy and/or oral hypoglycemic drugs. Besides, whole retinal thickness showed no statistically significant difference among T1DM, T2DM, and CON individuals. Noteworthily, the T1DM patients in DR preclinical period had a significantly lower ERG amplitude, especially in b wave (dark-adapted 3.0 response) and OPs2 wave, when compared to the T2DM and CON individuals (all $p < 0.05$). However, the b wave (dark-adapted 3.0 response) of the ERG test in T2DM and CON individuals showed no significant difference ($p > 0.05$).

3.2. The Gene Polymorphisms of ALDH2 in Preclinical DR Patients. The above results indicated that the retinal function had been decreased more in T1DM compared with T2DM before clinically detectable DR. To investigate the potential role of ALDH2, ALDH2 gene types (ALDH2 rs671 polymorphisms: including ALDH2GG, ALDH2GA, and ALDH2AA) in different cohorts were detected. It was known that those who carried an A allele are related to deficient ALDH2 activity. As shown in Table 2, we found the number of patients or healthy individuals with ALDH2GA/AA genotype was small, and there is no significant difference in the distribution of ALDH2 genotypes. However, the allele frequencies for ALDH2GA/AA in T1DM patients were statistically more than T2DM patients and CON individuals (all $p < 0.05$). In contrast, there was no significant difference in ALDH2-GA/AA genotype distribution between T2DM patients and healthy individuals ($p > 0.05$). Taken together, our data suggested that the risk of DR development in patients with T1DM was potentially associated with ALDH2 deficiency.

3.3. ALDH2 Activity and SIRT1 Expression in Preclinical DR Patients. To further explore whether the ALDH2 activity could be related to preclinical DR patients' retinal function, serum ALDH2 activity was estimated. As showed in Figure 1(a), T1DM patients presented a significantly lower level of serum ALDH2 activity compared with CON individuals ($p < 0.01$). Interestingly, the serum ALDH2 activity in T1DM patients was evidently decreased compared with that in T2DM patients ($p < 0.01$). Additionally, the potential associations between ALDH2 and SIRT1 were once revealed by our previous work [20]. As shown in Figure 1(b), the serum SIRT1 level in T1DM patients was downregulated compared to T2DM patients and CON individuals (all $p < 0.05$). Moreover, there existed a significant difference in serum SIRT1 level between T2DM patients and CON individuals ($p < 0.05$).

3.4. The Blood Glucose Level, Insulin Concentration, and Retinal Function in Diabetic Rats. The blood glucose of the CON group was 6.24 ± 0.97 mmol/L at the initial. And the blood glucose level of the T1DM group was 19.67 ± 3.85

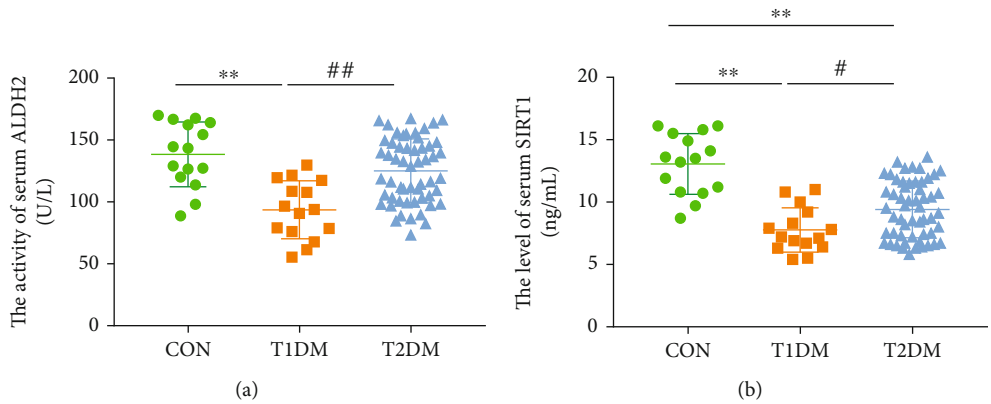

Figure 1: ALDH2 activity and SIRT1 expression in preclinical DR patients and healthy individuals; (a) the activity of serum ALDH2; (b) the level of serum SIRT1. Values are presented as mean ± SD, $n = 15$, 55, and 15. $^{**}p < 0.01$: T1DM cohort and T2DM cohort vs. CON cohort; $^{\#}p < 0.05$ and $^{\#\#}p < 0.01$: T2DM cohort vs. T1DM cohort.

mmol/L, and the T2DM group was 20.23 ± 4.26 mmol/L. There existed no significant difference between the T1DM group and the T2DM group ($p > 0.05$). After a 12-week study, the level of blood glucose in the T1DM group was 23.84 ± 2.85 mmol/L and the T2DM group was 24.51 ± 4.63 mmol/L with no statistically significant difference ($p > 0.05$) (Figure 2(a)). Moreover, the level of blood insulin in the T1DM group was 0.17 ± 0.02 ng/mL and that in the T2DM group was 0.24 ± 0.05 ng/mL, while the blood insulin level in the CON group was 0.30 ± 0.08 ng/mL after a 12-week study (Figure 2(b)). As we could see, the blood insulin level in the CON and T2DM groups was all higher than the T1DM group (all $p < 0.05$), while there existed no significant difference between the CON group and the T2DM group ($p > 0.05$).

To evaluate the retinal function of both types of DM at 12 week's durations, ffERG and FFA were performed. As shown in Figures 2(c)–2(e) and 2(h), the amplitude of a wave (dark-adaptation 3.0 response) and OPs2 wave (dark-adaptation 3.0 oscillatory potential response) in both the T1DM and T2DM groups obviously declined at 12-week diabetic duration compared to the CON group (all $p < 0.05$). And the T2DM group showed much better performances in the amplitude of a and OPs2 waves relative to T1DM. Furthermore, Figures 2(f) and 2(g) show the amplitude of b wave (dark-adaptation 3.0 response) in the T1DM group was significantly lower than that in the CON group ($p < 0.01$) and the peak time of b wave (dark-adaptation 3.0 response) in the T1DM group was significantly longer than the CON group ($p < 0.01$). Interestingly, in the T2DM group, the amplitude of b wave (dark-adaptation 3.0 response) was obviously higher than that in the T1DM group ($p < 0.05$); meanwhile, the peak time of b wave was significantly shorter ($p < 0.05$). However, the amplitude and peak time of b wave (dark-adaptation 3.0 response) existed no statistically significant difference between the T2DM group and the CON group (all $p > 0.05$). As for rats' retinal vessel microcirculation function, it is shown in Figure 2(i) and 2(j) that the fluorescein sodium appearing time in the retinal vein in the T1DM group (28.44 ± 4.85 s) was evidently prolonged compared to the CON (14.45 ± 2.24 s) and T2DM groups (18.67 ± 3.28 s) (all $p < 0.05$), whereas the difference between the T2DM group and the CON group did not achieve statistical significance ($p > 0.05$).

3.5. Retinal Morphological Structure and Apoptosis in Diabetic Rats. HE staining and TUNEL assay were applied to evaluate retinal morphometric structure changes and determine whether cell apoptosis partly caused this phenomenon. As shown in Figures 3(a) and 3(b), compared with the CON group, an extremely decreasing thickness of photoreceptors' inner and outer segment layer (IS/OS) was observed in both DM groups (all $p < 0.05$). Moreover, T1DM had significantly lesser cell layers of outer nuclear layer (ONL) which consists of photoreceptors' (cone and rod cells) nucleus, compared to the CON group ($p < 0.05$) (Figure 3(c)). Significantly, T1DM exhibited thinner IS/OS and ONL layers relative to T2DM retinas (all $p < 0.05$). When it came to the cell layers of the inner nuclear layer (INL), despite the T1DM group showed a decreasing tendency compared with the CON group, there existed no statistically significant difference among CON, T1DM, and T2DM ($p > 0.05$) (Figure 3(d)). Subsequently, it is shown in Figure 3(e) that apoptosis obviously occurred in T1DM retinas rather than T2DM retinas, especially in photoreceptor layers (ONL), compared with CON retinas according to TUNEL assay (all $p < 0.01$). This was further proved by the prominent elevated expression of proapoptotic molecules Bax and Caspase 3 and depressed antiapoptotic Bcl-2 in T1DM retinas, when compared to the CON and T2DM groups ($p < 0.05$) (Figures 3(f)–3(i)).

3.6. Retinal ALDH2 and SIRT1 Expression in Diabetic Rats. The mRNA expression of retinal ALDH2 and SIRT1 was detected by the RT-PCR method. Meanwhile, the protein expression of ALDH2 and SIRT1 was measured both via immunofluorescence and Western blotting assays. As shown in Figure 4(a), SIRT1 was strongly expressed in ONL, INL, and ganglion cell layer (GCL), which consisted with ALDH2, which was wildly expressed in metabolically active position. The mRNA expression of retinal ALDH2 and SIRT1 in the

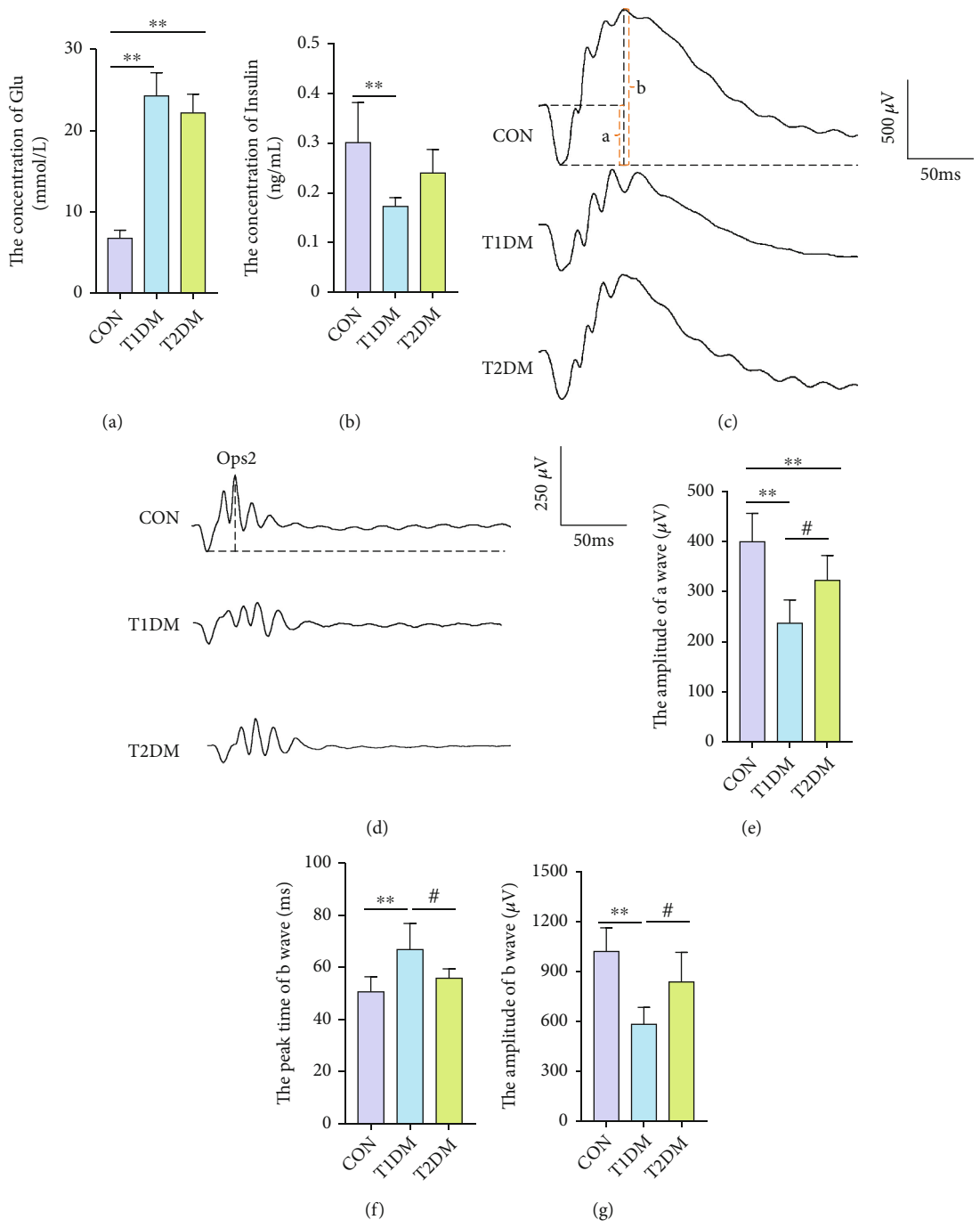

Figure 2: Continued.

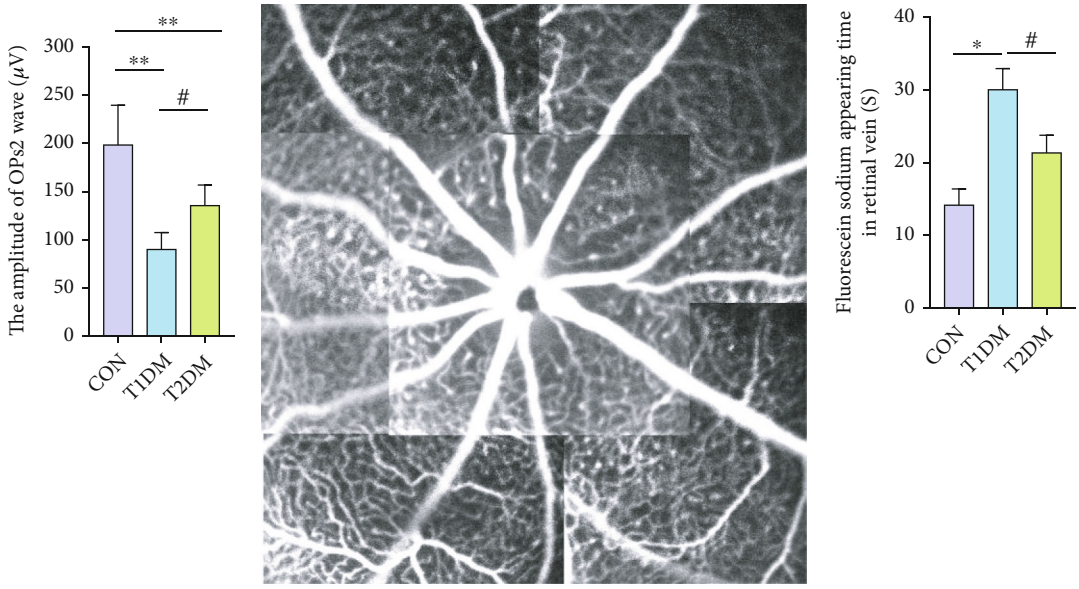

(h) (i) (j)

Figure 2: The retinal electrical activity and retinal vessel microcirculation function in the CON, T1DM, and T2DM groups after a 12-week study: (a) the concentration of blood glucose; (b) the concentration of blood insulin; (c) presentive images of a, b wave (dark-adaptation 3.0 response) and (d) OPs2 wave (dark-adaptation 3.0 oscillatory potential response); (e) the amplitude of a wave; (f) the peak time of b wave; (g) the amplitude of b wave; (h) the amplitude of OPs2 wave; (i) the representative fundus fluorescein angiography picture; (j) the fluorescein sodium appearing time in the retinal vein. Values are presented as mean ± SD, $n = 15$ or 6, respectively. $^{*}p < 0.05$ and $^{**}p < 0.01$: the T1DM group and the T2DM group vs. the CON group; $^{\#}p < 0.05$: the T2DM group vs. the T1DM group.

T1DM group was lesser than the CON and T2DM groups (all $p < 0.05$) (Figures 4(b) and 4(c)). However, the mRNA expression of ALDH2 and SIRT1 in the CON group and the T2DM group existed no significant difference (all $p > 0.05$). Moreover, the protein expression of ALDH2 and SIRT1 in the T1DM group was significantly decreased compared with both the CON and T2DM groups indicated by immunofluorescence and Western blotting detections (all $p < 0.05$) (Figures 4(a) and 4(d)–4(f)). Interestingly, the protein expression of ALDH2 and SIRT1 showed no significant difference between the T2DM and CON groups according to Western blotting (all $p > 0.05$) (Figures 4(d)–4(f)). The outcomes of Western blotting were in accordance with immunofluorescence staining.

3.7. Retinal VEGF-α, HIF-1α, and VEGFR2 Expressions in Diabetic Rats. To estimate the reaction of neovascularization in the retina, angiogenesis mediators VEGF-α, HIF-1α, and VEGFR2 were measured at 12-week diabetic duration. As shown in Figures 5(a) and 5(d), VEGF-α was strongly expressed in the external limiting membrane (ELM), inner plexiform layer (IPL), and ganglion cell layer (GCL); meanwhile, HIF-1α and VEGFR2 immunoreactivities were observed in ONL and INL, and GCL. It was found that the protein expression of VEGF-α in T1DM retinas was more than those in the CON and T2DM groups (all $p < 0.05$), while there existed no significant difference between CON and T2DM (all $p > 0.05$) (Figures 5(e) and 5(f)). Moreover, VEGFR2, the angiogenic receptor of VEGF, was extremely increased in T1DM, compared to CON and T2DM (all $p < 0.05$) (Figures 5(b), 5(e), and 5(h)). Additionally, although retinal HIF-1α, a VEGF transcriptional regulator, was increased in both types of DM relative to CON as demonstrated in Figure 5(c), T1DM exhibited a much greater increase of HIF-1α expression compared to T2DM, which was confirmed by both Western blotting and immunofluorescence (Figures 5(e) and 5(g)). It could indicate that the changes of retinal HIF-1α and VEGFR2 levels in T1DM were closely correlated to the elevating expression of VEGF-α.

3.8. The Retinal iNOS/eNOS Ratio and Inflammation in Diabetic Rats. Immunofluorescence assay was further performed to identify iNOS/eNOS imbalance in the diabetic retina. According to our study (data not shown), the retinal iNOS level was notably elevated in T1DM ($p < 0.05$) at 12-week diabetic duration, compared to CON and T2DM, whereas there existed no statistically significant difference of retinal eNOS expression among all groups ($p > 0.05$). Surprisingly, the iNOS/eNOS ratio in T1DM and T2DM retinas exhibited an obvious increase compared with CON retinas, which denoted an imbalance of iNOS/eNOS in diabetic retinas, especially in T1DM when compared to T2DM (all $p < 0.05$) ((Figures 6(a) and 6(b)). Undoubtedly, enhanced iNOS level could be a biomarker of the vicious inflammatory milieu in the diabetic retina. Accordingly, proinflammatory cytokines IL-1 and IL-6 were also measured via ELISA assay. As shown in Figure 6(c), retinal IL-1 production in the T1DM group was significantly increased compared with both the CON and T2DM groups (all $p < 0.01$), while there existed no significant difference between the CON group and the T2DM group ($p > 0.05$). As for IL-6, the retinal

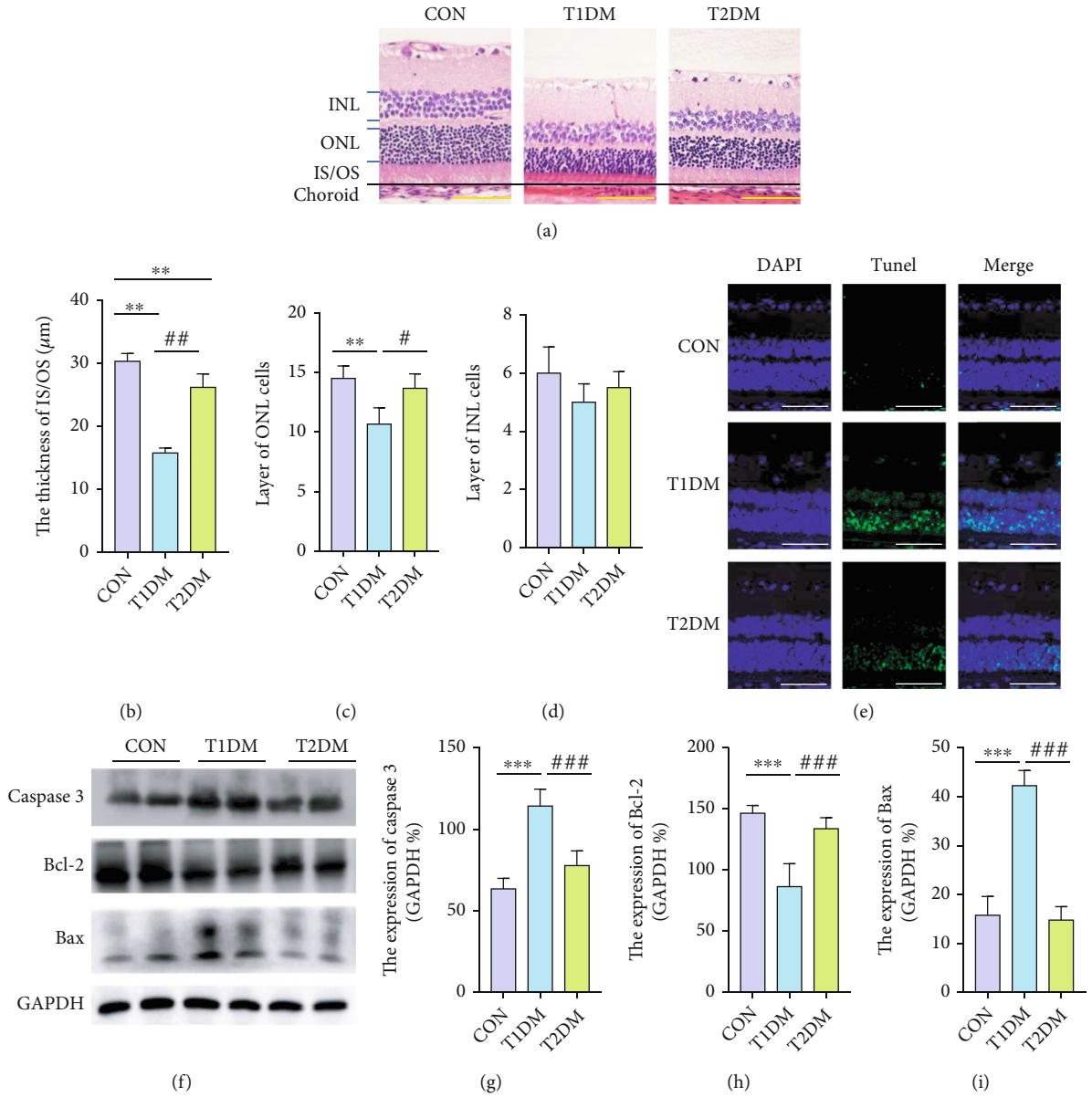

Figure 3: The number of retinal cell layers in the CON, T1DM, and T2DM groups detected by HE staining after a 12-week study: (a) the representative HE staining picture; (b) the thickness of OS/IS layer; (c) the layer of ONL cells; (d) the layer of INL cells; (e) the presented TUNEL images; (f) the representative Western blotting picture of Caspase 3, Bcl-2, and Bax; (g) the relative protein expression of Caspase 3; (h) the relative protein expression of Bcl-2; (i) the relative protein expression of Bax. INL: inner nuclear layer; ONL: outer nuclear layer; IS/OS: inner and outer segment layer; RPE: retinal pigment epithelial. Scale bar: 100 μm. Values are presented as mean ± SD, $n = 4$-6. $^{**}p < 0.01$, and $^{***}p < 0.001$: the T1DM group and the T2DM group vs. the CON group; $^{\#}p < 0.05$, $^{\#\#}p < 0.01$, and $^{\#\#\#}p < 0.001$: the T2DM group vs. the T1DM group.

production in T1DM was also increased compared with both the CON and T2DM groups (all $p < 0.05$), while there existed no significant difference between the CON and the T2DM ($p > 0.05$) at 12-week diabetic duration (Figure 6(d)).

3.9. Retinal Oxidative and Mitochondrial DNA Damage Level in Diabetic Rats. It was found that antioxidative enzyme superoxide dismutase 1 (SOD1) and ROS-producer NADPH oxidase 4 (NOX4) were both actively expressed mainly in retinal ONL, INL, and GCL (Figure 7(a)). SOD1 was notably declined in T1DM compared to the CON and T2DM retina, while NOX4 was notably elevated in T1DM compared to the CON retina (all $p < 0.05$) (Figures 7(b) and 7(c)). Although there were prominent reductions of retinal SOD1 in T2DM, there existed no statistically significant difference in NOX4 expressions between CON and T2DM. According to Figure 7(d), the retinal total ROS level was notably elevated in both T1DM and T2DM rats at 12-week diabetic duration, while there was a relatively lower level of ROS in the T2DM retina compared to the T1DM retina (all $p < 0.05$). It is known that mtDNA is highly susceptible to oxidative stress. As shown in

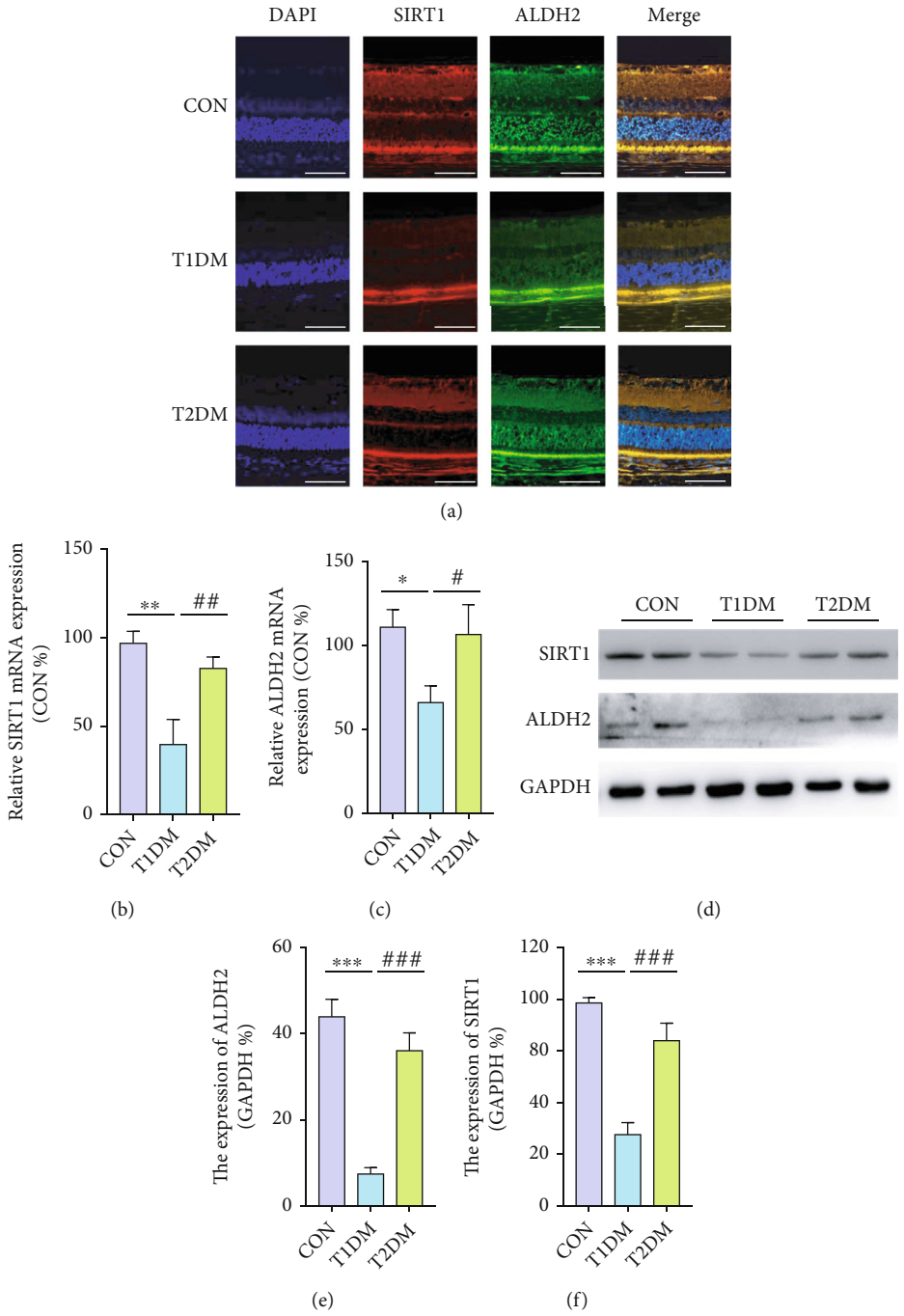

Figure 4: The protein and mRNA expressions of retinal SIRT1 and ALDH2 detected by immunofluorescence, RT-PCR, and Western blotting in the CON, T1DM, and T2DM groups after a 12-week study: (a) the representative immunofluorescence picture of ALDH2 and SIRT1; (b) the relative mRNA expression of ALDH2; (c) the relative mRNA expression of SIRT1; (d) the representative Western blotting picture of ALDH2 and SIRT1; (e) the relative protein expression of ALDH2; (f) the relative protein expression of SIRT1. Scale bar: 100 μm. Values are presented as mean ± SD, $n = 3$-4. $^{*}p < 0.05$, $^{**}p < 0.01$, and $^{***}p < 0.001$: the T1DM group and the T2DM group vs. the CON group; $^{\#}p < 0.05$, $^{\#\#}p < 0.01$, and $^{\#\#\#}p < 0.001$: the T2DM group vs. the T1DM group.

Figure 7(e), despite increased ROS in the retina, mtDNA was not statistically significantly damaged in the T2DM retina ($p > 0.05$). Nevertheless, evident mtDNA damage was observed in the T1DM retina compared to that in the T2DM and CON groups ($p < 0.05$).

4. Discussion

Our clinical investigation found an identifiable retinal dysfunction in both T1DM and T2DM patients at preclinical diabetic retinopathy stage. To our surprise, although the

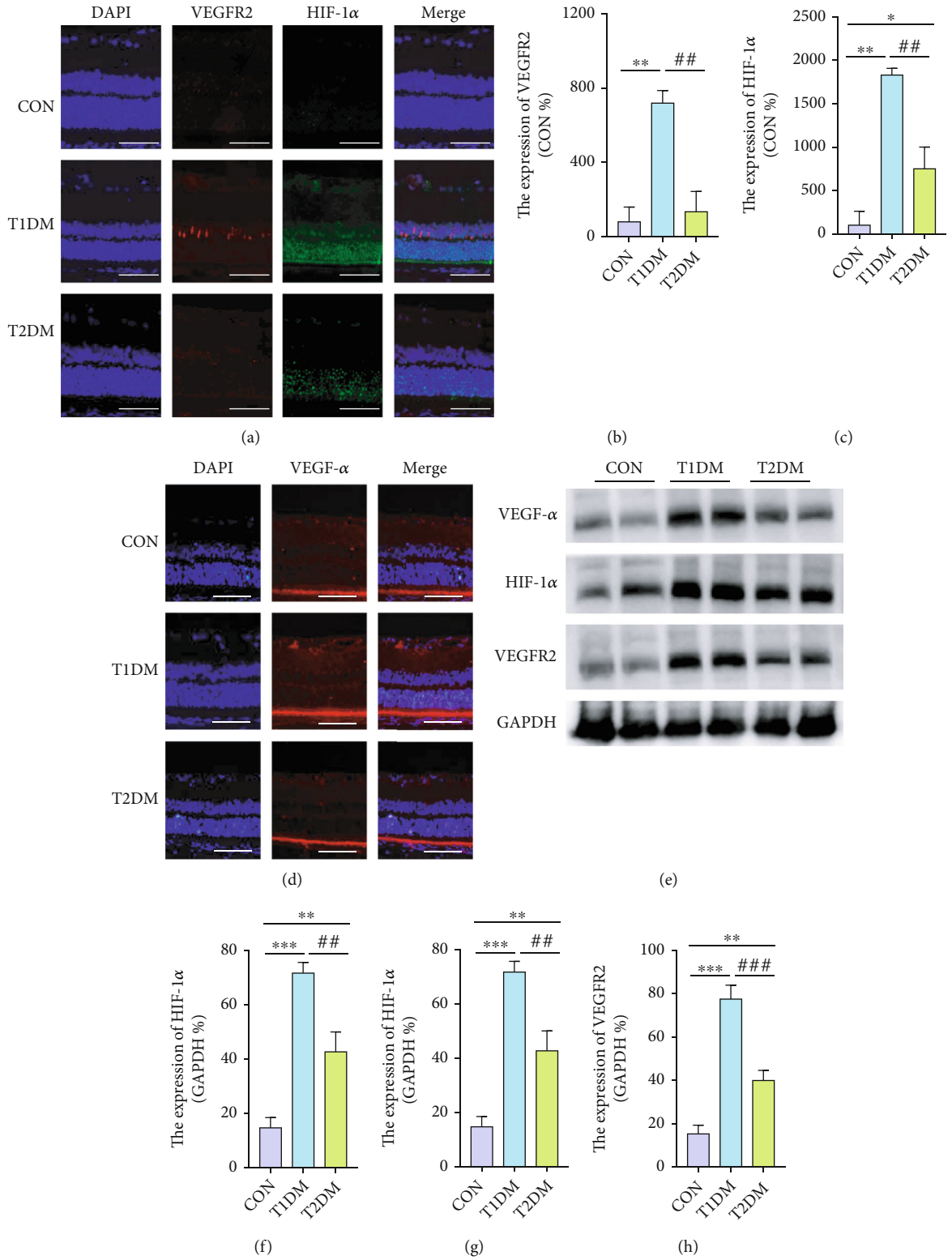

Figure 5: The expressions of retinal VEGF-α, HIF-1α, and VEGFR2 in the CON, T1DM, and T2DM groups after a 12-week study: (a, d) the representative immunofluorescence picture of VEGF-α, HIF-1α, and VEGFR2; (b) the relative expression of VEGFR2; (c) the relative expression of HIF-1α; (e) the representative Western blotting picture of VEGF-α, HIF-1α, and VEGFR2; (f–h) the relative protein expression of VEGF-α, HIF-1α, and VEGFR2. Scale bar: 100 μm. Values are presented as mean ± SD, $n = 3$-4. $^{*}p < 0.05$, $^{**}p < 0.01$, and $^{***}p < 0.001$: the T1DM group and the T2DM group vs. the CON group; $^{\#}p < 0.05$, $^{\#\#}p < 0.01$, and $^{\#\#\#}p < 0.001$: the T2DM group vs. the T1DM group.

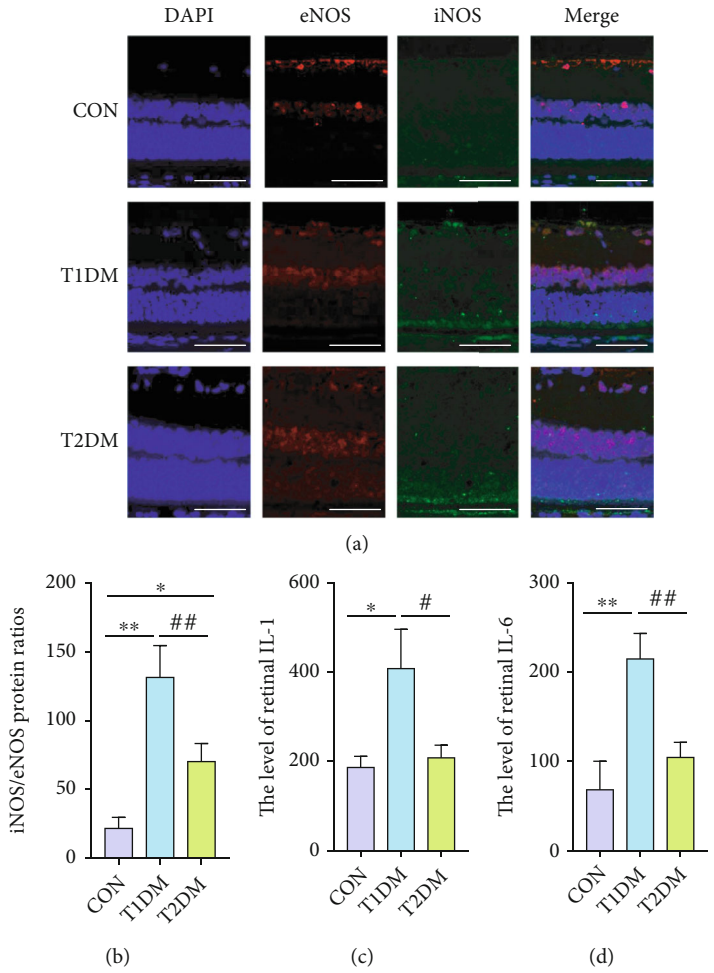

FIGURE 6: The level of retinal iNOS, eNOS, IL-1, and IL-6 in the CON, T1DM, and T2DM groups after a 12-week study: (a) the representative immunofluorescence picture of iNOS and eNOS; (b) the ratio of iNOS expression to eNOS expression; (c) the level of retinal IL-6; (d) the concentration of retinal IL-1. Scale bar: 100 μm. Values are presented as mean ± SD, $n = 3$-4. $^{*}p < 0.05$ and $^{**}p < 0.01$: the T1DM group and the T2DM group vs. the CON group; $^{\#}p < 0.05$ and $^{\#\#}p < 0.01$: the T2DM group vs. the T1DM group.

disease duration of T1DM patients was shorter, the retinal function of the patients was seriously poor. Additionally, serum ALDH2 activity and SIRT1 expression in T1DM patients were significantly lower than those in T2DM patients. To further verify this phenomenon, we constructed the T1DM and T2DM rats' model to study the potential difference in retinal morphology, function, and molecular biological marker and explore the possible mechanism.

As we all know, diabetic retinopathy can both trigger retinal microvessel and neuron cell damages. The oscillatory potential (OPs) wave, a component of the electroretinographic test, is regarded as a valuable indicator to evaluate retinal vessel-related disorders (retinal ischemia caused by reduced circulation) [34, 35]. Our results showed retinal vessel microcirculation function in both T1DM and T2DM rats attenuated to a lower level, but T1DM deteriorated much more rapidly and seriously, which has also been proved by increased fluorescein sodium appearing time. In fact, this was in line with other findings which revealed that diminished OPs wave amplitudes were found in persons with DM and no photographic evidence of background retinopathy [35].

In the study, we demonstrated that T1DM and T2DM jeopardized rats' retinas mainly at outer layers. This finding was supported by our several observations: (1) typical thinning occurred at the outer layers/photoreceptor layer (including ONL and IS/OS); (2) the prominent apoptotic cells were largely concentrated at the outer layers; (3) the negative wave of ERG (dark-adaptation 3.0 response) called a wave, reflecting the light absorption activity of the photoreceptors, depressed significantly. So, why was the outer retina extremely vulnerable to hyperglycemia? Primarily, there exists vigorous energy metabolism activity in the outer retina accompanied with a great number of metabolic wastes and mitochondrial damages all the time. The similar finding was also verified, in which, mtDNA damage was obviously occurred and even continued when hyperglycemia state continued in T1DM Wistar rat [36, 37]. Secondly, photoreceptors are fragile in some way, with limited nutritional supply and restricted resistant ability to adverse environments. Finally, the protective threshold of cellular stress response is limited, and the sophisticated cellular metabolism pathways are involved, which results in infaust resistance ability. Interestingly, the inner nuclear layers did not

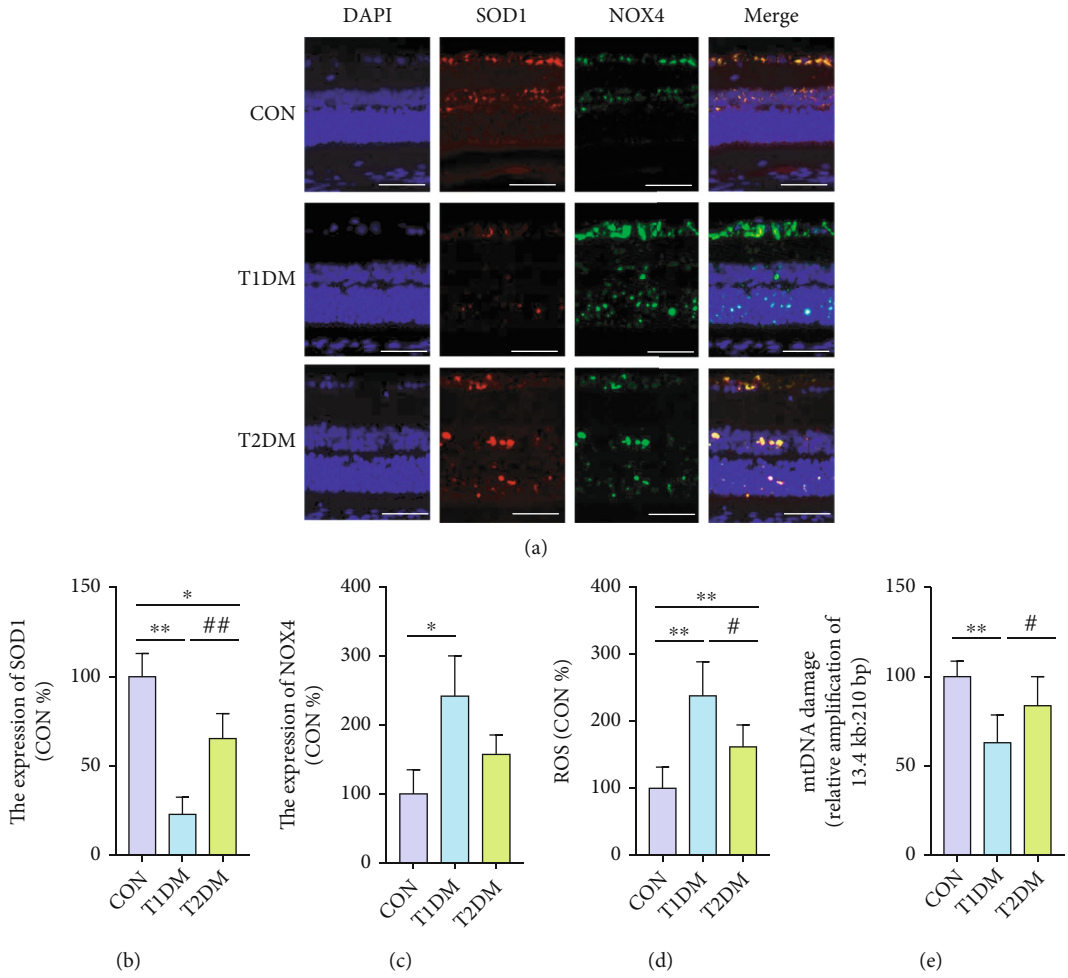

Figure 7: The levels of retinal SOD1, NOX4, total ROS, and mtDNA damage in the CON, T1DM, and T2DM groups after a 12-week study: (a) the representative immunofluorescence picture of SOD1 and NOX4; (b) SOD1 immunofluorescence levels normalized to CON; (c) NOX4 immunofluorescence levels normalized to CON; (d) the retinal total ROS level; (e) damage of mtDNA in the retina. Scale bar: 100 μm. Values are presented as mean ± SD, $n = 3$-4. $^{*}p < 0.05$ and $^{**}p < 0.01$: the T1DM group and the T2DM group vs. the CON group; $^{\#}p < 0.05$ and $^{\#\#}p < 0.01$: the T2DM group vs. the T1DM group.

significantly decrease in both T1DM and T2DM rats, and we supposed that despite the obvious dysfunction in photoreceptors, Müller, and bipolar cells, the morphological changes of inner retinal would probably intact at this early stage of DR.

It is widely realized that increasing reactive oxygen species (ROS) generation could impair antioxidant defenses, which decreases the ability of retinal cell homeostasis sustaining [38]. The data collected in our study showed that the level of retinal total ROS and ROS-producer NOX4 was significantly elevated in T1DM rats, while the expression of antioxidant SOD1 was obviously diminished. Moreover, oxidative stress levels and proinflammatory factors, such as IL-1, IL-6, and iNOS, were notably increased in T1DM rats. Recently, studies found that DM was well-recognized as a result of subclinical chronic low-grade inflammation event [39, 40]. Epidemiological studies revealed that levels of inflammatory cytokines, such as IL-6, IL-1β, and TNF-α, were prominently increased in DM patients [40]. In the case of the dynamic inflammation level alterations in different retinopathy stages, clinical studies showed that serum IL-6 was significantly increased in both the nonproliferative DR and proliferative DR but not in no DR patients with T2DM [26, 41]. Undeniably, higher IL-6 levels are potential risk factors for DR in T2DM. In the present study, diabetic rats with T2DM also showed no statistically significant difference in retinal IL-1 and IL-6 level compared with CON rats. We postulated that 12-week diabetic duration was not the advanced retinopathy stage for T2DM rats.

As we all know, hyperglycemia impairs vascular endothelium resulting in the breakdown of the blood-retinal barrier (BRB) integrity, the enhanced retinal microvascular permeability, and subsequently neovascularization [42–45]. In our animal study, despite the varying increased retinal proangiogenic reaction in both DM, the expression of VEGF-α was dramatically lesser in the T2DM group compared with the T1DM group. This relatively slighter

angiogenic reaction in the diabetic retina of T2DM was also convincingly verified by the less increasing of HIF-1α and VEGFR2, the transcriptional regulator, and receptor of VEGF, respectively. A previous clinical study proved that an increase of serum VEGF level is associated with the severity of diabetic retinopathy in T2DM patients [46]. Particularly, it demonstrated the level of VEGF showed a significant difference between controls and DR, while no significant difference was observed between controls and no DR in patients with clinically T2DM [46]. However, it was reported that the increased level of VEGF was found already in type 1 diabetic children and adolescents without clinical signs of retinopathy or in the early stages of nonproliferative retinopathy [47]. It suggests that VEGF activation occurs in both types of diabetes but increases less radically and slower in T2DM. Our results in the animal study were consistent with these studies. Meantime, it is convinced that the shift in eNOS and iNOS, the endothelial isoform, and inducible isoform of NO synthase, respectively, are implicated in vascular pathologic processes in DR [25, 48]. In line with those studies, we observed a significant increase of the iNOS/eNOS ratio in T1DM retinas. This imbalance was the consequence of oxidative stress injuries and stimulated by proinflammatory cytokines, indicating the presence of radical inflammatory events and vascular endothelial dysfunction in the T1DM retina which somehow explained the poor ERG outcome.

Interestingly, in the present study, mitochondrial ALDH2 was diminished much more in T1DM patients/rats. It was found that ALDH2 was wildly expressed in ONL, inner nuclear layer (INL), and ganglion cell layer (GCL), which featured with an active metabolism. Interestingly, nuclear SIRT1 was also wildly expressed in ONL, INL, and GCL, which was colocated with ALDH2 confirmed by immunofluorescent staining. In addition to that, the distinguished overall mtDNA damage which was extremely sensitive to oxidative stress [33, 36] was observed in the T1DM retina. We speculated that the mitochondrial-nuclear communication between ALDH2 and SIRT1 could alleviate oxidative stress, restore redox homeostasis, and improve the mitochondrion function. To some extent, the present study demonstrated an improved understanding of the ALDH2/-SIRT1 interplays, which may elucidate new therapeutic targets for the treatment of DR.

Accordingly, the functional and structural pathological alterations and deleterious oxidative stress reactions have been demonstrated in diabetic rats' retina, especially in T1DM when compared with T2DM. Moreover, the relative lower retinal ALDH2 and SIRT1 expressions, and elevated angiogenic factors were observed in the T1DM retina. Besides, the potential role of ALDH2 in DR and the highly accordant variation tendency of ALDH2 and SIRT1 were once elucidated by our previous work. We supposed that ALDH2/SIRT1 could be related to protecting the retina from ROS damage, alleviating hypoxic ischemic situation and attenuating angiogenic reaction. Thus, it is revealed that ALDH2/SIRT1 may play important roles during physiological and pathological processes of DR.

While the preliminary clinical retrospective observation study demonstrated the potential association between ALDH2/SIRT1 deficiency and DR progression, it is undeniable that the quantity of clinical cases was not sufficient and some essential tests were missed. Therefore, the findings need further thorough study with longer follow-up times for more reliable clinical results to verify the role of ALDH2/SIRT1 in different types of DM during DR development. As for the animal study, the 12-week observation period also seems not long enough and a single detection point was limited. Actually, in the beginning, we were interested in whether T1DM and T2DM showed a different diabetes-related retinal disorder in preclinical DR stage/a certain lasting period. Fortunately, the clinical observations were impressive and some common results were found in animal tests. As for the underlying reason for such difference of retinal ALDH2/SIRT1 and oxidative stress between T1DM and T2DM, further exploration is needed. On the basis of insulin secretion deference, we suspected that the insulin signaling pathway (insulin resistance and reduced glucose utilization), such as phosphoinositide 3-kinase (PI3K)/protein kinase B (AKT) signaling, could be involved in inducing differential protein changes in retinal tissue. Therefore, in the near future, we would like to thoroughly design experiments in both clinical cases and animal models to observe the specific diabetic retinal function and structure changes along with T1DM and T2DM duration and explore the potential role of ALDH2/SIRT1 in the process of diabetic retinal damage.

In summary, we found retinal function and structure injury induced by T1DM was more severe than T2DM in the certain period through clinical and animal study. And we first demonstrated that the slighter retinal disorders in T2DM would be related to the activation of the ALDH2/-SIRT1 pathway.

Abbreviations

4-HNE: 4-Hydroxynonenal
AGEs: Advanced glycation end products
ALDH2: Aldehyde dehydrogenase 2
ALEs: Advanced lipoxidation end-products
BCVA: Best-corrected visual acuity
DM: Diabetes mellitus
DR: Diabetic retinopathy
eNOS: Endothelial nitric acid synthase
ERG: Electroretinograms
GCL: Ganglion cell layer
HIF-1α: Hypoxia-inducible factor-1α
IL-1: Interleukin-1
IL-6: Interleukin-6
INL: Inner nuclear layer
iNOS: Inducible nitric acid synthase
IS/OS: Inner and outer segment layer
ISCEV: International Society for Clinical Electrophysiology of Vision
MtDNA: Mitochondrial DNA
NAD: Nicotinamide adenine dinucleotide
NOX4: NADPH oxidases 4
OCT: Optical coherence tomography
ONL: Outer nuclear layer

OS: Oxidative stress
SIRT1: Silent information regulator 1
SOD1: Superoxide dismutase1
T1DM: Type 1 diabetes mellitus
T2DM: Type 2 diabetes mellitus
VEGF-α: Vascular endothelial growth factor-α.

Data Availability

The data sets used and analyzed in the present study are available from the corresponding authors on reasonable request.

Disclosure

The abstract of the manuscript has been partially presented as a poster in the 24th Congress of the Chinese Ophthalmological Society (Suzhou, China).

Conflicts of Interest

All authors have read the journal's policy on authorship agreement and conflict of interest. The authors have declared that no conflict of interest exists.

Authors' Contributions

Mengshan He, Pan Long, and Tao Chen are co-first authors that contributed equally to the work.

Acknowledgments

The authors wish to thank Dr. Jinwen Wang of department of Pharmacy, Xijing Hospital, Fourth Military Medical University for supporting this study and helping for review & editing. This work was supported by the National Nature Science Foundation of China (Nos. 82074321 and 82001484), the Shaanxi Science and Technology Innovation Project (Nos. 2015SF2-08-01 and 2017ZDCXL-SF-01-01), the Key Research Laboratory of Traditional Chinese Medicine and Natural Medicine in Shaanxi Province (No. 2015-164), the subsidy after the Project of Shaanxi Engineering Technology Research Center (No. S2018-ZC-GCZXXY-SF-0005), and the Biomedicine Key Laboratory of Shaanxi Province (No. 2018SZS41).

References

[1] L. Yang, J. Shao, Y. Bian et al., "Prevalence of type 2 diabetes mellitus among inland residents in China (2000-2014): a meta-analysis," *Journal of Diabetes Investigation*, vol. 7, pp. 845–852, 2016.

[2] P. Saeedi, I. Petersohn, P. Salpea et al., "Global and regional diabetes prevalence estimates for 2019 and projections for 2030 and 2045: Results from the International Diabetes Federation Diabetes Atlas, 9th edition," *Diabetes Research and Clinical Practice*, vol. 157, article 107843, 2019.

[3] C. C. Wykoff, R. N. Khurana, Q. D. Nguyen et al., "Risk of blindness among patients with diabetes and newly diagnosed diabetic retinopathy," *Diabetes Care*, vol. 44, no. 3, pp. 748–756, 2021.

[4] Collaborators GBAV; Study VLEG, "Causes of blindness and vision impairment in 2020 and trends over 30 years, and prevalence of avoidable blindness in relation to VISION 2020: the right to sight: an analysis for the global burden of disease study," *The Lancet Global Health*, vol. 9, pp. e144–e160, 2021.

[5] S. P. Narayanan, E. Shosha, and C. D Palani, "Spermine oxidase: a promising therapeutic target for neurodegeneration in diabetic retinopathy," *Pharmacological Research*, vol. 147, article 104299, 2019.

[6] R. Klein, M. D. Knudtson, K. E. Lee, R. Gangnon, and B. E. Klein, "The Wisconsin Epidemiologic Study of Diabetic Retinopathy XXII: The Twenty- Five-Year Progression of Retinopathy in Persons with Type 1 Diabetes," *Ophthalmology*, vol. 115, no. 11, pp. 1859–1868, 2008.

[7] R. Klein, B. E. Klein, S. E. Moss, M. D. Davis, and D. L. DeMets, "The Wisconsin epidemiologic study of diabetic retinopathy," *Archives of Ophthalmology*, vol. 107, no. 2, pp. 244–249, 1989.

[8] S. Kusuhara, Y. Fukushima, S. Ogura, N. Inoue, and A. Uemura, "Pathophysiology of diabetic retinopathy: the old and the new," *Diabetes and Metabolism Journal*, vol. 42, no. 5, pp. 364–376, 2018.

[9] J. W. Yau, S. L. Rogers, R. Kawasaki et al., "Global prevalence and major risk factors of diabetic retinopathy," *Diabetes Care*, vol. 35, no. 3, pp. 556–564, 2012.

[10] A. W. Stitt, T. M. Curtis, M. Chen et al., "The progress in understanding and treatment of diabetic retinopathy," *Progress in Retinal and Eye Research*, vol. 51, pp. 156–186, 2016.

[11] Y. Wu, L. Tang, and B. Chen, "Oxidative stress: implications for the development of diabetic retinopathy and antioxidant therapeutic perspectives," *Oxidative Medicine and Cellular Longevity*, vol. 2014, Article ID 752387, 12 pages, 2014.

[12] C. Li, X. Miao, F. Li et al., "Oxidative stress-related mechanisms and antioxidant therapy in diabetic retinopathy," *Oxidative Medicine and Cellular Longevity*, vol. 2017, Article ID 9702820, 15 pages, 2017.

[13] M. W. Park, H. W. Cha, J. Kim et al., "NOX4 promotes ferroptosis of astrocytes by oxidative stress-induced lipid peroxidation via the impairment of mitochondrial metabolism in Alzheimer's diseases," *Redox Biology*, vol. 41, article 101947, 2021.

[14] R. E. McDowell, M. K. McGahon, J. Augustine, M. Chen, J. G. McGeown, and T. M. Curtis, "Diabetes impairs the aldehyde detoxifying capacity of the retina," *Investigative Ophthalmology & Visual Science*, vol. 57, no. 11, pp. 4762–4771, 2016.

[15] J. Augustine, E. P. Troendle, P. Barabas et al., "The role of lipoxidation in the pathogenesis of diabetic retinopathy," *Frontiers in Endocrinology*, vol. 11, article 621938, 2020.

[16] P. J. O'Brien, A. G. Siraki, and N. Shangari, "Aldehyde sources, metabolism, molecular toxicity mechanisms, and possible effects on human health," *Critical Reviews in Toxicology*, vol. 35, no. 7, pp. 609–662, 2005.

[17] A. Swiader, C. Camare, P. Guerby, R. Salvayre, and A. Negre-Salvayre, "4-Hydroxynonenal contributes to fibroblast senescence in skin photoaging evoked by UV-A radiation," *Antioxidants*, vol. 10, no. 3, p. 365, 2021.

[18] G. Y. Li, Z. B. Li, F. Li et al., "Meta-analysis on the association of ALDH2 polymorphisms and type 2 diabetic mellitus, diabetic retinopathy," *International Journal of Environmental Research and Public Health*, vol. 14, no. 2, p. 165, 2017.

[19] C. N. Spracklen, M. Horikoshi, Y. J. Kim et al., "Identification of type 2 diabetes loci in 433,540 East Asian individuals," *Nature*, vol. 582, no. 7811, pp. 240–245, 2020.

[20] M. He, P. Long, W. Yan et al., "ALDH2 attenuates early-stage STZ-induced aged diabetic rats retinas damage *via* Sirt1/Nrf2 pathway," *Life Sciences*, vol. 215, pp. 227–235, 2018.

[21] M. Mishra, A. J. Duraisamy, and R. A. Kowluru, "Sirt1: a guardian of the development of diabetic retinopathy," *Diabetes*, vol. 67, no. 4, pp. 745–754, 2018.

[22] S. Caito, S. Rajendrasozhan, S. Cook et al., "SIRT1 is a redox-sensitive deacetylase that is post-translationally modified by oxidants and carbonyl stress," *The FASEB Journal*, vol. 24, no. 9, pp. 3145–3159, 2010.

[23] P. Long, M. He, W. Yan et al., "ALDH2 protects naturally aged mouse retina via inhibiting oxidative stress-related apoptosis and enhancing unfolded protein response in endoplasmic reticulum," *Aging*, vol. 13, pp. 2750–2767, 2020.

[24] R. Othman, S. Berbari, E. Vaucher, and R. Couture, "Differential expression of kinin receptors in human wet and dry age-related macular degeneration retinae," *Pharmaceuticals*, vol. 13, no. 6, p. 130, 2020.

[25] D. Tonade and T. S. Kern, "Photoreceptor cells and RPE contribute to the development of diabetic retinopathy," *Progress in Retinal and Eye Research*, vol. 83, article 100919, 2021.

[26] K. Kaviarasan, M. Jithu, M. Arif Mulla et al., "Low blood and vitreal BDNF, LXA_4 and altered Th1/Th2 cytokine balance are potential risk factors for diabetic retinopathy," *Metabolism*, vol. 64, no. 9, pp. 958–966, 2015.

[27] T. N. Crawford, D. Alfaro III, J. B. Kerrison, and E. P. Jablon, "Diabetic retinopathy and angiogenesis," *Current Diabetes Reviews*, vol. 5, no. 1, pp. 8–13, 2009.

[28] Z. Zhong, J. Hou, B. Li et al., "Genetic polymorphisms of the mitochondrial aldehyde dehydrogenase ALDH2 gene in a large ethnic Hakka population in southern China," *Medical Science Monitor*, vol. 24, pp. 2038–2044, 2018.

[29] M. Kimura, A. Yokoyama, and S. Higuchi, "Aldehyde dehydrogenase-2 as a therapeutic target," *Expert Opinion on Therapeutic Targets*, vol. 23, no. 11, pp. 955–966, 2019.

[30] A. Yasgar, S. A. Titus, Y. Wang et al., "A high-content assay enables the automated screening and identification of small molecules with specific ALDH1A1-inhibitory activity," *PLoS One*, vol. 12, no. 1, article e170937, 2017.

[31] W. Yan, P. Long, T. Chen et al., "A natural occurring mouse model with Adgrv1 mutation of usher syndrome 2C and characterization of its recombinant inbred strains," *Cellular Physiology and Biochemistry*, vol. 47, no. 5, pp. 1883–1897, 2018.

[32] S. Leutner, A. Eckert, and W. E. Muller, "ROS generation, lipid peroxidation and antioxidant enzyme activities in the aging brain," *Journal of Neural Transmission*, vol. 108, no. 8, pp. 955–967, 2001.

[33] R. A. Kowluru, A. Kowluru, R. Veluthakal et al., "TIAM1–RAC1 signalling axis-mediated activation of NADPH oxidase-2 initiates mitochondrial damage in the development of diabetic retinopathy," *Diabetologia*, vol. 57, no. 5, pp. 1047–1056, 2014.

[34] L. Wachtmeister, "Oscillatory potentials in the retina: what do they reveal," *Progress in Retinal and Eye Research*, vol. 17, no. 4, pp. 485–521, 1998.

[35] N. Pescosolido, A. Barbato, A. Stefanucci, and G. Buomprisco, "Role of electrophysiology in the early diagnosis and follow-up of diabetic retinopathy," *Journal Diabetes Research*, vol. 2015, article 319692, pp. 1–8, 2015.

[36] S. A. Madsen–Bouterse, G. Mohammad, M. Kanwar, and R. A. Kowluru, "Role of mitochondrial DNA damage in the development of diabetic retinopathy, and the metabolic memory phenomenon associated with its progression," *Antioxidants & Redox Signaling*, vol. 13, no. 6, pp. 797–805, 2010.

[37] J. M. Santos, S. Tewari, and R. A. Kowluru, "A compensatory mechanism protects retinal mitochondria from initial insult in diabetic retinopathy," *Free Radical Biology & Medicine*, vol. 53, no. 9, pp. 1729–1737, 2012.

[38] Q. Zhong, M. Mishra, and R. A. Kowluru, "Transcription factor Nrf2-mediated antioxidant defense system in the development of diabetic retinopathy," *Investigative Ophthalmology & Visual Science*, vol. 54, no. 6, pp. 3941–3948, 2013.

[39] R. Sarangi, S. Padhi, S. Mohapatra et al., "Serum high sensitivity C-reactive protein, nitric oxide metabolites, plasma fibrinogen, and lipid parameters in Indian type 2 diabetic males," *Diabetes and Metabolic Syndrome: Clinical Research and Reviews*, vol. 6, no. 1, pp. 9–14, 2012.

[40] C. Liu, X. Feng, Q. Li, Y. Wang, Q. Li, and M. Hua, "Adiponectin, TNF-α and inflammatory cytokines and risk of type 2 diabetes: a systematic review and meta-analysis," *Cytokine*, vol. 86, pp. 100–109, 2016.

[41] J. H. Lee, W. Lee, O. H. Kwon et al., "Cytokine profile of peripheral blood in type 2 diabetes mellitus patients with diabetic retinopathy," *Annals of Clinical and Laboratory Science*, vol. 38, pp. 361–367, 2008.

[42] S. Cai, Q. Yang, M. Hou et al., "*A*-Melanocyte-Stimulating hormone protects early diabetic retina from blood-retinal barrier breakdown and vascular leakage via MC4R," *Cellular Physiology and Biochemistry*, vol. 45, no. 2, pp. 505–522, 2018.

[43] A. Reis, C. Mateus, P. Melo, J. Figueira, J. Cunha-Vaz, and M. Castelo-Branco, "Neuroretinal dysfunction with intact blood-retinal barrier and absent vasculopathy in type 1 diabetes," *Diabetes*, vol. 63, no. 11, pp. 3926–3937, 2014.

[44] H. H. Parving, "Impact of blood pressure and antihypertensive treatment on incipient and overt nephropathy, retinopathy, and endothelial permeability in diabetes mellitus," *Diabetes Care*, vol. 14, no. 3, pp. 260–269, 1991.

[45] K. Miyamoto, S. Khosrof, S. E. Bursell et al., "Prevention of leukostasis and vascular leakage in streptozotocin-induced diabetic retinopathy via intercellular adhesion molecule-1 inhibition," *Proceedings of the National Academy of Sciences of the United States of America*, vol. 96, no. 19, pp. 10836–10841, 1999.

[46] A. Jain, S. Saxena, V. K. Khanna, R. K. Shukla, and C. H. Meyer, "Status of serum VEGF and ICAM-1 and its association with external limiting membrane and inner segment-outer segment junction disruption in type 2 diabetes mellitus," *Molecular Vision*, vol. 19, pp. 1760–1768, 2013.

[47] K. Zorena, D. Raczynska, and K. Raczynska, "Biomarkers in diabetic retinopathy and the therapeutic implications," *Mediators of Inflammation*, vol. 2013, Article ID 193604, 11 pages, 2013.

[48] N. Toda and M. Nakanishitoda, "Nitric oxide: ocular blood flow, glaucoma, and diabetic retinopathy," *Progress in Retinal and Eye Research*, vol. 26, no. 3, pp. 205–238, 2007.

Hindawi
Oxidative Medicine and Cellular Longevity
Volume 2021, Article ID 2207125, 16 pages
https://doi.org/10.1155/2021/2207125

Research Article

Redox Imbalance and Methylation Disturbances in Early Childhood Obesity

Pedro Barbosa,[1,2,3] Stepan Melnyk,[4] Sirish C. Bennuri,[4] Leanna Delhey,[4,5] Andreia Reis,[6] Gabriela R. Moura,[6] Elisabet Børsheim,[4,7,8,9] Shannon Rose,[4,8] and Eugenia Carvalho[2,3,4,9]

[1]*PhD Programme in Experimental Biology and Biomedicine, Institute for Interdisciplinary Research (IIIUC), University of Coimbra, Coimbra, Portugal*
[2]*Center for Neuroscience and Cell Biology, University of Coimbra, Coimbra, Portugal*
[3]*Institute for Interdisciplinary Research, University of Coimbra, Coimbra, Portugal*
[4]*Arkansas Children's Research Institute, Little Rock, AR, USA*
[5]*Department of Epidemiology, University of Arkansas for Medical Sciences, Little Rock, AR, USA*
[6]*Institute of Biomedicine (iBiMED) & Department of Medical Sciences (DCM), University of Aveiro, Aveiro, Portugal*
[7]*Arkansas Children's Nutrition Center, Little Rock, AR, USA*
[8]*Department of Pediatrics, University of Arkansas for Medical Sciences, Little Rock, AR, USA*
[9]*Department of Geriatrics, University of Arkansas for Medical Sciences, Little Rock, AR, USA*

Correspondence should be addressed to Eugenia Carvalho; ecarvalh@cnc.uc.pt

Received 5 June 2021; Revised 13 July 2021; Accepted 2 August 2021; Published 18 August 2021

Academic Editor: Daniela Ribeiro

Obesity is increasing worldwide in prepubertal children, reducing the age of onset of associated comorbidities, including type 2 diabetes. Sulfur-containing amino acids, methionine, cysteine, and their derivatives play important roles in the transmethylation and transsulfuration pathways. Dysregulation of these pathways leads to alterations in the cellular methylation patterns and an imbalanced redox state. Therefore, we tested the hypothesis that one-carbon metabolism is already dysregulated in prepubertal children with obesity. Peripheral blood was collected from 64 children, and the plasma metabolites from transmethylation and transsulfuration pathways were quantified by HPLC. The cohort was stratified by BMI z-scores and HOMA-IR indices into healthy lean (HL), healthy obese (HO), and unhealthy obese (UHO). Fasting insulin levels were higher in the HO group compared to the HL, while the UHO had the highest. All groups presented normal fasting glycemia. Furthermore, high-density lipoprotein (HDL) was lower while triglycerides and lactate levels were higher in the UHO compared to HO subjects. S-adenosylhomocysteine (SAH) and total homocysteine levels were increased in the HO group compared to HL. Additionally, glutathione metabolism was also altered. Free cystine and oxidized glutathione (GSSG) were increased in the HO as compared to HL subjects. Importantly, the adipocyte secretory function was already compromised at this young age. Elevated circulating leptin and decreased adiponectin levels were observed in the UHO as compared to the HO subjects. Some of these alterations were concomitant with alterations in the DNA methylation patterns in the obese group, independent of the impaired insulin levels. In conclusion, our study informs on novel and important metabolic alterations in the transmethylation and the transsulfuration pathways in the early stages of obesity. Moreover, the altered secretory function of the adipocyte very early in life may be relevant in identifying early metabolic markers of disease that may inform on the increased risk for specific future comorbidities in this population.

1. Introduction

Obesity is a rapidly growing epidemic that is contributing to the significant increase in metabolic diseases worldwide. It is characterized by excess adipose tissue expansion and is associated with low-grade inflammation and metabolic dysfunction [1]. The continuous release of proinflammatory cytokines [1] and adipokines (e.g., leptin) by dysregulated adipose tissue may contribute to the obesity-associated inflammation [2]. It is thought that chronic low-grade inflammation induces chronic oxidative stress, and that both contribute to the obesity-related insulin resistance (IR) and type 2 diabetes (T2D) development [3]. Due to the drastic increase in early childhood obesity, the journey to T2D development is starting earlier in life. This in turn increases the risk for other severe health complications over the lifespan, such as hypertension, cardiovascular diseases (CVD), retinopathy, and neuropathy, that appear to increase as the age of T2D onset decreases [4–6]. Further, there are several important differences in the pathophysiology of obesity-associated comorbidities in adults compared to children, including early β-cell decline and time to T2D treatment failure, as well as the lack of appropriate pharmacological medications approved for earlier ages, and longer duration of the disease [7–10].

Early alterations in the redox and methylation status that are associated with obesity may play a significant role in the early onset of metabolic disturbances in children with obesity. The thiol group plays an important role in biological systems [11]. It appears in the sulfur-containing amino acids methionine and cysteine, and their derivatives, such as glutathione (GSH) and other low molecular weight intermediates in the transmethylation and transsulfuration pathways [11, 12], also known as aminothiols. Thiols are responsible for scavenging reactive oxygen species (ROS) and maintaining redox homeostasis [13]. In particular, cysteine is primarily responsible for maintaining the redox state in plasma [14], while GSH maintains intracellular redox homeostasis, acting directly or indirectly through enzymatic activity [13]. Recent studies postulate dysfunction in the redox homeostasis in obese children [15, 16]. Lechuga-Sancho et al. [15] have identified an altered oxidative status in erythrocytes from obesity-associated insulin resistant children, even before those changes occurred in plasma. Besides, Zalewska et al. [16] reported alterations in the saliva redox status followed by higher oxidative damage in obese when compared to overweight children.

Transmethylation and transsulfuration intermediates are also critically important for methylation of DNA, proteins, and lipids [14] with methionine-derived S-adenosylmethionine (SAM), being the primary methyl group donor [17]. Imbalance in the transmethylation and transsulfuration pathways is linked with obesity-related inflammation [18]. It has also been shown that high levels of circulating homocysteine, resulting from the S-adenosylhomocysteine (SAH) degradation, are linked to an increased oxidation status in circulation [19]. Moreover, the hyperhomocysteinemia resulting from the imbalance of transsulfuration and transmethylation metabolites has been linked to further risk of obesity-associated CVD, such as atherosclerosis [18, 19]. Interestingly, a study conducted in mice suggested that high levels of SAH in the circulation could be involved with alterations at the epigenetic levels by inhibiting the DNA methyltransferase enzymes. The same study also indicated a possible relation between high levels of SAH and endothelial dysfunction [20].

One-carbon metabolism pathways, including those described above, have been implicated in important metabolic processes that include redox defenses and epigenetic alterations, which are both altered in obesity [11]. However, it is not known how soon this can happen in life and whether these pathways, if becoming altered in prepubertal children with obesity, can facilitate the early onset of obesity-related comorbidities.

Therefore, the present study is mainly aimed at testing the hypothesis that one-carbon metabolism perturbation is already present in the early stages of obesity development, in prepubertal children. Therefore, transsulfuration and transmethylation metabolite levels were quantified and related with their systemic oxidative stress, genomic methylation status, and inflammatory marker levels in children of normal weight or with overweight/obesity.

2. Material and Methods

2.1. Study Cohort. A group of 64 prepubertal children (5-9 years old, Tables 1 and 2 from Results) were recruited after approval of the study by the Institutional Review Board (IRB) (protocol number 206164) at the University of Arkansas for Medical Science and following the guidelines of Declaration of Helsinki (1964). This clinical study was registered at ClinicalTrials.gov (NCT03323294). The inclusion criteria were age 5-9 years at the date of the visit (i.e., 5- <10 years), and the exclusion criteria were the presence of known chronic illnesses/disorders that might affect study outcome measures, such as type 1 diabetes mellitus, neurologic, developmental, endocrine, hepatic, autoimmune, cardiac, and renal disorders; use of any medication could affect study outcomes, e.g., antipsychotics, thyroid hormone replacement therapy, inhalation/oral steroids, insulin, anabolic drugs and stimulants, or being classified as underweight based on the CDC growth charts (http://www.cdc.gov/growthcharts).

Anthropometric variables were collected for all study participants and sex (male/female), age (years), weight (kg), height (cm), and waist circumference (cm) were included (Tables 1 and 2). For data analyses, children with an age ≥ 9 years and 6 months, but <10 years, were considered 10 years old (Tables 1 and 2). The weight was measured using a calibrated Avery Berkel, HL122 Series Platform Scale (Dynamic Scales, Terre Haute, IN, USA) wearing minimal clothing, while height was obtained using a stadiometer (Novel Products, Rockton, IL, USA). The waist circumference was measured as reported previously [21].

Body mass index (BMI) was calculated from body mass and height as kg/m^2 and adjusted for age and sex according to the Centers for Diseases Control and Prevention (http://www.cdc.gov/growthcharts). The participants

Table 1: Physiologic and biochemical characteristics of healthy prepubertal children stratified per BMIz.

Characteristics	n	HL	n	HO	p value
Sex: male/female	20	14/6	28	15/13	
Age (years)	20	7.0 (6.0–8.0)	28	7.0 (6.0–8.3)	ns
BMIz	20	0.078 ± 0.663	28	1.846 ± 0.557	<0.01
WC (cm)	20	55.0 (51.4-56.6)	28	61.5 (56.8-75.1)	<0.01
Systolic BP (mmHg)	20	99.7 ± 9.71	28	106.71 ± 10.39	0.047
Diastolic BP (mmHg)	20	58.7 ± 9.30	28	62.29 ± 7.65	ns
Heart rate (bpm)	20	78 ± 12	28	79 ± 11	ns
Fat mass (kg)	20	3.9 (3.3-5.2)	28	9.4 (6.5-14.4)	<0.01
Free-fat mass (kg)	20	19.0 (18.1-21.7)	28	23.3 (20.3-26.0)	<0.01
Total body water (kg)	20	13.9 (13.3-15.9)	28	17.1 (14.8-19.0)	<0.01
Insulin (μU/mL)	20	3.65 ± 1.55	28	5	<0.01
Glucose (mmol/L)	20	4.91 (4.75-5.12)	27	5.03 (4.60-5.35)	ns
HOMA-IR	20	0.79 (0.54-0.92)	27	1.21 (1.00-1.49)	<0.01
HOMA-β	20	50.17 (30.65-66.85)	27	72.05 (44.40-128.60)	0.015
HDL cholesterol (mmol/L)	20	1.47 ± 0.31	27	1.40 ± 0.29	ns
LDL cholesterol (mmol/L)	20	2.16 ± 0.61	27	2.35 ± 0.76	ns
Triglycerides (mmol/L)	20	0.52 (0.41-0.65)	27	0.53 (0.37-0.82)	ns
Total cholesterol (mmol/L)	20	3.73 ± 0.68	27	3.89 ± 0.81	ns
NEFA (mmol/L)	20	0.10 (0.06-0.16)	27	0.08 (0.04-0.13)	ns
Glycerol (μmol/L)	20	77.27 (64.19-130.24)	27	82.77 (68.20-92.10)	ns
Lactate (mmol/L)	20	2.07 ± 0.57	27	2.03 ± 0.47	ns

HL: healthy lean; HO: healthy obese; BMIz: BMI z-score; WC: waist circumference; BP: blood pressure; BMR: basal metabolic rate; HOMA-IR: homeostatic model assessment of insulin resistance; HOMA-β: homeostatic model assessment of β-cell function; LDL: low-density lipoprotein; HDL: high-density lipoprotein; NEFA: nonesterified fatty acids; ns: nonsignificant; p value <0.05 was considered significant.

were considered overweight or obese if their age- and sex-adjusted BMI was above the 85th percentile (i.e., BMI z – score (BMIz) > 1.04). Although during the stratification present in Statistical Analysis, all the participants with overweight and obesity were included in obese groups. Clinical outcomes such as systolic and diastolic blood pressure (mmHg), as well as heart rate (bpm), were also measured using a digital sphygmomanometer (Tables 1 and 2). The measurement was performed on an arm rested at heart level, and the cuff was placed two fingers above the brachial artery. These measurements were performed at the Pediatric Clinical Research Unit from Arkansas Children's Hospital using a GE Carescape V100 Dinamap vital sign monitor following the standard procedures for this unit. The instrument is calibrated for children.

Fat-free mass, fat mass, and total body water were also measured using the Tanita Body Composition Analyzer (Model TBF-300A; Tanita Corporation of America, Inc., Arlington Heights, IL, USA).

2.2. Blood Collection and Processing. Fasting venous blood samples were collected in EDTA tubes to isolate peripheral blood mononuclear cells (PBMCs), as previously described [21]. Plasma samples were collected after whole blood centrifugation (1,500 × g for 30 min at 4°C). Thereafter, samples were stored up to 1-2 years at -80°C, until the study was concluded, so that all samples could be measured together to reduce batch effects. Then, the plasma volume was replaced with wash buffer consisting of Ca^{2+}/Mg^{2+}-free PBS supplemented with 2 mM EDTA and 0.1% BSA (Sigma Aldrich, St. Louis, MO). To perform the gradient separation, Histopaque-1077 (Sigma Aldrich) was used. The diluted blood was layered on histopaque and centrifuged at 400 × g for 30 min at room temperature. The white cloudy layer of PBMCs was collected and washed two times with ~20 ml of room temperature wash buffer. PBMCs were counted using a hemocytometer (Bright-Line; Hausser Scientific, Horsham, PA), and 2-5 million PBMCs were pelleted, snap frozen on dry ice, and stored up to two years at -80°C, until the study was concluded [21].

2.3. Biochemical Measures. Fasting insulin concentration was measured in plasma using the Mesoscale Discovery Platform (MSD Multi-Array Assay System, Gaithersburg, MD, USA) according to the manufacturer's protocol. Fasting plasma glucose was measured using YSI 2900 biochemistry analyzer (YSI Life Sciences, Yellow Springs, OH, USA). The lipid profile was quantified in plasma using a RX Daytona clinical analyzer accordingly to the manufacturer's instructions (Randox Laboratories-IS Limited, Kearneysville, WV, USA)—nonesterified fatty acids (NEFA: mmol/L), glycerol (μmol/L), high-density lipoprotein (HDL: mmol/L), low-

Table 2: Physiologic and biochemical characteristics of prepubertal children with obesity stratified per HOMA-IR.

Characteristics	n	HO	n	UHO	p value
Sex: male/female	28	15/13	16	7/9	
Age: years	28	7.0 (6.0–8.3)	16	8.0 (7.0–9.0)	ns
BMIz	28	1.85 ± 0.56	16	2.45 ± 0.55	<0.01
WC (cm)	28	65.6 ± 12.1	16	77.5 ± 12.3	ns
Systolic BP (mmHg)	28	106.7 ± 10.4	16	113.5 ± 9.1	0.035
Diastolic BP (mmHg)	28	62.3 ± 7.7	16	64.75 ± 8.4	ns
Heart rate (bpm)	28	79 ± 11	16	83 ± 10	ns
Fat mass (kg)	28	9.4 (6.5-14.4)	16	19.3 (16.8-23.9)	<0.01
Fat-free mass (kg)	28	23.3 (20.3–26.0)	16	29.2 (26.4-31.8)	<0.01
Total body water (kg)	28	17.0 (14.8-19.0)	16	21.4 (19.3-23.3)	<0.01
Insulin (μU/mL)	28	5.75 (4.56-7.10)	16	15.19 (10.33-25.20)	<0.01
Glucose (mmol/L)	27	4.94 ± 0.52	16	5.28 ± 0.79	ns
HOMA-IR	27	1.21 (1.00-1.49)	16	3.00 (2.24-6.24)	<0.01
HOMA-β	27	72.05 (44.40-128.60)	16	200.74 (143.46-300.65)	<0.01
HDL cholesterol (mmol/L)	27	1.33 (1.18-1.59)	14	1.19 (1.05-1.24)	0.010
LDL cholesterol (mmol/L)	27	2.27 (2.01-2.97)	14	3.03 (2.16-3.25)	ns
Triglycerides (mmol/L)	27	0.53 (0.37-0.82)	14	0.75 (0.65-1.20)	0.041
Total cholesterol (mmol/L)	27	3.81 (3.47-4.51)	14	4.37 (3.47-4.58)	ns
NEFA (mmol/L)	27	0.08 (0.03-0.13)	16	0.09 (0.07-0.11)	ns
Glycerol (μmol/L)	27	82.77 (68.20-92.10)	14	91.12 (73.80-111.00)	ns
Lactate (mmol/L)	27	2.03 ± 0.47	14	2.62 ± 0.60	<0.01

HO: healthy obese; UHO: unhealthy obese; BMIz: BMI z-score; WC: waist circumference; BP: blood pressure; BMR: basal metabolic rate; HOMA-IR: homeostatic model assessment of insulin resistance; HOMA-β: homeostatic model assessment of β-cell function; LDL: low-density lipoprotein; HDL: high-density lipoprotein; NEFA: nonesterified fatty acids; ns: nonsignificant; p value <0.05 was considered significant.

density lipoprotein (LDL: mmol/L), and triglycerides (TGs: mmol/L). Additionally, plasma lactate (mmol/L) and CRP were measured using the same methodology.

Fasting insulin (μU/mL) and glucose concentrations (mmol/L) were used to calculate HOMA-IR and HOMA-β using the following equations:

$$\text{HOMA} - \text{IR} = \frac{\text{fGlucose}\,(\text{mmol/L}) \times \text{fInsulin}\,(\mu\text{U/mL})}{22.5},$$
$$\text{HOMA} - \beta = \frac{\text{fInsulin}\,(\mu\text{U/mL}) \times 20}{\text{fGlucose}\,(\text{mmol/L}) - 3.5}. \quad (1)$$

HOMA-IR was used to determine the insulin sensitivity status for each participant. When HOMA − IR ≥ 2, the participant was considered insulin resistant [22–24].

2.4. Sample Preparation for Aminothiol Analysis. Plasma was prepared for analysis as previously described by Melnyk et al. [25] in order to determine free reduced and oxidized or total reduced aminothiols. Briefly, to assess the total concentration of aminothiols, 50 μL of a solution containing 1.43 M of sodium borohydride, 66 mM sodium hydroxide, 1.5 μM EDTA, and 10 μL n-amyl alcohol was added to 200 μL of plasma and incubated for 30 min at 40°C. Thereafter, the proteins were precipitated by incubation for 10 min with cold 10% meta-phosphoric acid, the samples were centrifuged for 15 min at 14,000 RPM, and 20 μL of supernatant was measured by HPLC. To assess the free and oxidized aminothiol concentration, an equal volume of 10% meta-phosphoric acid was added to the plasma samples and treated as previously described [25].

2.5. Aminothiols and Oxidative Damage Marker Identification. Total and free aminothiols were separated using a Shimadzu HPLC with a Shimadzu pump model 580 on a 5 μm, 4.6 × 150 mm i.d. reverse-phase C_{18} column (MCM, Inc., Tokyo, Japan) with the thermostat at 25°C. An isocratic mobile phase composed of 50 mM sodium phosphate, 1.0 mM of reagent OSA, and 2% acetonitrile (v/v) at pH 2.7 was used. The detection of all compounds was carried out using a Coulochem II EC detector, model 5200A (ESA, Inc.). The identification was carried out using external standards for each compound: methionine, homocysteine, cysteine, cystine, cysteinylglycine, reduced and oxidized glutathione, gamma-glutamylcysteine, 3-nitro-tyrosine, and 3-chloro-tyrosine, as previously described [25].

The percentage of oxidized GSH was obtained using the following equation [14]:

$$\%\text{oxidized GSH} = \frac{2\text{GSSG}}{\text{free GSH} + 2\text{GSSG}} \times 100. \quad (2)$$

2.6. Plasma Adipokines and Cytokine Quantification. A plasma adipokine and cytokine kit was used to measure leptin, IL-1β, IL-6, IL-8, MCP-1, and TNF-α by multiplexing using a Milliplex® Map Human Adipokine Panel (Millipore®, MA, USA). Adiponectin was also measured using a human Adiponectin ELISA (Millipore®, MA, USA). All procedures were performed according to the manufacturer's instructions.

2.7. DNA Methylation Profile. DNA methylation was assessed in the isolated PBMCs. The Puregene Blood Kit (Gentra Systems, Inc., Minneapolis, MN, USA) was used to extract the DNA, and it was further bisulfite-converted and purified using an EZ DNA Methylation-Gold kit (Zymo Research, Irvine, CA, USA) according to the manufacturer's protocol [26]. After bisulfite-conversion, the methylation was determined using the Infinium MethylationEPIC bead chip from Illumina®. The acquired data was followed by a quality control analysis of samples and probes, followed by further normalization using the Bioconductor packages *minfi* v1.34.0 and *watermelon* version 1.32.0 [27, 28] in R version 4.0.2 [29, 30]. In order to reduce the bias within-array, the data was normalized combining Noob+BMIQ (β-mixture quantile normalization) in order to improve signal intensities [27, 31]. After normalization, the data was filtered and probes that failed (p value >0.01) were removed. All probes mapped to the X and Y chromosomes were also removed to avoid sex chromosome bias. Finally, cross-reactive probes [32] and probes including known SNPs were also removed, according to Illumina recommendations, before final statistical analysis [33].

2.8. Statistical Analysis. The original statistical power for the present study was computed with a total of 110 children based on a one-factor ANOVA, 80% power and $\alpha = 0.05$ were assumed, and a minimum detectable Cohen's f effect size of 0.33 was used. To test the differences between HL and HO and between HO and UHO, a t-test was performed when data fulfilled all the assumptions—the normal distribution was tested by the Shapiro-Wilk test, and the variance homogeneity was tested by the Levene's test. Otherwise, a Wilcoxon signed-rank test was performed. Results are presented as mean ± standard deviation (sd) and median (Q1–Q3) according to the respective test. The correlation between continuous variables was assessed using the Spearman's Rank-Order correlation, and the coefficient (rho) is shown for each correlation. A p value <0.05 was considered statistically significant. These tests were performed using the R version 4.0.2 [29, 30].

For statistical analysis of methylation results, differentially methylated positions (DMPs) were tested among groups using limma v3.44.3 [34] R package, after converting β values into M values. Covariates such as sex, age, and race were adjusted to the linear model. The p values were adjusted by the Benjamini-Hochberg method (false discovery rate [FDR]) [35]. DMPs were considered significative for FDR < 0.1. Gene set enrichment analyses were performed using the webtool STRING database v11.0b [36], for Gene Ontology (GO), KEGG (Kyoto Encyclopedia of Genes and Genomes), and Reactome pathways. Significant results were defined as FDR < 0.05.

3. Results

3.1. Physiologic and Biochemical Characterization of Study Population. The physiologic and biochemical characteristics of the study population were stratified according to the BMIz and HOMA-IR, as shown in Tables 1 and 2, respectively. The HO showed a significantly higher BMIz ($p < 0.01$) and waist circumference ($p < 0.01$), as compared with the HL subjects. In addition, the HO displayed a significantly higher fat-free mass ($p < 0.01$) and fat mass ($p < 0.01$) compared with HL. Interestingly, the HO showed significantly elevated plasma insulin levels ($p < 0.01$) when compared with the HL, despite normal fasting glucose levels and a HOMA − IR < 2. The HL presented a better β-cell insulin secretory function (HOMA-β) compared to the HO group (Table 1). Although obesity is normally characterized by dyslipidemia, this was not observed in the HO group, as their lipid profile was similar to that of HL. The systolic blood pressure was elevated in the HO as compared to HL subjects ($p = 0.047$).

Differences between the HO and UHO groups are presented in Table 2. The data indicate that UHO participants had higher BMIz as compared to the HO. Their higher BMIz was caused by a significant higher fat mass, as well as fat-free mass, that was accompanied by a significantly higher total body water in UHO compared to the HO. Insulin was significantly higher in the UHO group, in comparison to the HO group. This was also accompanied by a significant insulin secretory dysfunction, as represented by the HOMA-β index ($p = 0.0145$). Interestingly, these metabolic defects are already present in this prepubertal cohort of obese children, even in the presence of normal fasting plasma glycemia. The fasting glucose levels are similar among all the groups. While there were no differences in plasma cholesterol levels in the HL vs. HO, the UHO presented dyslipidemia which was characterized by a decrease in HDL cholesterol ($p = 0.01$) and significant increase in triglycerides levels ($p = 0.041$). The LDL cholesterol levels were slightly increased in the UHO compared to the HO participants, but the difference did not reach statistical significance ($p = 0.34$) in the UHO vs. HO participants. In spite of the young age of this cohort of UHO subjects, they already presented significantly elevated systolic blood pressure, as compared to the HO. Furthermore, the plasma lactate concentration was also significantly higher in the UHO compared to the HO. The lactate concentration was fairly well correlated with high levels of plasma insulin (Spearman's correlation, rho = 0.42, p value <0.01) and with HOMA-IR (Spearman's correlation, rho = 0.44, p value ≤0.01) (Supplementary Table 1B).

3.2. Transmethylation Metabolites. Transmethylation metabolites, such as methionine, SAH, SAM, adenosine, and homocysteine were quantified in the three groups of participants (Table 3). Of the evaluated metabolites, SAH levels were significantly increased in the HO group compared with the HL subjects. Interestingly, similar results were also observed for homocysteine levels. However, there was no

Table 3: Plasma transmethylation metabolite concentrations in prepubertal children stratified per BMIz and HOMA-IR.

Metabolites	HL ($n = 20$)	HO ($n = 28$)	p value*	UHO ($n = 16$)	p value**
Methionine (μmol/L)	19.22 ± 3.14	20.70 ± 3.53	ns	19.81 ± 3.44	ns
SAH (nmol/L)	19.32 (17.13-20.94)	23.34 (18.42-25.31)	0.027	21.76 (20.41-26.56)	ns
SAM (nmol/L)	45.24 ± 7.69	49.65 ± 8.00	ns	49.83 ± 9.75	ns
SAM/SAH ratio	2.35 ± 0.47	2.29 ± 0.53	ns	2.16 ± 0.53	ns
Adenosine (μmol/L)	0.16 ± 0.06	0.19 ± 0.06	ns	0.19 ± 0.06	ns
Total homocysteine (μmol/L)	5.06 (4.68-5.62)	6.23 (5.33-7.18)	<0.01	6.36 (5.46-6.86)	ns

HL: healthy lean; HO: healthy obese; UHO: unhealthy obese; SAM: S-adenosylmethyonine; SAH: S-adenosylhomocysteine; *LH-HO comparison; **HO-UHO comparison; ns: nonsignificant; p value <0.05 was considered significant.

Table 4: Circulating transsulfuration and oxidative damage metabolites in prepubertal children stratified per BMIz and HOMA-IR.

Metabolites	HL ($n = 20$)	HO ($n = 28$)	p value*	UHO ($n = 16$)	p value**
Total cysteine (μmol/L)	183.80 (165.43-195.58)	199.75 (178.20-214.20)	0.020	195.60 (184.80-207.13)	ns
Free cysteine (nmol/L)	19.23 ± 2.50	20.75 ± 3.09	ns	20.86 ± 2.73	ns
Cystine (nmol/L)	18.45 (17.35-19.50)	20.30 (19.28-21.83)	0.005	20.15 (17.55-21.43)	ns
Free cysteine/cystine	1.04 ± 0.11	1.04 ± 0.10	ns	1.05 ± 0.13	ns
Total ?-glutamylcysteine (μmol/L)	1.65 ± 0.22	1.67 ± 0.25	ns	1.71 ± 0.17	ns
Total reduced GSH (μmol/L)	5.63 ± 1.04	5.70 ± 1.08	ns	5.60 ± 0.71	ns
Free reduced GSH (μmol/L)	1.75 (1.57-1.92)	1.77 (1.60-1.87)	ns	1.79 (1.61-1.84)	ns
GSSG (μmol/L)	0.17 (0.15-0.20)	0.21 (0.17-0.26)	0.014	0.19 (0.17-0.23)	ns
Total reduced GSH/GSSG	32.81 ± 11.12	26.72 ± 8.66	0.038	30.15 ± 10.00	ns
Free reduced GSH/GSSG	10.00 ± 2.73	8.28 ± 2.43	0.026	9.36 ± 2.68	ns
Cysteinylglycine (μmol/L)	31.73 ± 6.52	38.67 ± 7.99	0.003	38.68 ± 6.69	ns
Oxidized GSH (%)	16.17 (14.56–18.93)	19.05 (17.07–21.42)	0.021	17.40 (15.66–21.14)	ns
3-Chloro-tyrosine (nmol/L)	42.35 ± 7.34	46.44 ± 10.19	ns	44.88 ± 9.10	ns
3-Nitro-tyrosine (nmol/L)	30.38 ± 8.63	33.24 ± 7.77	ns	33.46 ± 5.50	ns

HL: healthy lean; HO: healthy obese; UHO: unhealthy obese; GSH: reduced glutathione; GSSG: glutathione dissulfide; *HL-HO comparison; **HO-UHO comparison; ns: nonsignificant; p value <0.05 was considered significant.

difference in the SAM/SAH ratio. This ratio is frequently used to predict the methylation capacity of the cells. When UHO were compared with HO, no significant differences were found between groups.

3.3. Transsulfuration Metabolites. In parallel to the measurements of plasma transmethylation metabolites, Table 4 shows the levels of plasma metabolites related with the redox state as well as the transsulfuration pathway. When comparing the HL with the HO prepubertal children, several metabolites were significantly altered. The HO children exhibited increased levels of total cysteine (tCysteine; free circulating +protein-bound), while free cysteine (fCysteine) was not different as compared to the HL. Similarly, increased levels of cystine were observed. The cysteine oxidation ratio (fCysteine/cystine) is an important redox buffer responsible for maintaining the plasma redox state. However, the ratio was not different between groups. The homocysteine levels described above play an important role in the transsulfuration pathway, since it acts as an intermediary metabolite between both the transmethylation and the transsulfuration pathways. In fact, homocysteine is the main source of cysteine that is used to synthetize glutathione (GSH). Total reduced GSH (tGSH) and free reduced GSH (fGSH) were also measured but showed no significant differences between groups. On the other hand, the oxidized glutathione (GSSG) was significantly elevated in the HO compared with the HL subjects. The evaluation of tGSH/GSSG and fGSH/GSSG ratios showed a significant reduction in the antioxidant capacity and consequently an increase in oxidative stress in plasma of the HO children. The percentage of oxidized GSH was also higher in HO subjects compared to HL. Additionally, the levels of cysteinylglycine in HO group were also significantly higher, when compared with the HL.

Biomarkers of nitrosative stress, 3-chloro-tyrosine and 3-nitro-tyrosine, showed no significant differences between groups.

3.4. Inflammation Patterns. Oxidative stress is normally accompanied by an increase in the systemic inflammatory status. Therefore, we measured inflammatory cytokines as well as the inflammatory marker, C-reactive protein (CRP) in the plasma (Table 5). While CRP was elevated in HO as compared with the HL, no significant alterations were observed for inflammatory cytokines except for the unexpected finding of reduced TNF alpha levels in UHO as

Table 5: Markers of inflammation and adipocyte function in prepubertal children stratified per BMIz and HOMA-IR.

	HL		HO		p value*	UHO		p value**
	n		n			n		
CRP (mg/L)	20	0.15 (0.15-0.19)	27	0.80 (0.35-2.28)	<0.01	14	1.16 (0.41-2.87)	ns
IL-6 (pg/mL)	19	13.73 (5.32-49.58)	28	8.31 (3.45-37.77)	ns	16	8.95 (2.13-13.08)	ns
IL-8 (pg/mL)	18	4.88 (4.09-13.75)	22	5.55 (4.22-10.40)	ns	9	3.39 (3.08-7.60)	ns
MCP1 (pg/mL)	19	127.78 ± 36.691	28	125.614 ± 41.909	ns	16	115.94 ± 39.06	ns
TNF alpha (pg/mL)	19	6.49 (5.43-7.91)	28	6.12 (4.32-7.67)	ns	16	3.86 (2.40-5.18)	0.015
IL-1beta (pg/mL)	16	0.90 (0.54-1.40)	23	0.76 (0.57-2.19)	ns	12	0.57 (0.57-0.80)	ns
Leptin (ng/mL)	19	88.77 (51.30-104.25)	28	662.30 (187.46-1620.67)	<0.01	16	1439.34 (951.73-1647.30)	0.036
Adiponectin (ng/mL)	20	13928.27 (11255.19-17488.51)	27	13917.50 (10686.40-18460.15)	ns	16	7800.46 (7091.7-9684.40)	<0.01
Leptin/adiponectin	19	0.006 (0.003-0.008)	27	0.057 (0.012-0.114)	<0.01	16	0.165 (0.121-0.249)	<0.01

HL: healthy lean; HO: healthy obese; UHO: unhealthy obese; CRP: C-reactive protein; IL: interleukin; MCP-1: monocyte chemoattractant protein 1; *HL-HO comparison; **HO-UHO comparison; ns: nonsignificant; p value <0.05 was considered significant.

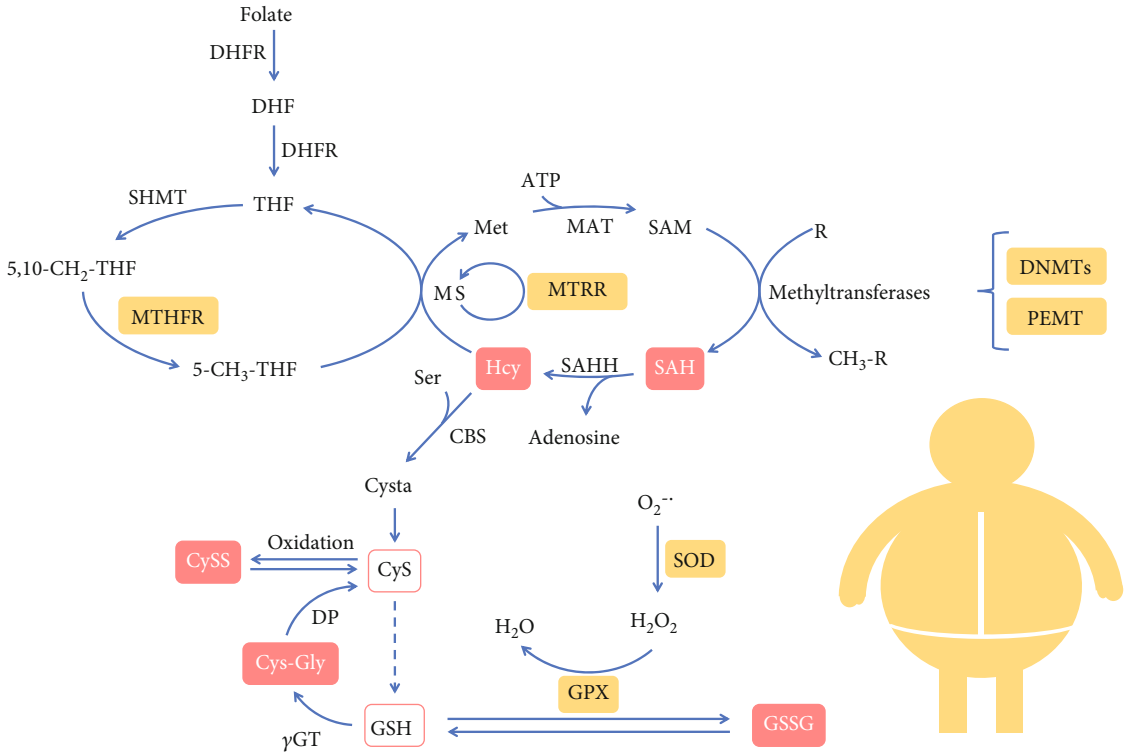

Highlights

- Alterations in one-carbon metabolism during childhood obesity;
- High levels of SAH in metabolic healthy obese;
- Biomarkers for identification of high risk to develop CVD and T2D;

Figure 1: One-carbon metabolism perturbations during childhood obesity. Yellow squares represent the enzymes that have altered DNA methylation pattern; pink squares represent increased metabolites found associated to obesity; bold symbols represent enzymes; DHFR: dihydrofolate reductase; DHF: dihydrofolate; THF: tetrahydrofolate; Met: methionine; MAT: S-adenosylmethionine synthetase; SAM: S-adenosylmethionine; SAH: S-adenosylhomocysteine; SAHH: SAH hydrolase; Hcy: homocysteine; MS: methionine synthase; MTRR: methionine synthase reductase; Ser: serine; Cysta: cystationine; CyS: cysteine; CySS: cystine; GSH: glutathione; γGT: γ-glutamyl transpeptidase; Cys-Gly: cysteinylglycine; DP: dipeptidase; GPX: glutathione peroxidase; GSSG: oxidized glutathione; SOD: superoxide dismutase.

Table 6: Differentially methylated positions in healthy lean (HL) and OverallObese prepubertal children that are related with genes involved in one-carbon metabolism.

DMP	Chr	Position	Genes	$\Delta\beta$	Log_2 fold change	p value*
cg14819132	17	17495032	PEMT	0.011	0.553	0.050
cg00214165	5	7869652	MTRR; FASTKD3	0.026	0.617	0.056
cg02956320	2	169643050	NOSTRIN	-0.073	-0.137	0.056
cg05065230	3	49395807	GPX1	0.012	0.651	0.063
cg06293195	22	36878654	TXN2	-0.078	-0.146	0.064
cg19948014	21	33032656	SOD1	0.007	0.552	0.070
cg22473973	10	133794911	BNIP3	0.012	0.437	0.073
cg19014302	19	18303893	MPV17L2	0.017	1.148	0.076
cg07941301	6	42928277	GNMT	0.015	0.740	0.078
cg01495361	20	31369590	DNMT3B	-0.055	-0.089	0.079
cg27619163	17	7982806	ALOX12B	0.044	1.474	0.083
cg05065765	3	38206519	OXSR1	0.016	0.632	0.084
cg04550070	11	73694480	UCP2	0.011	0.565	0.085
cg26978822	16	56622779	MT3	-0.019	-0.029	0.084
cg03452047	1	53067911	GPX7	0.012	0.391	0.087
cg26748435	14	64854866	MTHFD1	0.022	0.600	0.088
cg04372675	8	107283146	OXR1	0.019	0.510	0.094
cg06858294	17	7983203	ALOX12B	0.030	0.834	0.093
cg19642128	8	26240703	BNIP3L	0.031	1.068	0.094
cg13722539	11	64085131	PRDX5; TRMT112	0.006	0.406	0.094
cg10216074	2	25467197	DNMT3A	0.015	0.025	0.097
cg22545535	17	17495014	PEMT	0.024	0.941	0.096
cg08869383	1	11865661	MTHFR; CLCN6	0.010	0.464	0.098
cg09692733	19	10249298	DNMT1	0.006	0.009	0.096

DMP: differentially methylated position; Chr: chromosome; *adjusted p value using false discovery rate (FDR).

compared to HO subjects. Also, presented in Table 5 are the circulating levels of leptin and adiponectin, which are important cytokines secreted by adipose tissue. Adiponectin was reduced in the UHO as compared to the HO subjects while leptin levels and the leptin/adiponectin ratio were significantly elevated in the UHO as compared to the HO as well as in HO when compared to the HL groups. Increased levels of CRP were correlated with the leptin levels (Spearman's correlation, rho = 0.69, $p < 0.01$) (Supplementary Table 1A).

3.5. DNA Methylation Pattern. Since the transmethylation and transsulfuration pathways have a complementary loop as shown in Figure 1, and to further support our described findings of metabolic perturbations with possible effect at the DNA methylation mechanism, we analyzed the DNA methylation profile in PBMCs from a subset of the participants ($N = 14$ HL, $N = 16$ HO, and $N = 11$ UHO). Since no significant differences were observed between the HO and the UHO groups, both groups were merged (OverallObese) to achieve higher statistical power. Therefore, the HL ($n = 14$) were compared with the OverallObese subjects ($n = 27$) adjusting the model for HOMA-IR, thus enabling us to better isolate the effect of obesity.

From the cytosine-phosphate-guanines (CpGs) analyzed, 4677 were differentially methylated between the two groups (FDR < 0.1) (Supplementary Table 2). Furthermore, 35% of the significant DMPs presented a reduction in the methylation status (hypomethylation) in the OverallObese group, while 65% of the DMPs were hypermethylated in the same group. Moreover, 24 DMPs were selected from the list of 4677 DMPs based on their association with genes that are directly or indirectly related with one-carbon metabolism and consequently associated with oxidative stress and/or methylation processes [37–39], as explained before (Table 6).

Some of these DMPs are associated with genes involved in the expression of important enzymes, such as methionine synthase reductase (*MTRR* gene), methylenetetrahydrofolate dehydrogenase (*MTHFD1* gene), methylenetrahydrofolate reductase (*MTHFR* gene), and glycine-N-methyltransferase (*GNMT* gene). These enzymes are key in one-carbon metabolism and are responsible for methionine regeneration through the homocysteine conversion and the transmethylation pathway [40]. From these important results, it is possible to predict a downregulation in these enzymes since their genes are hypermethylated (positive β value or fold change in Table 6). The alteration in the methylation status of these enzymes could indeed explain the observed increase in SAH and homocysteine plasma levels observed in the HO (Table 3). Moreover, the methylation results also showed alteration in the regulation of genes involved in oxidative stress, which include glutathione peroxidase 1 and 7 (*GPX1*

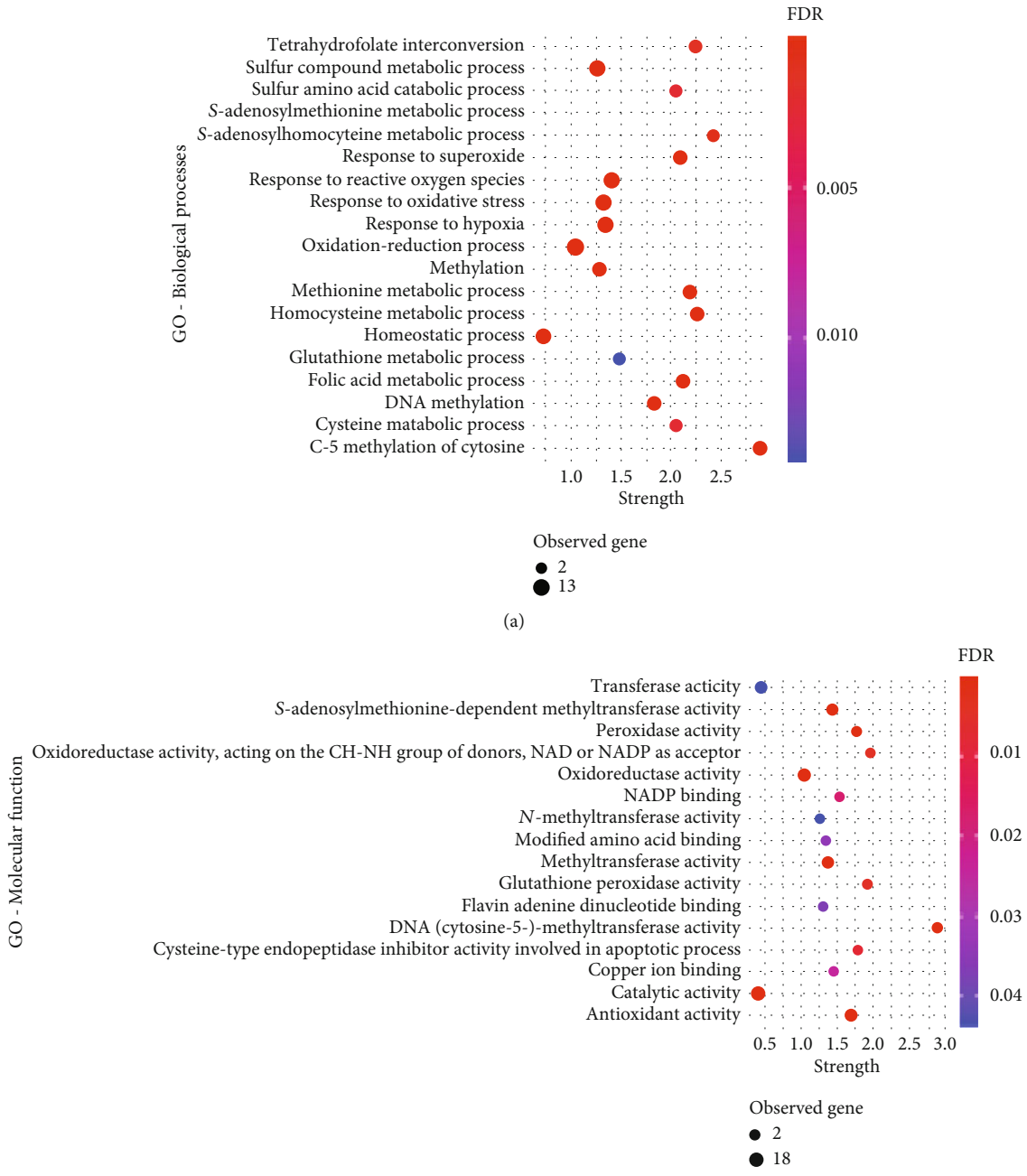

Figure 2: Continued.

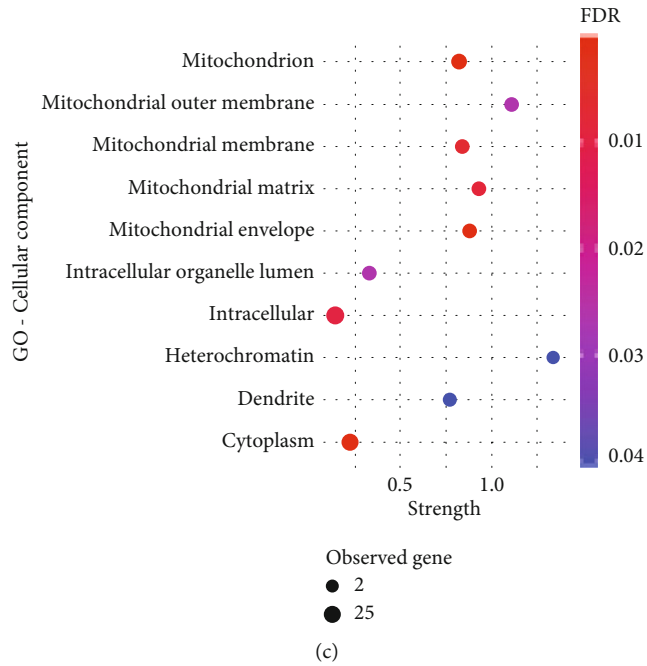

Figure 2: Gene Ontology (GO) term enrichment analysis for the genes related to the selected 24 DMPs. (a) GO terms for biological process terms; (b) GO terms for molecular function terms; (c) GO terms for cellular component terms; strength—enrichment effect, measured by the $\log_{10}$ of the number of proteins observed divided by the number of expected proteins. GO: Gene Ontology; FDR: false discovery rate; observed genes: number of genes (DMPs) involved in each GO term.

and GPX7), oxidation resistance 1 (*OXR1*), and superoxide dismutase 1 (*SOD1*). All these genes were hypermethylated in the OverallObese group, suggesting epigenetic-mediated downregulation. Interestingly, the enzymes responsible for DNA methylation, i.e., DNA methyltransferases (transcribed by the gene *DNMT1*), seem to be downregulated in the OverallObese group as well.

In order to disclose the biological meaning of these results, gene enrichment analysis was performed for the 24 DMP set, using the STRING database [36]. Importantly, the enrichment analysis showed 207 significant biological processes (Supplementary Table 3). Furthermore, 19 of them are terms involved in aminothiol metabolism, such as "response to oxidative stress," "methylation," "S-adenosylhomocysteine metabolic process," and "homocysteine metabolic process" (Figure 2(a)). In addition, 16 molecular functions, including SAM-dependent methyltransferase and peroxidase activity and 10 cellular components, including mitochondrial components, appear to be affected through the methylation pattern (Figures 2(b) and 2(c)). Interestingly, mitochondria seem to be of the most affected cellular component (Figure 2(c)). The KEGG pathway analysis, shown in Figure 3(a), indicates alterations in cysteine, methionine, and glutathione metabolism, as well as "one-carbon pool by folate." The Reactome pathway enrichment corroborates previous findings by showing alterations in metabolism and their association to epigenetic regulation (Figure 3(b)).

4. Discussion

Overnutrition and poor-quality diets are triggering a severe increase in obesity worldwide, with resulting metabolic disorders starting early in life, in particular during childhood [41]. Our results show that obesity has already caused profound changes in several aspects of metabolism in a cohort of prepubertal children, particularly in the one-carbon metabolism, of particular importance in the folate, transmethylation, and transsulfuration pathways. These studies, evaluating early childhood obesity, can inform on the potential origin of the related comorbidities that start plaguing many, already in young adulthood. We first chose to stratify children with obesity into two groups, the healthy and unhealthy obese, in order to understand the main differences between both conditions, where the unhealthy obese already presented insulin resistance. Our main criteria for this stratification were based on the HOMA – IR ≥ 2, although different phenotypes could be used to characterize and differentiate the metabolic state of this population, as reviewed by Phillips [41], who described various valid ways to characterize and distinguish between metabolically healthy and metabolically unhealthy obese children [41]. This separation between obese groups may give some important insights into adulthood comorbidities linked to obesity [41], and our analyses have revealed essential differences in several metabolic processes already emerging in this pediatric cohort. All pediatric subjects in this study presented normoglycemia, while the state of insulin resistance driven by the high circulating insulin concentrations observed in the UHO group likely reflects an attempt to maintain their euglycemia [42]. This is in agreement with other studies indicating that the insulin-resistant state could be present years before any alteration in circulating glucose are detected [43, 44]. Chronic periods of insulin resistance, even in the absence of elevated fasting glucose, may be an important contributing factor to the early

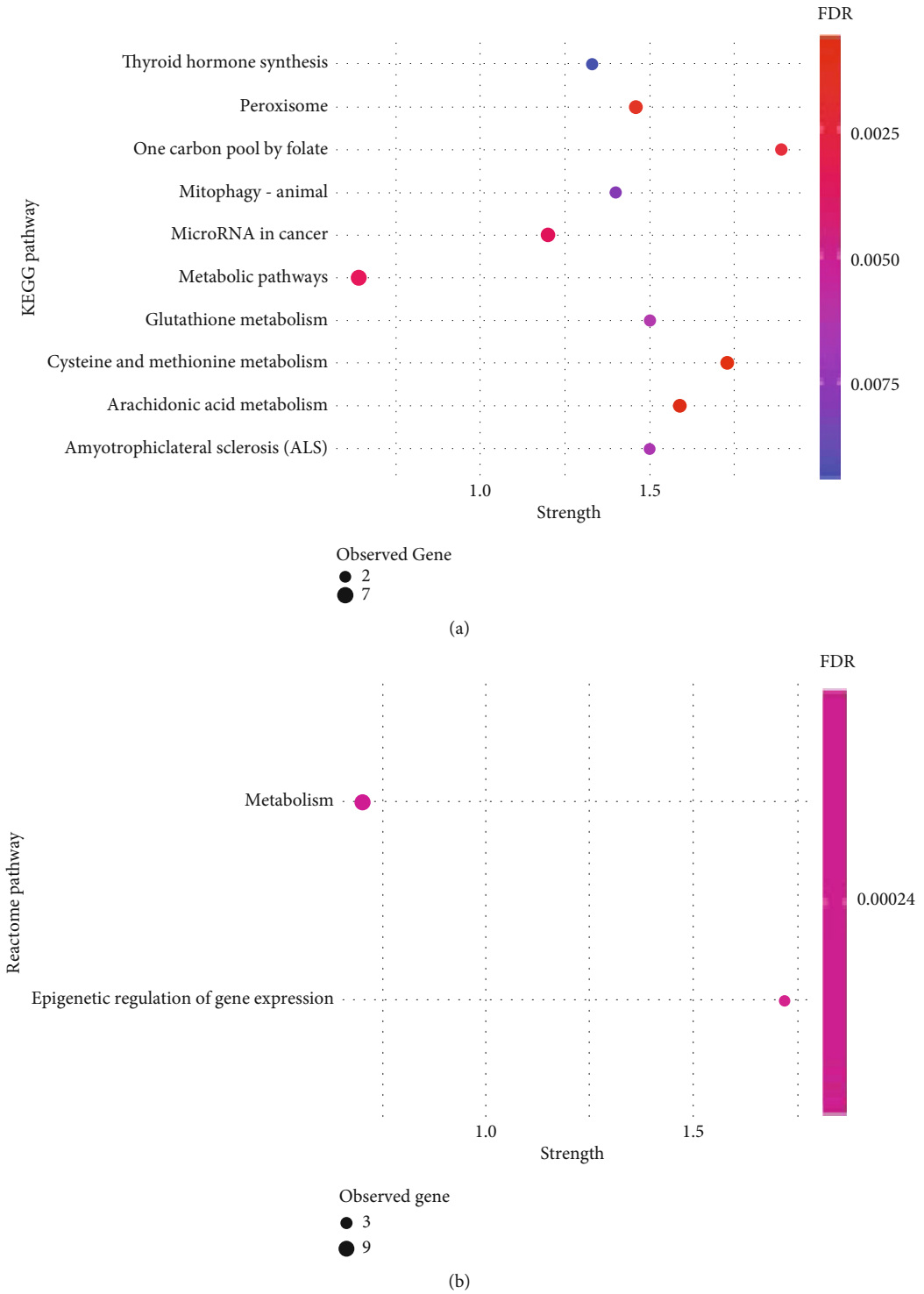

Figure 3: Pathway enrichment analysis for genes related to the selected 24 DMPs. (a) KEGG pathways; (b) Reactome pathways; strength—enrichment effect, measured by the $\log_{10}$ of the number of proteins observed divided by the number of expected proteins. GO: Gene Ontology; FDR: false discovery rate; observed genes: number of genes (DMPs) involved in a particular pathway.

blood pressure alterations also observed in our cohort [45, 46]. The increase in insulin production is reflected by the increased HOMA-β observed in the obese unhealthy subjects, reflecting increased β-cell activity. Similar to insulin, lactate levels were also elevated in the insulin-resistant obese group. This phenomenon has already been observed by Hosking et al. [47] in children with insulin resistance, indicating a positive correlation between insulin resistance and lactate levels during childhood and adolescence, even after controlling for BMIz as covariate BMIz. Furthermore,

Berhane et al. [48] have shown that plasma lactate was increased in adults during a hyperinsulinemic euglycemic clamp, a method that mimics the hyperinsulinemic state. Besides, they also indicated that high levels of lactate were present even before the insulin resistance was clinically detected [48]. Our data show that children as young as 5 to 10 years of age already show significantly elevated levels of lactate in the circulation, when comparing the HO to the UHO subjects. Moreover, there was a positive correlation between insulin and lactate levels as previously demonstrated [47]. Obesity-related insulin resistance has been involved in the development of other metabolic conditions, including CVD [49, 50] and lipid dysregulation [51, 52]. The insulin-resistant UHO subjects also presented lipid dysregulation and increased systolic blood pressure, risk factors for CVD. Furthermore, chronic low-grade inflammation and increased oxidative stress are characteristics of obesity [15]. The quantification of thiol molecules during prepubertal obesity and insulin resistance has not been well described. Some of these molecules are intermediaries of one-carbon metabolism and are important for the maintenance of redox homeostasis and the methylation capacity of cells by acting on transsulfuration and transmethylation pathways. Our data clearly show important differences in the transmethylation pathway, especially when comparing the HL and HO subjects. The HO showed higher levels of SAH and total homocysteine, similarity to the previously reported findings by Kumar et al. [53]. These molecules have already been implicated in the development of atherosclerosis and CVD [20, 54]. Similar alterations have been identified in diabetic patients with renal dysfunction, and the homocysteine levels were also positively correlated with insulin levels [40]. In addition, Chiang et al. [40] have observed the effect of insulin (1 μM) in HepG2 cell lines and showed that mRNA expression of different enzymes related with one-carbon metabolism, such as MTRR, was reduced during the treatment with insulin. In agreement, the HO subjects in the present study had higher fasting insulin levels that are accompanied with high levels of homocysteine in plasma, compared to their lean counterparts. Importantly, DNA methylation analysis, from PBMCs isolated from the prepubertal children with obesity, showed hypermethylation of different CpGs that are localized in the vicinity of important metabolic genes, including *PEMT*, *MTRR*, and *MTHFR*, suggesting that an epigenetic effect could be the cause for this downregulation. Gene Ontology enrichment analysis also showed alteration in different key biological processes, molecular functions, and cellular components related with one-carbon metabolism, as shown in Figure 2. Even though the SAM/SAH ratio was not altered in our cohort, there were already alterations in the methylation profile of PBMCs in the obese subjects. Yi et al. [55] correlated high levels of homocysteine and SAH with a decrease in DNA methylation of lymphocytes. High SAH levels are also described as inhibitors of methyltransferase processes [20]. Furthermore, alterations in the transsulfuration pathway were also identified, in particular when comparing the HL with the HO subjects. This pathway is important in the redox state maintenance, since it is responsible for the synthesis of molecules, such as cysteine and GSH, that act as important ROS scavengers [14]. Interestingly, increased insulin levels have been shown to disrupt the redox homeostasis and consequently alter the defense mechanisms against excess ROS production [56]. Elshorbagy et al. [57] indicated that alterations in plasma total cysteine are associated with an increase in BMI, in adults. Similarly, we also observed higher levels of total cysteine in the HO subjects compared to their lean counterparts. On the other hand, the levels of fCysteine remain unchanged between groups even in the presence of higher levels of cystine, especially in the obese groups. Furthermore, the fCysteine/cystine ratio is an important plasma marker that defines an imbalance in redox homeostasis [58]. However, no differences were identified in that ratio between groups in our cohort, although the levels of GSSG were increased in the obese groups. Similar results were postulated by Choromańska et al. [59] who reported high levels of GSSG in plasma of obese adults with hypertension. While the fCysteine/cystine ratio was not altered, we observed significant alterations in the GSH/GSSG ratio in the HO group, with an increase in the percentage of GSH oxidation compared to HL. Few studies of this kind have been performed in prepubertal children with obesity; however, it is known that in adults, insulin resistance and dyslipidemia have a significant impact on oxidative stress [3, 60]. In line with the alterations detected in the redox homeostasis, increased plasma inflammation was also observed, in the children with obesity, in particular CRP and leptin levels. Pedersen et al. [61] demonstrated that hyperinsulinemia during obesity induced the expression of inflammation-associated genes. Importantly, the role leptin plays in inflammatory exacerbation has been reviewed [2]. Interestingly, high levels of homocysteine have also previously been implicated with inflammation [62].

These metabolic alterations are key factors for future development of obesity-related comorbidities, particularly in people with insulin resistance, and have been described, particularly in adults, as important predictive markers of CVD, including atherosclerosis [20, 54, 63]. Additionally, our data show significant differences in adipocyte secretion of adipokines. While leptin levels were increased in both obese groups, adiponectin levels were decreased in the UHO group. Our results are in agreement with other studies indicating low adiponectin levels, as a marker of adipocyte secretory dysfunction, together with elevated leptin secretion [64, 65]. Our data indicate an evident alteration in adipocyte secretory patterns, especially in the obese- and insulin-resistant subjects. Landgraf et al. [66] corroborate the presence of adipose tissue dysfunction during childhood obesity, making the correlation between adipocyte expansion and inflammation. Interestingly, the high leptin and low adiponectin levels together with the increased plasma lactate are early important markers that differentiate obese subjects with insulin resistance from their metabolic healthy counterpart. Our results show a deregulated adipocyte secretory function, even under normoglycemia in prepubertal children with obesity.

Moreover, our data also show significant changes in the methylation patterns of PBMCs. Circulating cells have been considered important surrogate markers for different type of diseases, since they are in contact with the continuous

changing circulating molecules from surrounding tissues. Therefore, small metabolic changes that may occur in the body will induce key modifications in the biology of these cells [67]. In agreement, our results reflect the impact of obesity on the epigenetic patterns of PBMC DNA. In particular, we noticed alterations of the methylation degree in the vicinity of genes that are involved in one-carbon metabolism, such as the transmethylation and transsulfuration pathways. Previous studies have shown alterations in methylation patterns associated with obesity and obesity-related insulin resistance [68–70]. The lack of significant differences in these metabolic pathways and in the DNA methylation results when comparing the HO and the UHO subjects might likely be due to the low study power when we split the obese subjects into two different groups. Our study is limited by relatively small sample sizes as we were unable to fully reach our recruitment goals. Unfortunately, we do not have the DNA methylation data for the entire cohort. In future studies, we would like to increase the *N* in each group and invite the subjects back two years later for a follow-up visit.

Finally, the physiological and biochemical characteristics of the young prepubertal children show that among the obese subjects, there are indeed a group of HO that are still metabolically healthy as the HL, while the UHO already presented metabolic dysfunction, even under normoglycemia. This suggests that the adult obesity phenotype is starting to set in at an early age, raising important questions about the reversibility of this condition and the future health of these subjects.

In conclusion, our study showed the presence of deep alteration in one-carbon metabolism and related pathways in children with obesity (Figure 1), as young as 5-9 years of age. These alterations are mainly driven by obesity and elevated insulin levels. Most importantly, even the metabolic healthy obese subjects show increased levels of important metabolic markers, such as SAH, that is related with developing future comorbidities. This may reflect an important transition phase between different stages of obesity and insulin resistance. Specific markers that could identify this transition would be extremely important in identifying populations early at high risk of developing CVD and T2D. The data presented provide insight on important metabolic changes that occur in obesity early in life (summarized in Figure 1). Importantly, the metabolic healthy obese children seem to have some compensatory mechanisms to maintain important features unchanged, including the lipid profile and glucose levels. Also, some important alterations are already established at the epigenetic level, although some of these alterations could still be reversed by possible changing lifestyle habits [39].

Data Availability

Additional data can be found in supplementary tables.

Conflicts of Interest

The authors have no conflicts of interests to declare.

Authors' Contributions

Shannon Rose and Eugenia Carvalho contributed equally to this work and are considered senior authors.

Acknowledgments

Research reported in this publication was financed by the National Institute of General Medical Sciences of the National Institutes of Health under a COBRE Award Number P20GM109096 and the Arkansas Biosciences Institute/Arkansas Children' Research Institute, through the Discovery Acceleration Initiative/Program Project Planning Grants and bridging funds. Further funds were obtained by the European Regional Development Fund, through the Centro 2020 Regional Operational Programme Healthy Aging2020-CENTRO-01-0145-FEDER-000012 and through COMPETE 2020–Operational Programme for Competitiveness and Internationalisation and Portuguese national funds via FCT—Fundação para a Ciência e a Tecnologia, projects POCI-01-0145-FEDER-007440, POCI-01-0145-FEDER-022184 (GenomePT), UIDB/04539/2020, UIDP/04539/2020, UIDP/04501/2020 (iBiMED-UA), and PB PhD grant SFRH/BD/143849/2019. EB was partly funded by NIH/-NIGMS UL1 TR003107 and KL2 TR003108 and USDA/ARS 6026-51000-012-06-S. The content is solely the responsibility of the authors and does not necessarily represent the official views of the funding agencies. We thank all the participants in the study. We acknowledge the technical assistance of Matthew Cotter, Oleksandra Pavliv, Stewart Macleod, Stefan Graw, and Stephanie Byrum.

Supplementary Materials

Supplementary 1. Supplementary Table 1: correlation of clinical and biochemical parameters (A) in healthy lean and healthy obese participants and (B) in healthy obese and unhealthy obese participants.

Supplementary 2. Supplementary Table 2: complete list of differentially methylated positions (DMPs).

Supplementary 3. Supplementary Table 3: GO term enrichment results for biological processes.

References

[1] E. Kilic, Ö. F. Özer, A. Erek Toprak et al., "Oxidative stress status in childhood obesity: a potential risk predictor," *Medical Science Monitor*, vol. 22, pp. 3673–3679, 2016.

[2] N. Iikuni, Q. Kwan Lam, L. Lu, G. Matarese, and A. Cava, "Leptin and inflammation," *Current Immunology Reviews*, vol. 4, no. 2, pp. 70–79, 2008.

[3] S. Hurrle and W. H. Hsu, "The etiology of oxidative stress in insulin resistance," *Biomedical Journal*, vol. 40, no. 5, pp. 257–262, 2017.

[4] L. G. Bjerregaard, B. W. Jensen, L. Ängquist, M. Osler, T. I. A. Sørensen, and J. L. Baker, "Change in overweight from childhood to early adulthood and risk of type 2 diabetes," *New England Journal of Medicine*, vol. 378, no. 14, pp. 1302–1312, 2018.

[5] S. H. Song and C. A. Hardisty, "Early onset type 2 diabetes mellitus: a harbinger for complications in later years–clinical observation from a secondary care cohort," *An International Journal of Medicine*, vol. 102, no. 11, pp. 799–806, 2009.

[6] C. Graf and N. Ferrari, "Metabolic syndrome in children and adolescents," *Visceral Medicine*, vol. 32, no. 5, pp. 357–362, 2016.

[7] T. S. Hannon and S. A. Arslanian, "The changing face of diabetes in youth: lessons learned from studies of type 2 diabetes," *Annals of the New York Academy of Sciences*, vol. 1353, no. 1, pp. 113–137, 2015.

[8] F. Bacha, N. Gungor, S. Lee, and S. A. Arslanian, "Progressive deterioration of β-cell function in obese youth with type 2 diabetes," *Pediatric Diabetes*, vol. 14, no. 2, pp. 106–111, 2013.

[9] D. A. Elder, L. N. Hornung, J. C. Khoury, and D. A. D'Alessio, "β-Cell Function Over Time in Adolescents With New Type 2 Diabetes and Obese Adolescents Without Diabetes," *Journal of Adolescent Health*, vol. 61, no. 6, pp. 703–708, 2017.

[10] P. Zeitler, K. Hirst, L. Pyle et al., "A clinical trial to maintain glycemic control in youth with type 2 diabetes," *New England Journal of Medicine*, vol. 366, no. 24, pp. 2247–2256, 2012.

[11] L. Turell, R. Radi, and B. Alvarez, "The thiol pool in human plasma: the central contribution of albumin to redox processes," *Free Radical Biology and Medicine*, vol. 65, pp. 244–253, 2013.

[12] S. Jill James, S. Melnyk, S. Jernigan, A. Hubanks, S. Rose, and D. W. Gaylor, "Abnormal transmethylation/transsulfuration metabolism and DNA hypomethylation among parents of children with autism," *Journal of Autism and Developmental Disorders*, vol. 38, no. 10, pp. 1966–1975, 2008.

[13] G. M. de Donatis, R. Moschini, M. Cappiello, A. del Corso, and U. Mura, "Cysteinyl-glycine in the control of glutathione homeostasis in bovine lenses," *Molecular Vision*, vol. 16, pp. 1025–1033, 2010.

[14] S. Melnyk, G. J. Fuchs, E. Schulz et al., "Metabolic imbalance associated with methylation dysregulation and oxidative damage in children with autism," *Journal of Autism and Developmental Disorders*, vol. 42, no. 3, pp. 367–377, 2012.

[15] A. M. Lechuga-Sancho, D. Gallego-Andujar, P. Ruiz-Ocaña et al., "Obesity induced alterations in redox homeostasis and oxidative stress are present from an early age," *PLoS One*, vol. 13, no. 1, article e0191547, 2018.

[16] A. Zalewska, A. Kossakowska, K. Taranta-Janusz et al., "Dysfunction of Salivary Glands, Disturbances in Salivary Antioxidants and Increased Oxidative Damage in Saliva of Overweight and Obese Adolescents," *Journal of Clinical Medicine*, vol. 9, no. 2, p. 548, 2020.

[17] N. Mahmood, D. Cheishvili, A. Arakelian et al., "Methyl donor S-adenosylmethionine (SAM) supplementation attenuates breast cancer growth, invasion, and metastasisin vivo; therapeutic and chemopreventive applications," *Oncotarget*, vol. 9, no. 4, pp. 5169–5183, 2018.

[18] Y. Chen, M. Han, A. Matsumoto, Y. Wang, D. C. Thompson, and V. Vasiliou, "Glutathione and transsulfuration in alcohol-associated tissue injury and carcinogenesis," in *Advances in Experimental Medicine and Biology*, vol. 1032, Springer, 2018.

[19] Y. M. Go and D. P. Jones, "Cysteine/cystine redox signaling in cardiovascular disease," *Free Radical Biology & Medicine*, vol. 50, no. 4, pp. 495–509, 2011.

[20] Y. Xiao, J. Xia, J. Cheng et al., "Inhibition of S-adenosylhomocysteine hydrolase induces endothelial dysfunction via epigenetic regulation of p66shc-mediated oxidative stress pathway," *Circulation*, vol. 139, no. 19, pp. 2260–2277, 2019.

[21] S. Rose, E. Carvalho, E. C. Diaz et al., "A comparative study of mitochondrial respiration in circulating blood cells and skeletal muscle fibers in women," *American Journal of Physiology-Endocrinology and Metabolism*, vol. 317, no. 3, pp. E503–E512, 2019.

[22] B. Hedblad, P. Nilsson, L. Janzon, and G. Berglund, "Relation between insulin resistance and carotid intima-media thickness and stenosis in non-diabetic subjects. Results from a cross-sectional study in Malmo, Sweden," *Diabetic Medicine*, vol. 17, no. 4, pp. 299–307, 2000.

[23] M. A. Tomé Martínez de Rituerto, M. A. Botana, C. Cadarso-Suárez et al., "Prevalence of metabolic syndrome in Galicia (NW Spain) on four alternative definitions and association with insulin resistance," *Journal of Endocrinological Investigation*, vol. 32, no. 6, pp. 505–511, 2009.

[24] K. Omiya, K. Minami, Y. Sato et al., "Impaired β-cell function attenuates training effects by reducing the increase in heart rate reserve in patients with myocardial infarction," *Journal of Cardiology*, vol. 65, no. 2, pp. 128–133, 2015.

[25] S. Melnyk, M. Pogribna, I. Pogribny, R. J. Hine, and S. J. James, "A new HPLC method for the simultaneous determination of oxidized and reduced plasma aminothiols using coulometric electrochemical detection1," *The Journal of Nutritional Biochemistry*, vol. 10, no. 8, pp. 490–497, 1999.

[26] M. Bibikova, B. Barnes, C. Tsan et al., "High density DNA methylation array with single CpG site resolution," *Genomics*, vol. 98, no. 4, pp. 288–295, 2011.

[27] R. Pidsley, C. C. Y Wong, M. Volta, K. Lunnon, J. Mill, and L. C. Schalkwyk, "A data-driven approach to preprocessing Illumina 450K methylation array data," *BMC Genomics*, vol. 14, no. 1, pp. 293–303, 2013.

[28] M. J. Aryee, A. E. Jaffe, H. Corrada-Bravo et al., "Minfi: a flexible and comprehensive Bioconductor package for the analysis of Infinium DNA methylation microarrays," *Bioinformatics*, vol. 30, no. 10, pp. 1363–1369, 2014.

[29] R Core Team, *R: A language and environment for statistical computing*, R Foundation for Statistical Computing, Vienna, Austria, 2021, https://www.r-project.org/.

[30] RStudio Team, *RStudio: Integrrated Development Environment for R*, RStudio, PBC, Boston, MA, 2021.

[31] J. Liu and K. D. Siegmund, "An evaluation of processing methods for HumanMethylation450 BeadChip data," *BMC Genomics*, vol. 17, no. 1, 2016.

[32] R. Pidsley, E. Zotenko, T. J. Peters et al., "Critical evaluation of the Illumina MethylationEPIC BeadChip microarray for whole-genome DNA methylation profiling," *Genome Biology*, vol. 17, no. 1, 2016.

[33] J. Maksimovic, B. Phipson, and A. Oshlack, "A cross-package Bioconductor workflow for analysing methylation array data," *F1000Research*, vol. 5, p. 1281, 2016.

[34] M. E. Ritchie, B. Phipson, D. Wu et al., "Limma powers differential expression analyses for RNA-sequencing and microarray studies," *Nucleic Acids Research*, vol. 43, no. 7, article e47, 2015.

[35] Y. Benjamini and Y. Hochberg, "Controlling the false discovery rate: a practical and powerful approach to multiple

testing," *Journal of the Royal Statistical Society: Series B (Methodological)*, vol. 57, no. 1, pp. 289–300, 1995.

[36] D. Szklarczyk, A. L. Gable, D. Lyon et al., "STRING v11: protein-protein association networks with increased coverage, supporting functional discovery in genome-wide experimental datasets," *Nucleic Acids Research*, vol. 47, D1, pp. D607–D613, 2019.

[37] A. Leone, M. S. Roca, C. Ciardiello, S. Costantini, and A. Budillon, "Oxidative stress gene expression profile correlates with cancer patient poor prognosis: identification of crucial pathways might select novel therapeutic approaches," *Oxidative Medicine and Cellular Longevity*, vol. 2017, Article ID 2597581, 18 pages, 2017.

[38] Y. L. Lee, X. Xu, S. Wallenstein, and J. Chen, "Gene expression profiles of the one-carbon metabolism pathway," *Journal of Genetics and Genomics*, vol. 36, no. 5, pp. 277–282, 2009.

[39] J. A. Martínez, F. I. Milagro, K. J. Claycombe, and K. L. Schalinske, "Epigenetics in Adipose Tissue, Obesity, Weight Loss, and Diabetes," *Advances in Nutrition*, vol. 5, no. 1, pp. 71–81, 2014.

[40] E. P. I. Chiang, Y. C. Wang, W. W. Chen, and F. Y. Tang, "Effects of Insulin and Glucose on Cellular Metabolic Fluxes in Homocysteine Transsulfuration, Remethylation,S-Adenosylmethionine Synthesis, and Global Deoxyribonucleic Acid Methylation," *The Journal of Clinical Endocrinology & Metabolism*, vol. 94, no. 3, pp. 1017–1025, 2009.

[41] C. M. Phillips, "Metabolically healthy obesity across the life course: epidemiology, determinants, and implications," *Annals of the New York Academy of Sciences*, vol. 1391, no. 1, pp. 85–100, 2017.

[42] J. A. J. Martyn, M. Kaneki, S. Yasuhara, D. S. Warner, and M. A. Warner, "Obesity-induced insulin resistance and hyperglycemia: etiologic factors and molecular mechanisms," *Anesthesiology*, vol. 109, no. 1, pp. 137–148, 2008.

[43] E. Carvalho, P. A. Jansson, M. Axelsen et al., "Low cellular IRS 1 gene and protein expression predict insulin resistance and NIDDM," *The FASEB Journal*, vol. 13, no. 15, pp. 2173–2178, 1999.

[44] M. M. Adeva-Andany, E. Ameneiros-Rodríguez, C. Fernández-Fernández, A. Domínguez-Montero, and R. Funcasta-Calderón, "Insulin resistance is associated with subclinical vascular disease in humans," *World Journal of Diabetes*, vol. 10, no. 2, pp. 63–77, 2019.

[45] R. Tarray, S. Saleem, D. Afroze et al., "Role of insulin resistance in essential hypertension," *Cardiovascular Endocrinology*, vol. 3, no. 4, pp. 129–133, 2014.

[46] A. R. Sinaiko, J. Steinberger, A. Moran, R. J. Prineas, and D. R. Jacobs, "Relation of insulin resistance to blood pressure in childhood," *Journal of Hypertension*, vol. 20, no. 3, pp. 509–517, 2002.

[47] J. Hosking, J. Pinkney, A. Jeffery et al., "Insulin resistance during normal child growth and development is associated with a distinct blood metabolic phenotype (Earlybird 72)," *Pediatric Diabetes*, vol. 20, no. 7, pp. 832–841, 2019.

[48] F. Berhane, A. Fite, N. Daboul et al., "Plasma lactate levels increase during hyperinsulinemic euglycemic clamp and oral glucose tolerance test," *Journal of Diabetes Research*, vol. 2015, Article ID 102054, 7 pages, 2015.

[49] A. Deeb, S. Attia, S. Mahmoud, G. Elhaj, and A. Elfatih, "Dyslipidemia and fatty liver disease in overweight and obese children," *Journal of Obesity*, vol. 2018, Article ID 8626818, 6 pages, 2018.

[50] M. Bastien, P. Poirier, I. Lemieux, and J. P. Després, "Overview of epidemiology and contribution of obesity to cardiovascular disease," *Progress in Cardiovascular Diseases*, vol. 56, no. 4, pp. 369–381, 2014.

[51] B. M. Wolfe, E. Kvach, and R. H. Eckel, "Treatment of obesity," *Circulation Research*, vol. 118, no. 11, pp. 1844–1855, 2016.

[52] J. Vekic, A. Zeljkovic, A. Stefanovic, Z. Jelic-Ivanovic, and V. Spasojevic-Kalimanovska, "Obesity and dyslipidemia," *Metabolism: Clinical and Experimental*, vol. 92, pp. 71–81, 2019.

[53] K. Jagadish Kumar, K. Saldanha, K. Sushma, D. Srinivasa Murthy, and P. Vishwanath, "A prospective study of homocysteine and its relation to body mass index and lipid profile in school children," *Indian Pediatrics*, vol. 54, no. 11, pp. 935–937, 2017.

[54] Y. Xiao, X. Su, W. Huang et al., "Role of S-adenosylhomocysteine in cardiovascular disease and its potential epigenetic mechanism," *International Journal of Biochemistry and Cell Biology*, vol. 67, pp. 158–166, 2015.

[55] P. Yi, S. Melnyk, M. Pogribna, I. P. Pogribny, R. J. Hine, and S. J. James, "Increase in Plasma Homocysteine Associated with Parallel Increases in Plasma *S*-Adenosylhomocysteine and Lymphocyte DNA Hypomethylation," *Journal of Biological Chemistry*, vol. 275, no. 38, pp. 29318–29323, 2000.

[56] A. M. Mahmoud, M. M. Ali, E. R. Miranda et al., "Nox2 contributes to hyperinsulinemia-induced redox imbalance and impaired vascular function," *Redox Biology*, vol. 13, pp. 288–300, 2017.

[57] A. K. Elshorbagy, M. Valdivia-Garcia, I. M. Graham et al., "The association of fasting plasma sulfur-containing compounds with BMI, serum lipids and apolipoproteins," *Nutrition, Metabolism and Cardiovascular Diseases*, vol. 22, no. 12, pp. 1031–1038, 2012.

[58] Y. M. Go and D. P. Jones, "Redox compartmentalization in eukaryotic cells," *Biochimica et Biophysica Acta - General Subjects*, vol. 1780, no. 11, pp. 1273–1290, 2008.

[59] B. Choromańska, P. Myśliwiec, M. Łuba et al., "The impact of hypertension and metabolic syndrome on nitrosative stress and glutathione metabolism in patients with morbid obesity," *Oxidative Medicine and Cellular Longevity*, vol. 2020, Article ID 1057570, 10 pages, 2020.

[60] R. L. Yang, Y. H. Shi, G. Hao, W. Li, and G. W. Le, "Increasing oxidative stress with progressive hyperlipidemia in human: relation between malondialdehyde and atherogenic index," *Journal of Clinical Biochemistry and Nutrition*, vol. 43, no. 3, pp. 154–158, 2008.

[61] D. J. Pedersen, A. Guilherme, L. V. Danai et al., "A major role of insulin in promoting obesity-associated adipose tissue inflammation," *Molecular Metabolism*, vol. 4, no. 7, pp. 507–518, 2015.

[62] M. OudiEl, Z. Aouni, C. Mazigh et al., "Homocysteine and markers of inflammation in acute coronary syndrome," *Experimental and Clinical Cardiology*, vol. 15, no. 2, pp. e25–e28, 2010.

[63] E. Golia, G. Limongelli, F. Natale et al., "Inflammation and cardiovascular disease: from pathogenesis to therapeutic target," *Current Atherosclerosis Reports*, vol. 16, no. 9, p. 435, 2014.

[64] P.-A. Jansson, F. Pellmé, A. Hammarstedt et al., "A novel cellular marker of insulin resistance and early atherosclerosis in

humans is related to impaired fat cell differentiation and low adiponectin," *The FASEB Journal*, vol. 17, no. 11, pp. 1434–1440, 2003.

[65] X. Yang, P. A. Jansson, I. Nagaev et al., "Evidence of impaired adipogenesis in insulin resistance," *Biochemical and Biophysical Research Communications*, vol. 317, no. 4, pp. 1045–1051, 2004.

[66] K. Landgraf, D. Rockstroh, I. V. Wagner et al., "Evidence of early alterations in adipose tissue biology and function and its association with obesity-related inflammation and insulin resistance in children," *Diabetes*, vol. 64, no. 4, pp. 1249–1261, 2015.

[67] M. Mosallaei, N. Ehtesham, S. Rahimirad, M. Saghi, N. Vatandoost, and S. Khosravi, "PBMCs: a new source of diagnostic and prognostic biomarkers," *Archives of Physiology and Biochemistry*, pp. 1–7, 2020.

[68] F. He, A. Berg, Y. Imamura Kawasawa et al., "Association between DNA methylation in obesity-related genes and body mass index percentile in adolescents," *Scientific Reports*, vol. 9, no. 1, p. 2079, 2019.

[69] S. Sayols-Baixeras, I. Subirana, A. Fernández-Sanlés et al., "DNA methylation and obesity traits: an epigenome-wide association study. The REGICOR study," *Epigenetics*, vol. 12, no. 10, pp. 909–916, 2017.

[70] J. Zhao, J. Goldberg, J. D. Bremner, and V. Vaccarino, "Global DNA methylation is associated with insulin resistance: a monozygotic twin study," *Diabetes*, vol. 61, no. 2, pp. 542–546, 2012.

Hindawi
Oxidative Medicine and Cellular Longevity
Volume 2021, Article ID 4009308, 9 pages
https://doi.org/10.1155/2021/4009308

Research Article

Nrf2 Pathway Ameliorates Bladder Dysfunction in Cyclophosphamide-Induced Cystitis via Suppression of Oxidative Stress

Bin Ni, Zhengsen Chen, Le Shu, Yunpeng Shao, Yi Huang, Nebiyu Elias Tamrat, Zhongqing Wei, and Baixin Shen

Department of Urology, The Second Affiliated Hospital of Nanjing Medical University, Nanjing 210000, China

Correspondence should be addressed to Zhongqing Wei; weizq1@163.com and Baixin Shen; baixinshen@njmu.edu.cn

Received 21 April 2021; Revised 12 May 2021; Accepted 10 June 2021; Published 7 July 2021

Academic Editor: Daniela Ribeiro

Objective. To investigate the protective effect and molecular mechanism of nuclear factor E2-related factor 2 (Nrf2) pathway in interstitial cystitis (IC). *Methods*. We established a mouse model of IC by cyclophosphamide (CYP) in wild-type mice and Nrf2 gene knockout mice. We examined the histological and functional alterations, the changes of oxidative stress markers, and the expression of the antioxidant genes downstream of Nrf2 pathway. *Results*. After CYP administration, the mice showed urinary frequency and urgency, pain sensitization, decreased contractility, bladder edema, and oxidative stress disorder. Notably, the $Nrf2^{-/-}$ CYP mice had more severe symptoms. The mRNA and protein levels of antioxidant genes downstream of Nrf2 pathway were significantly upregulated in the $Nrf2^{+/+}$ CYP mice, while there were no significant changes in the $Nrf2^{-/-}$ CYP mice. *Conclusion*. Nrf2 pathway protects bladder injury and ameliorates bladder dysfunction in IC, possibly by upregulating antioxidant genes and inhibiting oxidative stress.

1. Introduction

Interstitial cystitis (IC), also known as bladder painful syndrome (BPS), is a chronic inflammatory bladder disease that clinically manifests as pain or pelvic discomfort related to bladder filling, accompanied by lower urinary tract symptoms such as urinary urgency and frequency [1]. There is wide variation in reported incidence and prevalence of IC depending on the criteria used for diagnosis, but approximately 90% of the patients are women [2]. At present, the therapeutic alternatives are still limited and unsatisfactory. Therefore, further research is needed to clarify the related mechanism of IC.

Recently, increasing studies have found that oxidative stress is closely associated with pathological mechanisms of various diseases [3]. Reactive oxygen species (ROS) produced by oxidative stress may contribute to bladder dysfunction [4]. Previous research has found that diverse antioxidants could suppress oxidative stress induced by IC [5, 6]. The nuclear factor E2-related factor 2 (Nrf2) pathway is a transcription factor involved in regulating the cellular antioxidative responses by promoting the expression of ant genes through binding to antioxidant response element (ARE, 5′-TGACXXXGC-3′) [7]. Under homeostatic conditions, two molecules of keap1 are bound to Nrf2 and isolate Nrf2 in the cytoplasm [8]. In response to oxidative stress, Keap1 inactivation promotes the dissociation of Nrf2 from Keap1 and translocation into the nucleus. The Nrf2-sMaf complex binds, in a sequence-specific manner, to the ARE in the promoter region of Nrf2 target genes and then initiates the expression of a series of antioxidant genes, such as heme oxygenase-1 (HO-1), NAD (P)H : quinone oxidoreductase 1 (NQO1), glutathione reductase (GR), and superoxide dismutase (SOD) [9]. However, the specific molecular mechanism of Nrf2 in IC is still unclear and the functional evaluation of IC animal models remains vague.

In this study, wild-type and Nrf2 knockout mice were obtained to establish the IC model by cyclophosphamide

(CYP). Moreover, our study is the first to establish an objective functional evaluation system for the study of the bladder function and behavior in IC animal models, according to the typical clinical manifestation of IC. Micturition behavior, pain hypersensitivity, and urodynamics were performed to assess the IC animal models. In summary, the protective effect and regulation mechanism of the Nrf2 pathway in IC were explored, in order to provide new options for the clinical treatment of IC.

2. Materials and Methods

2.1. Animals. Wild-type C57BL/6J mice were obtained from the Animal Center of Nanjing Medical University and the Nrf2 knockout mice were purchased from the Model Animal Research Center of Nanjing University. All mice were housed five per cage in a room under a 12 h light/dark cycle with free access to food and water under the condition of 20–26°C with 40–60% relative humidity. The animals in this study were sacrificed by a physical method of euthanasia under anesthetized with isoflurane. All experimental procedures were approved by the Animal Ethical and Welfare Committee of Nanjing Medical University (IACUC-1904032).

A total of 80 mice were randomly divided into four groups ($n = 20$): $Nrf2^{+/+}$ control group, $Nrf2^{-/-}$ control group, $Nrf2^{+/+}$ CYP group, and $Nrf2^{-/-}$ CYP group. The control groups received saline treatment, and the CYP groups received a single intraperitoneal injection of cyclophosphamide (CYP, 150 mg/kg) [10]. The mice were sacrificed 24 hours after administration. Mice in the same group received homogeneous treatment.

2.2. Void Spot Assays (VSA). Urinary frequency and mean voided volume were studied using the void spot assay [11]. We performed the VSA experiments 24 hours after CYP administration in a circle metabolic cage (Yuyan, Shanghai). Individual mice were gently removed into the metabolic cage with circular filter paper (Whatman No.1) taped to the bottom without a grid. The mice were provided with standard food and water for the duration of the assay. The micturition cages were kept in a quiet area for 2 hours. At the end of 2 hours, the mice were returned to normal housing, and the filter paper was recovered and imaged using an imaging system. The images were analyzed by the Fiji version of the ImageJ software. Urine volumes were determined using an area-to-volume standard curve as shown in Figure 1. We performed the VSA experiments at approximately the same time every afternoon between 9 AM and 4 PM.

2.3. Pelvic Nociceptive Response Using von Frey Filaments. Mice were placed individually in Plexiglas cubicles on a wire grid on a raised platform (Yuyan, Shanghai). Mice were allowed to acclimate to the environment for a minimum of 30 minutes before testing. Filaments were applied vertically to the pelvic area close to the bladder. The 50% withdrawal threshold was determined using the up-down method of Dixon (1980) [12]. We chose 0.008 g, 0.02 g, 0.04 g, 0.07 g, 0.16 g, 0.4 g, 1 g, 2 g (North coast, USA) as a series and the testing was initiated with the 0.07 g hair, in the middle of the series. Withdrawal or retraction of the lower abdominal/-pelvic area from the filament stimulation was considered a positive response. In the absence of a withdrawal response to the initially selected filament, a stronger stimulus was chosen; in the event of withdrawal, a weaker stimulus was chosen. According to Dixon, once the two responses straddle the threshold, four additional responses are required.

2.4. Urodynamic Measurements. Urodynamic measurements were performed 24 hours after CYP administration in mice as previously described [13]. The mice were anesthetized with isoflurane (2%). Before the start of the recording, the air in the system was emptied and the catheter was connected via a T-tube to a pressure transducer (Taimeng, Chengdu) and microinjection pump (Silugao, Beijing). Normal saline was infused at room temperature into the bladder at a rate of 3 ml/h to elicit repetitive bladder contractions. Continuous urodynamic curves were digitized and recorded using a multichannel signal processing system (Taimeng, Chengdu) for at least 30 minutes. The micturition pressure and intercontractile interval were analyzed, which represent the bladder contractility and urinary frequency. We performed the urodynamic measurements at approximately the same time every afternoon between 9 AM and 4 PM.

2.5. Bladder Histology. Mice bladders were obtained and processed with 4% paraformaldehyde fixation, paraffin embedment, 5 μm section preparation, dewaxing, hematoxylin and eosin (HE) staining, dehydration, and photography, according to the standard steps.

2.6. Oxidative Stress Markers Determination. This study uses the method of Liu et al., and the method description partly reproduces their wording [14]. The contents of MDA, SOD, and GSH-Px in the bladder tissues were determined by spectrophotometry according to the manufacturer's protocols (Jiancheng, Nanjing). Briefly, the MDA level was detected using the thiobarbituric acid (TAB) method, and the maximum absorbance was read at 532 nm. The activity of SOD was based on the combination of xanthine and xanthine oxidase, and the maximum absorbance was read at 450 nm. The activity of GSH-Px was measured using the enzyme-catalyzed reaction product, and the maximum absorbance was read at 412 nm.

2.7. Western Blot. Mice bladders were lysed in RIPA lysis buffer (Beyotime, Shanghai) to extract total protein. Protein concentrations were measured with BCA. Then, 30-50 μg protein aliquots were separated using 10% sodium dodecyl sulfate polyacrylamide gel electrophoresis (SDS-PAGE) gels and transferred to polyvinylidene fluoride (PVDF) membranes. After being blocked with 5% skim milk dissolved in TBST at room temperature for 2 h, the membranes were incubated overnight at 4°C with various primary antibodies: HO-1 (1 : 1000, Affinity), NQO1 (1 : 1000, Affinity), and β-actin (1 : 5000, Proteintech). Following incubation with horseradish peroxidase-conjugated secondary antibodies (1 : 5000, Proteintech), antibody–antigen complexes were detected using an ECL substrate and visualized with an imaging system.

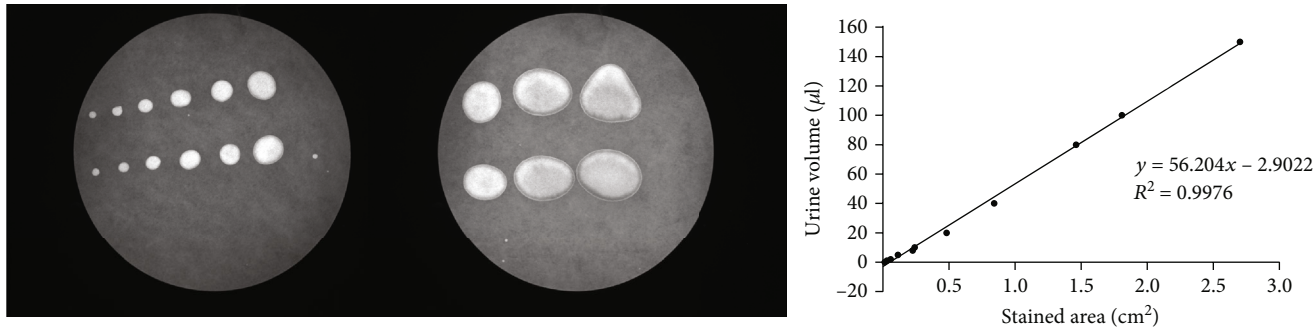

Figure 1: Urine was collected to construct the standard curve and the urine was pipetted onto filter paper in different volumes (1, 2, 4, 10, 20, 40, 80, 100, 150 μl). The formula Y (volume) = 56.204 $*$ X (stained area) − 2.9022 (R^2 = 0.9976) was used to calculate individual void on the filter paper.

Table 1: Prime sequence.

Gene	GeneBank	Primer sequence (5′-3′)	Product size (bp)
Nrf2	NM_010902	F: TTCCTCTGCTGCCATTAGTCAGTC R: GCTCTTCCATTTCCGAGTCACTG	215
HO-1	NM_010442	F: ATCGTGCTCGCATGAACACT R: CCAACACTGCATTTACATGGC	339
NQO1	NM_008706	F: ACTCGGAGAACTTTCAGTACC R: TTGGAGCAAAGTAGAGTGGT	492
β-Actin	NM_007393	F: AGTGTGACGTTGACATCCGTA R: GCCAGAGCAGTAATCTCCTTCT	150

2.8. qRT-PCR. RNAs in tissues were extracted using TRIzol (Invitrogen, USA). The extracted RNA was quantified and stored at -80°C. Reverse transcription experiments were performed according to the instructions of the PrimeScript™ RT reagent Kit with gDNA Eraser (Takara) on GeneAmp PCR System 9700 (Applied Biosystems, USA). Quantitative real-time PCR (qRT-PCR) was performed by TB Green® Premix Ex Taq™ II (Takara) on the Applied Biosystems StepOnePlus Real-Time PCR system (Applied Biosystems, USA). The PCR was performed as follows: incubation at 95°C for 3 min followed by 35 cycles for 30 s at 94°C, 30 s at 57°C, and 30 s at 72°C. The relative expression of mRNA was evaluated using the $2^{-\Delta\Delta Ct}$ method. β-Actin was used as a reference housekeeper gene [15]. Primer sequences were list in Table 1.

2.9. Statistical Analysis. All data are shown as mean ± SD. GraphPad Prism 8 was used to evaluate data. Student's t -test was used to analyze the differences between the groups. A value of $P < 0.05$ was considered statistically significant.

3. Result

3.1. Nrf2 Ameliorated Bladder Dysfunction in CYP-Induced Cystitis. As shown, there was no difference between the control groups ($P > 0.05$). After CYP administration, the mice showed urinary frequency and urgency (Figure 2(a)). We found the number of micturition increased and mean voided volume decreased compared with the corresponding control mice. Compared with $Nrf2^{+/+}$ CYP mice, $Nrf2^{-/-}$ CYP mice had more severe performance (Figures 2(c) and 2(d)).

Furthermore, the urodynamics of the mice were examined under anesthesia, and the parameters of cystometry were measured according to the urodynamic curve (Figure 2(b)). The inter contractile interval was significantly shorter in CYP mice than in control mice. However, the intercontractile interval in $Nrf2^{-/-}$ CYP mice significantly decreased compared with that in $Nrf2^{+/+}$ CYP mice (Figure 2(e)). Micturition pressure significantly decreased in CYP mice; however, no significant difference was observed in micturition pressure between $Nrf2^{+/+}$ CYP mice and $Nrf2^{-/-}$ CYP mice (Figure 2(f)). The results showed that Nrf2 ameliorated bladder dysfunction in CYP-induced cystitis.

3.2. Nrf2 Alleviated the Pelvic Hypersensitivity in CYP-Induced Cystitis. As a typical clinical manifestation of IC, allodynia in the suprapubic area was determined using von Frey filaments (Figure 3(a)). The pelvic hypersensitivity was represented by 50% withdrawal threshold, which significantly decreased in CYP mice than in control mice. Importantly, $Nrf2^{-/-}$ CYP mice showed lower withdrawal threshold compared with $Nrf2^{+/+}$ CYP mice (Figure 3(b)).

3.3. Nrf2 Rescued the Histological Changes in CYP-Induced Cystitis. CYP administration caused bladder injury, as manifested by the appearance of bladder edema and congestion (Figure 4(a)). The bladder weight significantly increased in CYP mice and $Nrf2^{-/-}$ CYP mice had higher wet weight than $Nrf2^{+/+}$ CYP mice (Figure 4(b)). HE staining revealed that CYP administration resulted in bladder edema and structural destruction. However, $Nrf2^{-/-}$ CYP mice showed more severe

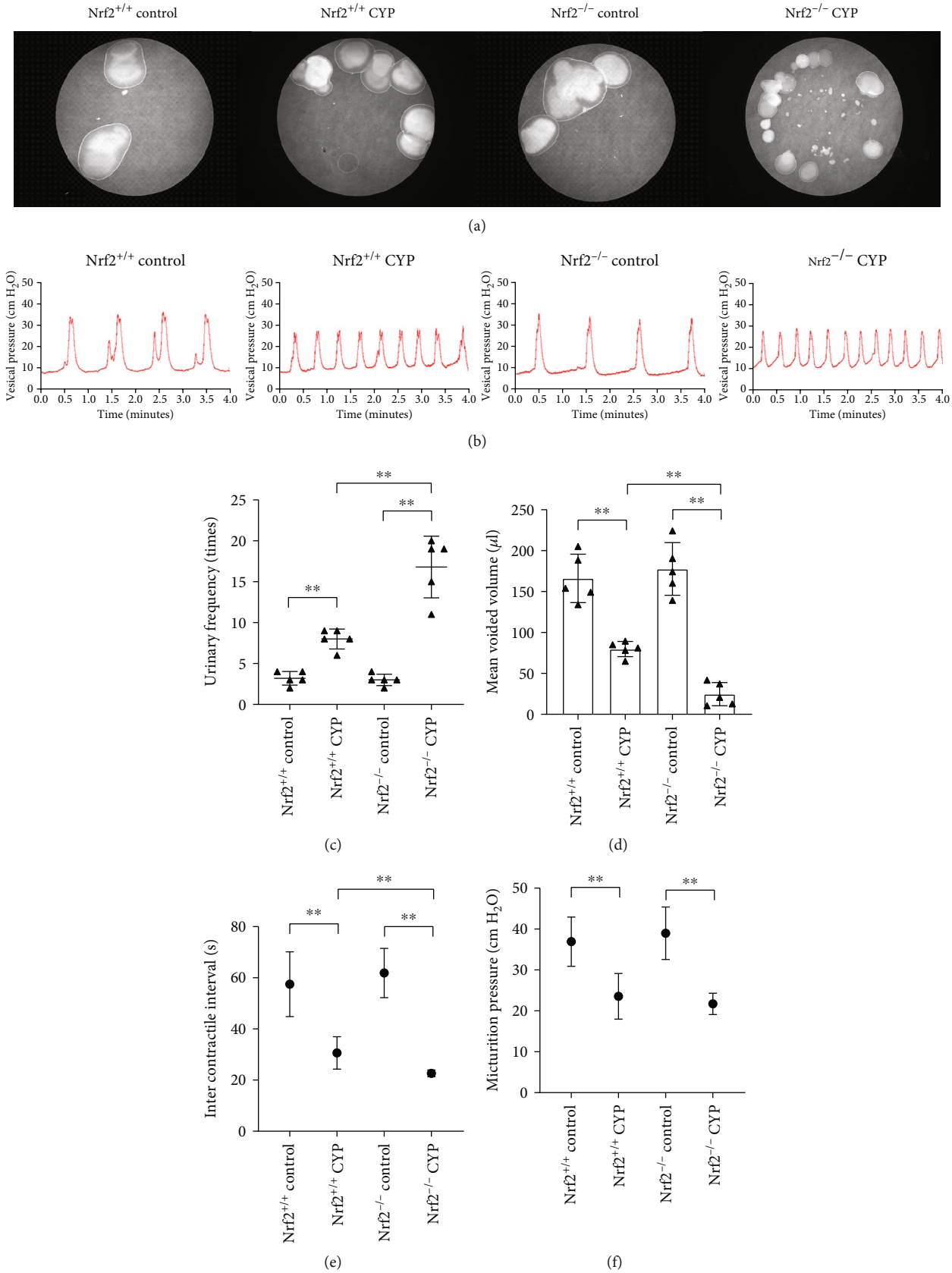

FIGURE 2: Nrf2 ameliorated bladder dysfunction in CYP-induced cystitis. (a) Sample VSA blots from four groups. (b) Urodynamic curves of four groups. Comparison of urinary frequency (c), mean voided volume (d), micturition pressure (e), and inter contractile interval (f) in four groups. $^{*}P < 0.05$, $^{**}P < 0.01$. Data are presented as mean ± SD.

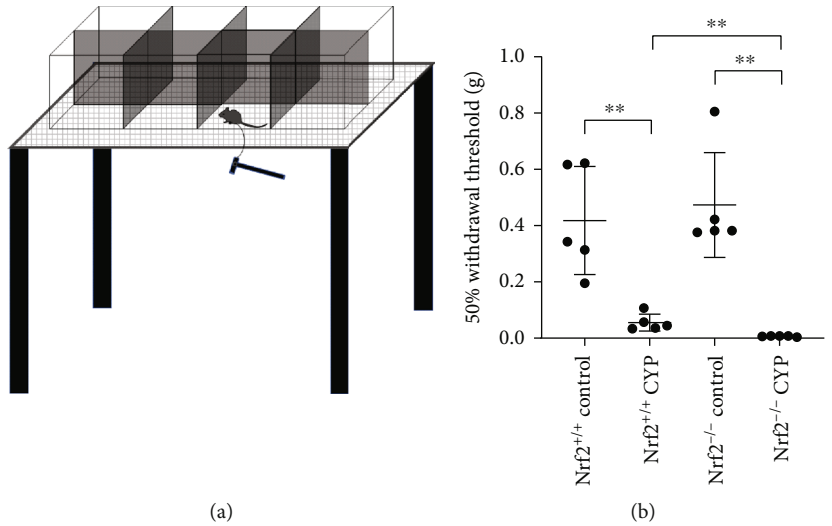

Figure 3: Nrf2 alleviated the pelvic hypersensitivity in CYP-induced cystitis. (a) Schematic diagram of determination of withdrawal threshold using von Frey filaments. (b) 50% withdrawal threshold of four groups. $^{*}P < 0.05$, $^{**}P < 0.01$. Data are presented as mean ± SD.

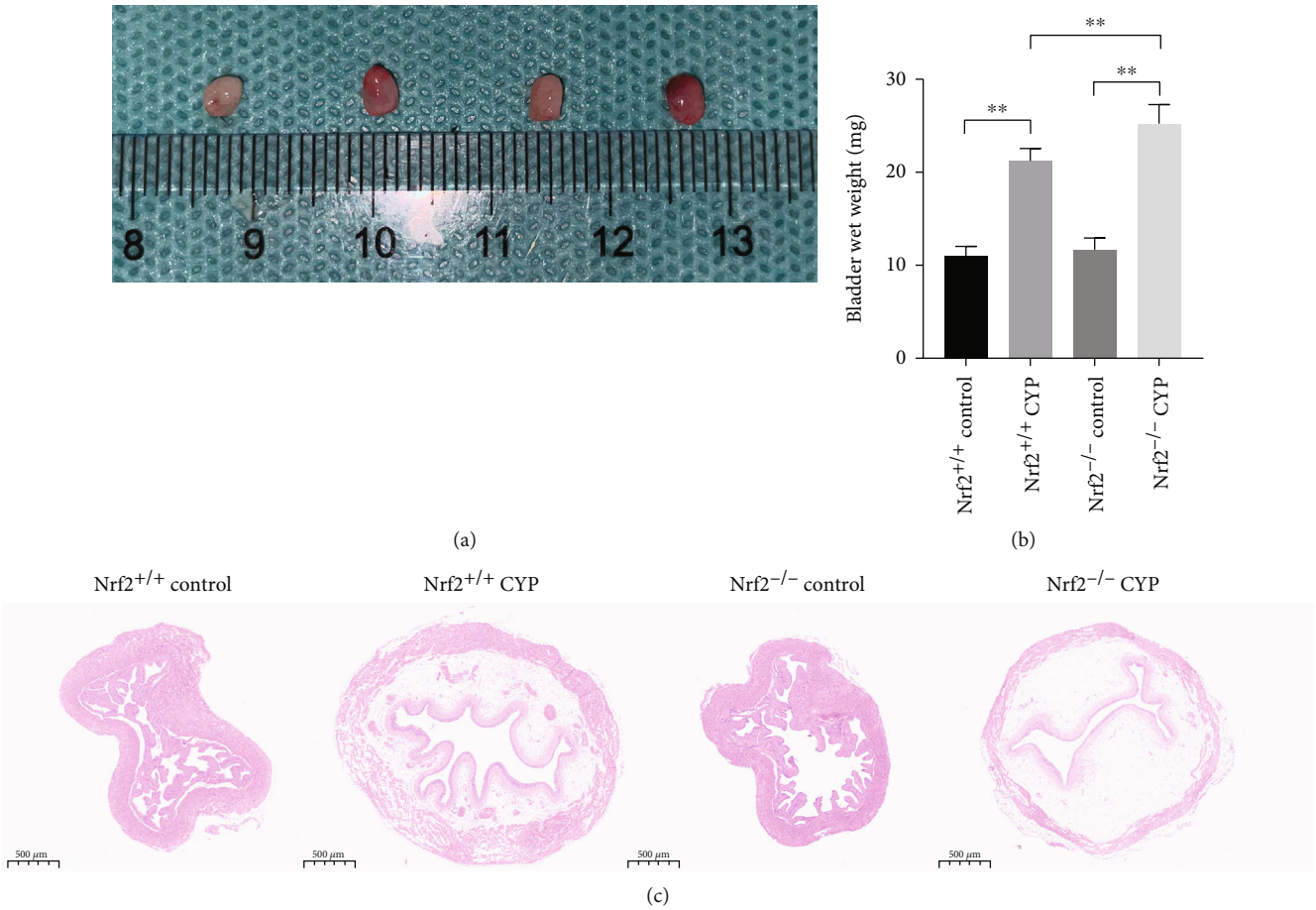

Figure 4: Nrf2 rescued the histological changes in CYP-induced cystitis. (a) Representative images of bladder from four groups. (b) Comparison of bladder weight in four groups. (c) Representative histological bladder sections from four groups (magnification: 20x). $^{*}P < 0.05$, $^{**}P < 0.01$. Data are presented as mean ± SD.

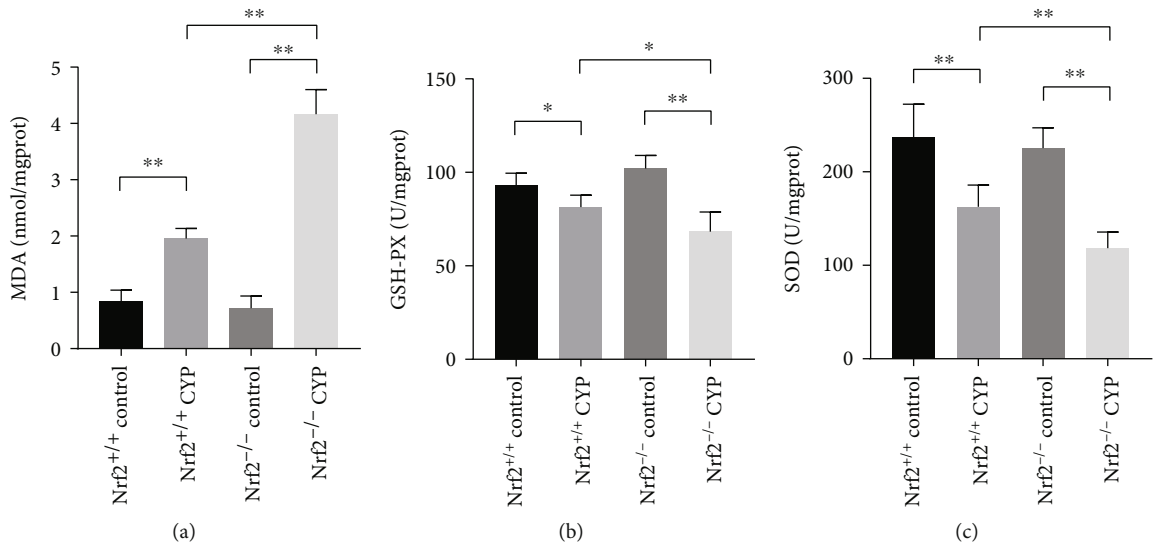

Figure 5: Nrf2 attenuated oxidative stress in CYP-induced cystitis. (a) MDA level in the bladder of the four groups. (b) The activities of GSH-Px in the bladder of the four groups. (c) The activities of SOD in the bladder of the four groups. $^{*}P < 0.05$, $^{**}P < 0.01$. Data are presented as mean ± SD.

damage in histology (Figure 4(c)). The findings indicated that Nrf2 rescued the histological changes in CYP-induced cystitis.

3.4. Nrf2 Attenuated Oxidative Stress in CYP-Induced Cystitis. MDA, SOD, and GSH-Px were measured to evaluate the level of oxidative stress. Our study showed that the content of MDA in bladder was significantly increased in CYP mice compared with the corresponding control mice. Furthermore, the level of MDA was higher in $Nrf2^{-/-}$ CYP mice than in $Nrf2^{+/+}$ CYP mice (Figure 5(a)). The activities of SOD and GSH-Px significantly decreased in CYP mice compared with the corresponding control mice. However, the activities of SOD and GSH-Px was lower in $Nrf2^{-/-}$ CYP mice than in $Nrf2^{+/+}$ CYP mice (Figures 5(b) and 5(c)). The results indicated that Nrf2 attenuated oxidative stress in CYP-induced cystitis.

3.5. Nrf2 Might Protect against Bladder Injury by Activating Its Downstream Antioxidant Genes. In order to explore the mechanism of Nrf2 in CYP-induced cystitis, we investigated the expression of its downstream antioxidant genes. We found that both the mRNA and protein levels of HO-1 and NQO1 were upregulated in $Nrf2^{+/+}$ CYP mice compared with $Nrf2^{+/+}$ control mice. As expected, there was no obvious expression in $Nrf2^{-/-}$ mice (Figures 3(a)–3(d)). The results demonstrated that Nrf2 protected mice against bladder injury, possibly through activating its downstream antioxidant genes. The Figure 6 is shown below.

4. Discussion

The etiology of IC is unknown and there are few effective clinical treatments for IC. Therefore, exploration of more alternative treatments for IC is necessary. Nrf2 pathway has been proven to inhibit oxidative stress damage in cardiac myocyte damage [16], lung injury [17, 18], and liver damage [19, 20]. Increasing studies have shown that oxidative stress participates in IC [21]. Moreover, a study demonstrates that the serum antioxidant capacity in IC patients is lower than that in controls [22]. As the crucial regulator of antioxidant defense system, Nrf2 pathway may play a critical role in the occurrence and development of IC. According to relevant studies, CYP-induced cystitis is the most stable, reliable, and widely used mode for the study of IC [23]. The typical clinical manifestations of IC can be induced after a single high-dose injection, such as pain-related behavior, bladder edema, urinary frequency, and urgency [24]. According to the symptoms above, our study is the first to establish an objective functional evaluation system for the study of the function and behavior in IC animal models, which provides a reference method for the related research in the future. However, animal models for the study of IC need further optimization.

It has been reported that Nrf2 could ameliorate bladder dysfunction through suppressing oxidative stress [25, 26]. In this study, we performed some interesting experiments, such as void spot assay, determination of pain threshold using von Frey filaments, and urodynamic examination. Previous researches just adapted some of them to evaluate bladder hyperreflexia induced by CYP [27]. As reported, we observed the urination frequency and mean voided volume. The 50% withdrawal threshold was determined using the up-down method of Dixon. At the same time, the micturition pressure and the micturition interval are measured in the urodynamic examination. We found that the CYP mice showed varying degrees of bladder dysfunction and behavioral changes, but $Nrf2^{-/-}$ CYP mice had more severe symptoms. The results indirectly indicated that Nrf2 might play a vital role in ameliorating IC-induced bladder dysfunction.

In addition, we performed HE staining on the mice bladder. CYP administration could result in extensive cystitis,

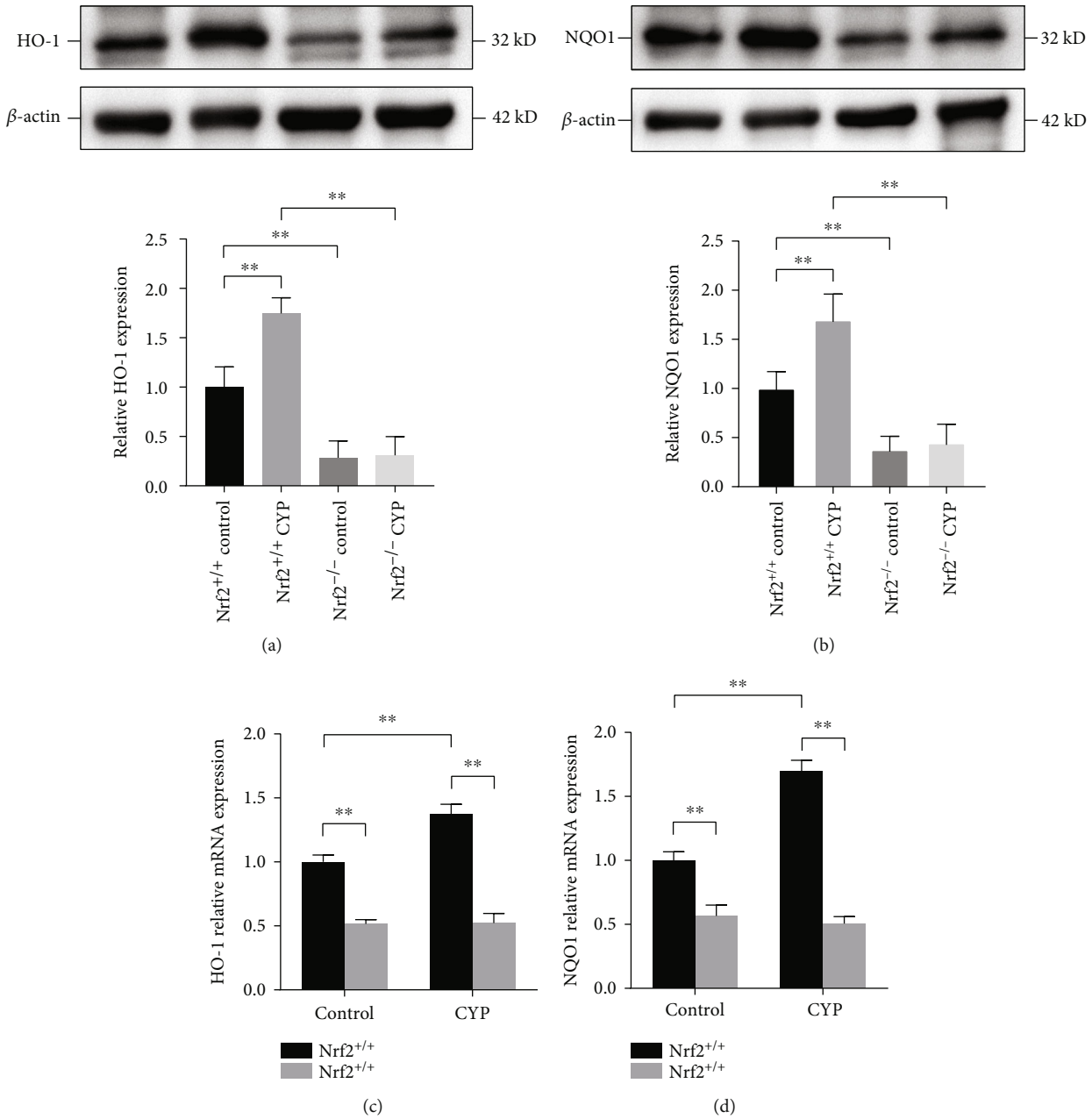

Figure 6: Nrf2 might protect bladder injury by activating its downstream antioxidant genes. (a) The protein expression of HO-1 in the bladder of the four groups. (b) The protein expression of NQO1 in the bladder of the four groups. Relative mRNA expression levels of HO-1 (c) and NQO1 (d) in the bladder of the four groups. $^{*}P < 0.05$, $^{**}P < 0.01$. Data are presented as mean ± SD.

bladder edema and structural destruction [28]. Notably, $Nrf2^{-/-}$ CYP mice had more severe symptoms. Our study demonstrated that Nrf2 could protect mice against IC-induced morphological damage. Furthermore, we measured the oxidative stress markers in mice bladder. We found that knockout of Nrf2 caused higher sensitivity to oxidative stress in CYP mice. $Nrf2^{-/-}$ CYP mice showed higher level of MDA and decreased activities of SOD and GSH-Px compared with $Nrf2^{+/+}$ CYP mice. The results indicated that Nrf2 might alleviate oxidative stress in IC.

Finally, we further studied the potential mechanism of Nrf2 pathway in IC. The expression of the antioxidant enzymes downstream of Nrf2 pathway, including HO-1 and NQO1, was determined. HO-1 is an antioxidant enzyme encoded by the HMOX1 gene, which can catalyze the decomposition of heme and exert antioxidant effects through the decomposition products [29]. NQO1 is a ubiquitous cytosolic phase II biotransformation enzyme whose primary physiological role is catalysis of two-electron reduction of quinones and thereby their detoxification. Knockout of NQO1 gene in mice led to increased reactive oxygen species, alterations in factors regulating energy metabolism and adhesion, and loss of mitochondrial structures including cristae structures [30]. We found that after knocking out Nrf2, the

endogenous HO-1 and NQO1 levels were significantly lower than those in normal mice. Importantly, their activities could not be upregulated after CYP administration, which suggested that Nrf2 is an essential translation factor for regulating the expression of antioxidant genes. It has been reported that the expression of Nrf2 and its downstream antioxidant genes decreased after other drug administration [31, 32]. Difference of drugs and the duration of intervention may contribute to the discrepancy. Some poison administration may directly or indirectly cause DNA damage, thereby affecting gene transcription regulation. Moreover, in response to oxidative stress injury, Nrf2 translocates into the nucleus and then activates its downstream antioxidant genes, which may show a curvilinear change. Our previous study showed that the expression of Nrf2 and its downstream antioxidant genes gradually increased after CYP administration. However, the expression levels reached their peak at 24 hours and gradually decreased subsequently, which is consistent with previous research [33, 34]. The results indicated that Nrf2 might protect mice against bladder dysfunction and oxidative stress by activating its downstream antioxidant genes in IC. Based on current findings, it is significant to explore Nrf2-related pharmaceutical treatments for IC.

In summary, our study is the first to adopt Nrf2 knockout mice in the study of IC and establish an objective functional evaluation system for IC animal models. We found that Nrf2 pathway protected mice against CYP-induced cystitis, possibly by activating the expression of antioxidant genes to inhibit oxidative stress and ameliorate bladder dysfunction. These findings may provide strong evidence for the Nrf2 pathway as a new target for clinical treatment of IC.

Data Availability

All of data were presented in the main paper. The data that support the findings of this study are available on request from the corresponding author. All authors take responsibility for the integrity of the data and the accuracy of the data analysis.

Conflicts of Interest

The authors declare that they have no conflicts of interest.

Authors' Contributions

BN, ZSC, BXS, and ZQW were involved in the study, design of the experiments. BN, ZSC, and BXS performed the experiments, evaluated data and wrote the manuscript. BN, LS, YPS, YH, NET, and BXS were involved in data analysis and manuscript editing. All authors read and approved the final manuscript. Bin Ni and Zhengsen Chen are co-first author.

Acknowledgments

This research was supported by the National Natural Science Foundation of China (81400758, 81873627), Jiangsu Province "333" project (BRA2020392), and "789" project of The Second Affiliated Hospital of Nanjing Medical University (789ZYRC202080120). The funds were used in the design of the study, collection of data, statistical analysis, data interpretation, and writing of the manuscript and revision.

References

[1] J. P. van de Merwe, J. Nordling, P. Bouchelouche et al., "Diagnostic Criteria, Classification, and Nomenclature for Painful Bladder Syndrome/Interstitial Cystitis: An ESSIC Proposal," *European Urology*, vol. 53, no. 1, pp. 60–67, 2008.

[2] A. Cox, N. Golda, G. Nadeau et al., "CUA guideline: diagnosis and treatment of interstitial cystitis/bladder pain syndrome," *Canadian Urological Association Journal*, vol. 10, no. 5-6, pp. E136–E155, 2016.

[3] D. Sun, C. Sun, G. Qiu et al., "Allicin mitigates hepatic injury following cyclophosphamide administration via activation of Nrf2/ARE pathways and through inhibition of inflammatory and apoptotic machinery," *Environmental Science and Pollution Research*, 2021.

[4] Y. Miyata, T. Matsuo, K. Mitsunari, A. Asai, K. Ohba, and H. Sakai, "A review of oxidative stress and urinary dysfunction caused by bladder outlet obstruction and treatments using antioxidants," *Antioxidants*, vol. 8, no. 5, p. 132, 2019.

[5] E. J. Gonzalez, A. Peterson, S. Malley et al., "The effects of tempol on cyclophosphamide-induced oxidative stress in rat micturition reflexes," *Scientific World Journal*, vol. 2015, article 545048, pp. 1–13, 2015.

[6] P. R. Gore, C. P. Prajapati, U. B. Mahajan et al., "Protective effect of thymoquinone against cyclophosphamide-induced hemorrhagic cystitis through inhibiting DNA damage and upregulation of Nrf2 expression," *International Journal of Biological Sciences*, vol. 12, no. 8, pp. 944–953, 2016.

[7] T. H. Rushmore, M. R. Morton, and C. B. Pickett, "The antioxidant responsive element. Activation by oxidative stress and identification of the DNA consensus sequence required for functional activity," *The Journal of Biological Chemistry*, vol. 266, no. 18, pp. 11632–11639, 1991.

[8] K. I. Tong, Y. Katoh, H. Kusunoki, K. Itoh, T. Tanaka, and M. Yamamoto, "Keap1 recruits Neh2 through binding to ETGE and DLG motifs: characterization of the two-site molecular recognition model," *Molecular and Cellular Biology*, vol. 26, no. 8, pp. 2887–2900, 2006.

[9] C. Tonelli, I. I. C. Chio, and D. A. Tuveson, "Transcriptional regulation by Nrf2," *Antioxidants & Redox Signaling*, vol. 29, no. 17, pp. 1727–1745, 2018.

[10] K. Tooke, B. Girard, and M. A. Vizzard, "Functional effects of blocking VEGF/VEGFR2 signaling in the rat urinary bladder in acute and chronic CYP-induced cystitis," *American Journal of Physiology Renal Physiology*, vol. 317, no. 1, pp. F43–F51, 2019.

[11] K. A. Wegner, L. L. Abler, S. R. Oakes et al., "Void spot assay procedural optimization and software for rapid and objective quantification of rodent voiding function, including overlapping urine spots," *American Journal of Physiology Renal Physiology*, vol. 315, no. 4, pp. F1067–F1080, 2018.

[12] S. R. Chaplan, F. W. Bach, J. W. Pogrel, J. M. Chung, and T. L. Yaksh, "Quantitative assessment of tactile allodynia in the rat paw," *Journal of Neuroscience Methods*, vol. 53, no. 1, pp. 55–63, 1994.

[13] D. E. Bjorling, Z. Wang, C. M. Vezina et al., "Evaluation of voiding assays in mice: impact of genetic strains and sex," *American Journal of Physiology Renal Physiology*, vol. 308, no. 12, pp. F1369–F1378, 2015.

[14] C. Liu, H. Xu, S. Fu et al., "Sulforaphane ameliorates bladder dysfunction through activation of the Nrf2-ARE pathway in a rat model of partial bladder outlet obstruction," *Oxidative Medicine and Cellular Longevity*, vol. 2016, Article ID 7598294, 12 pages, 2016.

[15] S. A. Bustin, V. Benes, J. A. Garson et al., "The MIQE guidelines: minimum information for publication of quantitative real-time PCR experiments," *Clinical Chemistry*, vol. 55, no. 4, pp. 611–622, 2009.

[16] Q. M. Chen and A. J. Maltagliati, "Nrf2 at the heart of oxidative stress and cardiac protection," *Physiological Genomics*, vol. 50, no. 2, pp. 77–97, 2018.

[17] Q. Liu, Y. Gao, and X. Ci, "Role of Nrf2 and its activators in respiratory diseases," *Oxidative Medicine and Cellular Longevity*, vol. 2019, Article ID 7090534, 17 pages, 2019.

[18] Y. Lv, H. Jiang, S. Li et al., "Sulforaphane prevents chromium-induced lung injury in rats via activation of the Akt/GSK-3β/Fyn pathway," *Environmental Pollution*, vol. 259, article 113812, 2020.

[19] X. Ma, Q. Luo, H. Zhu et al., "Aldehyde dehydrogenase 2 activation ameliorates CCl4-induced chronic liver fibrosis in mice by up-regulating Nrf2/HO-1 antioxidant pathway," *Journal of Cellular and Molecular Medicine*, vol. 22, no. 8, pp. 3965–3978, 2018.

[20] S. Li, X. Zheng, X. Zhang et al., "Exploring the liver fibrosis induced by deltamethrin exposure in quails and elucidating the protective mechanism of resveratrol," *Ecotoxicology and Environmental Safety*, vol. 207, article 111501, 2021.

[21] J. Li, H. Luo, X. Dong et al., "Therapeutic effect of urine-derived stem cells for protamine/lipopolysaccharide-induced interstitial cystitis in a rat model," *Stem Cell Research & Therapy*, vol. 8, no. 1, p. 107, 2017.

[22] K. Ener, M. Keske, M. Aldemir et al., "Evaluation of oxidative stress status and antioxidant capacity in patients with painful bladder syndrome/interstitial cystitis: preliminary results of a randomised study," *International Urology and Nephrology*, vol. 47, no. 8, pp. 1297–1302, 2015.

[23] C. Augé, X. Gamé, N. Vergnolle, P. Lluel, and S. Chabot, "Characterization and validation of a chronic model of cyclophosphamide-induced interstitial cystitis/bladder pain syndrome in rats," *Frontiers in Pharmacology*, vol. 11, article 1305, 2020.

[24] L. Birder and K. E. Andersson, "Animal modelling of interstitial cystitis/bladder pain syndrome," *International Neurourology Journal*, vol. 22, pp. S3–S9, 2018.

[25] H. C. Tai, S. D. Chung, C. T. Chien, and H. J. Yu, "Sulforaphane improves ischemia-induced detrusor overactivity by downregulating the enhancement of associated endoplasmic reticulum stress, autophagy, and apoptosis in rat bladder," *Scientific Reports*, vol. 6, no. 1, article 36110, 2016.

[26] M. Gu, C. Liu, X. Wan et al., "Epigallocatechin gallate attenuates bladder dysfunction via suppression of oxidative stress in a rat model of partial bladder outlet obstruction," *Oxidative Medicine and Cellular Longevity*, vol. 2018, Article ID 1393641, 10 pages, 2018.

[27] L. Arms and M. A. Vizzard, "Role for pAKT in rat urinary bladder with cyclophosphamide (CYP)-induced cystitis," *American Journal of Physiology. Renal Physiology*, vol. 301, no. 2, pp. F252–F262, 2011.

[28] A. Fathollahi, F. Daneshgari, and A. T. Hanna-Mitchell, "Melatonin and its role in lower urinary tract function: an article review," *Current Urology*, vol. 8, no. 3, pp. 113–118, 2015.

[29] A. Grochot-Przeczek, J. Dulak, and A. Jozkowicz, "Haem oxygenase-1: non-canonical roles in physiology and pathology," *Clinical Science*, vol. 122, no. 3, pp. 93–103, 2012.

[30] B. A. Patrick, A. Das, and A. K. Jaiswal, "NAD(P)H:quinone oxidoreductase 1 protects bladder epithelium against painful bladder syndrome in mice," *Free Radical Biology & Medicine*, vol. 53, no. 10, pp. 1886–1893, 2012.

[31] B. Liu, H. Yu, R. Baiyun et al., "Protective effects of dietary luteolin against mercuric chloride-induced lung injury in mice: Involvement of AKT/Nrf2 and NF-κB pathways," *Food and Chemical Toxicology*, vol. 113, pp. 296–302, 2018.

[32] Y. Lv, Q. Bing, Z. Lv et al., "Imidacloprid-induced liver fibrosis in quails via activation of the TGF-β1/Smad pathway," *Science of The Total Environment*, vol. 705, article 135915, 2020.

[33] Y. Hong, W. Yan, S. Chen, C. R. Sun, and J. M. Zhang, "The role of Nrf2 signaling in the regulation of antioxidants and detoxifying enzymes after traumatic brain injury in rats and mice," *Acta Pharmacologica Sinica*, vol. 31, no. 11, pp. 1421–1430, 2010.

[34] W. Yan, H. D. Wang, X. M. Feng, Y. S. Ding, W. Jin, and K. Tang, "The expression of NF-E2-related factor 2 in the rat brain after traumatic brain injury," *The Journal of Trauma*, vol. 66, no. 5, pp. 1431–1435, 2009.